MATHEMATICAL MODELLING OF THE COMPLEX MECHANICS OF BIOLOGICAL GELS

JAMES RICHARD REOCH

A thesis submitted in fulfilment of
the requirements for the degree of
Doctor of Philosophy

School of Mathematical Sciences
The University of Adelaide

2020

ABSTRACT

Biological tissues are comprised of cells surrounded by the extracellular matrix (ECM). The ECM can be thought of as a fibrous polymer network, acting as a natural scaffolding to provide mechanical support to the cells. Reciprocal mechanical and chemical interactions between the cells and the ECM are crucial in regulating the development of tissues and maintaining their functionality. Hence, to maintain *in vivo*-like behaviour when cells are cultured *in vitro*, they are often seeded in a gel, which aims to mimic the ECM. A range of natural and synthetic gels are used in such experiments, with these gels primarily consisting of solvent and polymer.

In this thesis, we develop mathematical models that incorporate cell-gel interactions together with osmotic pressure to better understand the mechanical behaviour of biological gels. In particular, we consider an experiment where cells are seeded within a gel, which gradually compacts due to forces exerted on it by the cells. We investigate how cell traction forces interact with osmotic effects (which can lead to either gel swelling or contraction depending on the gel's composition) and the types of behaviour that can arise as a result.

We begin by developing a multiphase model to study gel swelling and contraction. In this model, the volume fractions of polymer and solvent (which together form the gel) are tracked alongside cell density as the gel evolves. We consider the novel addition of cell traction forces in this framework alongside chemical potentials in the polymer and solvent.

We then study this model in one-dimensional coordinates. We find that a number of qualitatively different behaviours are possible, depending on the composition of the gel and the strength of cell traction forces. We discover spatially varying steady states as well as an unusual case where the components of the gel oscillate between swelling and contraction.

Since gels used in experiments are often formed as thin layers, we extend the model to study the gel as a two-dimensional thin sheet. We derive an extensional flow model by using the gel's thinness to scale certain parameters; in this model, key variables are functions of axial position and time. This allows us to derive a new leading order, one dimensional model from the initial 2D system of equations.

We consider the thin film model for uniform and non-uniform initial conditions separately. With uniform initial conditions, we find that the model reduces to a system driven by an ordinary differential equation in the gel's height. For non-uniform initial conditions, spatially varying equilibrium solutions can be found.

In this thesis, we develop and analyse new mathematical models for a cell-gel system incorporating cell-induced gel contraction alongside osmotic effects. We find new emergent behaviours, derive a new leading order model from the two-dimensional thin film problem, and compare the gel's behaviours in 1D and 2D settings. We show that adding cells can provide a switch between gel swelling and contraction, and that the balance between chemical potentials and cell forces is pivotal in the system's stability and equilibrium outcomes.

THESIS DECLARATION

I certify that this work contains no material which has been accepted for the award of any other degree or diploma in my name in any university or other tertiary institution and, to the best of my knowledge and belief, contains no material previously published or written by another person, except where due reference has been made in the text. In addition, I certify that no part of this work will, in the future, be used in a submission in my name for any other degree or diploma in any university or other tertiary institution without the prior approval of the University of Adelaide and where applicable, any partner institution responsible for the joint award of this degree.

I give permission for the digital version of my thesis to be made available on the web, via the University's digital research repository, the Library Search and also through web search engines, unless permission has been granted by the University to restrict access for a period of time.

Signed: Date:

ACKNOWLEDGEMENTS

Most of all, thank you to my partner Shila, whose encouragement and belief has meant the world to me over the last seven years.

To my supervisors Yvonne Stokes and Edward Green, thank you so much for your guidance, patience and flexibility through a PhD that has taken some unexpected turns. Thank you for your understanding with me switching firstly to remote, then part-time (and recently, spare-time) study. I've very much enjoyed learning from you and feel like I've become a much better researcher and mathematician as a result.

Thank you to my associate supervisor Mary Myerscough for your help and support when called on over the last few years. Thank you as well to Peter Kim for previously occupying this position and for helping to facilitate my move back to the University of Sydney.

Thank you to the University of Adelaide for their support and accommodation over the course of my candidature and for providing me with a Faculty of Engineering, Mathematics and Computer Sciences Divisional Scholarship. Thank you to the University of Sydney for hosting me over the majority of my candidature and for providing a welcoming community to be a part of.

Thanks to the teams in the Westpac STEM PhD program and Financial Markets for giving me an opportunity and an interesting beginning to my career beyond my PhD. In particular, thank you to my managers in the eCommerce team for their flexibility and understanding as I've juggled work and study over the last three years, and to Seb for your advice and friendship.

I owe a big thank you to my parents Clare and Andrew who have always encouraged me to learn new things and take opportunities to study, and who will unfailingly provide support whenever and however I need it. Thank you to Anna and Angus for always being there.

Finally, thank you to all my friends who have helped to make the majority of this time as enjoyable as it was. To Adrianne, Sara, Kerry and Matthew among others, thanks for making the PhD bearable and sorry I was so distracting. Thank you to Sara and Shila for proofreading my thesis as well and giving helpful feedback. To Libby, Anthony and Oleg, thanks for the lunches and advice. To everyone not mentioned, thanks for being there and I hope to see more of everyone soon.

CONTENTS

1

INTRODUCTION

1.1 PROBLEM STATEMENT

Biological tissues are comprised of cells living in extracellular matrix, hereafter designated ECM. The ECM provides mechanical support to the cells *in vivo* and helps to regulate cell behaviour, as well as playing a key role in the mechanical behaviour of the tissues themselves (Frantz *et al.*, 2010). The ECM *in vivo* can be thought of as a fibrous polymer network; it can consist of a number of different substances, including proteoglycans, collagens and glycoproteins (Rozario and DeSimone, 2010). To reproduce *in vivo*-like behaviour when cells are cultured *in vitro*, they are often seeded in a gel, which aims to mimic the ECM. Since the structural protein collagen is the primary component of the ECM in many animal tissues (Shoulders and Raines, 2009), collagen gels are frequently used in laboratory studies (*e.g.* Moon and Tranquillo (1993); Stevenson *et al.* (2010)), but a wide range of other natural (*e.g.* Matrigel (Krause *et al.*, 2008)) or synthetic (*e.g.* poly(lactic acid) (Wayne *et al.*, 2005)) gels are also used. Improved understanding of the mechanical behaviour of biological gels, together with cell-cell and cell-gel interactions, will lead to better understanding of the development and functioning of tissues.

The mechanical characteristics of a tissue can have a powerful effect on cell behaviours such as proliferation, differentiation and cell motility (Rozario and DeSimone, 2010); this effect is, in fact, reciprocal, since the tissue is maintained by these cells (Frantz *et al.*, 2010). *In vitro* experiments aimed at gaining more insight into the cell-ECM relationship and how each regulates and affects the other are conducted using cell-seeded gels; these gels are studied in different physical configurations such as thin films and small spheres. One such experiment, presented by Moon and Tranquillo (1993), involves the contraction of a sphere of collagen gel under the influence of cell traction forces. The cells' mechanical interactions with the polymer network surrounding them lead to this polymer network being reorganised and compacted. This process of ECM remodelling is important in tissue growth and development and, accordingly, is important in a range of related topics such as wound healing and tissue engineering (Moon and Tranquillo, 1993).

Mathematical modelling of this experiment assumed that the only forces acting on the gel were those exerted by the cells. However, biological gels can swell or contract in the absence of cells, for example, due to osmotic effects whereby solvent molecules enter or leave the gel's polymer network until the gel equilibrates with the surrounding solvent (Hong *et al.*, 2010). Osmotic swelling and contraction of gels and gel-like substances is often studied mathematically using multiphase flow models, in which the behaviour of the polymer and solvent components of the gel are each distinctly considered. Recent experiments have suggested that these osmotic effects could be used to manipulate the mechanical environment of cells *in vitro* by, for example, applying a compressive force to the gel in which they reside (Monnier *et al.*, 2016).

In this thesis, we will model the behaviour of a biological gel. The gel is comprised of a polymer network and a solvent and sits surrounded by a bath of pure solvent. Initially, the gel is seeded with cells. As time progresses, the interface between the gel and the surrounding solvent expands or contracts with the movement of solvent into or out of the gel. This movement is a result of the underlying force balance in the system, affected by factors like cell traction and osmotic pressure. Swelling or contraction occurs until either a steady state is reached when the system is in equilibrium, or the gel reaches a fully dissolved or contracted state. We will study the emergent behaviours of this system in 1D and thin film geometries, reflecting different gel configurations.

Our aim is to gain better understanding of how cell and osmotic forces interact within cell-seeded gels grown *in vitro* through the development and investigation of these mathematical models. In particular, we are interested in the different qualitative outcomes that may arise (*e.g.* gel contraction, swelling or dissolution), and how these outcomes, together with the dynamics of the process, depend on factors such as the gel composition, osmotic pressure, cell traction strength, and drag between the network and solution phases of the gel.

This introduction provides an overview of current literature dealing with key aspects of this problem. In Section 1.2, we look at modelling of the cells' mechanical interactions with the ECM *in vitro*. Section 1.3 discusses the mechanics of polymer-solvent multiphase flow models, including osmotic effects. Finally, Section 1.4 describes mod-

els for thin fluid layers. We conclude the introduction with an outline of the thesis in Section 1.5.

1.2 CELL-ECM MODELLING

Mechanochemical interactions between cells and the ECM they inhabit have been studied in a number of works (*e.g.* Murray (2001); Murray *et al.* (1983)). These models describe the movement of cells in ECM due to factors such as advection, chemotaxis and diffusion, together with mechanical interactions between the cells and matrix. Cells migrate within the ECM and, due to the traction forces they generate, deform the ECM as they move. The mechanochemical model presented in Murray (2001) consists of mass conservation equations for each of the cell and ECM densities, together with a force balance equation, wherein stresses in the ECM and cell traction stresses balance body forces.

Moon and Tranquillo (1993) used this theory to model the experiment already mentioned in Section 1.1. In this experiment, cells were seeded in a collagen gel and acted to compact the gel over approximately two days through the traction stresses they generated. The use of a spherical gel in this experiment, as opposed to a thin disc, allows for simpler modelling through the spherical symmetry of the gel; the isotropic distribution of collagen fibres also assists modelling. The model and experimental results are then used in the second part of this study by Barocas *et al.* (1995) to quantify the force exerted by the cells by means of a cell traction parameter. Although the degree of gel contraction can provide a measure of the cell forces exerted, we note that it is also dependent on the specific procedures employed in the experiment (*e.g.* cell density, gel composition and size, cell type, etc.).

The mechanochemical model is presented here as set out by Moon and Tranquillo (1993), with the notation changed where possible for consistency with our models. We let $n(\mathbf{x}, t)$ and $\rho(\mathbf{x}, t)$ denote the cell density and ECM density respectively at position $\mathbf{x}$ and time t, while $\mathbf{S}_p(\mathbf{x}, t)$ denotes the displacement vector of the ECM. Cells are

advected with the gel and also move randomly; therefore, the conservation equation for cell density is given by

$$\frac{\partial n}{\partial t} + \nabla \cdot \left(n \frac{\partial \mathbf{S}_p}{\partial t} \right) = D \nabla^2 n, \tag{1.1}$$

where D is a constant diffusion coefficient. For simplicity, cell death and proliferation are ignored. The velocity $\mathbf{v}_p \approx \partial \mathbf{S}_p / \partial t$; this approximation assumes small displacements in the ECM.

The ECM is modelled as a single, viscoelastic material. Mass conservation then gives

$$\frac{\partial \rho}{\partial t} + \nabla \cdot \left(\rho \frac{\partial \mathbf{S}_p}{\partial t} \right) = 0. \tag{1.2}$$

There is no growth term in the conservation equation for the ECM since polymer production and degradation is negligible over the experimental time scales of interest (Green *et al.*, 2013).

Momentum balance for the system is described by the equation

$$\nabla \cdot \boldsymbol{\sigma} + \mathbf{F} = 0, \tag{1.3}$$

where $\boldsymbol{\sigma}$ is the gel stress tensor and $\mathbf{F}$ is the force per unit volume acting on the gel; $\mathbf{F}$ is taken to be zero here as there are negligible body forces acting on the gel. We note that inertial effects have been neglected in this model, since the time scale of deformation is very long and the spatial scales are small (Murray, 2001).

The stress tensor $\boldsymbol{\sigma}$ is the sum of ECM and cell contributions, $\boldsymbol{\sigma} = \boldsymbol{\sigma}_{\text{ECM}} + \boldsymbol{\sigma}_{\text{cell}}$. The ECM is assumed to be a viscoelastic material. Hence, $\boldsymbol{\sigma}_{\text{ECM}}$ is the sum of viscous and elastic stress terms involving the strain tensor and rate of strain tensor. The cell contribution $\boldsymbol{\sigma}_{\text{cell}}$ captures the traction forces arising as cells pull on the ECM; it is proportional to the cell and ECM densities and includes the parameter τ_0, which is a measure of the traction force exerted by a cell on the local ECM (Moon and Tranquillo, 1993). From equation (1.3), we see that cell traction forces are assumed to be in mechanical balance with the viscoelastic forces in the ECM as well as external forces (Murray, 2001).

An issue arising in these models is that cells are treated as a continuum material, including a stress tensor to capture cell traction effects. However, given that the fraction of cells existing in experimental gels is small, this treatment may not be appropriate. Furthermore, these mechanochemical models treat the gel as a single material (either fluid or solid) which must be assumed to be compressible for it to be able to contract. However, many types of biological gel are largely made up of water, an incompressible fluid, bringing the appropriateness of this assumption into question. Therefore, in this thesis, we will investigate the possibility that gel contraction can be a result of syneresis, *i.e.* fluid being separated out from the gel. This possibility was noted in Moon and Tranquillo (1993), but was not pursued further. In order to address this separation of fluid from the gel, the presence of the solvent surrounding the gel must be incorporated into the mathematical model. This also allows us to introduce osmotic effects into our model, and to consider their role in any syneresis seen. Osmotic pressure gradients can induce the movement of solvent across the gel's boundary, encouraging either swelling or contraction depending on the gel's composition.

Green *et al.* (2013) built on the work of Moon and Tranquillo (1993) in developing a model for cell-induced gel contraction. Alongside the mechanical interactions present in the model of Moon and Tranquillo (1993), they also hypothesised that chemotactic signals secreted by cells may influence the gel's contraction. These chemical effects are incorporated through a diffusion equation describing the evolution of the chemical concentration. Green *et al.* (2013) considered a range of forms for the cell force function, including force being a prescribed function of the radial distance, a mechanically-driven cell force function akin to that proposed in Murray (2001), and a chemically-driven force. They found best agreement with the results in Moon and Tranquillo (1993) using the mechanically-driven function. Green *et al.* also highlighted that syneresis may be a factor in the gel's contraction that is not covered in the mechanochemical models; they suggested that multiphase gel models with appropriate boundary conditions for the solvent could be used to address this. In this thesis, we therefore investigate multiphase flow models as a way to incorporate the flow of fluid into and out of gels through syneresis, particularly focusing on osmotic effects. We note that Barocas and Tranquillo (1994) studied the gel contraction problem in a multiphase flow setting; how-

ever, they did not consider fluid flow across the interface of the gel, the surrounding solvent, or any osmotic effects.

Outside the context of cell-seeded gels, a number of studies by Oster *et al.* have considered combinations of osmotic and cell traction stresses, looking at problems like cell crawling (Oster, 1984; Oster and Perelson, 1985) and limb growth (Oster *et al.*, 1985). However, these studies differ significantly in other ways from the problem that we will analyse. One such difference is that they do not consider the movement of solvent, instead considering it to be stationary. Secondly, the osmotic pressure is driven by sol-gel polymerisation and depolymerisation inside the cell, as opposed to osmotic pressure driven by chemical potential gradients between a gel and surrounding fluid. Furthermore, the traction in some of these models is due to the cytogel pulling the cells, as opposed to cells contracting the polymer network like in Moon and Tranquillo (1993). The model presented in Oster *et al.* (1985) is not a multiphase flow model and similarly does not consider solvent movement, with the osmotic component driven by cell-produced chemical concentrations.

1.3 Multiphase flow models and osmotic pressure

The models discussed in the previous section treated the gel or ECM as a single material. However, more detailed models have been developed using multiphase flow theory that study gels as a mixture of interacting polymer and solvent components, each with its own properties. These include studies into polyelectrolyte gels (Mori *et al.*, 2013; Wolgemuth *et al.*, 2004), biofilms (Cogan and Keener, 2004; Winstanley *et al.*, 2011), active cell motion (Oliver *et al.*, 2005), and swelling polymer gels (Doi, 2011; Doi and Onuki, 1992; Keener *et al.*, 2011a,b). The polyelectrolyte and swelling gel models listed here focus on the movement of solution across the boundaries of gels. Multiphase flow theory is ideal for looking at gel behaviour, as it provides a mathematical framework in which the mechanics of both polymer and solvent phases can be considered, together with the interaction between phases (Cogan and Guy, 2010). It provides a macroscopic model of the behaviour of the different phases, achieved through averaging the equations of motion (mass and momentum conservation) for each component over a rep-

resentative volume (Drew, 1983). For the development and some general discussion of two-phase flow models, see Drew (1983).

A general two-phase model is described by Oliver *et al.* (2005), where it is applied to the actin network inside crawling cells. They consider a polymer network phase with volume fraction θ_p and a solvent phase with volume fraction θ_s; these volume fractions satisfy the no-voids condition $\theta_p + \theta_s = 1$ throughout the domain. We have again modified the notation here where possible for consistency throughout the thesis. Conservation of mass gives the equations

$$\rho_p \left(\frac{\partial \theta_p}{\partial t} + \nabla \cdot (\theta_p \boldsymbol{v}_p) \right) = -\mathcal{J}, \tag{1.4}$$

$$\rho_s \left(\frac{\partial \theta_s}{\partial t} + \nabla \cdot (\theta_s \boldsymbol{v}_s) \right) = \mathcal{J}, \tag{1.5}$$

where ρ_p and ρ_s denote the respective phase densities, $\boldsymbol{v}_p$ and $\boldsymbol{v}_s$ the respective phase velocities, and $\mathcal{J}$ the average flux of mass between phases.

Given that inertial effects are negligible for biological gels, conservation of momentum gives the equations

$$\nabla \cdot (\theta_p \boldsymbol{\sigma}_p) + \mathbf{F}_{ps} = \mathbf{0}, \tag{1.6}$$

$$\nabla \cdot (\theta_s \boldsymbol{\sigma}_s) - \mathbf{F}_{ps} = \mathbf{0}, \tag{1.7}$$

where $\boldsymbol{\sigma}_p$ and $\boldsymbol{\sigma}_s$ are the average network and solvent stress tensors respectively, and $\mathbf{F}_{ps}$ denotes the inter-phase force exerted on the network by the solution.

The network is treated as an incompressible viscous fluid with stress tensor $\boldsymbol{\sigma}_p = -P_p \mathbf{I} + \eta_p (\nabla \boldsymbol{v}_p + (\nabla \boldsymbol{v}_p)^T)$, where P_p is the intra-network phase pressure, $\mathbf{I}$ the identity matrix, and the second term is the rate of strain tensor with viscosity η_p and polymer velocity $\boldsymbol{v}_p$. The solvent is assumed to be inviscid and so has the stress tensor $\boldsymbol{\sigma}_s = -P_s \mathbf{I}$, where P_s is the intra-solvent pressure. The inter-phase force has the form $\mathbf{F}_{ps} = -\xi \theta_p \theta_s (\boldsymbol{v}_p - \boldsymbol{v}_s) + P_{ps} \nabla \theta_p$. The first term describes drag between the two phases, while the second describes the pressure applied by the solvent on the network due to surface traction between the phases.

Oliver *et al.* define two pressure coefficients for use in their momentum equation: the solvation coefficient $\Psi = P_s - P_{ps}$, and the contractile coefficient $\Phi = P_s - P_p$. The solvation coefficient defines the difference between the intra-solvent pressure and the pressure across the interface between network and solution, while the contractile coefficient gives the difference in pressure between solvent and network phases. They note that there are not strong physical interpretations for these pressure coefficients, due to the artificial nature of the pressure terms coming out of the multiphase averaging process.

Incorporating these pressure terms, the force balance on the polymer and solvent phase respectively is given as

$$\nabla \cdot (\theta_p \eta_p (\nabla \boldsymbol{v}_p + (\nabla \boldsymbol{v}_p)^T)) = \theta_p \nabla P_p + \Psi \nabla \theta_p + \xi \theta_p \theta_s (\boldsymbol{v}_p - \boldsymbol{v}_s) - \Phi \nabla \theta_p, \tag{1.8}$$

$$0 = \theta_s \nabla P_s + \Psi \nabla \theta_s - \xi \theta_p \theta_s (\boldsymbol{v}_p - \boldsymbol{v}_s). \tag{1.9}$$

Adding equations (1.8) and (1.9) gives the typical conservation of momentum equation,

$$\nabla \cdot (\theta_p \eta_p (\nabla \boldsymbol{v}_p + (\nabla \boldsymbol{v}_p)^T)) = \nabla P, \tag{1.10}$$

where $\nabla P = \theta_p P_p + \theta_s P_s$ can be thought of as the overall pressure existing in the mixture. In this model, there is assumed to be no solvent flow across the free boundary.

This type of model has been built upon by Keener *et al.* (2011a,b) and Mori *et al.* (2013) to study the dynamics of gel swelling and contraction. The osmotic movement of solvent across the gel boundary is incorporated in these models through particular choices of functional forms for the force and pressure functions F_{ps}, Ψ and Φ; typically spatial gradients of chemical potential functions are used. These chemical potentials are in turn functions of the volume fractions of network and solvent, and are defined by Flory-Huggins free energy functions.

Osmotically-driven movement of solution into and out of gels has been studied in the context of gel mechanics using Flory-Huggins theory. This theory is derived from statistical thermodynamics, giving a measure of the entropy and enthalpy of the mixture (Kumar and Gupta, 2003). Using these measures, we can calculate the free energy

of the mixture per unit volume, and, thereby, the osmotic pressure (Kumar and Gupta, 2003; Winstanley *et al.*, 2011). In experiments where pure solvent is separated from a mixture of solute and solvent by a semi-permeable membrane, the osmotic pressure can be measured as the additional pressure that must be applied to the mixture to prevent the flow of solvent (Hong *et al.*, 2010); it is thus a function of the difference in the chemical potentials in the mixture and external solvent. In a gel, the cross-linked polymers perform the role of a semi-permeable membrane; the cross-links allow the flow of solvent into or out from the gel, but prevent polymers from leaving (Hong *et al.*, 2010). Osmotic pressure appears widely throughout multiphase treatments of gel mechanics (Keener *et al.*, 2011a); it will be included in our model through chemical potential functions. This is discussed further in Section 2.4.

Keener *et al.* (2011b) evaluated the impact of free energy on the kinetics of gel swelling. The aim was to extend multiphase flow models for gel swelling to incorporate free energies; this allows for a better understanding of the manner in which the gel evolves. Their model is comparable to that in Oliver *et al.* (2005), with osmotic pressure entering the model through the particular choice of pressure functions. They have advection equations akin to equations (1.4) and (1.5), with phase densities $\rho_p = \rho_s = 1$ and flux between phases $\mathcal{J} = 0$. A key difference is that the solvent stress tensor in Keener *et al.* (2011b) incorporates viscous stresses as well. Further, the pressures P_p and P_s are taken to be identical, hence the contractile pressure $\Phi = 0$. Osmotic pressure is incorporated through the solvation coefficient Ψ, where in Keener *et al.* (2011b),

$$\Psi = \theta_s \frac{\partial \mu_s}{\partial \theta_s} = \theta_p \frac{\partial \mu_p}{\partial \theta_p}.$$

μ_s and μ_p are the chemical potentials of solvent and network respectively; this is consistent with the relations discussed later in Section 2.4. In this model, these solvation terms therefore describe the osmotic pressure gradients working to drive solvent into or out of the gel.

In their work, Keener *et al.* found that these chemical potential gradients are the forces driving the gel's evolution. These chemical potentials can induce gel swelling or contraction depending on the interaction energies between polymer and solvent

which determine whether it is energetically advantageous for the phases to mix or to minimise contact. The manner in which the gel evolves spatially and temporally depends on physical factors such as drag between phases and viscosity in the polymer and solvent.

Keener *et al.* closed their system of equations with boundary conditions at the interface of the gel. There is a kinematic boundary condition governing the position of the moving gel-solvent interface. There is also a continuity of stress condition at the free boundary which imposes that the jump in normal stress is zero across the interface. We note that this condition is corrected in a later work (Sircar *et al.*, 2013) to incorporate the free energy of the solvent outside the gel. While this boundary condition captures the relation between velocity and free energy across the interface, it does not consider the permeability of the boundary, which may significantly affect the flow of solvent across this interface, and hence the dynamics of the gel. The permeability of the interface is incorporated in other models such as Mori *et al.* (2013).

Mori *et al.* (2013) studied the dynamics of polyelectrolyte gels, in which the polymer network contains a fixed charge. They noted that most biological gels are polyelectrolyte gels. They developed a multiphase model similar to those discussed previously, in which Flory-Huggins free energy drives gel evolution, and extended the model to also include ionic electrodiffusion. A key contribution of this work is the development of a novel class of boundary conditions at the free boundary. One such boundary condition is that the movement of solvent across the interface is proportional to the difference in normal solvent stress. This condition was scaled by the parameter $\mathcal{R}$, which describes the permeability of the boundary, that is, how resistant the boundary is to fluid flow. There is another interface condition similar to that in Keener *et al.* (2011b) requiring that normal force across the gel-solvent interface is continuous.

We aim to combine the approaches taken in Keener *et al.* (2011b) and Mori *et al.* (2013) with the mechanochemical theory presented in Section 1.2 to produce new mathematical models for the mechanics of cell-seeded gels which incorporate osmotic effects.

While many of the cell-ECM and multiphase flow models discussed so far are typically presented in a general, three-dimensional form, the analysis is often carried out for 1D cases (see *e.g.* Green *et al.* (2013); Keener *et al.* (2011b); Moon and Tranquillo (1993)). Modelling the gel as a two-dimensional thin film allows us to study gel behaviour in another experimentally relevant geometry, while simplifying the analysis compared to a general 2D geometry.

Thin film models are employed in a range of mathematical problems. Such studies include modelling thin viscous sheets in both two and three dimensions (Howell (1996); King and Oliver (2005)), pattern formation in cell aggregation (Green *et al.* (2017); Green (2006)), and osmotically-driven biofilm growth (Trinschek *et al.* (2016, 2017)). Howell (1996) considered a number of basic thin film problems, including the stretching flow of a thin, single-phase viscous sheet, with the length or tension prescribed. The model we will develop in this thesis is more complex, involving numerous interacting components and with the length to be determined as part of the solution. Consequently, we will build on the frameworks described in this section to develop our model.

Howell (1996) studied the dynamics of a two-dimensional thin viscous sheet through the use of asymptotic methods to derive tractable, leading order equations to describe the sheet's evolution. The model considered an incompressible Newtonian fluid which flows between two free surfaces; the centre line of the sheet is a variable function of time and space like the free boundaries. The asymptotic approach relies on the fact that the inverse aspect ratio of the sheet (*i.e.* the ratio of its height to length) is small; this ratio is represented by the small parameter ε. Accordingly, the height and velocities in the y-direction were scaled by ε. The fluid was assumed to be governed by 2D Stokes equations describing mass and momentum conservation of the fluid alongside kinematic and dynamic boundary conditions.

To derive a leading order model for the thin sheet's dynamics, the dependent variables were expanded in powers of ε^2 and substituted into the system of equations. Through analysing the equations at leading order and at $\mathcal{O}(\varepsilon^2)$, a reduced system of

equations was found where the leading order axial velocity $u_0 = u_0(x,t)$, *i.e.* it is independent of the y-coordinate and so is uniform across the height of the sheet; this is described as an extensional flow. The Trouton model was recovered, which consists of the following equations for the axial velocity and the height of the sheet,

$$\frac{\partial}{\partial x}\left(4h_0\frac{\partial u_0}{\partial x}\right) = 0, \tag{1.11}$$

$$\frac{\partial h_0}{\partial t} + \frac{\partial}{\partial x}(u_0 h_0) = 0, \tag{1.12}$$

where h_0 is the leading order height. The Trouton ratio (the ratio of extensional to shear viscosity) is 4 in this problem; this ratio changes depending on the dimensionality of the system.

Howell explored this model further under different scaling regimes for the system, finding particular scalings describing how the sheet buckles as it is compressed, and generalised the model to obtain equations governing three-dimensional sheets. It was noted that these methods should be extendable to find leading order solutions for more complicated problems.

Green *et al.* (2017) used similar techniques to study pattern formation in chemotactic cell aggregation with a thin film model. They modelled cells and culture medium as a two-phase mixture in a culture well. The culture well was studied in 2D Cartesian coordinates and included a free boundary describing the height of the film, while the film's length was fixed. The aim of this paper was to determine the conditions under which small perturbations to homogeneous steady states can lead to spatially varying steady state solutions.

Key differences in Green *et al.* (2017) compared to other multiphase models such as Keener *et al.* (2011b) and Mori *et al.* (2013) are the absence of osmotically-driven fluid movement as well as the inclusion of cells. The model consists of coupled equations describing conservation of mass and momentum for the cell and medium volume fractions. It was assumed that the inverse aspect ratio of the thin film is small, so the dependent variables were expanded in powers of ε^2 and then, as in Howell (1996), substituted into the model equations to derive leading order expressions.

A key factor in deriving a leading order 1D model from their initial 2D equations is the scaling of parameters. The parameters describing drag and cell chemotactic effects relative to viscosity were scaled to be $\mathcal{O}(1/\varepsilon^2)$, *i.e.* they were assumed to be large. The chemotaxis scaling encodes the assumption that cell forces are large and a significant determinant of behaviour, while the drag scaling couples together the movement of cell and culture medium phases. These scalings were crucial for a non-trivial leading order model to be derived.

The resulting model describes an extensional flow where the leading order variables are independent of the y-coordinate. The system consists of equations averaged across the height of the film, including mass conservation for cell and mixture phases as well as the chemoattractant, and a force balance equation for the cell layer. Through integrating across y in the model derivation, the free boundary at $y = h$ was included in the 1D model through a mass conservation equation. We will use a similar methodology in Chapter 4 when deriving a reduced model for our 2D thin film problem.

Similar modelling techniques were explored in multiphase, three-dimensional thin films in King and Oliver (2005). They developed thin film models for poroviscous flow, which were then applied to the active motion of crawling animal cells. Since the cell was assumed to be 'well-spread', it was represented as a thin film on a substrate. The cell was modelled as a two-phase material with network and solution phases; the solution flows through the poroviscous network, with mass transfer between the solution and network phases occurring due to the polymerisation and de-polymerisation process. Unlike the previous works discussed, the gel length is a free boundary in this instance. We note that this model also does not include osmotic solvent flow, or indeed, solvent flow outside the film.

As discussed with respect to the Green *et al.* (2017) study, the choice of parameter scalings played a significant role in the resulting model derived. In their paper, King and Oliver (2005) explored different thin film scaling limits, with a key result being to demonstrate how the particular choice of scaling regime allows for different models to be derived with a reduction in spatial dimensional dependency. The paper also showed how scaling regimes can be applied to extract useful models from seemingly intractable systems of equations. King and Oliver perturbed variables in powers of ε^2

like the previous studies discussed, and then obtained equations at leading order and $\mathcal{O}(\varepsilon^2)$ to derive an extensional flow model.

King and Oliver (2005) and Green (2006) also considered a lubrication scaling limit in their models alongside the extensional limits discussed so far. The lubrication problem differs from the extensional case through the presence of a no-slip condition on at least one boundary. Green (2006) considered a similar model to that presented in Green *et al.* (2017); the key difference in the lubrication limit is that while chemotaxis and drag were still scaled to be large, the ECM pressure and surface tension were also scaled to be $\mathcal{O}(1/\varepsilon^2)$. These scalings indicate that the pressures created in the system are large, and that significant surface tension and ECM pressure are required to accommodate continuity of pressure and normal stress across the boundaries. In the culture medium domain, equivalent to our gel, the pressure was found to be equal to the surface tension; the balance between cell stresses and surface tension then played a significant role in the evolution of the cell volume fraction. As in the extensional case, a 1D model for the governing equations was derived.

These thin film models do not consider the effects of osmotic swelling. Indeed, to our knowledge, osmotic pressure has not been included in a mechanical thin film model similar to those discussed thus far. We will incorporate osmotic fluid flow in the thin film gel model we develop in Chapter 4.

1.5 THESIS OUTLINE

The thesis proceeds as follows. In Chapter 2, we develop a multiphase model for gel-solvent interaction. An important contribution of this work is that, unlike the models discussed in Section 1.2, we account for the flow of both polymer and solvent components of the gel together with osmotic effects. We build on the multiphase flow models discussed in Section 1.3 to incorporate cell-gel interactions, thereby creating a more comprehensive model of the system.

In Chapter 3, we analyse this model in 1D Cartesian coordinates, finding small time analytic solutions and studying the model numerically to better understand the possible qualitative behaviours. We see in this analysis that the gel swells or contracts

depending on the balance of cell and chemical potentials and their gradients. We find non-uniform spatial equilibria in this setting as well as cases where the polymer fraction and cell density of the gel oscillate as it evolves.

In Chapter 4, we extend the theory discussed in Section 1.4 to develop a new thin film model for the gel in 2D Cartesian coordinates. Exploiting that the gel height is small relative to its length, we show that in particular scaling limits, a 1D extensional flow model can be derived from the initial 2D system of equations. We then study this model in Chapter 5 for uniform initial conditions. We show that a reduced model can be derived which is governed by an ordinary differential equation (ODE) for the gel height. We then find small time solutions and implement the model numerically, evaluating the behaviours arising from the reduced system of equations. In Chapter 6, we study the thin film model for non-uniform initial conditions. We consider the stability of equilibria in the thin film, followed by numerical evaluation of the model. We find that spatially varying equilibria can be found when taking spatially non-uniform initial conditions.

We conclude in Chapter 7 with a summary of the key findings in this thesis and an outline of possible future work.

2

MODEL DEVELOPMENT

In this chapter, we develop a general model for gel mechanics which will be studied throughout this thesis. We detail the problem to be modelled, the equations describing the dynamics of the gel's evolution, and appropriate initial and boundary conditions to complete this system of equations. We use a multiphase flow approach based on the work of Keener *et al.* (2011b) and Mori *et al.* (2013), modified to incorporate cells.

In this thesis, we will study a gel seeded with cells, which sits within a surrounding bath of liquid solvent (*e.g.* nutrient medium). This gel-solvent system is sketched in Fig. 2.1. The domain Ω is divided into two regions: the gel region Ω_g, and the surrounding region of pure solvent Ω_s. We note that the problem can be studied in different geometries, *i.e.* Ω_g does not necessarily have to be spherical. Let $\mathbf{x}$ denote position in Ω and t denote time. The centroid of the gel is at $\mathbf{x} = 0$ and the gel-solvent interface, denoted $\Gamma_g(\mathbf{x}, t) = 0$, is the boundary between Ω_g and Ω_s. This interface between the gel and surrounding solvent can move over time with the movement of solvent between the two regions.

The gel is assumed to be made up of two phases, polymer and solvent, each of constant density, with volume fractions denoted by $\theta_p(\mathbf{x}, t)$ and $\theta_s(\mathbf{x}, t)$ respectively. Hence, we define Ω_g to be the region where $\theta_p > 0$ and $\theta_s > 0$, and Ω_s to be that where $\theta_p = 0$ and $\theta_s = 1$. Cells are only present in the gel region Ω_g, and for simplicity, we assume that the volume they occupy within the gel is negligible; we therefore do not include a cell volume fraction and instead consider cell density $n(\mathbf{x}, t)$, where $n(\mathbf{x}, t) = 0$ in Ω_s (similar to Barocas and Tranquillo (1994)). Thus, the no-voids condition

$$\theta_p + \theta_s = 1, \tag{2.1}$$

is satisfied everywhere in the domain $\Omega = \Omega_g + \Omega_s$. Moreover, the model given below, while written for the gel region Ω_g, is also applicable to the solvent region Ω_s on setting $\theta_p = n = 0$ and $\theta_s = 1$.

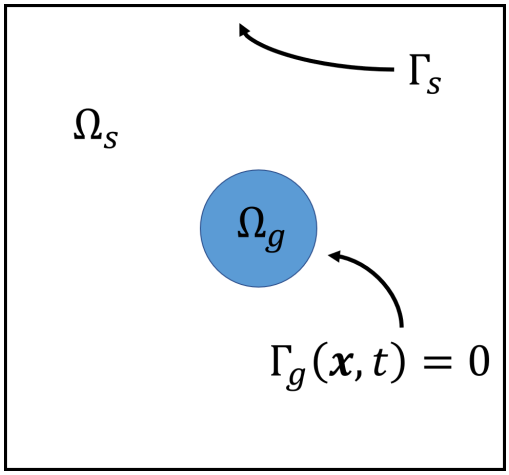

Figure 2.1: Gel-solvent domain $\Omega = \Omega_g \cup \Omega_s$. Ω_g contains the cell population as well as positive volume fractions for both the polymer network and solvent, whereas Ω_s contains only solvent. $\Gamma_g(\mathbf{x}, t) = 0$ is the moving boundary of the gel, also referred to as the gel-solvent interface. Γ_s is the external boundary of the domain.

2.2 MASS AND MOMENTUM CONSERVATION EQUATIONS

We assume the mass of both polymer and solvent is conserved (*i.e.* production and degradation of both species is neglected), so that

$$\frac{\partial \theta_p}{\partial t} + \nabla \cdot (\theta_p \boldsymbol{v}_p) = 0, \tag{2.2}$$

$$\frac{\partial \theta_s}{\partial t} + \nabla \cdot (\theta_s \boldsymbol{v}_s) = 0, \tag{2.3}$$

where $\boldsymbol{v}_p(\mathbf{x}, t)$ and $\boldsymbol{v}_s(\mathbf{x}, t)$ are the polymer and solvent velocities respectively. Given the no-voids condition (2.1), adding equations (2.2) and (2.3) yields

$$\nabla \cdot \boldsymbol{v} = 0, \tag{2.4}$$

where $\boldsymbol{v} = \theta_p \boldsymbol{v}_p + \theta_s \boldsymbol{v}_s$ is the volume-averaged velocity of the polymer-solvent mixture (Keener *et al.*, 2011b); we choose to replace (2.3) with (2.4). Note that in the solvent region Ω_s we simply have $\nabla \cdot \boldsymbol{v}_s = 0$.

For simplicity, cell proliferation and death are neglected, so the cell population is fixed. Cells are assumed to move by a combination of advection with the polymer net-

work and unbiased random motion, modelled by Fick's Law with diffusion coefficient D. Conservation of cells then gives

$$\frac{\partial n}{\partial t} + \nabla \cdot (n \boldsymbol{v}_p) = D\nabla^2 n. \tag{2.5}$$

We obtain equations for $\boldsymbol{v}_p(\boldsymbol{x}, t)$ and $\boldsymbol{v}_s(\boldsymbol{x}, t)$ by considering the momentum balance throughout the domain. Green *et al.* (2013) note that the Deborah number (which gives the ratio of elastic to viscous effects) found experimentally for gels like collagen is small ($\mathcal{O}(10^{-1}) - \mathcal{O}(10^{-2})$), meaning that elastic effects can be ignored. Hence, following Keener *et al.* (2011b) and Mori *et al.* (2013), we model both the polymer and the solvent phases as viscous fluids with a common pressure, P. The viscous stresses in the two phases are encapsulated by the deviatoric tensors $\boldsymbol{\sigma}_p$ and $\boldsymbol{\sigma}_s$, where the polymer stress tensor $\boldsymbol{\sigma}_p$ and the rate of strain tensor $\boldsymbol{e}_p$ are defined by

$$\boldsymbol{\sigma}_p = 2\eta_p \boldsymbol{e}_p + \kappa_p \mathbf{I} \nabla \cdot \boldsymbol{v}_p, \tag{2.6}$$

$$\boldsymbol{e}_p = \frac{1}{2}\left(\nabla \boldsymbol{v}_p + \nabla \boldsymbol{v}_p{}^T\right), \tag{2.7}$$

with the solvent tensors $\boldsymbol{\sigma}_s$ and $\boldsymbol{e}_s$ similarly defined with subscript s in place of p. The constants η_i and κ_i ($i = p, s$) are the dynamic and bulk viscosities of each phase i respectively, and $\mathbf{I}$ is the identity tensor.

As in Keener *et al.* (2011b), we assume that the forces exerted on the two phases come from inter-phase drag (which is proportional to the product of the volume fractions of the two phases) and chemical potential gradients. In addition, we include traction stresses exerted by cells on the polymer network. Inertia can be neglected on the time and length scales typical of experiments such as Moon and Tranquillo (1993), so that the momentum balances for the two phases are given by

$$\nabla \cdot (\theta_p \boldsymbol{\sigma}_p) - \xi \theta_p \theta_s (\boldsymbol{v}_p - \boldsymbol{v}_s) - \theta_p \nabla \mu_p - \theta_p \nabla P + \nabla(\theta_p G) = 0, \tag{2.8}$$

$$\nabla \cdot (\theta_s \boldsymbol{\sigma}_s) - \xi \theta_p \theta_s (\boldsymbol{v}_s - \boldsymbol{v}_p) - \theta_s \nabla \mu_s - \theta_s \nabla P = 0. \tag{2.9}$$

In equations (2.8) and (2.9), $\mu_p(\theta_p)$ and $\mu_s(\theta_p)$ are the chemical potentials for the polymer and solvent respectively, while ξ is the constant drag coefficient. The traction

force exerted by the cells on the polymer network is a novel addition in this context of multiphase gel modelling; it is incorporated as a body force acting on the gel and is given by the gradient of $\theta_p G(n)$, where G is a scalar potential energy function (Mori *et al.*, 2013). The forms of the cell potential function G and the chemical potentials μ_p and μ_s are detailed in Sections 2.3 and 2.4 below.

2.3 CELL POTENTIAL ENERGY FUNCTION

We assume the energy potential associated with the cells to be given by the Hill equation

$$G(n) = \frac{\tau_0 n^2}{1 + \lambda n^2}. \tag{2.10}$$

This differs from the function described in previous works (Green *et al.*, 2013; Moon and Tranquillo, 1993; Murray, 2001) in having n^2 rather than n in the numerator. This means that $\partial G/\partial n > 0$ for all n, which ensures that the cell traction force,

$$\boldsymbol{\nabla} G = \frac{\partial G}{\partial n} \boldsymbol{\nabla} n, \tag{2.11}$$

acts in the direction of increasing cell concentration. The positive parameter τ_0 provides a measure for the strength of cell traction forces, and λ is a positive contact inhibition parameter, which reflects that the force exerted by cells decreases as the cells become more densely populated.

The chemical potential functions μ_p and μ_s describe the work done by the free energy in the polymer and solvent to affect the swelling or compaction of the gel. These are defined as

$$\mu_p(\theta_p) = f + \theta_s \frac{\partial f}{\partial \theta_p}, \tag{2.12}$$

$$\mu_s(\theta_p) = f - \theta_p \frac{\partial f}{\partial \theta_p}, \tag{2.13}$$

where $f(\theta_p)$ is the free energy per unit volume of gel (Keener *et al.*, 2011b). The free energy function, derived from polymer physics, is defined below. The polymer chemical potential μ_p describes the change in free energy resulting from an additional polymer unit being added to the gel, while the solvent chemical potential μ_s describes the change in free energy from an additional solvent unit being added (Keener *et al.*, 2011b).

The free energy of the system per unit volume of gel is

$$f(\theta_p) = \frac{k_B \mathcal{T}}{\nu_m} \left(\frac{\theta_p}{N} \log(\theta_p) + \theta_s \log(\theta_s) + \chi \theta_p \theta_s + \mu_p^0 \theta_p + \mu_s^0 \theta_s \right), \tag{2.14}$$

where k_B is the Boltzmann constant, $\mathcal{T}$ is temperature, ν_m is the characteristic volume of a monomer in our system, N is the chain length of the polymer, χ is the Flory interaction parameter and the constants μ_p^0 and μ_s^0 are dimensionless quantities known as the standard free energies of the polymer and solvent respectively. The logarithmic terms in the function describe the entropy of mixing polymer and solvent; these terms always encourage swelling in the gel. The latter terms involving χ, μ_p^0 and μ_s^0 can increase the tendency for the gel to swell or contract depending on the signs of these parameters. The χ term describes the energy of mixing, while the terms involving μ_p^0 and μ_s^0 describe the interaction energy in a pure polymer or solvent state respectively (Rubinstein *et al.*, 2003).

In most of the relevant literature (*e.g.* Mori *et al.* (2013); Rubinstein *et al.* (2003); Zhang *et al.* (2008)) the standard free energy parameters μ_p^0 and μ_s^0 are not included, so that

the free energy function represents only the interaction or mixing of the phases as opposed to the total free energy (Keener *et al.*, 2011a). However, following the work of Keener *et al.* (see Keener *et al.* (2011a,b); Sircar *et al.* (2013)), we retain the standard free energy terms for generality. In the framework of Mori *et al.* (2013) that we adopt, we will see that these terms do not contribute explicitly to the final model, due to cancellations of terms involving $f(\theta_p)$ and its derivatives. They are, nevertheless, contained implicitly through the derivation of the mixing parameter χ (see Rubinstein *et al.* (2003) for further detail).

The Flory interaction parameter χ is a dimensionless parameter that characterises the nature of the interaction between the phases in the mixture: $\chi < 0$ indicates attraction between the phases, and accordingly, mixing of these components being energetically advantageous; $\chi > 0$ corresponds to repulsion between the polymer and solvent, resulting in the phases preferring to separate (Rubinstein *et al.*, 2003).

As in Keener *et al.* (2011b), from equations (2.12) and (2.13), we can derive further useful relations between the chemical potentials and free energy. Firstly, we have the relation,

$$\theta_p \mu_p + \theta_s \mu_s = f(\theta_p). \tag{2.15}$$

We also have that

$$\mu_p - \mu_s = \frac{\partial f}{\partial \theta_p}, \tag{2.16}$$

which indicates that at stationary points of $f(\theta_p)$, the chemical potentials μ_p and μ_s must be equal.

2.5 INITIAL AND BOUNDARY CONDITIONS

To close our system of equations, we need to impose suitable initial and boundary conditions.

The initial conditions for the volume fractions and cell density are given by

$$\theta_p(\mathbf{x},0) = \theta_i(\mathbf{x}), \quad \theta_s(\mathbf{x},0) = 1 - \theta_i(\mathbf{x}), \quad n(\mathbf{x},0) = n_i(\mathbf{x}), \tag{2.17}$$

where $0 < \theta_i(\mathbf{x}) < 1$ and $n_i(\mathbf{x}) \geqslant 0$ for $\mathbf{x} \in \Omega_p$, and $\theta_i(\mathbf{x}) = n_i(\mathbf{x}) = 0$ for $\mathbf{x} \in \Omega_s$. The initial gel-solvent interface is given by

$$\Gamma_g(\mathbf{x},0) = \Gamma_{g_i}(\mathbf{x}) = 0. \tag{2.18}$$

We take the centroid of the gel to be fixed in space and, therefore, have zero velocity at the origin for all time,

$$\boldsymbol{v}_p(\mathbf{0},t) = \mathbf{0}, \tag{2.19}$$

while no slip and no penetration on the external boundary of the domain Γ_s is given by

$$\boldsymbol{v}_s = \mathbf{0}. \tag{2.20}$$

The gel-solvent interface $\Gamma_g(\mathbf{x},t) = 0$ moves over time due to movement of the polymer phase, so that its position is given by the kinematic condition

$$\frac{\partial \Gamma_g}{\partial t} + \boldsymbol{v}_p \cdot \nabla \Gamma_g = 0. \tag{2.21}$$

We assume there is no diffusive flux of cells out of the gel at the interface, so that

$$(D\nabla n) \cdot \hat{\mathbf{n}} = 0 \text{ on } \Gamma_g = 0, \tag{2.22}$$

where $\hat{\mathbf{n}}$ is the unit normal vector on $\Gamma_g = 0$. Continuity of stress across $\Gamma_g = 0$ is described by

$$[\theta_p \boldsymbol{\sigma}_p + \theta_s \boldsymbol{\sigma}_s + f - \theta_p f' + \theta_p G] \cdot \hat{\mathbf{n}} - [P + \mu_s] \cdot \hat{\mathbf{n}} = 0, \tag{2.23}$$

where the prime denotes differentiation with respect to θ_p (Mori *et al.*, 2013). The bracket notation $[J]$ in equation (2.23) denotes the jump in the function J across the boundary; thus $[J] = 0$ indicates that J is continuous across the boundary. Using equation (2.13), we simplify interface condition (2.23) to

$$[\theta_p \boldsymbol{\sigma}_p + \theta_s \boldsymbol{\sigma}_s + \theta_p G - P] \cdot \hat{\mathbf{n}} = 0. \tag{2.24}$$

Finally, at the interface, we have

$$\mathcal{R}\theta_s(\boldsymbol{v}_s - \boldsymbol{v}_p) \cdot \hat{\mathbf{n}} = (\hat{\mathbf{n}} \cdot \boldsymbol{\sigma}_s^e \hat{\mathbf{n}}) - (\hat{\mathbf{n}} \cdot \boldsymbol{\sigma}_s \hat{\mathbf{n}}) + [P + \mu_s], \tag{2.25}$$

where we have introduced the superscript e to clearly designate a quantity in the solvent domain Ω_s external to the gel. This condition describes how the difference in pressure, chemical potential, and solvent stress across the interface drives fluid flow into or out from the gel, at a rate proportional to the resistance $\mathcal{R} \geqslant 0$ of the boundary (see equation (3.15) in Mori *et al.* (2013)). We note that an increase in $\mathcal{R}$ increases the resistance of the boundary so that it is more impervious to solvent flow, while a decrease indicates that it is easier for fluid to move across the boundary in and out of the gel. With the resistance $\mathcal{R} = 0$, the normal solvent stresses are equal to the pressure difference across the interface.

2.6 DISCUSSION

We have developed a new, multiphase model to study a gel-solvent system including cells. This model extends those presented in Keener *et al.* (2011b) and Mori *et al.* (2013), incorporating cell traction stresses alongside osmotic pressure. This will allow us to study the gel's emergent behaviours and characteristics under these competing forces. Having derived the model here in a general, three-dimensional form, we will now study particular cases representing different gel constructions. Chapter 3 presents an analysis of the model in 1D Cartesian coordinates, this being the most tractable

geometry for analytical and numerical investigations. The later chapters of the thesis study thin films of gel, adapting the model to 2D Cartesian coordinates.

3

1D MODEL FOR CELL-GEL MECHANICS

3.1 INTRODUCTION

We now consider the model developed in Chapter 2 in 1D Cartesian coordinates. We study the gel in this simple setting to understand the behaviours that emerge from the model. In this chapter, we set out the model equations in this 1D coordinate system, non-dimensionalise the model, and transform it onto a fixed spatial domain. We then consider equilibrium and short time behaviour, through which we can derive insights into the stability of equilibrium states. We implement a numerical scheme to simulate the model, exploring the forces driving gel swelling and contraction and the manner in which this occurs.

3.2 ONE-DIMENSIONAL CARTESIAN MODEL

For simplicity, we investigate the behaviour of a one-dimensional gel in the Cartesian coordinate x, which is symmetrical about $x = 0$. We also assume that all quantities are continuous and differentiable at $x = 0$. Thus, we consider $0 \leqslant x \leqslant L(t)$ as the gel domain Ω_g in which $0 < \theta_p(x,t) < 1$, $\theta_s(x,t) = 1 - \theta_p(x,t)$, and $n(x,t) \geqslant 0$, while the polymer and solvent velocities are $v_p(x,t)$ and $v_s(x,t)$. There is a fixed symmetry boundary at $x = 0$ and a moving boundary at $x = L(t)$ (equivalently, $\Gamma_g(x,t) = x - L(t) = 0$) on which the kinematic condition (2.21) becomes

$$\frac{dL}{dt} = v_p(L(t),t). \tag{3.1}$$

Outside the gel domain ($x > L(t)$), we have the solvent domain Ω_s with $\theta_p^e(x,t) = 0$ and $\theta_s^e(x,t) = 1$, where we have introduced the superscript e to clearly designate the solvent domain external to the gel. From hereon, this superscript notation will be used for all quantities in Ω_s, while lack of the superscript e denotes quantities in Ω_g.

Since, by symmetry, $v_p(0,t) = v_s(0,t) = 0$, the continuity condition (2.4) implies that throughout Ω_g we have

$$\theta_p v_p + \theta_s v_s = 0. \tag{3.2}$$

Similarly, throughout Ω_s we simply have $v_s^e = 0$, which satisfies the no-penetration condition (2.20) on the boundary Γ_s. In gel domain Ω_g, from the mass conservation equation (2.2) we also have

$$\frac{\partial \theta_p}{\partial t} + \frac{\partial}{\partial x}(\theta_p v_p) = 0, \tag{3.3}$$

while the advection-diffusion equation for cell density (2.5) becomes

$$\frac{\partial n}{\partial t} + \frac{\partial}{\partial x}(n v_p) = D\frac{\partial^2 n}{\partial x^2}, \tag{3.4}$$

and the momentum equations (2.8) and (2.9) are now

$$\begin{aligned}\frac{\partial}{\partial x}\left(2\eta_p\theta_p\frac{\partial v_p}{\partial x} + \kappa_p\theta_p\frac{\partial v_p}{\partial x}\right) - \xi\theta_p\theta_s(v_p - v_s) - \theta_p\frac{\partial \mu_p}{\partial x} - \theta_p\frac{\partial P}{\partial x} \\ + \frac{\partial}{\partial x}(\theta_p G) = 0, \end{aligned} \tag{3.5}$$

$$\frac{\partial}{\partial x}\left(2\eta_s\theta_s\frac{\partial v_s}{\partial x} + \kappa_s\theta_s\frac{\partial v_s}{\partial x}\right) - \xi\theta_p\theta_s(v_s - v_p) - \theta_s\frac{\partial \mu_s}{\partial x} - \theta_s\frac{\partial P}{\partial x} = 0. \tag{3.6}$$

On multiplying (3.5) by θ_s and (3.6) by θ_p and taking the difference, we eliminate the pressure terms from the momentum equations, yielding

$$\begin{aligned}(2\eta_p + \kappa_p)\theta_s\frac{\partial}{\partial x}\left(\theta_p\frac{\partial v_p}{\partial x}\right) + (2\eta_s + \kappa_s)\theta_p\frac{\partial}{\partial x}\left(\theta_s\frac{\partial}{\partial x}\left(\frac{\theta_p v_p}{\theta_s}\right)\right) \\ - \xi\theta_p\theta_s(v_p - v_s) - \theta_p\theta_s\frac{\partial}{\partial x}(\mu_p - \mu_s) + \theta_s\frac{\partial}{\partial x}(\theta_p G) = 0. \end{aligned} \tag{3.7}$$

From equation (3.2), we have

$$v_s = -\frac{\theta_p}{\theta_s}v_p, \tag{3.8}$$

and differentiating equation (2.16) with respect to x gives

$$\frac{\partial}{\partial x}(\mu_p - \mu_s) = f''(\theta_p)\frac{\partial \theta_p}{\partial x}. \tag{3.9}$$

On substituting equations (3.8) and (3.9), (3.7) becomes

$$(2\eta_p + \kappa_p)\theta_s \frac{\partial}{\partial x}\left(\theta_p \frac{\partial v_p}{\partial x}\right) + (2\eta_s + \kappa_s)\theta_p \frac{\partial}{\partial x}\left(\theta_s \frac{\partial}{\partial x}\left(\frac{\theta_p v_p}{\theta_s}\right)\right) - \xi\theta_p v_p$$
$$- \theta_p \theta_s f''(\theta_p)\frac{\partial \theta_p}{\partial x} + \theta_s \frac{\partial}{\partial x}(\theta_p G) = 0. \tag{3.10}$$

We use (3.10) to replace (3.5).

In the solvent region Ω_s, where $v_s^e = 0$, $\theta_p^e = 0$ and $\theta_s^e = 1$, the solvent viscous stress tensor $\boldsymbol{\sigma}_s^e$ is zero, and from (2.13) and (2.14),

$$\mu_s^e = f - \theta_p f'\big|_{\theta_p = 0} = f(0), \tag{3.11}$$

where $f(0)$ is a constant. From the definition of $f(\theta_p)$ in equation (2.14), we see that $f(0) = \mu_s^0$. The momentum equation (2.9) therefore simplifies to

$$\frac{\partial P^e}{\partial x} = 0 \tag{3.12}$$

and we see that P^e is at most a function of time t.

The 1D form of the interface condition (2.24) on $x = L(t)$ becomes

$$(2\eta_p + \kappa_p)\theta_p \frac{\partial v_p}{\partial x} + (2\eta_s + \kappa_s)\theta_s \frac{\partial v_s}{\partial x} + \theta_p G - (P - P^e) = 0, \tag{3.13}$$

while (2.25) on $x = L(t)$ becomes

$$\mathcal{R}\theta_s(v_s - v_p) = -(2\eta_s + \kappa_s)\frac{\partial v_s}{\partial x} + (P - P^e) + (\mu_s - \mu_s^e). \tag{3.14}$$

Using (3.14) to eliminate pressure from (3.13) and using (3.8) to substitute for v_s, we obtain

$$(2\eta_p + \kappa_p)\theta_p \frac{\partial v_p}{\partial x} + (2\eta_s + \kappa_s)\theta_p \frac{\partial}{\partial x}\left(\frac{\theta_p v_p}{\theta_s}\right) + \theta_p G + \mathcal{R} v_p$$
$$+ \mu_s - \mu_s^e = 0 \tag{3.15}$$

at $x = L(t)$.

From (2.19), the velocity at the origin is zero for all time,

$$v_p(0,t) = 0 \quad \text{for } t \geqslant 0. \tag{3.16}$$

From the mass conservation equation (3.3), given that $v_p(0,t) = 0$, there is a characteristic along $x = 0$. On this characteristic, $\theta_p(0,t)$ satisfies the ODE

$$\frac{d\theta_p(0,t)}{dt} = -\theta_p(0,t)\frac{\partial v_p(0,t)}{\partial x}, \tag{3.17}$$

subject to the initial condition $\theta_p(0,0) = \theta_i(0)$. Similarly, given that $v_p(L,t) = dL/dt$, there is a characteristic along $x = L(t)$, and as such, $\theta_p(L,t)$ must satisfy

$$\frac{d\theta_p(L,t)}{dt} = -\theta_p(L,t)\frac{\partial v_p(L,t)}{\partial x}, \tag{3.18}$$

subject to $\theta_p(L,0) = \theta_i(L)$. Therefore, assuming that v_p is smooth for $t \geqslant 0$, θ_p is determined from the initial condition and v_p, and no boundary conditions on θ_p are required.

Furthermore, given that v_p and $\partial v_p/\partial x$ are continuous and differentiable at $x = 0$ and that v_p is an odd function, it can be shown from equation (3.3) that if $\partial\theta_i(0)/\partial x = 0$, then $\partial\theta_p(0,t)/\partial x = 0$ for all t, *i.e.* if the polymer fraction θ_p is initially symmetric and continuous about the origin, then it will remain so for all time. Since we take $\theta_i(x)$ to be differentiable with $\partial\theta_i(0)/\partial x = 0$, we therefore have

$$\frac{\partial\theta_p(0,t)}{\partial x} = 0 \quad \text{for } t \geqslant 0. \tag{3.19}$$

Finally, the symmetry of the cell density at $x = 0$ requires

$$\frac{\partial n(0,t)}{\partial x} = 0 \quad \text{for } t \geqslant 0, \tag{3.20}$$

while no diffusive cell flux at $x = L(t)$ requires

$$D\frac{\partial n(L(t),t)}{\partial x} = 0 \quad \text{for } t \geqslant 0. \tag{3.21}$$

The no-voids condition (2.1), the conservation equations (3.2), (3.3), (3.4), the momentum equation (3.10), and boundary conditions (3.1), (3.15), (3.20), (3.21) comprise a complete model for the polymer and solvent volume fractions $\theta_p(x,t)$, $\theta_s(x,t)$, the cell density $n(x,t)$, and the polymer and solvent velocities $v_p(x,t)$, $v_s(x,t)$ in the gel, along with the length $L(t)$ of the gel. To solve for the pressure difference between the gel and solvent regions, $P(x,t) - P^e(t)$, we must add the momentum equation (3.6) and the boundary condition (3.14). However, we choose not to solve for pressure throughout the gel, given that we can study the mechanics driving the gel without its inclusion, and so drop (3.6) and (3.14) from the model.

3.3 NON-DIMENSIONALISATION

Let $\mathfrak{L} = L(0)$ be the length scale, $\mathfrak{N}$ be a characteristic cell density (typically the mean initial density), and let the time scale be the ratio of polymer viscosity η_p to the free energy scale $k_B\mathcal{T}/v_m$. Using these scales, we non-dimensionalise our model variables as follows, where tildes denote dimensionless quantities,

$$x = \mathfrak{L}\tilde{x}, \quad t = \frac{\eta_p v_m}{k_B\mathcal{T}}\tilde{t}, \quad L(t) = \mathfrak{L}\tilde{L}(\tilde{t}), \tag{3.22a}$$

$$v_p = \frac{k_B\mathcal{T}\mathfrak{L}}{\eta_p v_m}\tilde{v}_p, \quad v_s = \frac{k_B\mathcal{T}\mathfrak{L}}{\eta_p v_m}\tilde{v}_s, \quad n = \mathfrak{N}\tilde{n}. \tag{3.22b}$$

We also define the following dimensionless model parameters, again denoted by tildes,

$$\tilde{\kappa}_p = \frac{\kappa_p}{\eta_p}, \quad \tilde{\kappa}_s = \frac{\kappa_s}{\eta_p}, \quad \tilde{\eta}_s = \frac{\eta_s}{\eta_p}, \quad \tilde{\xi} = \frac{\mathfrak{L}^2\xi}{\eta_p}, \tag{3.23a}$$

$$\tilde{\tau}_0 = \frac{\tau_0\mathfrak{N}^2 v_m}{k_B\mathcal{T}}, \quad \tilde{\lambda} = \mathfrak{N}^2\lambda, \quad \tilde{D} = \frac{\eta_p v_m D}{k_B\mathcal{T}\mathfrak{L}^2}, \quad \tilde{\mathcal{R}} = \frac{\mathfrak{L}\mathcal{R}}{\eta_p}, \tag{3.23b}$$

and the dimensionless free energy, chemical potential functions, and cell potential energy,

$$\tilde{f}(\theta_p) = \frac{v_m}{k_B\mathcal{T}}f(\theta_p) = \left(\frac{\theta_p}{N}\log(\theta_p) + \theta_s\log(\theta_s) + \chi\theta_p\theta_s + \mu_p^0\theta_p + \mu_s^0\theta_s\right), \tag{3.24a}$$

$$\tilde{\mu}_s = \frac{v_m}{k_B\mathcal{T}}\mu_s, \quad \tilde{\mu}_p = \frac{v_m}{k_B\mathcal{T}}\mu_p, \quad \tilde{G} = \frac{\tilde{\tau}_0\tilde{n}^2}{1+\tilde{\lambda}\tilde{n}^2}. \tag{3.24b}$$

The mass balance equations (3.2), (3.3) and (3.4) are unchanged in form on writing them in terms of the scaled variables and parameters. Similarly, (2.12), (2.13), (2.15), (2.16) and the boundary conditions (3.1), (3.20), (3.21) are unchanged in form. Hence we do not re-write them here. The scaled forms of the momentum equation (3.10) and interface stress condition (3.15) become

$$(2+\tilde{\kappa}_p)\theta_s\frac{\partial}{\partial\tilde{x}}\left(\theta_p\frac{\partial\tilde{v}_p}{\partial\tilde{x}}\right)+(2\tilde{\eta}_s+\tilde{\kappa}_s)\theta_p\frac{\partial}{\partial\tilde{x}}\left(\theta_s\frac{\partial}{\partial\tilde{x}}\left(\frac{\theta_p\tilde{v}_p}{\theta_s}\right)\right)-\tilde{\xi}\theta_p\tilde{v}_p$$
$$-\theta_p\theta_s\tilde{f}''\frac{\partial\theta_p}{\partial\tilde{x}}+\theta_s\frac{\partial}{\partial\tilde{x}}\left(\theta_p\tilde{G}\right)=0, \tag{3.25}$$

over $0\leqslant\tilde{x}\leqslant\tilde{L}(\tilde{t})$ and, at $\tilde{x}=\tilde{L}(\tilde{t})$,

$$(2+\tilde{\kappa}_p)\theta_p\frac{\partial\tilde{v}_p}{\partial\tilde{x}}+(2\tilde{\eta}_s+\tilde{\kappa}_s)\theta_p\frac{\partial}{\partial\tilde{x}}\left(\frac{\theta_p\tilde{v}_p}{\theta_s}\right)+\theta_p\tilde{G}$$
$$+\tilde{\mu}_s-\tilde{\mu}_s^e+\tilde{\mathcal{R}}\tilde{v}_p=0. \tag{3.26}$$

We now introduce a change in coordinates to shift our moving boundary problem onto a fixed domain. We define new coordinates $X=\tilde{x}/\tilde{L}(\tilde{t})$ and $T=\tilde{t}$, so that the domain $0\leqslant\tilde{x}\leqslant\tilde{L}(\tilde{t})$ is mapped to the fixed domain $0\leqslant X\leqslant 1$. On this fixed domain the model becomes, using dots to denote differentiation with respect to time T, primes to denote differentiation with respect to θ_p, and dropping tildes on dimensionless variables and parameters for convenience,

$$\theta_s=1-\theta_p, \tag{3.27}$$

$$\theta_p v_p+\theta_s v_s=0, \tag{3.28}$$

$$\frac{\partial\theta_p}{\partial T}-\frac{X\dot{L}}{L}\frac{\partial\theta_p}{\partial X}+\frac{1}{L}\frac{\partial}{\partial X}(\theta_p v_p)=0, \tag{3.29}$$

$$\frac{\partial n}{\partial T}-\frac{X\dot{L}}{L}\frac{\partial n}{\partial X}+\frac{1}{L}\frac{\partial}{\partial X}(n v_p)=\frac{D}{L^2}\frac{\partial^2 n}{\partial X^2}, \tag{3.30}$$

$$(2+\kappa_p)\frac{\theta_s}{L^2}\frac{\partial}{\partial X}\left(\theta_p\frac{\partial v_p}{\partial X}\right)+(2\eta_s+\kappa_s)\frac{\theta_p}{L^2}\frac{\partial}{\partial X}\left(\theta_s\frac{\partial}{\partial X}\left(\frac{\theta_p v_p}{\theta_s}\right)\right)$$
$$-\xi\theta_p v_p-\frac{\theta_p\theta_s}{L}f''(\theta_p)\frac{\partial\theta_p}{\partial X}+\frac{\theta_s}{L}\frac{\partial}{\partial X}\left(\theta_p G\right)=0, \tag{3.31}$$

with boundary conditions at $X = 0$,

$$v_p = 0, \quad \frac{\partial n}{\partial X} = 0, \quad \frac{\partial \theta_p}{\partial X} = 0, \tag{3.32}$$

and boundary conditions at $X = 1$,

$$(2 + \kappa_p)\frac{\theta_p}{L}\frac{\partial v_p}{\partial X} + (2\eta_s + \kappa_s)\frac{\theta_p}{L}\frac{\partial}{\partial X}\left(\frac{\theta_p v_p}{\theta_s}\right) + \theta_p G + \mu_s - \mu_s^e + \mathcal{R} v_p = 0, \tag{3.33}$$

$$D\frac{\partial n}{\partial X} = 0, \tag{3.34}$$

$$\dot{L} = v_p. \tag{3.35}$$

In addition, we must specify suitable initial conditions

$$\theta_p(X, 0) = \theta_i(X), \qquad n(X, 0) = n_i(X), \qquad L(0) = 1, \tag{3.36}$$

with $\theta_i(X)$ chosen such that $\partial\theta_i(0)/\partial X = 0$. This completes our derivation of the 1D model.

3.4 STEADY STATE CONDITIONS

We now consider steady state (*i.e.* long time) solutions of our model. This allows us to understand the necessary conditions in the gel for it to equilibrate. These conditions will assist us in analysing the model's analytic and numerical behaviours throughout this chapter.

The system reaches equilibrium when θ_p and n are such that there is zero net force everywhere, the velocities of polymer and solvent are zero everywhere, and $\dot{L} = 0$, *i.e.* the free boundary stops moving. We find that both spatially uniform and non-uniform steady state solutions can occur in θ_p and n.

At a steady state, the mass and momentum conservation equations (3.29) - (3.31) are

$$\frac{1}{L}\frac{\partial}{\partial X}(\theta_p v_p) = 0, \tag{3.37}$$

$$\frac{1}{L}\frac{\partial}{\partial X}(n v_p) = \frac{D}{L^2}\frac{\partial^2 n}{\partial X^2}, \tag{3.38}$$

$$(2+\kappa_p)\frac{\theta_s}{L^2}\frac{\partial}{\partial X}\left(\theta_p\frac{\partial v_p}{\partial X}\right) + (2\eta_s+\kappa_s)\frac{\theta_p}{L^2}\frac{\partial}{\partial X}\left(\theta_s\frac{\partial}{\partial X}\left(\frac{\theta_p v_p}{\theta_s}\right)\right) - \xi\theta_p v_p - \frac{\theta_p\theta_s}{L}f''(\theta_p)\frac{\partial\theta_p}{\partial X} + \frac{\theta_s}{L}\frac{\partial}{\partial X}(\theta_p G) = 0. \tag{3.39}$$

To demonstrate that the velocities are zero at equilibrium, we evaluate the steady state polymer advection equation (3.37), which gives

$$\frac{1}{L}\frac{\partial}{\partial X}(\theta_p v_p) = 0. \tag{3.40}$$

Integrating with respect to X and applying the boundary condition $v_p = 0$ at $X = 0$, we find that

$$\theta_p v_p = 0. \tag{3.41}$$

Since we must have $\theta_p > 0$, we see that $v_p = 0$ must hold at equilibrium. Accordingly, we must also have $v_s = 0$ using equation (3.28).

The momentum balance equation (3.39) then gives us the equilibrium condition throughout the interior of the gel,

$$\frac{\partial}{\partial X}(\theta_p G) - \theta_p f''(\theta_p)\frac{\partial\theta_p}{\partial X} = 0. \tag{3.42}$$

From (2.13), we note that

$$\frac{\partial\mu_s}{\partial X} = -\theta_p f''(\theta_p)\frac{\partial\theta_p}{\partial X}, \tag{3.43}$$

and accordingly, equation (3.42) can be expressed in the form

$$\frac{\partial}{\partial X}(\theta_p G + \mu_s) = 0, \tag{3.44}$$

i.e. for the gel to be in equilibrium, the cell traction force must be balanced by the force due to chemical potential gradients. We note that with $n = 0$ (and hence $G = 0$), this is the same condition as in Keener *et al.* (2011b). Equation (3.44) is subject to the condition (3.33) at the interface $X = 1$, which, at equilibrium, gives

$$\theta_p G + \mu_s - \mu_s^e = 0. \tag{3.45}$$

After integrating (3.44) and using (3.45) to set the constant of integration, we obtain

$$\theta_p G + \mu_s - \mu_s^e = 0, \tag{3.46}$$

and we see that the condition (3.45) applies everywhere at equilibrium. We note that, as shown in (3.11), $\mu_s^e = f(0)$ is constant.

From the cell advection-diffusion equation (3.38), we see that, at equilibrium, we must have

$$D\frac{\partial^2 n}{\partial X^2} = 0. \tag{3.47}$$

For $D = 0$, this is trivially satisfied, and equation (3.46) is sufficient for the gel to equilibrate. In this case, it is possible to have equilibrium solutions in θ_p and n that depend on X.

With $D \neq 0$, after integrating (3.47) and applying the no-flux condition (3.34), we find that

$$\frac{\partial n}{\partial X} = 0, \tag{3.48}$$

i.e. at equilibrium, n must be spatially uniform.

Now, given spatially uniform n, equation (3.42) can be written

$$\left(G - \theta_p f''(\theta_p)\right) \frac{\partial \theta_p}{\partial X} = 0, \tag{3.49}$$

indicating that either $G - \theta_p f''$ or $\partial\theta_p/\partial X$ must equal zero for equilibrium. Given the functional form of $f(\theta_p)$ (see (2.14)), we have

$$f'' = \frac{1}{N\theta_p} + \frac{1}{1-\theta_p} - 2\chi. \tag{3.50}$$

Evaluating $G - \theta_p f'' = 0$, we find the following quadratic expression in θ_p,

$$\theta_p^2 + \left\{ \frac{1}{2\chi}\left(1 + G - \frac{1}{N}\right) - 1 \right\} \theta_p - \frac{1}{2\chi}\left(G - \frac{1}{N}\right) = 0. \tag{3.51}$$

This shows that, at most, we can have two positive solutions for θ_p, depending on the values of the model parameters. However, given that θ_p must be continuous, only a constant value of θ_p will satisfy this condition. Thus, we must have $\partial\theta_p/\partial X = 0$ to satisfy $G - \theta_p f'' = 0$ at equilibrium. Therefore, from equation (3.49), we see that we must have at equilibrium,

$$\frac{\partial\theta_p}{\partial X} = 0, \tag{3.52}$$

i.e. spatially uniform θ_p. Therefore, if diffusion $D \neq 0$, n and θ_p must be spatially uniform and satisfy equation (3.46) for the gel to reach a steady state.

We note that, given conservation of mass in equations (3.29) and (3.30), we have the relation between the mass of polymer at $T = 0$ and any later time T, and similarly for the mass of cells,

$$L(T)\int_0^1 \theta_p(X,T)\,dX = \int_0^1 \theta_i(X)\,dX, \qquad L(T)\int_0^1 n(X,T)\,dX = \int_0^1 n_i(X)\,dX, \tag{3.53}$$

where $L(0) = 1$ as required by our scaling. This demonstrates that any perturbations to the initial polymer fraction or cell density that change the total polymer or cell mass will lead to changes in L, θ_p and n at later points in time. In particular, this demonstrates that changing the initial mass of polymer or cells will result in a different equilibrium solution in θ_p, n and L, *i.e.* the long time behaviour is not independent of the initial conditions.

We can use equation (3.46) to calculate the spatially uniform equilibrium values of θ_p and n for a given set of parameter values (note that this does not preclude steady states that are X-dependent also existing for such parameter values when $D = 0$). This is useful for two reasons: firstly, it provides a method to confirm that numerical simulations (such as we will see in Section 3.7) find the correct equilibrium values; secondly, it allows us to analyse how the equilibrium values of polymer and cell density change as chosen parameter values are adjusted. Together with a condition derived from the short time solutions in Section 3.6, we will use this in Section 3.6.6 to analyse steady state values of particular variables and parameters, as well as the stability of these equilibria as different parameter values change.

3.5 SHORT TIME ANALYSIS

We next study the behaviour of the 1D Cartesian system (3.27) - (3.36) on a short time scale to investigate the early time evolution of the system from non-equilibrium initial conditions. In Section 3.6, we will determine how the system evolves over small time in response to small spatial perturbations to equilibria. Later, in Section 3.7.2, we will compare these short time solutions with numerical solutions at early time to verify the behaviour of our numerical scheme described in Section 3.7.

3.5.1 *Evolution from non-equilibrium initial conditions*

We proceed by introducing the short time scale $\delta \ll 1$ and define $T = \delta\hat{T}$. We then write the dependent variables as power series in δ, expanding about the initial conditions:

$$L(\hat{T}) = L_0 + \delta L_1(\hat{T}) + \delta^2 L_2(\hat{T}) + ..., \tag{3.54}$$

$$\nu_p(X, \hat{T}) = \nu_0(X) + \delta\nu_1(X, \hat{T}) + \delta^2\nu_2(X, \hat{T}) + ..., \tag{3.55}$$

with expansions for θ_p and n similar to that for ν_p. Here $L_0 = 1$, $\nu_0(X)$, $\theta_0(X)$, and $n_0(X)$ are the initial conditions. For simplicity, and in the interests of finding an analytic solution, we shall restrict our attention to spatially uniform initial conditions for θ_p and

n, *i.e.* $\theta_0(X) = \theta_i$ and $n_0(X) = 1$, where θ_i is constant and we have scaled n using the initial cell density as its characteristic value.

We substitute these expansions into (3.29) - (3.35). From the kinematic boundary condition (3.35) at $\mathcal{O}(\delta)$, we find

$$L_1(\hat{T}) = v_0(1)\hat{T}. \tag{3.56}$$

The momentum equation (3.31) at leading order becomes

$$(2+\kappa_p)(1-\theta_i)\theta_i\frac{\partial^2 v_0}{\partial X^2} + (2\eta_s+\kappa_s)\theta_i^2\frac{\partial^2 v_0}{\partial X^2} - \xi\theta_i v_0 = 0. \tag{3.57}$$

On applying the boundary condition $v_0(0) = 0$, we find that this has the solution

$$v_0 = A_0\sinh(\alpha X), \quad \alpha = \sqrt{\frac{\xi}{(2+\kappa_p)(1-\theta_i)+(2\eta_s+\kappa_s)\theta_i}}. \tag{3.58}$$

The constant A_0 is determined from the interface condition (3.33), where at leading order (remembering that $G = \tau_0 n^2/(1+\lambda n^2)$ and $n_0 = 1$), we have

$$(2+\kappa_p)\theta_i\frac{\partial v_0}{\partial X} + (2\eta_s+\kappa_s)\frac{\theta_i^2}{1-\theta_i}\frac{\partial v_0}{\partial X} + \frac{\theta_i\tau_0}{1+\lambda} + \mu_s(\theta_i) - \mu_s^e + \mathcal{R}v_0 = 0, \tag{3.59}$$

which yields,

$$\begin{aligned} A_0 = &-\left\{\alpha\cosh(\alpha)\left((2+\kappa_p)\theta_i + \frac{(2\eta_s+\kappa_s)\theta_i^2}{(1-\theta_i)}\right) + \mathcal{R}\sinh(\alpha)\right\}^{-1} \\ &\times\left(\frac{\theta_i\tau_0}{1+\lambda} + \mu_s(\theta_i) - \mu_s^e\right). \end{aligned} \tag{3.60}$$

We note that by (3.46), the term in the final brackets in (3.60) is equal to zero if our initial condition $\theta_0 = \theta_i$, $n_0 = 1$ is a steady state. We would then have $A_0 = v_0(X) = 0$, as required for an equilibrium. For the remainder of this section, we therefore consider the early time evolution from non-equilibrium initial conditions only.

Finally, at $\mathcal{O}(\delta)$ the polymer and cell advection equations (3.29) and (3.30) reduce to

$$\frac{\partial \theta_1}{\partial \hat{T}} = -\theta_i \frac{\partial v_0}{\partial X}, \tag{3.61}$$

$$\frac{\partial n_1}{\partial \hat{T}} = -\frac{\partial v_0}{\partial X}, \tag{3.62}$$

where $\theta_1(X,0) = n_1(X,0) = 0$. These have the solutions

$$\theta_1(X,\hat{T}) = -\theta_i \alpha A_0 \cosh(\alpha X)\hat{T}, \tag{3.63}$$

$$n_1(X,\hat{T}) = -\alpha A_0 \cosh(\alpha X)\hat{T}. \tag{3.64}$$

Thus, we have obtained the following short time solutions for the length of the gel, the polymer fraction and the cell density respectively,

$$L(\hat{T}) = 1 + \delta \hat{T} A_0 \sinh(\alpha) + \mathcal{O}(\delta^2), \tag{3.65}$$

$$\theta_p(X,\hat{T}) = \theta_i(1 - \delta \hat{T} \alpha A_0 \cosh(\alpha X)) + \mathcal{O}(\delta^2), \tag{3.66}$$

$$n(X,\hat{T}) = 1 - \delta \hat{T} \alpha A_0 \cosh(\alpha X) + \mathcal{O}(\delta^2), \tag{3.67}$$

with α and A_0 as defined above.

From these solutions we can determine how the gel will evolve away from uniform initial conditions. The sign of each $\mathcal{O}(\delta)$ term is determined by A_0, whose sign is, in turn, specified by the balance between the initial cell and chemical potentials. With positive A_0 (*e.g.* with a large negative mixing parameter χ in μ_s encouraging gel swelling), the length L increases as the gel stretches in response to the influx of solvent, causing θ_p and n to decrease. Meanwhile, for negative A_0 (*e.g.* driven by a large cell traction parameter τ_0), the gel contracts in length as solvent is forced out, with θ_p and n increasing accordingly.

Given that $\alpha > 0$ here, the $\cosh(\alpha X)$ functions in (3.66) and (3.67) increase monotonically with X; accordingly, the magnitude of these functions is greatest at $X = 1$. This indicates that θ_p and n will evolve most rapidly at the gel's interface over small time.

We also consider the small time solution for the model with no drag. Setting $\xi = 0$ in equation (3.57) and applying the boundary condition $v_0(0) = 0$, we find that

$$v_0 = k_1 X, \tag{3.68}$$

where, from the interface condition (3.59),

$$k_1 = -\left\{(2+\kappa_p)\theta_i + \frac{(2\eta_s+\kappa_s)\theta_i^2}{(1-\theta_i)} + \mathcal{R}\right\}^{-1} \times \left(\frac{\theta_i \tau_0}{1+\lambda} + \mu_s(\theta_i) - \mu_s^e\right). \tag{3.69}$$

After evaluating the model equations as done for $\xi \neq 0$ above, we arrive at the small time solution for the zero-drag case,

$$L(\hat{T}) = 1 + \delta \hat{T} k_1 + \mathcal{O}(\delta^2), \tag{3.70}$$

$$\theta_p(\hat{T}) = \theta_i(1 - \delta \hat{T} k_1) + \mathcal{O}(\delta^2), \tag{3.71}$$

$$n(\hat{T}) = 1 - \delta \hat{T} k_1 + \mathcal{O}(\delta^2). \tag{3.72}$$

We note that the zero-drag solution (3.70) - (3.72) is the same as that in equations (3.65) - (3.67) in the limit $\alpha \to 0$, which corresponds to drag $\xi \to 0$.

The behaviour here is again driven by the balance in cell and chemical potentials which appear in the constant k_1. The solution for this special case does not depend on hyperbolic functions as was seen for $\xi \neq 0$, and furthermore, θ_p and n are independent of X. Without drag, the gel therefore evolves in a spatially uniform manner over small time; this is in contrast to the case with $\xi \neq 0$, where as previously mentioned, θ_p and n evolve away from the initial conditions more rapidly with increasing X across the spatial domain.

These solutions allow us to assess the early time behaviour with arbitrary uniform initial conditions. We will use these small time solutions in Section 3.7 to verify that our numerical method evolves as expected.

3.6 SPATIAL PERTURBATIONS TO EQUILIBRIA OVER SMALL TIME

We now examine how the system evolves over short time from initial conditions that are small amplitude spatial perturbations to equilibrium solutions. This will suggest the stability of the equilibrium state: an equilibrium will be taken as unstable if spatial perturbations increase in amplitude over time, leading the system to evolve away from the equilibrium; an equilibrium will be taken as stable if the perturbations decay. We note that these stability criteria are supported by our numerical solutions to the model. To find analytic solutions, we restrict our attention to spatially uniform equilibria as required in the general case where $D \neq 0$, and owing to the difficulty of finding such solutions for the non-uniform case.

3.6.1 *Perturbations in space and time*

We denote the dimensionless steady state by asterisks, L^*, θ^*, n^*, v^*, where $v^* = 0$. The length and cell density are scaled on their equilibrium values such that $L^* = n^* = 1$. We take δ to be the short time scale as in the previous section and let ϵ be the amplitude of the spatial perturbation, where $\delta \ll \epsilon \ll 1$. Next, we take the series (3.54), (3.55), *etc.*, and expand each of the terms L_j, v_j, θ_j, n_j, $j = 1, 2, \ldots$, in powers of ϵ, for example,

$$L_j = L_{j0} + \epsilon L_{j1} + \epsilon^2 L_{j2} + \ldots, \tag{3.73}$$

$$v_j = v_{j0} + \epsilon v_{j1} + \epsilon^2 v_{j2} + \ldots, \tag{3.74}$$

while we take the initial conditions

$$L_0 = 1, \tag{3.75}$$

$$v_0 = \epsilon v_{01}(X) + \epsilon^2 v_{02}(X) + \ldots, \tag{3.76}$$

$$\theta_0 = \theta^* + \epsilon \theta_{01}(X), \tag{3.77}$$

$$n_0 = 1 + \epsilon n_{01}(X). \tag{3.78}$$

We set $\theta_{01} = \cos(\gamma X)$, $n_{01} = N_{01}\cos(\gamma X)$, such that

$$\theta_0 = \theta^* + \epsilon\cos(\gamma X), \tag{3.79}$$

$$n_0 = 1 + \epsilon N_{01}\cos(\gamma X), \tag{3.80}$$

where N_{01} is an $\mathcal{O}(1)$ constant describing the magnitude of the spatial perturbation to the cell density. We note that higher order terms of v_0 must be determined in such a way as is consistent with the other initial conditions.

Note that θ_0 and n_0 satisfy the symmetry boundary conditions (3.32) at $X = 0$ for any choice of γ, while the no-flux cell boundary condition (3.34) at $X = 1$ requires that $\gamma = Z\pi$ for some integer Z. For $Z = 0$, the spatial perturbation is constant and so effectively only shifts our initial condition, resulting in a similar solution to that presented in Section 3.5.1. Furthermore, changing the sign of Z does not change θ_0 or n_0. We therefore restrict our analysis to positive values of Z.

We ensure that our choices of θ_0 and n_0 are such that the total masses of polymer and cells over the domain $0 \leqslant X \leqslant 1$ are unchanged from the unperturbed initial masses (θ^* for the polymer fraction and 1 for the cell density). As such, we have

$$\theta^* = L_0\int_0^1 \theta_0(X)\,dX, \tag{3.81}$$

and similarly,

$$1 = L_0\int_0^1 n_0(X)\,dX. \tag{3.82}$$

On evaluating these expressions, we find that

$$\theta^* = \theta^* + \frac{\epsilon}{\gamma}\sin(\gamma), \tag{3.83}$$

and

$$1 = 1 + \frac{\epsilon N_{01}}{\gamma}\sin(\gamma). \tag{3.84}$$

Given the condition on γ above, we see that these equations are trivially satisfied, and as such, the perturbations do not change the initial masses of polymer and cells. Equation (3.84) also demonstrates that we are free to set N_{01} to any $\mathcal{O}(1)$ value and still satisfy (3.82).

Incorporating these spatial perturbations in ϵ, the expansions (3.54), (3.55), *etc.*, become

$$L(\hat{T}) = 1 + \delta L_{10}(\hat{T}) + \delta\epsilon L_{11}(\hat{T}) + \delta^2 L_{20}(\hat{T}) + ..., \tag{3.85}$$

$$\begin{aligned} \nu_p(X,\hat{T}) = {} & \epsilon\nu_{01}(X) + \delta\nu_{10}(X,\hat{T}) + \epsilon^2\nu_{02}(X) \\ & + \delta\epsilon\nu_{11}(X,\hat{T}) + \delta^2\nu_{20}(X,\hat{T}) + ..., \end{aligned} \tag{3.86}$$

and so on.

We now substitute these series into the governing equations for our gel to derive solutions for θ_p, n, ν_p and L describing the small time behaviour.

3.6.2 *Deriving small time solutions*

To determine ν_{01}, we consider the $\mathcal{O}(\epsilon)$ terms of the momentum balance equation (3.31), finding

$$\begin{aligned} H\frac{\partial^2\nu_{01}}{\partial X^2} - \xi\theta^*\nu_{01} - \theta^*(1-\theta^*)f''(\theta^*)\frac{\partial\theta_{01}}{\partial X} + (1-\theta^*)\frac{\tau_0}{1+\lambda}\frac{\partial\theta_{01}}{\partial X} \\ +(1-\theta^*)\theta^*\frac{2\tau_0}{(1+\lambda)^2}\frac{\partial n_{01}}{\partial X} = 0, \end{aligned} \tag{3.87}$$

where $H = (2+\kappa_p)\theta^*(1-\theta^*) + (2\eta_s + \kappa_s){\theta^*}^2$. On substituting $\theta_{01} = \cos(\gamma X)$, $n_{01} = N_{01}\cos(\gamma X)$ in (3.87), we obtain

$$\frac{\partial^2\nu_{01}}{\partial X^2} - \alpha^2\nu_{01} + \frac{(1-\theta^*)}{H}\gamma z\sin(\gamma X) = 0, \tag{3.88}$$

where α is as defined in (3.58) on replacing θ_i with θ^*, and

$$z = \theta^* f''(\theta^*) - \frac{\tau_0}{1+\lambda} - \theta^*\frac{2\tau_0 N_{01}}{(1+\lambda)^2}. \tag{3.89}$$

This has the solution

$$v_{01} = A_{01}\sinh(\alpha X) + \frac{(1-\theta^*)\gamma}{H(\alpha^2+\gamma^2)} z \sin(\gamma X). \tag{3.90}$$

Using the interface condition (3.33) at $\mathcal{O}(\epsilon)$, we find

$$A_{01} = \left(\frac{H}{(1-\theta^*)}\alpha\cosh\alpha + \mathcal{R}\sinh\alpha\right)^{-1} \times \left(\frac{\alpha^2}{\alpha^2+\gamma^2} z\cos(\gamma) - \frac{\mathcal{R}(1-\theta^*)\gamma}{H(\alpha^2+\gamma^2)} z\sin(\gamma)\right), \tag{3.91}$$

which, given the condition on γ, simplifies to

$$A_{01} = \left(\frac{H}{(1-\theta^*)}\alpha\cosh\alpha + \mathcal{R}\sinh\alpha\right)^{-1} \times \frac{\alpha^2}{\alpha^2+\gamma^2} z\cos(\gamma). \tag{3.92}$$

We stop at finding $v_{01}(X)$ and do not continue with higher order terms for the initial velocity v_0, since these do not feature in the $\mathcal{O}(\delta)$ and $\mathcal{O}(\delta\epsilon)$ corrections to θ_p and n.

Evaluating equations (3.29) and (3.30) at $\mathcal{O}(\delta)$, we find that θ_{10} and n_{10} are independent of time $\hat{T}$, hence $\theta_{10} = n_{10} = 0$. Similarly, evaluating the kinematic boundary condition (3.35) at $\mathcal{O}(\delta)$ yields $L_{10} = 0$.

At $\mathcal{O}(\delta\epsilon)$, we have

$$\frac{\partial\theta_{11}}{\partial\hat{T}} = -\theta^*\frac{\partial v_{01}}{\partial X}, \tag{3.93}$$

$$\frac{\partial n_{11}}{\partial\hat{T}} = -\frac{\partial v_{01}}{\partial X} + D\frac{\partial^2 n_{01}}{\partial X^2}, \tag{3.94}$$

with solutions

$$\theta_{11} = \left(-\theta^*\frac{\partial v_{01}}{\partial X}\right)\hat{T}, \tag{3.95}$$

$$n_{11} = \left(-\frac{\partial v_{01}}{\partial X} + D\frac{\partial^2 n_{01}}{\partial X^2}\right)\hat{T}. \tag{3.96}$$

Evaluating the kinematic boundary condition (3.35) at $\mathcal{O}(\delta\epsilon)$, we find

$$\frac{dL_{11}}{d\hat{T}} = v_{01}(X=1) = A_{01}\sinh(\alpha), \tag{3.97}$$

from which,

$$L_{11} = A_{01} \sinh(\alpha)\hat{T}. \tag{3.98}$$

Putting everything together, we have small time analytic solutions for the polymer volume fraction, cell density and gel length, respectively given as

$$\begin{aligned}\theta_p(X,\hat{T}) &= \theta^* + \epsilon\cos(\gamma X) - \epsilon\delta\hat{T}\theta^*\left(\alpha A_{01}\cosh(\alpha X) + \frac{(1-\theta^*)\gamma^2}{H(\alpha^2+\gamma^2)}z\cos(\gamma X)\right) \\ &\quad + \mathcal{O}(\delta^2), \end{aligned} \tag{3.99}$$

$$\begin{aligned}n(X,\hat{T}) &= 1 + \epsilon N_{01}\cos(\gamma X) - \epsilon\delta\hat{T}\Bigg(\alpha A_{01}\cosh(\alpha X) + \frac{(1-\theta^*)\gamma^2}{H(\alpha^2+\gamma^2)}z\cos(\gamma X) \\ &\quad + D\gamma^2 N_{01}\cos(\gamma X)\Bigg) + \mathcal{O}(\delta^2), \end{aligned} \tag{3.100}$$

$$L(\hat{T}) = 1 + \epsilon\delta A_{01}\sinh(\alpha)\hat{T} + \mathcal{O}(\delta^2). \tag{3.101}$$

We note that, at $\mathcal{O}(\delta\epsilon)$, equation (3.100) does not satisfy the no-flux cell boundary condition at $X = 1$ due to the $\cosh(\alpha X)$ term. In equation (3.94), we have neglected a higher-order term involving $\partial^2 n_{11}/\partial X^2$, meaning that we have a singular perturbation problem and cannot satisfy all boundary conditions for n_{11}. For the purposes of our analysis herein, we will continue to discuss this solution, as any possible error is confined to the small region near $X = 1$, hence not affecting behaviour in most of the gel. However, we will see in Section 3.6.3 that, in the zero-drag case where v_{01} is given by equation (3.103), the $\cosh(\alpha X)$ term does not appear in the solutions for θ_p and n, and accordingly, the boundary condition at $X = 1$ is satisfied.

3.6.3 *Zero-drag solution*

On setting the drag coefficient $\xi = 0$, we see in equation (3.58) that $\alpha = 0$, and hence one of the terms in equation (3.88) vanishes. Solving (3.88) then yields the following solution for v_{01},

$$v_{01} = \frac{(1-\theta^*)}{H\gamma}z\sin(\gamma X) + k_1(\hat{T})X + k_2(\hat{T}), \tag{3.102}$$

where k_1 and k_2 are constants of integration. Using the boundary conditions (3.32) and (3.33), we find that $k_1 = k_2 = 0$, and so the zero-drag solution for v_{01} reduces to

$$v_{01} = \frac{(1-\theta^*)}{H\gamma} z \sin(\gamma X). \tag{3.103}$$

We take this zero-drag solution for v_{01} and evaluate the higher order terms of θ_p, n and L in the same manner as Section 3.6.2. Given that $v_{01}(X = 1) = 0$ here, we find that $L_{11} = 0$ using the kinematic boundary condition. We therefore find the following zero-drag solutions for θ_p, n and L,

$$\theta_p(X, \hat{T}) = \theta^* + \epsilon \cos(\gamma X) - \epsilon\delta\hat{T}\theta^* \frac{(1-\theta^*)}{H} z \cos(\gamma X) + \mathcal{O}(\delta^2), \tag{3.104}$$

$$n(X, \hat{T}) = 1 + \epsilon N_{01} \cos(\gamma X) - \epsilon\delta\hat{T} \left(\frac{(1-\theta^*)}{H} z + D\gamma^2 N_{01} \right) \cos(\gamma X) + \mathcal{O}(\delta^2), \tag{3.105}$$

$$L(\hat{T}) = 1 + \mathcal{O}(\delta^2). \tag{3.106}$$

As was the case in Section 3.5, the zero-drag solution (3.104) - (3.106) here is the same as that for the non-zero-drag solution in equations (3.99) - (3.101) in the limit $\alpha \to 0$, corresponding to drag $\xi \to 0$.

As mentioned previously, in the absence of a $\cosh(\alpha X)$ term, equation (3.105) now satisfies the boundary condition $\partial n/\partial X = 0$ at $X = 1$. We now discuss the behaviour of both this solution and that with $\xi \neq 0$ over small time.

3.6.4 *Behaviour of the small time solutions*

We are interested in the temporal growth or decay of the spatial perturbations to the model variables. Therefore, we investigate the amplitude of the terms involving trigonometric and hyperbolic functions in the small time solutions.

We first describe the behaviour predicted by equations (3.99) - (3.101) over small time, with $\xi \neq 0$. From equation (3.101), we see that L increases or decreases depending on the sign of A_{01}, which in turn depends on the value of z and the choice of γ. This $A_{01} \sinh(\alpha)$ term describes the 1D stretching or shrinking of the gel over the short

time scale as a result of the spatial perturbation. The changes in θ_p and n due to this expansion or contraction are described by the $A_{01}\cosh(\alpha X)$ terms in their solutions; as seen previously, $\cosh(\alpha X)$ increases monotonically with X since $\alpha > 0$. Greater changes in θ_p and n therefore occur as X increases across the spatial domain. This is analogous to the solution given by equations (3.65) - (3.67), where the gel length is governed by a $\sinh(\alpha)$ term, while the $\cosh(\alpha X)$ terms determine the increase or decrease of the polymer fraction and cell density.

The trigonometric terms in the solutions for θ_p and n, (3.99) and (3.100) respectively, describe whether the initial spatial perturbations increase in amplitude or decay over time. Growth in these perturbations is akin to an unstable equilibrium where the gel evolves away from its steady state; decaying perturbations meanwhile correspond to a stable equilibrium. We note that the presence of non-zero diffusion in (3.100) works to dampen perturbations to n (even when the system is unstable).

In the zero-drag solution (3.104)-(3.106), L remains constant to $\mathcal{O}(\delta\epsilon)$ and no hyperbolic functions appear. Accordingly, θ_p and n evolve in space with no change in the gel's length, *i.e.* there is no flow at $X = 1$ when $\xi = 0$. Thus, a change in gel length only occurs over short time when $\xi > 0$.

Since we are primarily interested here in the evolution of the polymer and cell distributions, we focus our attention on the case where $\xi = 0$. In this case, changes in the amplitude of the perturbations are simply governed by the coefficients of the trigonometric terms, avoiding any complications resulting from the small changes in gel length with drag present.

3.6.5 *Steady state stability conditions*

As explained above, to simplify the interpretation of the stability results presented in this section, we restrict our attention to the case where $\xi = 0$.

From the $\mathcal{O}(\epsilon)$ and $\mathcal{O}(\delta\epsilon)$ terms, the solution for θ_p (3.104) includes the term

$$\left(1 - \theta^* \frac{(1-\theta^*)}{H} z\delta\hat{T}\right)\epsilon\cos(\gamma X), \tag{3.107}$$

while the solution for n (3.105) includes

$$\left\{1 - \left(\frac{(1-\theta^*)}{H} z + D\gamma^2 N_{01}\right) \delta\hat{T}\right\} \epsilon \cos(\gamma X). \tag{3.108}$$

For the amplitude of the initial perturbations to both θ_p and n to be decreasing, and accordingly, the equilibrium to revert back to a stable state, we require

$$z > 0, \tag{3.109}$$

which can be expressed in the form

$$f''(\theta^*) - \frac{\tau_0}{1+\lambda}\left(\frac{1}{\theta^*} + \frac{2N_{01}}{1+\lambda}\right) > 0. \tag{3.110}$$

In the case that $z < 0$, the perturbation will grow with time. We note that with $z = 0$, the system remains largely static, with only diffusive cell flux occurring. Hence, the growth or decay of perturbations in this system is dependent on the balance between free energy and cell force. Without cells, it is the sign of $f''(\theta^*)$ which determines the stability of an equilibrium. Given that

$$f''(\theta^*) = \frac{1}{N\theta^*} + \frac{1}{1-\theta^*} - 2\chi, \tag{3.111}$$

where N is typically large, we see that it is the sign and magnitude of the mixing parameter χ together with the equilibrium fraction of solvent $1-\theta^*$ that primarily determines this. Adding cells to the model will always reduce the value of z, and with other values held constant, move the equilibrium towards an unstable state. Similarly, with cells present, increasing cell traction strength τ_0 or reducing contact inhibition λ will make instability more likely.

3.6.6 *Analysis of steady state stability*

Using the stability condition (3.110) derived through the small time analysis, we can determine whether equilibria are stable or unstable. We can therefore study how both the equilibrium and its stability change as we adjust particular parameter values.

The diagrams presented in this section have been generated by solving the equilibrium condition (3.46), which, upon substituting for G and μ_S, becomes

$$\theta_p \frac{\tau_0 n^2}{1+\lambda n^2} + \log(\theta_s) + \chi\theta_p^2 - \theta_p\left(\frac{1}{N} - 1\right) = 0. \tag{3.112}$$

For non-zero cell density, we have scaled the system such that the equilibrium cell density $n^* = 1$. Noting this, (3.112) can be expressed as

$$\frac{\theta^*\tau_0}{1+\lambda} + \log(1-\theta^*) + \chi\theta^{*2} - \theta^*\left(\frac{1}{N} - 1\right) = 0, \tag{3.113}$$

while the first term vanishes for $n^* = 0$.

We solve this expression for a chosen parameter as we vary θ^* between 0 and 1, holding other parameters fixed. Alternatively, we find the relationship between two parameters using (3.113) while keeping θ^* and other parameters fixed. Through this analysis, we can also determine whether spatially uniform steady states exist for a particular set of parameter values and initial conditions.

Figs. 3.1 - 3.3 demonstrate how θ^* varies as we change the mixing parameter χ at different values of τ_0 (we note that changes in the dimensionless parameter τ_0 can correspond to changes in the characteristic cell density – here the physical steady state value – or the cell traction strength). In the majority of cases, larger values of χ indicate greater levels of contraction in the gel, corresponding to larger values of θ^*; this outcome should be expected, as increasing χ indicates that separation of the two phases in the gel is more favourable. In Fig. 3.1, it is shown that in the absence of cells ($n^* = 0$), two equilibrium values of θ^* – one stable and one unstable – exist for the same parameter values. Note that the stability of these steady states is determined using equation (3.110). We also see that, in the absence of cells, steady states θ^* exist

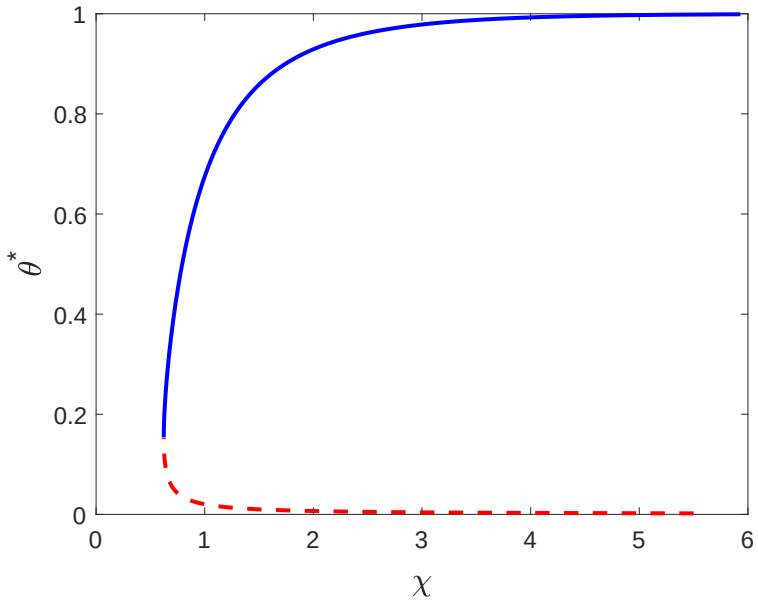

Figure 3.1: Equilibrium polymer fraction θ^* vs. mixing parameter χ. The solid blue curve shows stable equilibria while the red dashed curve shows unstable equilibria. Fixed values: $N = 100$, $n^* = 0$.

only for positive values of χ (given $N = 100$); with $\chi < 0$, the terms in the free energy function all promote mixing between solvent and polymer, and accordingly, the gel keeps expanding until it dissolves. In this example, if a gel's initial fraction of polymer θ_i is in the region beneath the blue solid line, the gel will contract to equilibrium with a greater value of θ_p, while if θ_i is above the branch of stable equilibria, the gel will swell to a steady state. For $\chi < 0.62$, there are no steady states possible for any initial condition θ_i (*i.e.* the gel dissolves). This indicates that small changes to the initial composition of a gel, *e.g.* the fraction of polymer or make-up of the solvent, could have significant impacts on its subsequent behaviour and possible steady state.

With cells introduced into the system, θ^* increases monotonically as χ increases, as seen in Figs. 3.2 and 3.3 where $\tau_0 = 0.25$ and $\tau_0 = 1$ respectively. In these examples, we see that there are no longer any unstable equilibria, and that stable equilibria now exist over the spectrum of χ values. We see that as the traction parameter increases from $\tau_0 = 0.25$ (Fig. 3.2) to $\tau_0 = 1$ (Fig. 3.3), the equilibrium polymer fraction is greater for the same values of χ. For example, in Fig. 3.2 where $\tau_0 = 0.25$, at $\chi = 0$ we have $\theta^* = 0.2$, while in Fig. 3.3 where $\tau_0 = 1$, at $\chi = 0$ we have $\theta^* = 0.58$. Similarly, we see

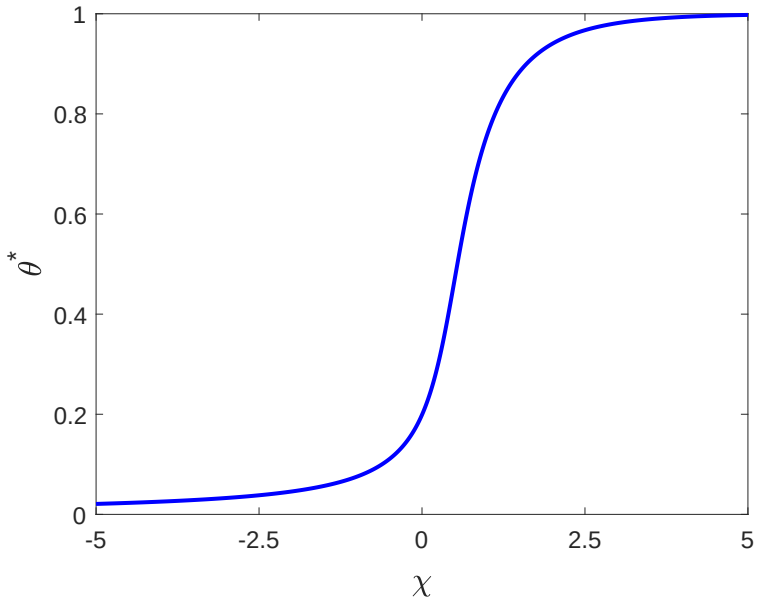

Figure 3.2: Equilibrium polymer fraction θ^* vs. mixing parameter χ with a small cell traction parameter $\tau_0 = 0.25$. Only stable equilibria (solid blue line) are present in this case. Fixed values: $N = 100$, $n^* = 1$, $\tau_0 = 0.25$, $\lambda = 1$.

in these figures that with τ_0 increasing from $\tau_0 = 0.25$ to $\tau_0 = 1$, the same particular equilibrium value θ^* is found with a decreasing value of the mixing parameter χ.

This relationship between τ_0 and χ is reinforced in Fig. 3.4, where χ is plotted against τ_0 for fixed $\theta^* = 0.5$. We see that χ decreases linearly with increasing τ_0; as the cells exert more force, lower values of the interaction parameter are needed to keep the system at the same equilibrium value of polymer. Similarly, with a larger value of χ, less cell traction is necessary to maintain this equilibrium. This linear relationship between χ and τ_0 when the polymer fraction is fixed can be clearly seen in equation (3.113).

In Fig. 3.5 it is shown that, as would be expected, larger values of τ_0 correspond to larger θ^*, *i.e.* greater compaction in the polymer network. We note that we must have $\tau_0 \geqslant 0$; therefore, the equilibria that cross the vertical line at $\tau_0 = 0$ are not biologically relevant. There is a very small branch of permissible unstable equilibria in the region approaching $\theta^* = 0$, but the vast majority of initial conditions here will reach a stable steady state. In the small region where two steady states exist, gels with an initial polymer fraction above the unstable values of θ^* will contract to the stable equilibrium, whereas those below the unstable values will swell until the gel dissolves.

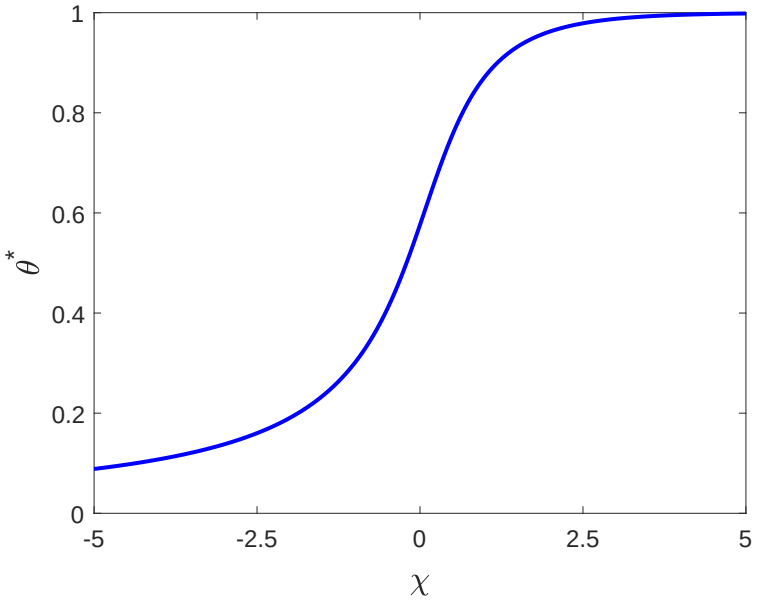

Figure 3.3: Equilibrium polymer fraction θ^* vs. mixing parameter χ with a larger cell traction parameter $\tau_0 = 1$. Again, only stable equilibria (solid blue line) are evident. Fixed values: $N = 100$, $n^* = 1$, $\tau_0 = 1$, $\lambda = 1$.

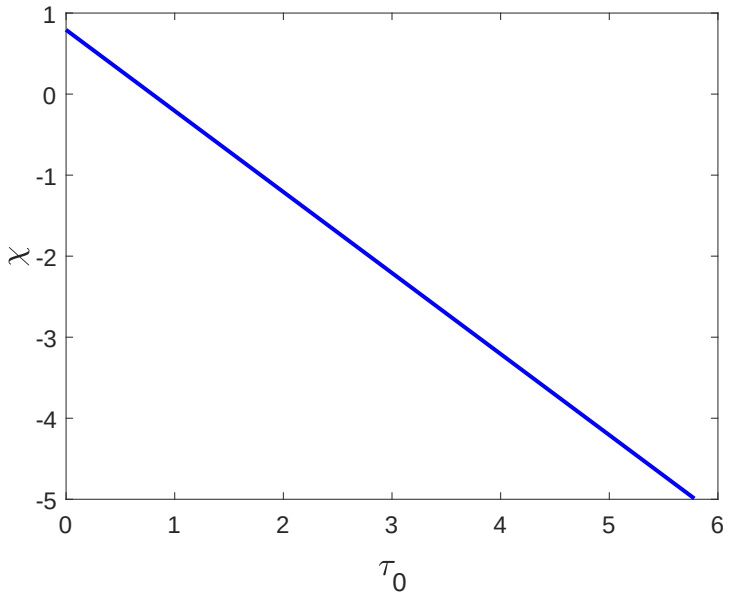

Figure 3.4: Relationship between τ_0 and χ with the polymer equilibrium fixed at $\theta^* = 0.5$; this steady state is stable for this range of parameters. Fixed values: $\theta^* = 0.5$, $N = 100$, $n^* = 1$, $\lambda = 1$.

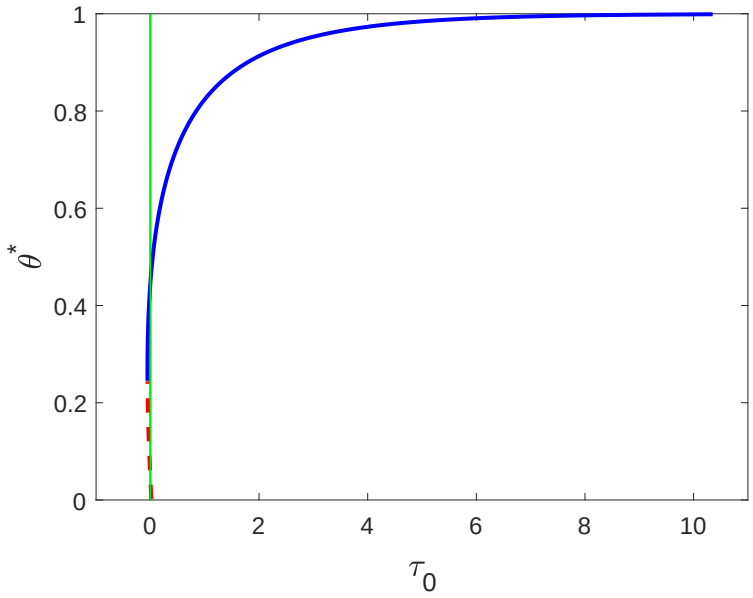

Figure 3.5: Equilibrium polymer fraction θ^* vs. cell traction parameter τ_0. The solid blue curve shows stable equilibria while the red dashed curve shows unstable equilibria. The solid green line is $\tau_0 = 0$; equilibria to the left of this have $\tau_0 < 0$ and are not relevant. Fixed values: $\chi = 0.75$, $N = 100$, $n^* = 1$, $\lambda = 1$.

3.7 NUMERICAL SIMULATIONS

We now perform numerical simulations to investigate the behaviours predicted by our model. We consider a range of initial conditions – both uniform and non-uniform – and parameter values to better understand the emergent behaviours that can arise as a result of the interacting forces in the system. We find uniform and non-uniform equilibria can eventuate, as well as a novel example where the polymer fraction and cell density in parts of the gel oscillate before the gel finally dissolves.

These simulations have been carried out in MATLAB using the 1D Cartesian system (3.27) - (3.36) presented in Section 3.2. We use finite difference methods to discretise these equations onto a uniform spatial grid. Central differencing is used in the velocity equation (3.31), excluding at $X = 1$, where a one-sided difference is used for derivatives of θ_p, and the boundary condition (3.33) is used to provide a ghost point for v_p. The Crank-Nicolson method is used for equations (3.29) and (3.30), with one-sided differences used for derivatives of v_p at $X = 1$ (see Morton and Mayers (2005) for discussion

of these numerical methods). We have found that this numerical scheme conserves mass effectively over time. To check this, we calculated the percentage change in the mass of polymer and cells at the initial and final points in time for each of the simulations presented in this section. With a time step of $dT = 0.0005$ and spatial step of $dX = 0.002$, the worst-case change in mass for θ_p or n between first and final time was 0.0076%.

The algorithm used to solve this model is as follows:

1. Set parameter values and initial conditions in θ_p, n and L.
2. Solve equation (3.31) using matrix inversion to find $v_p(T = 0)$ using the initial conditions in step 1, subject to the boundary conditions (3.32) and (3.33).
3. For $i = 1, 2, ...$
    a) Increment T by time step dT.
    b) Update θ_p in time by solving equation (3.29) using a Crank-Nicolson scheme, subject to the boundary condition on v_p in (3.32) (we note that from cancellation of terms in (3.29) at $X = 0$, this equation does not involve a $\partial\theta_p/\partial X$ term at $X = 0$).
    c) Update n in time by solving equation (3.30) using a Crank-Nicolson scheme, subject to boundary conditions (3.32) and (3.34).
    d) Update v_p by solving (3.31) with updated values of θ_p and n using the same method as in step 2.
    e) Update L(T) using the kinematic boundary condition (3.35) with an explicit Euler time step.

Steps 3a - 3e are repeated until the specified end time is reached. This end time is chosen such that the gel reaches a steady state or the system breaks down with the polymer fraction approaching 0 or 1. We can then study the solutions found for θ_p, n and L at each point in time to understand how the gel evolves temporally and how the spatial characteristics of the variables change with time.

3.7.1 *Overview of initial conditions and parameter choices*

We wish to study the effect that introducing cells has on the behaviour of a gel. Accordingly, we present simulations for a cell-free gel initially, then add cells into the system. We look at the effects of parameters like drag and viscosity, *e.g.* studying the impact they have on the spatial distribution of model variables and the speed at which the gel evolves. We start with uniform initial conditions for θ_p and n. We also consider how taking spatially non-uniform initial conditions in the polymer fraction and cell density affects the evolution of the system.

The aim of our simulations is to illustrate the qualitative behaviours of our model for different initial conditions and in different parameter regimes. Lacking experimental data to fit model parameters, we take the majority of parameters to be $\mathcal{O}(1)$.

Throughout these simulations, we will not change certain initial conditions and parameters (see Table 3.1) while investigating the effects of changing others between simulations (see Table 3.2). The terms which may vary between simulations in Table 3.2 will be discussed in the simulations that follow as they arise and are adjusted. We note here that the mixing parameter χ is the only term appearing in the final system of equations which allows negative values. As seen earlier, the length scale is set such that the initial length $L(0) = 1$. When cells are present, we will choose the average initial cell density as the characteristic value, so that $n_i = 1$ for an initially uniform cell distribution. Given that μ_p^0 and μ_s^0 do not appear in the final set of model equations due to cancellation of terms when taking $\mu_s - \mu_s^e$ in interface condition (3.33), we set these to zero. We set the bulk viscosities κ_p and κ_s to zero without loss of generality, as these terms only appear in linear combination with the dynamic viscosity parameters. The polymer chain length N is generally large for polymer and solution mixtures, therefore we set $N = 100$ (Rubinstein *et al.*, 2003). We set the contact inhibition parameter $\lambda = 1$.

Table 3.1: Dimensionless initial conditions and parameter values which we do not change between simulations.

Term	Symbol	Value used
Initial length	L_i	1
Contact inhibition parameter	λ	1
Polymer chain length	N	100
Polymer standard free energy	μ_p^0	0
Solvent standard free energy	μ_s^0	0
Polymer bulk viscosity	κ_p	0
Solvent bulk viscosity	κ_s	0

Table 3.2: Dimensionless initial condition and parameter values which we may change between simulations.

Term	Symbol	Range of values used
Initial polymer fraction	θ_i	0.2 - 0.7
Initial cell density	n_i	0 - 1
Cell traction coefficient	τ_0	0.1 - 1
Cell diffusion coefficient	D	0 - 1
Mixing parameter	χ	-0.1 - 1.5
Interface resistance	$\mathcal{R}$	0.1 - 5
Drag coefficient	ξ	0 - 5
Solvent dynamic viscosity	η_s	0.1 - 5

3.7.2 *Numerical comparison with small time solutions*

To validate our numerical method, we first compare simulation results with the analytic small time solutions derived in Sections 3.5 and 3.6. Fig. 3.6 compares the numerical solution for θ_p against the small time solution for θ_p with uniform initial conditions given by equation (3.66). We see good agreement between the two solutions for the polymer fraction θ_p at different points in the spatial domain. Similar agreement is found between the solutions for n over early time (result not shown). For this example, $A_0 = -0.145 < 0$, indicating that θ_p should increase over small time; this is evident in Fig. 3.6.

In Fig. 3.7, we compare the numerical solution for θ_p against the short time solution for spatially perturbed equilibrium initial conditions as given by equation (3.104) (noting that this is the zero-drag case). We do this using an arbitrary set of parameters which solves the equilibrium condition (3.46). We again see that the two solutions for θ_p are very close over the short time scale. Good agreement is also found between the numerical and analytic solutions for n (result not shown). In this example, $z = 0.98 > 0$, suggesting that this is a stable steady state and the perturbations will decay over time. This is supported by Fig. 3.7, with θ_p at different points in space converging towards a uniform value.

We also note that we have confirmed in the following simulations that the system reaches an appropriate steady state which satisfies the equilibrium condition (3.46).

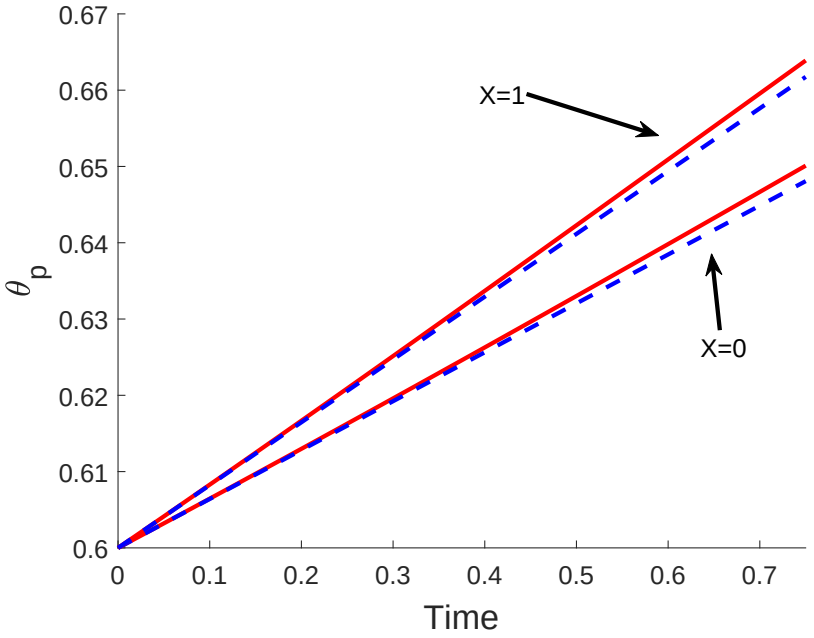

Figure 3.6: Comparing the small time solution (3.66) for θ_p with uniform initial conditions (blue dashed lines) with the numerical solution (red solid lines) over early time at $X = 0$ and $X = 1$. We see that the solutions evolve closely over this period of time. Values: $\theta_i = 0.6$, $n_i = 1$, $\chi = 0.75$, $\eta_s = 0.1$, $\xi = 0.5$, $\mathcal{R} = 0.5$, $\tau_0 = 1$, $D = 0$.

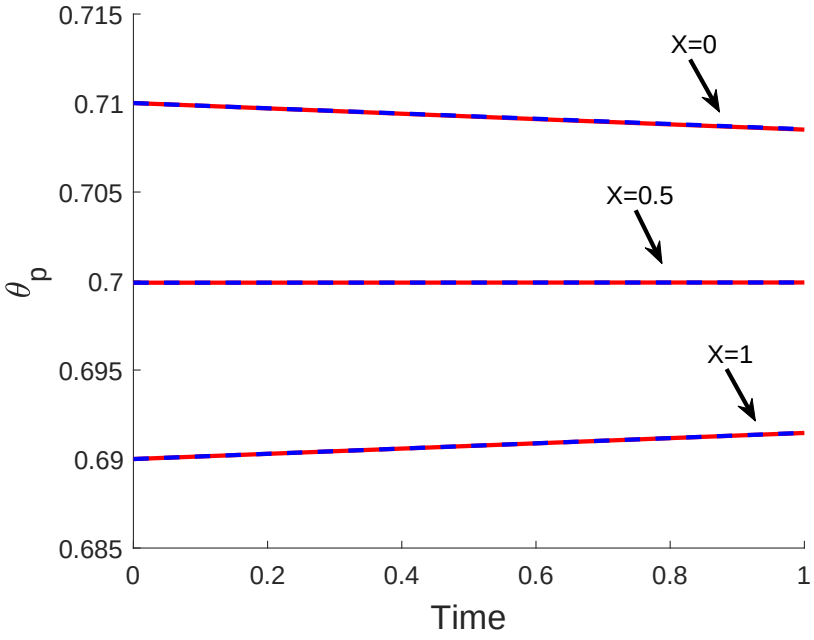

Figure 3.7: Comparing the small time solution (3.104) for θ_p with spatially perturbed equilibrium initial conditions (blue dashed lines) with the numerical solution (red solid lines) over early time at $X = 0$, $X = 0.5$ and $X = 1$. The solutions are closely matched over this period of time. Values: $\theta_i = 0.7 + 0.01\cos(3\pi X)$, $n_i = 1 + 0.01\cos(3\pi X)$, $\chi = 0.5785$, $\eta_s = 1$, $\xi = 0$, $\mathcal{R} = 1$, $\tau_0 = 0.65$, $D = 0.01$, $\gamma = 3\pi$, $\epsilon = 0.01$, $N_{01} = 1$.

3.7.3 *Cell-free gel, uniform initial conditions*

In a cell-free gel (where $n = 0$), swelling or contraction is driven by the free energy of the system; gradients in chemical potentials on either side of the gel-solvent interface induce the movement of solvent and polymer. This is similar to the results presented in Keener *et al.* (2011b). In Fig. 3.8, where $\theta_i = 0.6$ and $\chi = 0.75$, the balance in chemical potentials μ_p and μ_s produces an osmotic pressure gradient, causing solvent to enter the gel from the surrounding solvent region Ω_s; the gel thus swells until an equilibrium is reached with $\theta^* = 0.45$ and $L^* = 1.34$. Conversely, in Figs. 3.9 and 3.10, we see the gel contract to an equilibrium state. The free energy in the system has been altered in two different ways here to induce contraction. In Fig. 3.9, we have taken the same initial conditions as Fig. 3.8, but with an increased strength of mixing parameter $\chi = 1.5$. In Fig. 3.10, the initial fraction of polymer has been decreased to $\theta_i = 0.25$, with the value of χ remaining at $\chi = 0.75$. The effect in both instances is to increase the initial free energy in the gel, resulting in a situation where the gradient in chemical potentials will induce solvent to flow out from the gel to balance the potentials, and hence result in a smaller equilibrium length. The gel equilibrates with $\theta^* = 0.86$ and $L^* = 0.7$ in Fig. 3.9, and $\theta^* = 0.45$ and $L^* = 0.56$ in Fig. 3.10. These equilibria all clearly satisfy the mass conservation relation $L^*\theta^* = \theta_i$, as given in equation (3.53) (as indeed will all steady states found).

We note that the simulations in Figs. 3.8 and 3.10 reach the same equilibrium value, $\theta^* = 0.45$, for the two different initial conditions; this corresponds to the equilibrium predicted in Fig. 3.1 with $\chi = 0.75$ and the same fixed set of parameter values otherwise. Fig. 3.9 meanwhile confirms that, for the same initial conditions and parameter set, increasing the value of χ will result in an equilibrium with a larger polymer fraction ($\theta^* = 0.86$). This is also in agreement with Fig. 3.1.

We also note that the polymer fraction at $X = 1$ (shown by red dashed lines) evolves slightly faster than that at $X = 0$ (blue solid lines). This lag reflects the time taken for the solvent to flow into or away from the centre of the gel. We discuss the parameters affecting this lag and the spatial profiles of the polymer as the gel evolves in Section 3.7.5.

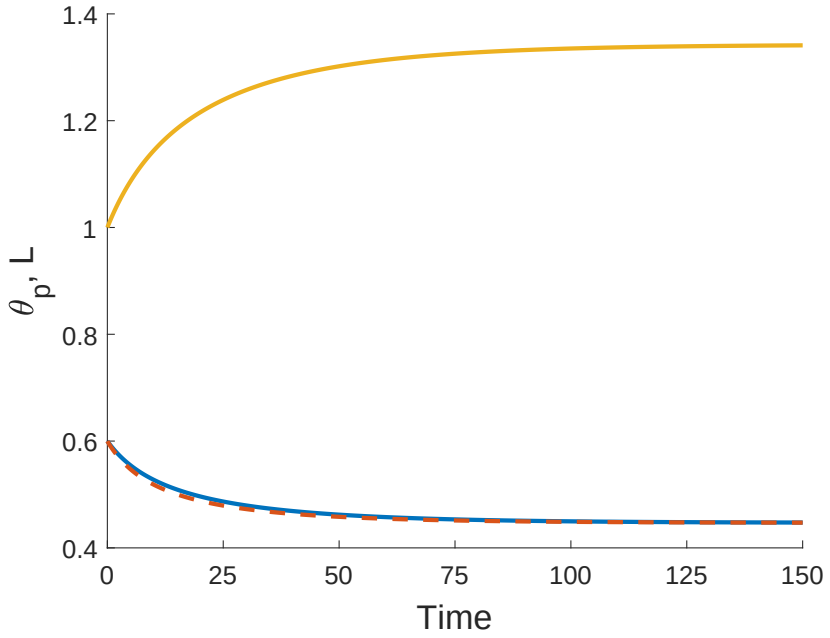

Figure 3.8: Time evolution of a cell-free gel. The gel swells to equilibrium due to osmotic pressure. $L(T)$ is the solid gold line, $\theta_p(X = 0)$ is the solid blue line, $\theta_p(X = 1)$ is the dashed red line. Values: $\theta_i = 0.6$, $n_i = 0$, $\chi = 0.75$, $\eta_s = 0.25$, $\xi = 0.5$, $\mathcal{R} = 0.5$. $(\theta^*, L^*) = (0.45, 1.34)$.

We have shown here that, in the absence of cells, the gel will swell or contract depending on the balance between chemical potential gradients across the gel-solvent interface. These behaviours echo those found by Keener *et al.* (2011b), which is expected since our gel model builds on their work. Comparing our model to that of Keener *et al.*, we note that while the inclusion of boundary resistance in our model only affects the rate of the gel's elongation or shrinking, the absence of any contribution from the standard free energy parameters μ_p^0 and μ_s^0 will change the final gel length and polymer fraction found here for the same set of parameters used in Keener *et al.*. We next introduce cells into the simulations to study their effect on the gel's behaviour.

3.7.4 *Cell-gel system*

In Fig. 3.11, we use the same gel parameters as for Fig. 3.8, and introduce a cell population with weak traction ($n_i = 1$, $\tau_0 = 0.1$; note also $D = 0.01$). We see that the gel still swells to a steady state with the cell traction parameter set at this low level. However,

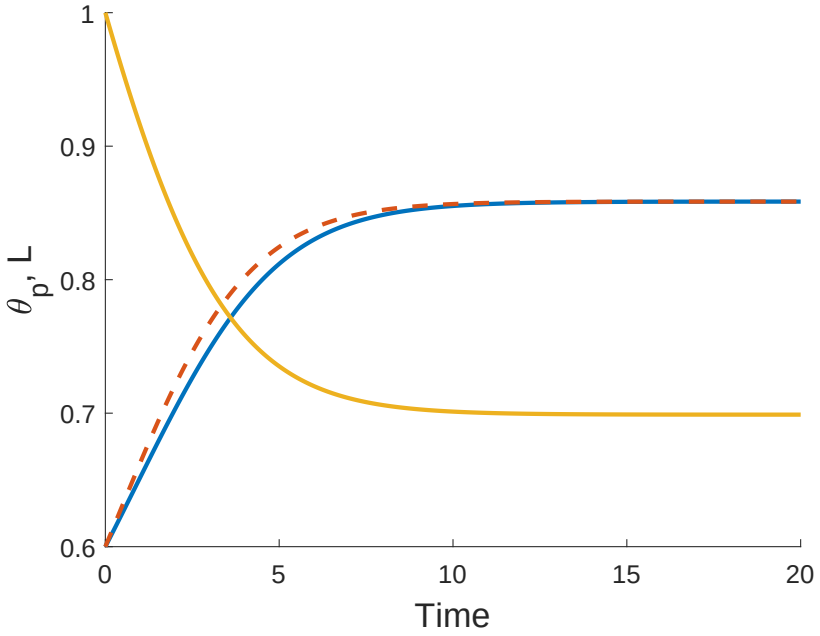

Figure 3.9: Time evolution of a cell-free gel. With increased χ, the gel now contracts to a smaller steady state length. $L(T)$ is the solid gold line, $\theta_p(X = 0)$ is the solid blue line, $\theta_p(X = 1)$ is the dashed red line. Values: $\theta_i = 0.6$, $n_i = 0$, $\chi = 1.5$, $\eta_s = 0.25$, $\xi = 0.5$, $\mathcal{R} = 0.5$. $(\theta^*, L^*) = (0.86, 0.7)$.

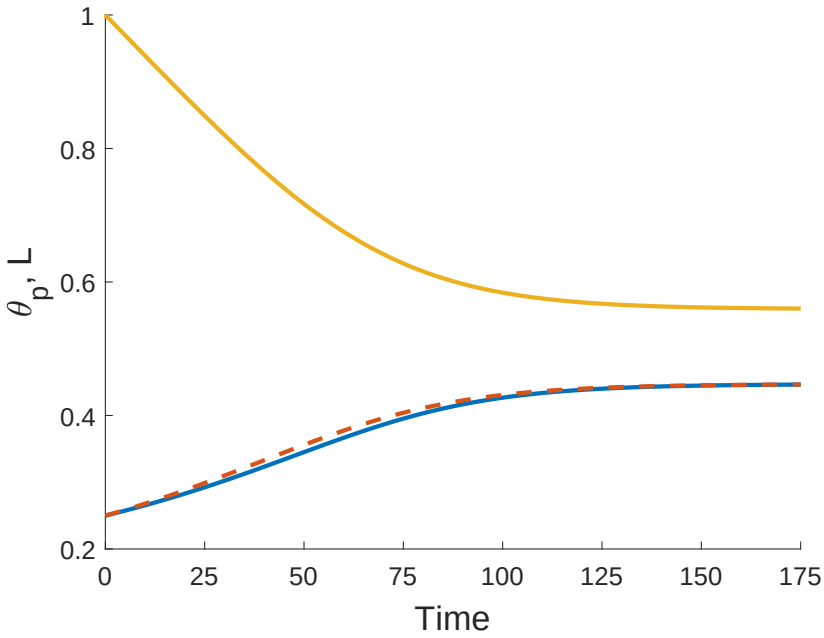

Figure 3.10: Time evolution of a cell-free gel. Decreasing the initial polymer fraction changes the free energy balance such that the gel now contracts. $L(T)$ is the solid gold line, $\theta_p(X = 0)$ is the solid blue line, $\theta_p(X = 1)$ is the dashed red line. Values: $\theta_i = 0.25$, $n_i = 0$, $\chi = 0.75$, $\eta_s = 0.25$, $\xi = 0.5$, $\mathcal{R} = 0.5$. $(\theta^*, L^*) = (0.45, 0.56)$.

compared to the simulation in Fig. 3.8, the final size of the gel is now smaller (equilibrating here at $\theta^* = 0.54$, $n^* = 0.91$, $L^* = 1.1$), indicating that the cells are exerting some contractile force that counters the expansion due to osmotic effects. We increase the traction parameter to $\tau_0 = 1$ in Fig. 3.12; once cell traction is increased over a certain threshold, the gel will switch from expansion to contraction. In this instance, the cell traction stresses are stronger than the chemical potential gradient, and as the cells compact the polymer network, solvent is squeezed from the gel until it reaches a steady state once the mechanical forces are in balance, where $\theta^* = 0.86$, $n^* = 1.44$, $L^* = 0.69$. We have therefore established that introducing cells into a gel that would otherwise swell can induce a switch in behaviour, resulting in a significantly different outcome for the gel. As in Section 3.7.3, the equilibria found here satisfy the mass conservation relations $L^*\theta^* = \theta_i$, $L^*n^* = 1$, as described in equation (3.53).

The time taken to equilibrate is noticeably different across the simulations seen so far, as the rate at which the gel evolves is affected by the strength of a number of competing forces. For example, we see in Fig. 3.8 that equilibrium is reached at approximately $T = 130$, while in Fig. 3.9, due to the larger value of χ, not only does the gel contract, but it equilibrates by $T = 15$. In a case like that presented in Fig. 3.9, where the free energy alone induces gel contraction, adding cells to this gel will lead to a steady state being reached more quickly (result not shown). Therefore, the magnitude of parameters like the interaction energy χ and cell traction τ_0 will affect the time taken to reach a steady state. Alongside this, mechanical factors like drag and viscosity will impact the gel's temporal evolution.

3.7.5 *Effects of mechanical parameters and diffusion on gel evolution*

We now study how the ratios of drag ξ, resistance $\mathcal{R}$, and solvent viscosity η_s relative to polymer viscosity η_p affect the rate at which a gel evolves to equilibrium and the manner in which it does so spatially. In the simulations presented in Figs. 3.13 - 3.16, we take a gel with the same initial conditions, free energy parameters, and cell force parameters as that presented in Fig. 3.12; this gel will therefore reach the same equilibrium regardless of parameters like drag and viscosity (given that the equilibrium is

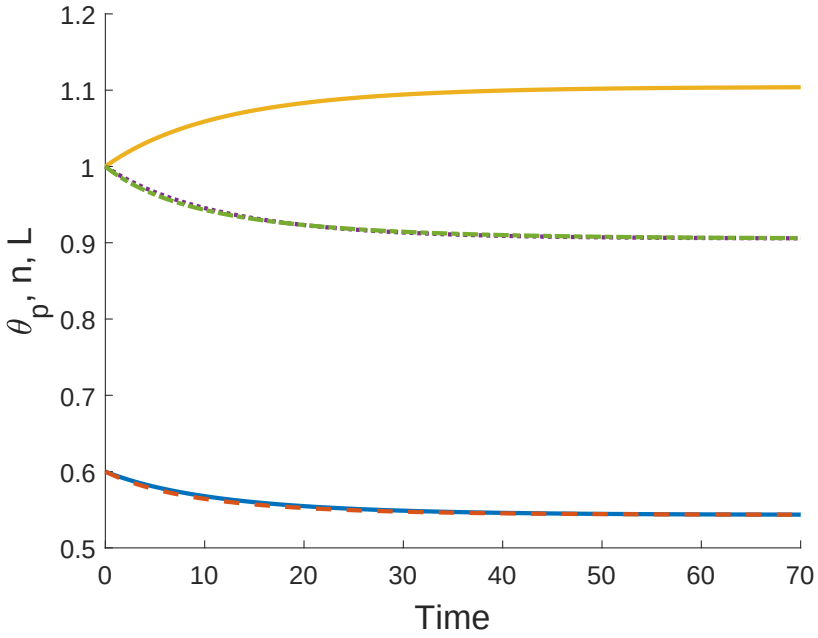

Figure 3.11: Time evolution of a cell-gel system. With weak cell traction, the gel still swells to an equilibrium state. $L(T)$ is the solid gold line, $\theta_p(X=0)$ is the solid blue line, $\theta_p(X=1)$ is the dashed red line, $n(X=0)$ is the dotted purple line, $n(X=1)$ is the dash-dotted green line. Values: $\theta_i = 0.6$, $n_i = 1$, $\chi = 0.75$, $\eta_s = 0.25$, $\xi = 0.5$, $\mathcal{R} = 0.5$, $\tau_0 = 0.1$, $D = 0.01$. $(\theta^*, n^*, L^*) = (0.54, 0.91, 1.1)$.

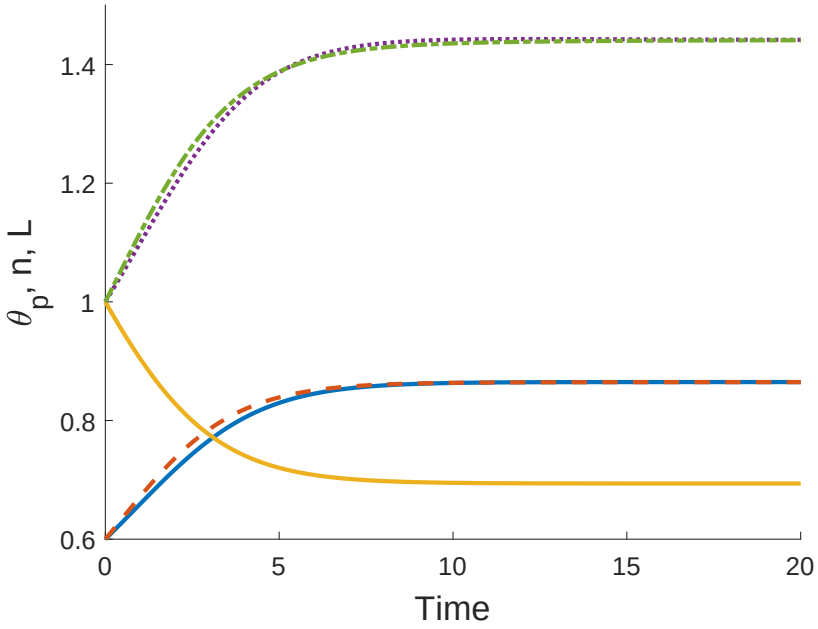

Figure 3.12: Time evolution of a cell-gel system. With increased cell traction, the gel switches to contraction as the cell-induced forces are stronger than the osmotic pressure. $L(T)$ is the solid gold line, $\theta_p(X=0)$ is the solid blue line, $\theta_p(X=1)$ is the dashed red line, $n(X=0)$ is the dotted purple line, $n(X=1)$ is the dash-dotted green line. Values: $\theta_i = 0.6$, $n_i = 1$, $\chi = 0.75$, $\eta_s = 0.25$, $\xi = 0.5$, $\mathcal{R} = 0.5$, $\tau_0 = 1$, $D = 0.01$. $(\theta^*, n^*, L^*) = (0.86, 1.44, 0.69)$.

determined by equation (3.46), in which these mechanical parameters do not appear). We first set ξ, $\mathcal{R}$ and η_s to be small, indicating that these effects are insignificant relative to polymer dynamic viscosity, and as such, polymer dynamic viscosity is the dominant mechanical characteristic; we will refer to this as the base case in the comparisons that follow. We note that due to the scaling used here, we have effectively set $\eta_p = 1$. To better understand the impact of each parameter on the gel's evolution, we then change one of ξ, $\mathcal{R}$ and η_s in turn while holding the others constant. We take $D = 0$ here so that diffusion has no impact on the cell and polymer distributions. The gel reaches the same steady state in each case ($\theta^* = 0.86$, $n^* = 1.44$, $L^* = 0.69$), albeit at different times and with different lags between $X = 1$ and $X = 0$.

In Fig. 3.13, we compare the evolution of θ_p for the base case with $\xi = \mathcal{R} = \eta_s = 0.1$ (shown by the red solid line for $X = 0$ and the red dashed line for $X = 1$) and for a gel with large drag, where $\xi = 5$ and $\mathcal{R} = \eta_s = 0.1$ (shown by the blue solid line for $X = 0$ and blue dashed line for $X = 1$). We see that increasing the drag coefficient slows down the evolution of the polymer fraction (with the gel equilibrating at $T \approx 25$ with large ξ compared to $T \approx 10$ with small ξ). Furthermore, for large drag, θ_p changes at a much slower rate at $X = 0$ than at $X = 1$, while there is little difference in θ_p between $X = 0$ and $X = 1$ when drag is small. This is reflected in Figs. 3.15 and 3.16, which show the spatial profiles for θ_p at increasing points in time for the base case and large drag case respectively. With polymer viscosity dominant in Fig. 3.15, the gel evolves across the spatial domain in a largely uniform manner. In Fig. 3.16, much stronger spatial variations are evident, reflecting that, while the gel evolves quickly at the interface, it takes much longer for solvent to flow through the domain due to the extra resistance when drag is large.

In Fig. 3.14 we similarly compare the gel's behaviour with interface resistance $\mathcal{R}$ and solvent viscosity η_s each large relative to polymer viscosity. For large resistance (shown by the green solid and dotted curves for $X = 0$ and $X = 1$ respectively), we take $\mathcal{R} = 5, \xi = \eta_s = 0.1$, while for large viscosity (shown by the black solid and dotted curves for $X = 0$ and $X = 1$ respectively), we set $\eta_s = 5, \xi = \mathcal{R} = 0.1$. Note that this figure should be compared to the base case given by the red curves in Fig. 3.13. Increasing the resistance parameter $\mathcal{R}$, the rate of change of θ_p is slowed at $X = 1$

compared to the base case (with equilibrium now reached at $T \approx 20$). This reflects the fact that the boundary of the gel is less permeable to fluid flow with larger $\mathcal{R}$. In this case, the polymer fraction remains almost uniform across the spatial domain, *i.e.* there is no additional lag induced between $X = 1$ and $X = 0$ with large $\mathcal{R}$. Large solvent viscosity η_s has the effect of slowing down gel contraction further still, with the gel not equilibrating until $T \approx 80$ (note that equilibrium for the large η_s case is not shown in Fig. 3.14). As with $\mathcal{R}$, in this case there is minimal lag between the evolution at $X = 1$ and $X = 0$.

We now study the effect of non-zero diffusion on the gel's behaviour. As diffusion increases, we expect to see more uniform spatial profiles in the cell density as well as the polymer fraction, as cells spread more evenly across the gel through random motion. In Fig. 3.16 we showed the spatial profiles of θ_p for a gel with a large drag coefficient and zero diffusion. In Fig. 3.17, we see that the spatial distribution of cells in this gel is similarly non-uniform over much of the gel's evolution. We now take this same gel with large drag, but introduce cell diffusion, setting $D = 0.005$; the time evolution in this case is shown in Fig. 3.18. In Fig. 3.19, we see that with large drag, the cell density initially increases rapidly at $X = 1$ (like in Fig. 3.17). Over time, cells move down their density gradient towards $X = 0$ due to the diffusion term now present. The cells become more dense in this region, eventually overshooting the equilibrium value (see n in Fig. 3.18); however, as time progresses, the diffusive movement leads n to converge to its equilibrium value across the domain. Increasing diffusion further to $D = 1$ in Fig. 3.20, the strength of the random motion is such that the cells remain well spread spatially for all time. We note that in this case, the polymer still evolves with a lag across the spatial domain, like seen in Fig. 3.16 (result not shown).

3.7.6 *Reduced initial polymer fraction*

Taking a smaller initial polymer fraction, we can see different dynamics emerge in the evolution of the gel. Setting $\theta_i = 0.2$ and all other parameters as in Fig. 3.12, we see in Figs. 3.21 and 3.22 that the polymer fraction and cell density evolve slowly over the beginning phases ($T = 0$ to $T \approx 2$), before a period of rapid increase ($T \approx 2$ to

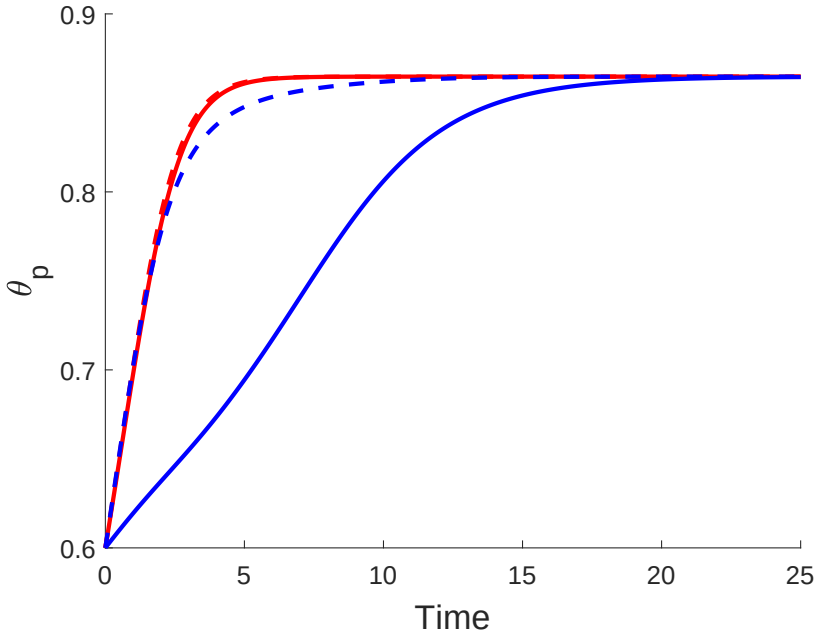

Figure 3.13: Comparison of the polymer fraction's evolution for the base case with polymer viscosity dominant vs. case with large drag. For the base case, ($\xi = \mathcal{R} = \eta_s = 0.1$), $\theta_p(X = 0)$ is the solid red line and $\theta_p(X = 1)$ is the dashed red line; for large drag ($\xi = 5, \mathcal{R} = \eta_s = 0.1$), $\theta_p(X = 0)$ is the solid blue line and $\theta_p(X = 1)$ is the dashed blue line. Other values: $\theta_i = 0.6$, $n_i = 1$, $\chi = 0.75$, $\eta_s = 0.1$, $\mathcal{R} = 0.1$, $\tau_0 = 1$, $D = 0$.

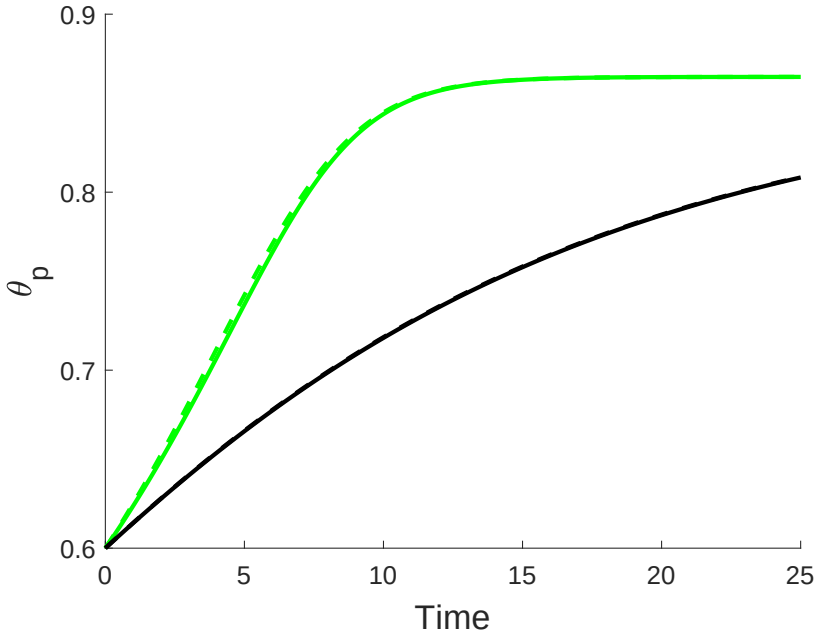

Figure 3.14: Comparison of the polymer fraction's evolution with large resistance and large solvent viscosity (note that these should be considered together with the base case in Fig. 3.13). For large resistance ($\mathcal{R} = 5, \xi = \eta_s = 0.1$), $\theta_p(X = 0)$ is the solid green line and $\theta_p(X = 1)$ is the dashed green line; for large solvent viscosity ($\eta_s = 5, \xi = \mathcal{R} = 0.1$), $\theta_p(X = 0)$ is the solid black line and $\theta_p(X = 1)$ is the dashed black line. Other values as in Fig. 3.13.

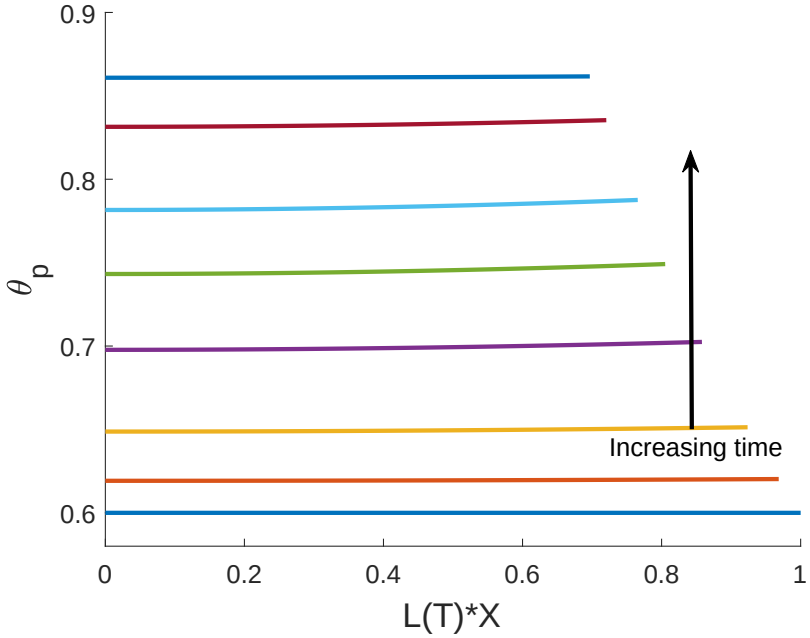

Figure 3.15: Spatial profile of θ_p as the gel contracts for the base case where polymer viscosity is dominant in Fig. 3.13 with $\xi = \mathcal{R} = \eta_s = 0.1$, showing that the gel evolves largely uniformly in space. Profiles are plotted (from bottom to top) at $T = 0, 0.2, 0.5, 1, 1.5, 2, 3, 5$. Other values as given in Fig. 3.13.

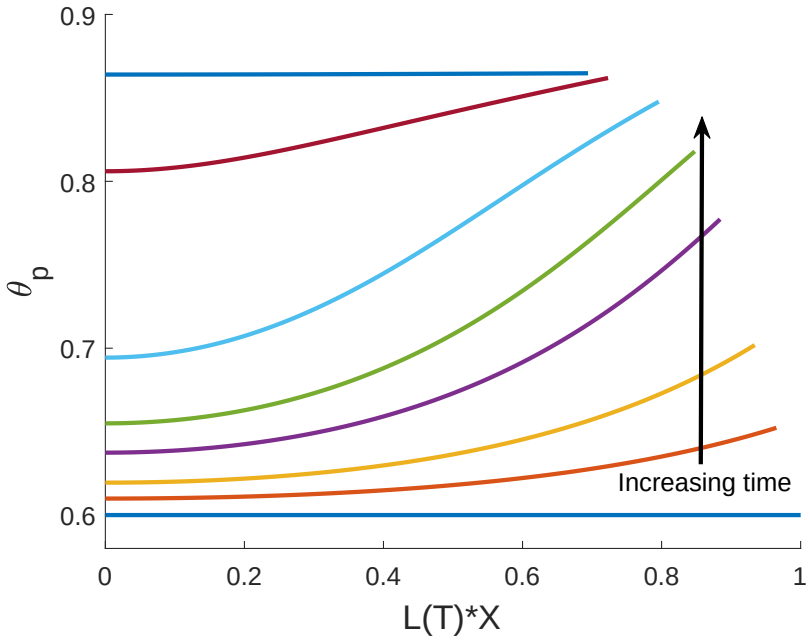

Figure 3.16: Spatial profile of θ_p as the gel contracts with large drag $\xi = 5$ and $\mathcal{R} = \eta_s = 0.1$, as seen in Fig. 3.13, showing that the gel evolves more rapidly at the boundary, with changes taking time to flow across the length of the gel. Profiles are plotted (from bottom to top) at $T = 0, 0.5, 1, 2, 3, 5, 10, 22$. Other values as given in Fig. 3.13.

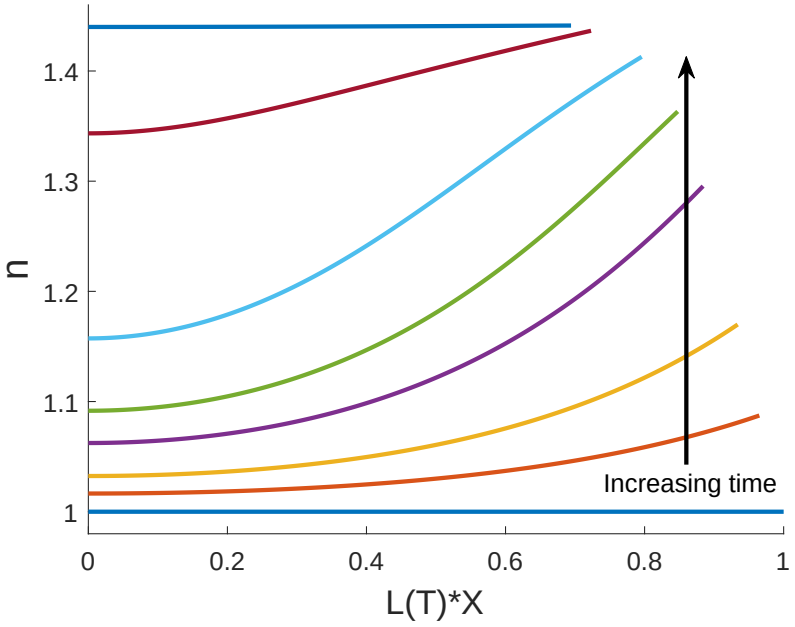

Figure 3.17: Spatial profile of n as the gel contracts with large drag $\xi = 5$ and $\mathcal{R} = \eta_s = 0.1$ as seen in Fig. 3.13, showing that, like θ_p, the cell density also increases most rapidly at $X = 1$. Profiles are plotted (from bottom to top) at $T = 0$, 0.5, 1, 2, 3, 5, 10, 22. Other values as given in Fig. 3.13.

$T \approx 7$), which slows down again as the gel moves towards its steady state ($T \approx 7$ to $T \approx 12$). From this lower initial value of θ_p, much greater contraction is evident in the gel, which reaches the steady state $\theta^* = 0.91$, $n^* = 4.54$, $L^* = 0.22$. The evolution of the gel length here is quite rapid until the gel approaches its steady state length ($T \approx 7$). With a larger initial polymer fraction, $\theta_i = 0.4$, the gel reaches the steady state $(\theta^*, n^*, L^*) = (0.89, 2.23, 0.45)$ (result not shown). In Fig. 3.12, we saw that with $\theta_i = 0.6$, the resulting steady state was $(\theta^*, n^*, L^*) = (0.86, 1.44, 0.69)$. This demonstrates that, with the initial cell density constant, there is a negative correlation between the initial fraction of polymer in the gel and the degree to which both the gel contracts (seen in L^*) and the polymer compacts (seen in θ^*). This negative correlation was seen in experiments presented in Stevenson *et al.* (2010). This example is discussed further in relation to other models in Section 3.8.

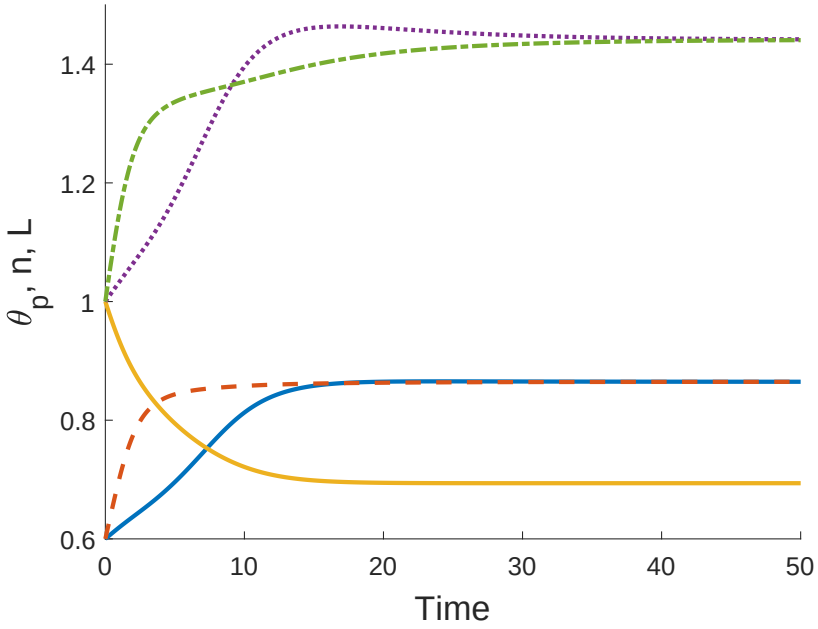

Figure 3.18: Time evolution of a cell-gel system. With small diffusion, the cell density and polymer fraction increase slightly above their equilibrium values at $X = 0$ before slowly reducing to the steady state. $L(T)$ is the solid gold line, $\theta_p(X = 0)$ is the solid blue line, $\theta_p(X = 1)$ is the dashed red line, $n(X = 0)$ is the dotted purple line, $n(X = 1)$ is the dash-dotted green line. Values as given in Fig. 3.13 with $\xi = 5$ and $D = 0.005$. $(\theta_p^*, n^*, L^*) = (0.86, 1.44, 0.69)$.

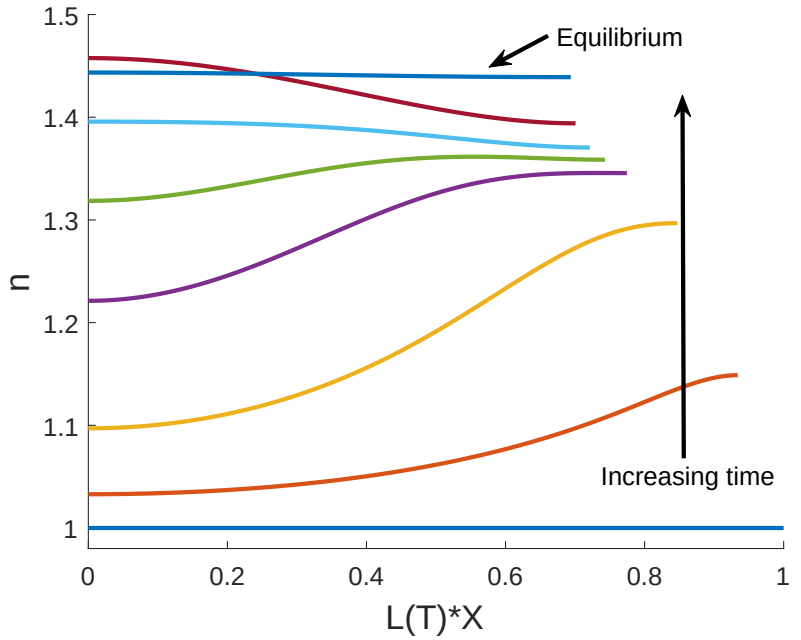

Figure 3.19: Spatial profile of n as the gel contracts with large drag $\xi = 5$ and a small diffusion coefficient $D = 0.005$. The added diffusion changes the dynamics compared to Fig. 3.17 as the gel contracts, with the cell density becoming larger towards $X = 0$ before easing back to a final uniform equilibrium. Profiles are plotted (from bottom to top) at $T = 0, 1, 3, 6, 8, 10, 14, 40$. Other values as given in Fig. 3.13.

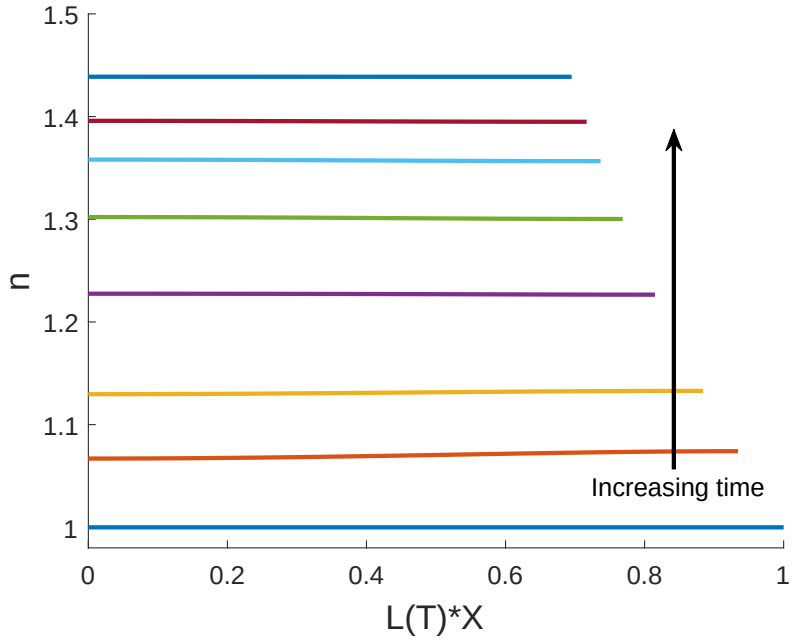

Figure 3.20: Spatial profile of n as the gel contracts with large drag $\xi = 5$ and large diffusion coefficient $D = 1$. Large diffusion means that, compared with Figs. 3.17 and 3.19, the cells remain spatially well spread as the gel contracts. Profiles are plotted (from bottom to top) at $T = 0, 1, 2, 4, 6, 8, 10, 18$. Other values as given in Fig. 3.13.

The negative correlation here is evident when looking at the mass conservation relations in equation (3.53) with spatially uniform steady states and initial conditions, which give

$$L^*\theta^* = \theta_i, \qquad L^*n^* = 1; \tag{3.114}$$

this also implies that $n^* = \theta^*/\theta_i$. We see that the decrease in θ^* and n^* with θ_i increasing, as in the examples above, requires an increase in the equilibrium length L^* to conserve mass for these quantities.

We note that we see similar behaviour take place in a cell-free gel. For example, amending the example in Fig. 3.21 such that $\theta_i = 0.2$, $n_i = 0$, $\chi = 1.5$, the gel evolves in a similar manner, with a slow initial phase of polymer compaction followed by rapid evolution and then slowing near the steady state (see Fig. 3.23). In this instance, the gel equilibrates with $\theta^* = 0.86$, $L^* = 0.23$. Furthermore, taking $\theta_i = 0.4$ and $\theta_i = 0.6$, we reach steady states of $(\theta^*, L^*) = (0.86, 0.47)$ and $(\theta^*, L^*) = (0.86, 0.70)$ respectively

(result not shown for $\theta_i = 0.4$; see Fig. 3.9 for $\theta_i = 0.6$). While the equilibrium fraction of polymer is the same regardless of the initial condition in the cell-free case (provided the same free energy parameters are used), we see that the change in gel length is also negatively correlated with the initial polymer fraction here. This is clear from the condition $L^*\theta^* = \theta_i$ in equation (3.114), given θ^* is fixed by the free energy parameters in the cell-free case. These results indicate that the presence of cells is therefore necessary to see the negative correlation between initial and final polymer fractions.

3.7.7 *Non-uniform initial conditions*

The numerical simulations presented thus far have been performed using spatially uniform initial conditions. Despite spatial variations being evident while the gel is evolving, these initial conditions eventually produce spatially uniform steady states. This matches previous work such as Keener *et al.* (2011b) looking at cell-free models, wherein only spatially uniform equilibria are found.

We now consider examples with spatially non-uniform initial conditions, finding that these initial conditions can result in spatially varying equilibrium solutions. This is a novel behaviour arising in our model from the presence of cells. We will consider non-uniform initial conditions in both the polymer and cells separately.

We first evaluate a cell-free gel with a spatially varying initial polymer distribution; this allows us to establish a baseline against which we can evaluate the impact of cells. We take a gel as specified in Fig. 3.8 where $\theta_i = 0.6$ and $\chi = 0.75$, for which the gel swells to an equilibrium with $\theta^* = 0.45$ and $L^* = 1.34$. We add a spatially varying component to the initial condition for the polymer fraction, such that $\theta_i = 0.6 + 0.025\cos(\pi X)$; this corresponds to a gel where the polymer is slightly bunched at the gel's centre (where $X = 0$) and less than the mean value at the gel's edge (where $X = 1$). We note that this initial condition satisfies the symmetry condition $\partial\theta_p/\partial X = 0$ at $X = 0$. In Fig. 3.24, we see that this gel swells to the same steady state as for uniform $\theta_i = 0.6$, and evolves on a similar time scale (see Fig. 3.8 for comparison). In Fig. 3.25, we see the spatial distribution of polymer across the length of the gel at increasing points in time; the polymer, initially more concentrated towards $X = 0$,

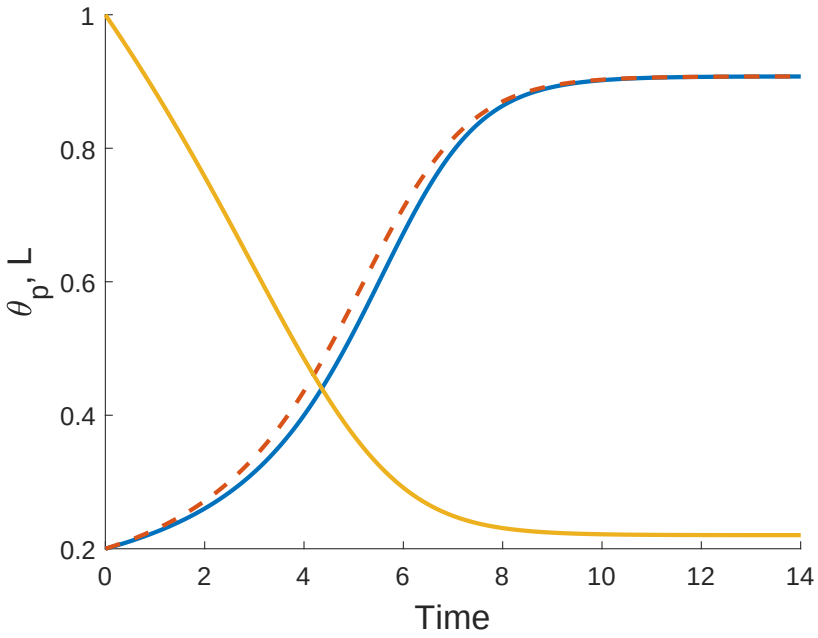

Figure 3.21: Time evolution of θ_p and L in a cell-gel system with a small initial polymer fraction $\theta_i = 0.2$. A significant degree of contraction occurs, resulting in a much smaller gel at equilibrium. $L(T)$ is the solid gold line, $\theta_p(X = 0)$ is the solid blue line, $\theta_p(X = 1)$ is the dashed red line. Values: $\theta_i = 0.2$, $n_i = 1$, $\chi = 0.75$, $\eta_s = 0.25$, $\xi = 0.5$, $\mathcal{R} = 0.5$, $\tau_0 = 1$, $D = 0.01$. $(\theta_p^*, n^*, L^*) = (0.91, 4.54, 0.22)$.

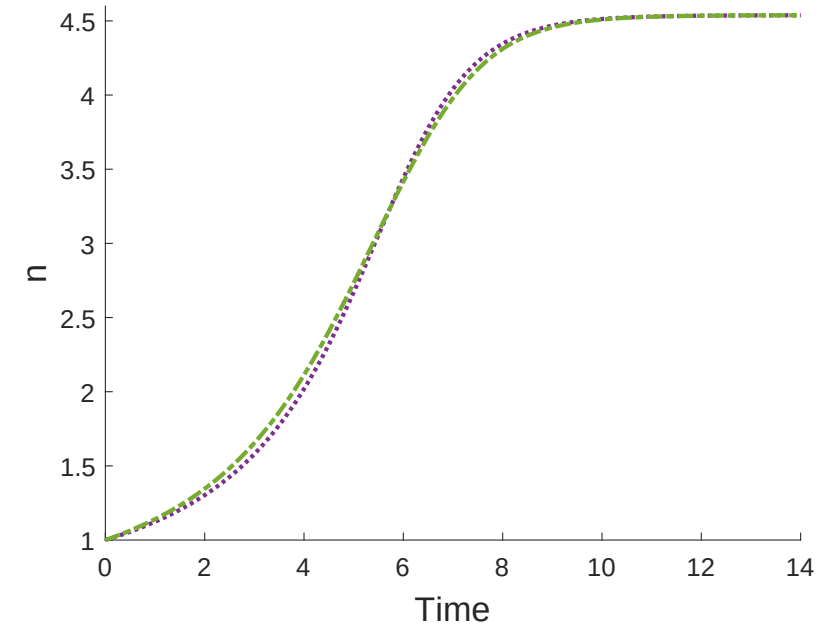

Figure 3.22: Time evolution of n in a cell-gel system with a small initial polymer fraction $\theta_i = 0.2$. A significant degree of contraction occurs, resulting in a much smaller gel at equilibrium. $n(X = 0)$ is the dotted purple line, $n(X = 1)$ is the dash-dotted green line. Values as given in Fig. 3.21.

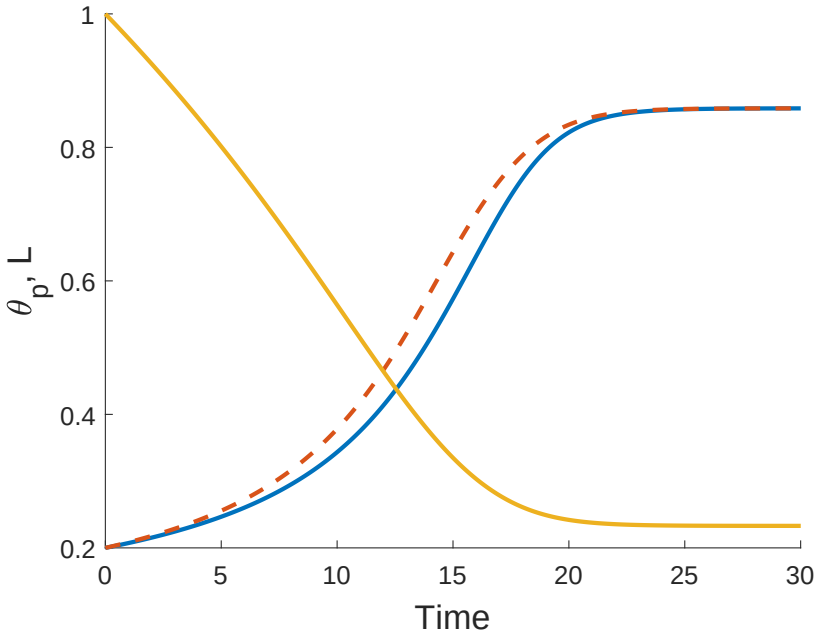

Figure 3.23: Time evolution of θ_p and L in a cell-free gel. In the absence of cells, the gel still contracts significantly from the small initial polymer fraction $\theta_i = 0.2$ and in a similar manner to Fig. 3.22. $L(T)$ is the solid gold line, $\theta_p(X = 0)$ is the solid blue line, $\theta_p(X = 1)$ is the dashed red line. Values: $\theta_i = 0.2$, $n_i = 0$, $\chi = 1.5$, $\eta_s = 0.25$, $\xi = 0.5$, $\mathcal{R} = 0.5$. $(\theta_p^*, L^*) = (0.86, 0.23)$.

smooths out over time as the gel swells, eventually becoming uniform as it expands to its steady state where θ^* is constant. Therefore, in the simulations we have seen, spatial variations in the initial polymer distribution in a cell-free gel do not affect the equilibrium outcome.

We now take the same gel with a spatially varying polymer initial condition and include a cell population where $n_i = 1$ and $\tau_0 = 1$, noting that $D = 0$. The time evolution for this gel is shown in Fig. 3.26; we see that the gel, which swelled in the absence of cells due to osmotic effects, now contracts to an equilibrium with spatially non-uniform solutions for both the polymer fraction and cell density. The mean equilibrium values of θ_p and n here, ($\bar{\theta}^* = 0.86$, $\bar{n}^* = 1.44$), are the same as the steady state found in Fig. 3.12. Figs. 3.27 and 3.28 show the spatial distributions of θ_p and n respectively over time. In contrast to the cell-free case, the cell forces present in the system are stronger than the chemical potentials, and so induce the gel to contract. We see that the polymer is initially less compacted towards $X = 1$; it must therefore contract more in this region to move to its steady state value. As the fraction of polymer increases in this region,

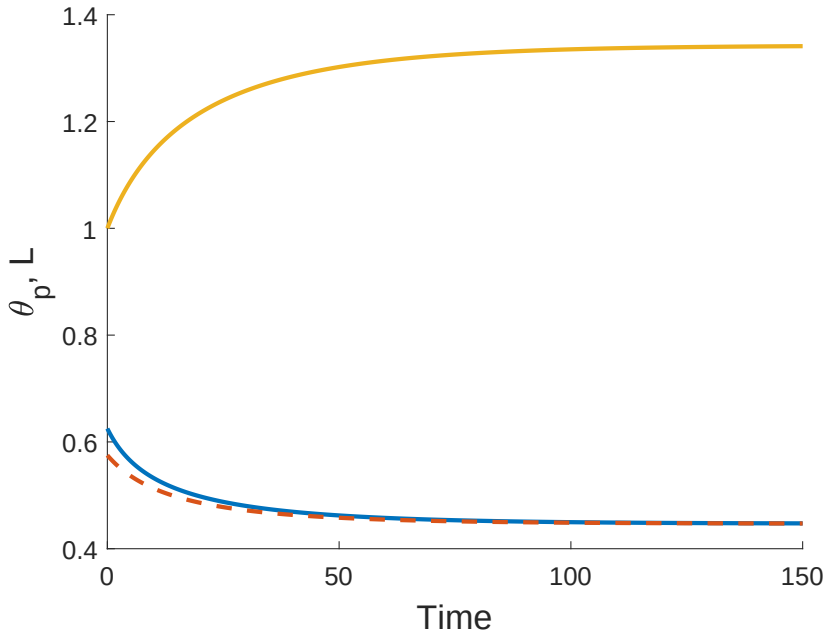

Figure 3.24: Time evolution of a cell-free gel with non-uniform initial polymer fraction. The gel swells to a spatially uniform steady state. $L(T)$ is the solid gold line, $\theta_p(X=0)$ is the solid blue line, $\theta_p(X=1)$ is the dashed red line. Values: $\theta_i = 0.6 + 0.025\cos(\pi X)$, $n_i = 0$, $\chi = 0.75$, $\eta_s = 0.25$, $\xi = 0.5$, $\mathcal{R} = 0.5$. $(\theta_p^*, L^*) = (0.45, 1.34)$.

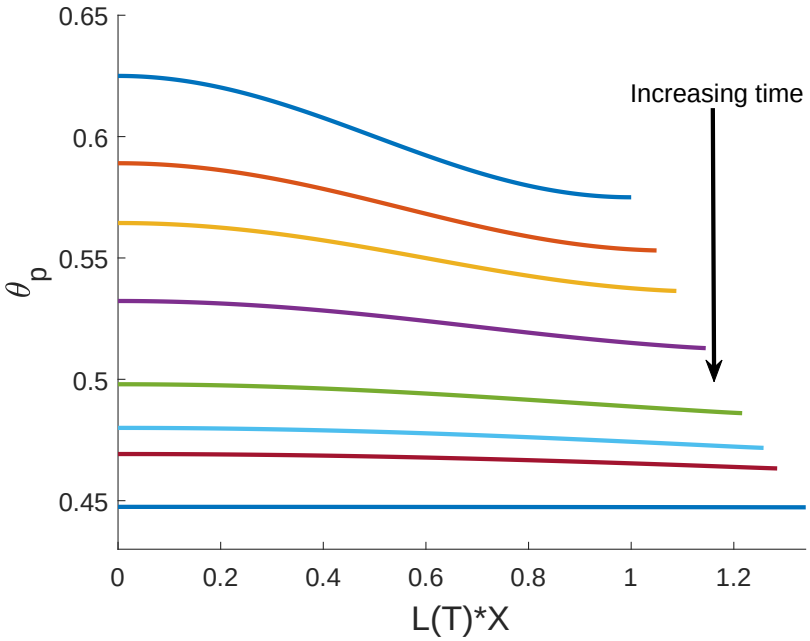

Figure 3.25: Spatial profile of θ_p for the case shown in Fig. 3.24 as the gel swells from a non-uniform initial condition. Profiles are plotted (from top to bottom) at $T = 0, 2.5, 5, 10, 20, 30, 40, 150$. Values as given in Fig. 3.24.

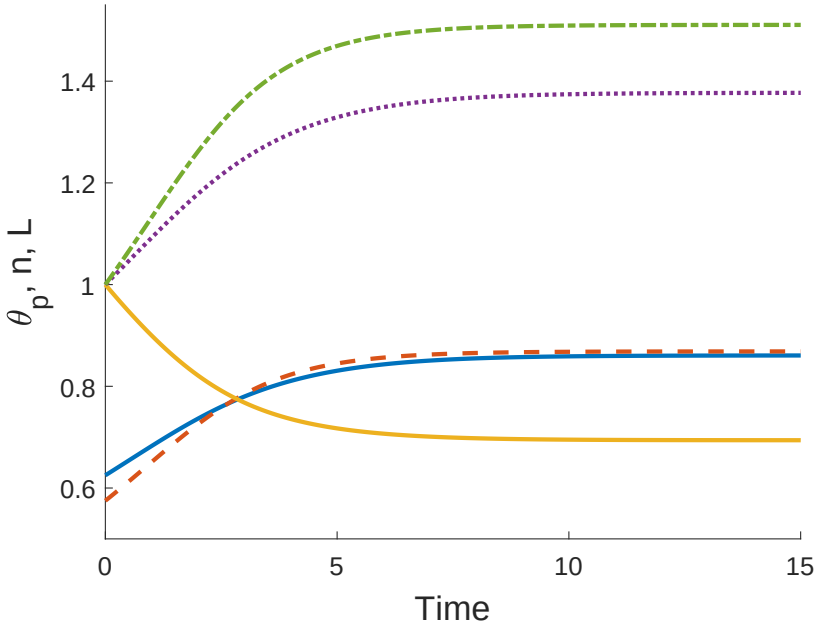

Figure 3.26: Time evolution of a cell-gel system with non-uniform initial polymer fraction. The gel contracts to a spatially-varying steady state. $L(T)$ is the solid gold line, $\theta_p(X=0)$ is the solid blue line, $\theta_p(X=1)$ is the dashed red line, $n(X=0)$ is the dotted purple line, $n(X=1)$ is the dash-dotted green line. Values: $\theta_i = 0.6 + 0.025\cos(\pi X)$, $n_i = 1$, $\chi = 0.75$, $\eta_s = 0.25$, $\xi = 0.5$, $\mathcal{R} = 0.5$, $\tau_0 = 1$, $D = 0$. $(\bar{\theta}^*, \bar{n}^*, L^*) = (0.86, 1.44, 0.69)$.

cells then become more concentrated, which reinforces this non-uniform evolution by pulling more polymer and cells towards the edge of the gel. The presence of non-zero drag also contributes to the formation of the spatial gradients seen, as discussed earlier. With $D = 0$, there is no requirement for the cells to even out over time, and therefore, we see a non-uniform distribution remaining at equilibrium. By the end of the process, the polymer fraction has ended slightly larger at $X = 1$ than at $X = 0$, reflecting the greater density of cells in that region.

We now take the same system and change the spatial perturbation to the initial condition from the polymer fraction to the cell density, such that our initial conditions are $n_i = 1 + 0.05\cos(\pi X)$, $\theta_i = 0.6$. This corresponds to a gel where the cells are now initially more densely seeded at $X = 0$ (*i.e.* the centre of a gel that is symmetric about the origin). In the time evolution for this system, shown in Fig. 3.29, we see the gel reaches a steady state with the same mean polymer fraction and cell density as the previous example, albeit with different spatial distributions. Fig. 3.30 confirms that the

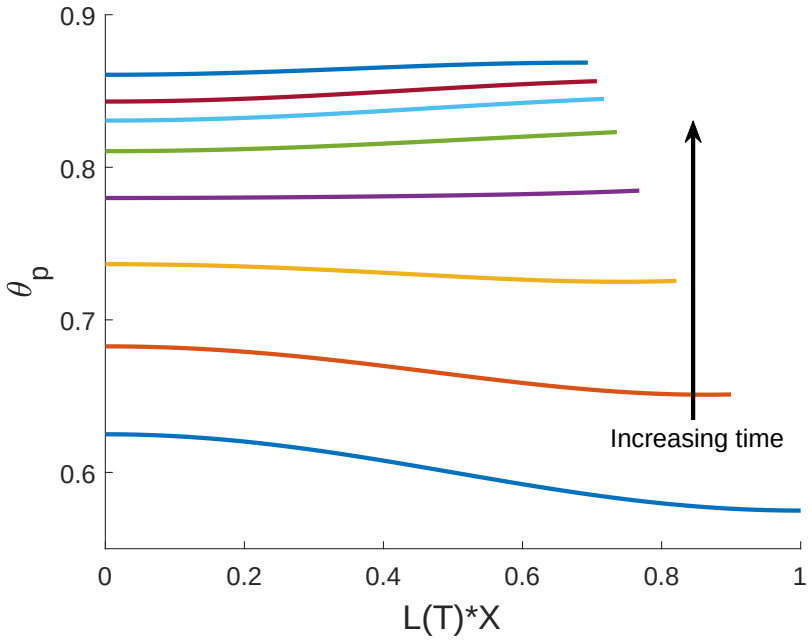

Figure 3.27: Spatial profile of θ_p for the case shown in Fig. 3.26 as the gel contracts from a non-uniform polymer initial condition. Profiles are plotted (from bottom to top) at $T = 0, 1, 2, 3, 4, 5, 6, 15$. Values as given in Fig. 3.26.

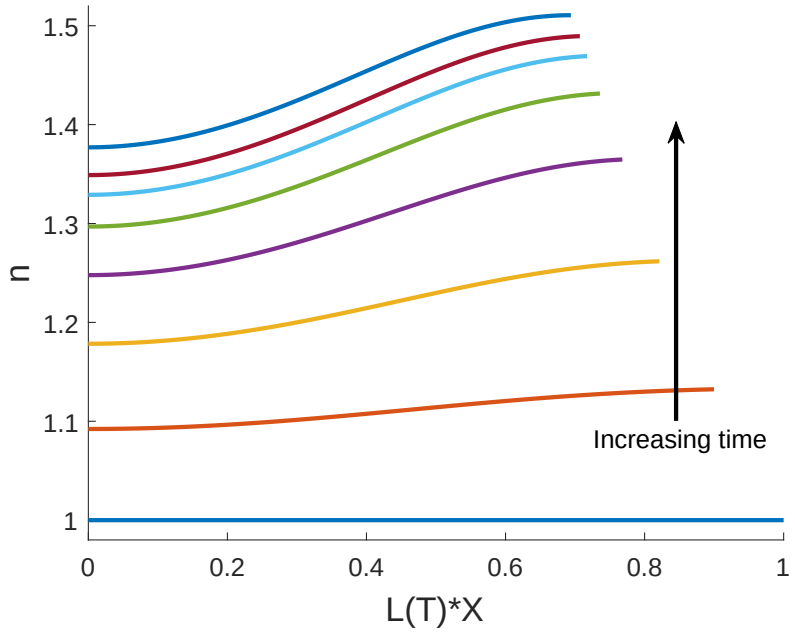

Figure 3.28: Spatial profile of n for the case shown in Fig. 3.26 as the gel contracts from a non-uniform polymer initial condition. Spatial variations appear in the cell profile in response to the non-uniformity in polymer. Profiles are plotted (from bottom to top) at $T = 0, 1, 2, 3, 4, 5, 6, 15$. Values as given in Fig. 3.26.

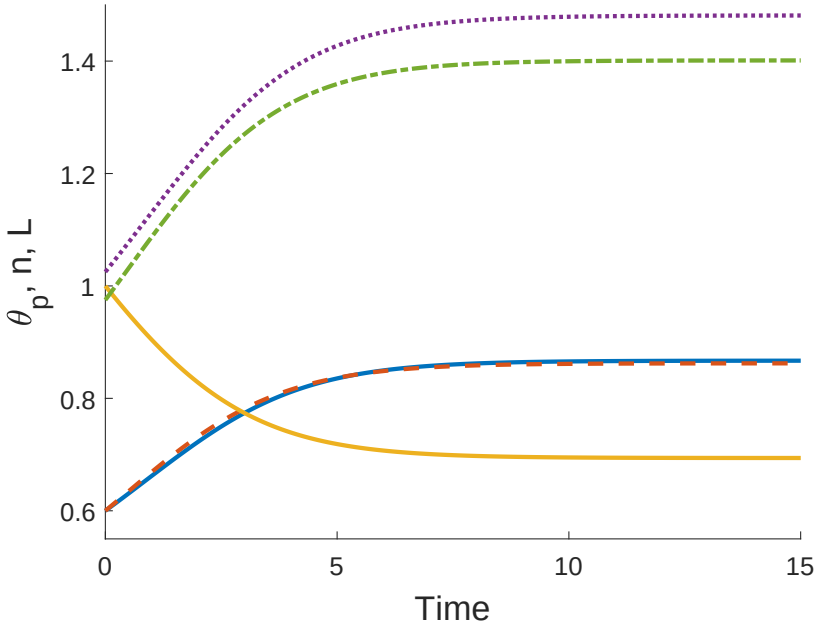

Figure 3.29: Time evolution of a cell-gel system with non-uniform initial cell density and uniform initial polymer fraction. The gel contracts to a steady state with non-uniform profiles for n and θ_p. $L(T)$ is the solid gold line, $\theta_p(X = 0)$ is the solid blue line, $\theta_p(X = 1)$ is the dashed red line, $n(X = 0)$ is the dotted purple line, $n(X = 1)$ is the dash-dotted green line. Values: $\theta_i = 0.6$, $n_i = 1 + 0.025\cos(\pi X)$, $\chi = 0.75$, $\eta_s = 0.25$, $\xi = 0.5$, $\mathcal{R} = 0.5$, $\tau_0 = 1$, $D = 0$. $(\bar{\theta}^*, \bar{n}^*, L^*) = (0.86, 1.44, 0.69)$.

polymer velocity v_p goes to zero across the spatial domain over time, demonstrating that the gel is maintaining its equilibrium state. The spatial profiles here are displayed in Figs. 3.31 and 3.32. The presence of drag creates a slight increase in both θ_p and n at $X = 1$ while the gel evolves. As the gel approaches its steady state, the evolution at $X = 1$ slows while the polymer fraction and cell density continue to increase across the rest of the domain. Greater cell concentrations around $X = 0$ result in polymer being pulled to the gel centre, and finally, a higher polymer fraction in this region at equilibrium. At this resulting steady state, we see that the amplitude of the cell profile is greater than the amplitude of n_i (the amplitude is approximately 0.04 at equilibrium and 0.025 initially), while the polymer fraction is slightly larger at $X = 0$ compared to $X = 1$, in contrast to the previous example.

These non-uniform equilibria have been found with diffusion $D = 0$. As shown in Section 3.4, for the gel to equilibrate with $D \neq 0$, n^* and θ^* must be spatially uniform. Therefore, adding diffusion to these simulations will always result in a spatially

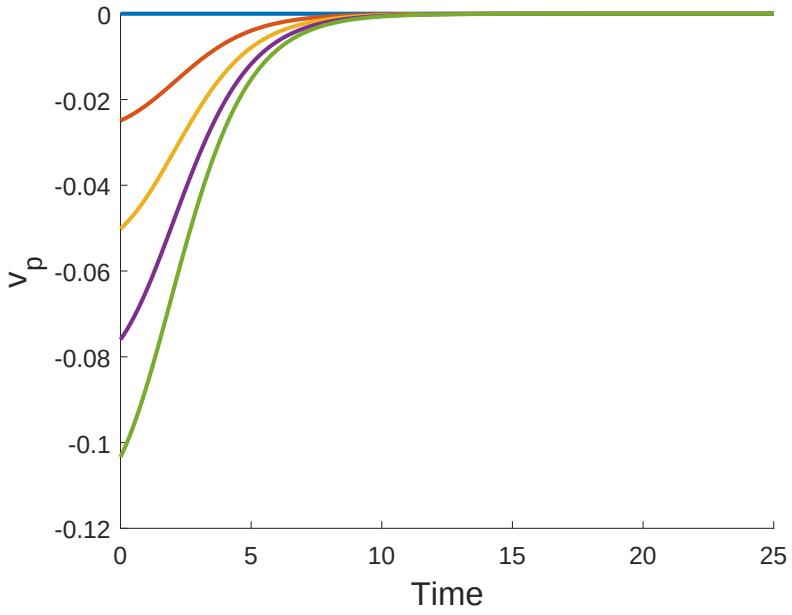

Figure 3.30: Time evolution of velocity v_p at different points in the spatial domain. The velocity goes to zero across the spatial domain as the gel reaches its spatially varying equilibrium before $T = 20$. In descending order initially, $v_p(0, T)$ is the blue line, $v_p(0.25, T)$ is the red line, $v_p(0.5, T)$ is the yellow line, $v_p(0.75, T)$ is the purple line, $v_p(1, T)$ is the green line. Values as given in Fig. 3.29.

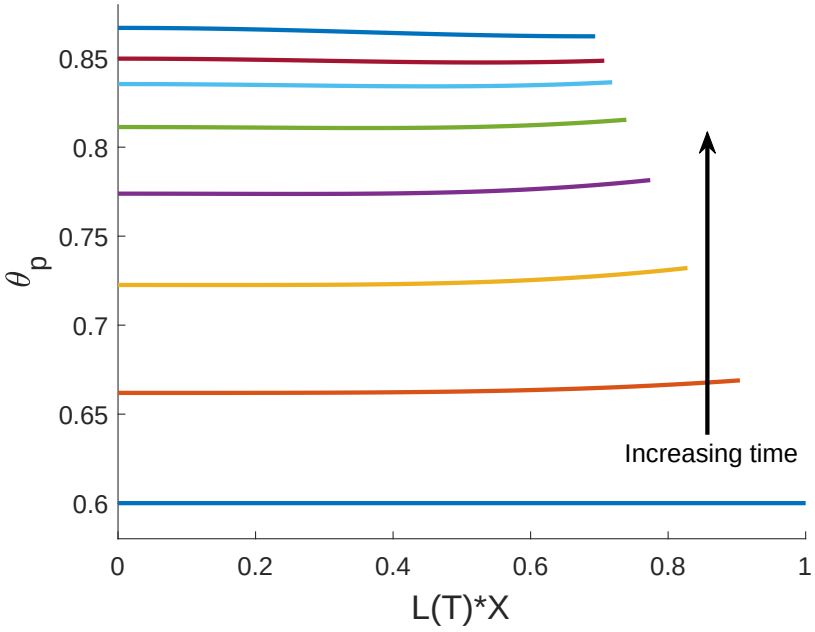

Figure 3.31: Spatial profile of θ_p for the case shown in Fig. 3.29 as the gel contracts from a non-uniform cell initial condition. Spatial variations emerge in the polymer profile which are maintained at equilibrium. Profiles are plotted (from bottom to top) at $T = 0$, 1, 2, 3, 4, 5, 6, 15. Values as given in Fig. 3.29.

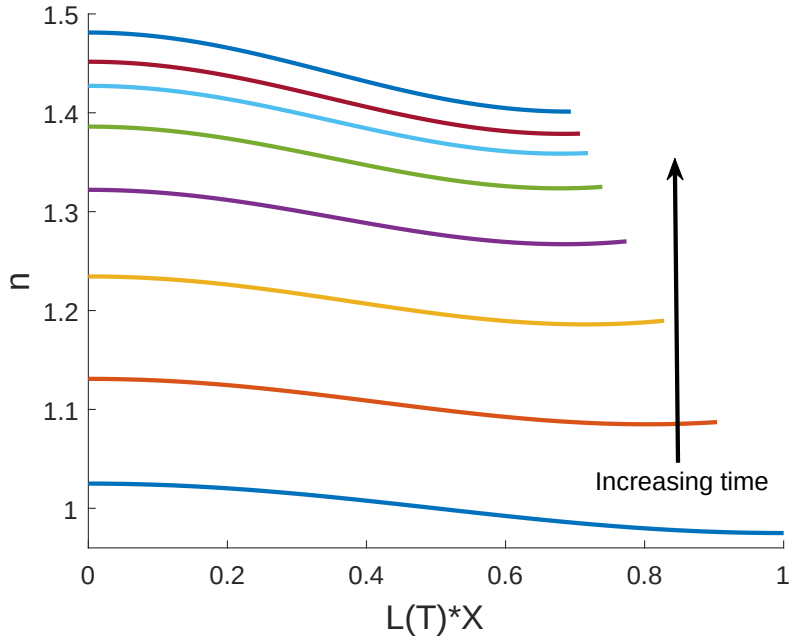

Figure 3.32: Spatial profile of n for the case shown in Fig. 3.29 as the gel contracts from a non-uniform cell initial condition. Spatial variations persist in the cell profile to equilibrium. Profiles are plotted (from bottom to top) at $T = 0$, 1, 2, 3, 4, 5, 6, 15. Values as given in Fig. 3.29.

uniform steady state on a long enough time horizon, with the additional random cell motion smoothing the cell profile, and subsequently, polymer profile as well. In Fig. 3.33, we see that with a non-uniform initial cell distribution as in the previous example, but with $D = 0.01$, the gel moves towards a uniform equilibrium in both cells and polymer. We have found that with small diffusion parameters (*e.g.* $D = 0.0005$), the gel will reach a quasi-steady state with non-uniform spatial profiles like those seen in Fig. 3.29; from this state, as seen in Fig. 3.34, the gel moves very slowly towards a uniform value over time due to diffusive motion (finally equilibrating at $T \approx 700$, not shown).

3.7.8 *Oscillating behaviour*

Our model exhibits a novel behaviour where the cell density and polymer fraction will spatially oscillate as the system evolves, *i.e.* parts of the gel will switch back and forth between swelling and contraction over time; this is displayed in Fig. 3.35. In this

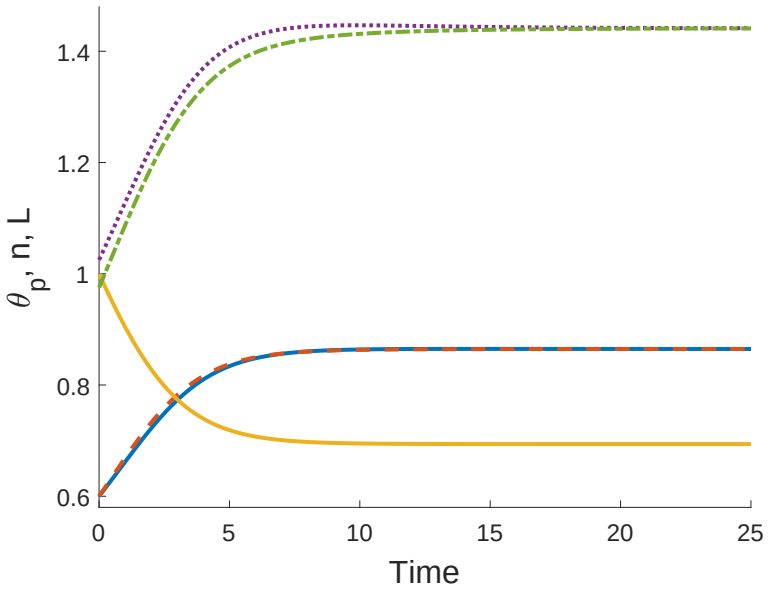

Figure 3.33: Time evolution of a gel with non-uniform cell initial condition. Adding diffusion $D = 0.01$ here to the example shown in Fig. 3.29 leads to uniform spatial equilibria, equal to the mean equilibrium values found in Fig. 3.29. $L(T)$ is the solid gold line, $\theta_p(X = 0)$ is the solid blue line, $\theta_p(X = 1)$ is the dashed red line, $n(X = 0)$ is the dotted purple line, $n(X = 1)$ is the dash-dotted green line. Values otherwise as given in Fig. 3.29. $(\theta^*, n^*, L^*) = (0.86, 1.44, 0.69)$.

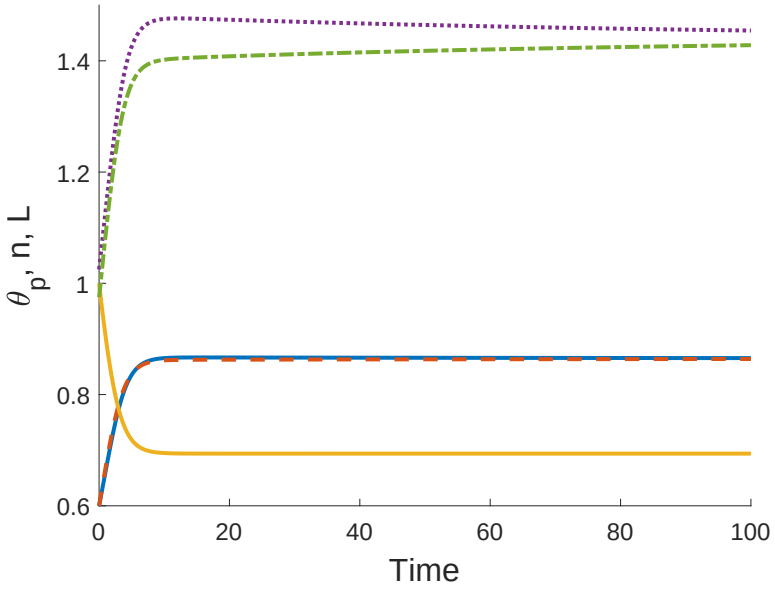

Figure 3.34: Time evolution of a gel with non-uniform cell initial condition and a very small diffusion coefficient $D = 0.0005$. The gel reaches a similar state to that in Fig. 3.29 by $T \approx 10$, before slowly moving to a uniform steady state over time. $L(T)$ is the solid gold line, $\theta_p(X = 0)$ is the solid blue line, $\theta_p(X = 1)$ is the dashed red line, $n(X = 0)$ is the dotted purple line, $n(X = 1)$ is the dash-dotted green line. Values otherwise as given in Fig. 3.29. $(\theta^*, n^*, L^*) = (0.86, 1.44, 0.69)$.

case, uniform initial conditions are used, with $\theta_i = 0.5$ and $n_i = 1$, while there is a negative mixing parameter $\chi = -0.1$ (indicating that the polymer and solvent would prefer to mix) and fairly strong cell traction $\tau_0 = 0.8$. This behaviour emerges from the combination of parameters leading to the cell traction stress being finely balanced with the free energy. We have found that it also requires both the drag parameter ξ and the resistance parameter $\mathcal{R}$ to be sufficiently large ($\xi = \mathcal{R} = 1.5$ here for example), otherwise these oscillations are not evident. We note that this behaviour occurs on a very long time scale and that the gel eventually dissolves in this situation (with $\theta_p \to 0$). The length of the gel increases monotonically over time (result not shown).

This behaviour comes about as a result of the competition between osmotic effects working to expand the gel and cell traction acting to contract it. The interface resistance slows the evolution at $X = 1$, while due to the presence of drag, steep gradients develop in the polymer fraction and cell density as the gel swells, with θ_p and n decreasing most near $X = 1$. These significant gradients can be seen in the spatial profiles for θ_p shown in Fig. 3.36. Large variations in the cell density are similarly evident between the two ends of the spatial domain (result not shown). The greater density of cells around $X = 0$ produces a gradient such that the cell force starts to pull polymer back towards $X = 0$. The gel then contracts locally in this region, while still swelling across the domain towards $X = 1$. Eventually, the chemical potential gradients are such across the domain that the gel starts swelling for all X again, with these local fluctuations repeating once more as the gel slowly expands in a non-uniform manner. Over a long enough time frame, the gel eventually dissolves.

In Figs. 3.37 - 3.39, we see the effect of reducing the interface resistance and drag in these simulations. With resistance and drag each taken separately to be small (Figs. 3.37 and 3.38 respectively), we see reduced oscillations in the gel; however, this behaviour still occurs. When both parameters are taken to be small, the oscillations are no longer present and the gel dissolves in a more typical manner (see Fig. 3.39). Similarly, with very small diffusion (*e.g.* $D \approx 0.0001$) the oscillations occur, but larger diffusion coefficients smooth out spatial gradients in the cell density and so prevent this oscillating behaviour from occurring (results not shown).

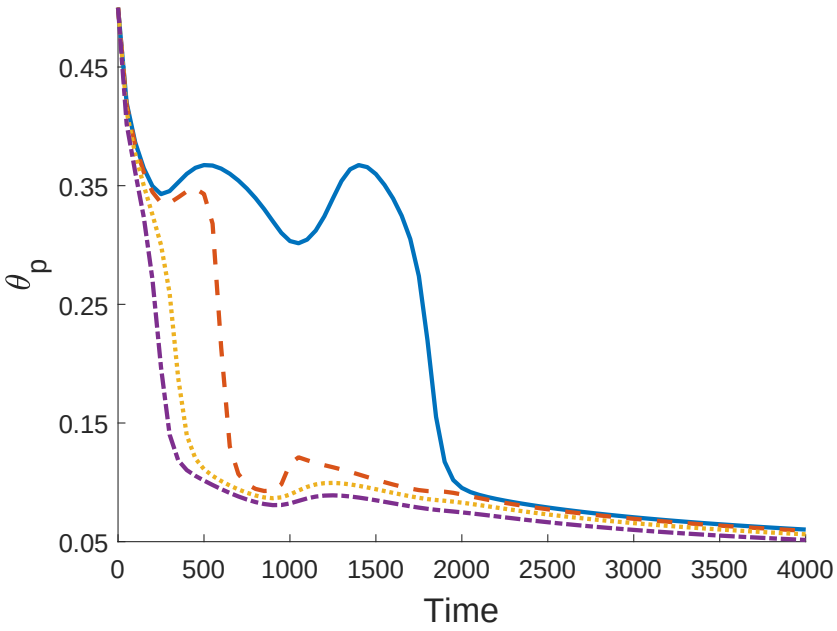

Figure 3.35: Time evolution of θ_p for a swelling gel with oscillating behaviour. The gel eventually dissolves as it continues to swell. $\theta_p(X = 0)$ is the solid blue line, $\theta_p(X = 0.33)$ is the dashed red line, $\theta_p(X = 0.66)$ is the dotted gold line, $\theta_p(X = 1)$ is the dash-dotted purple line. Values: $\theta_i = 0.5$, $n_i = 1$, $\chi = -0.1$, $\eta_s = 0.1$, $\xi = 1.5$, $\mathcal{R} = 1.5$, $\tau_0 = 0.8$, $D = 0$.

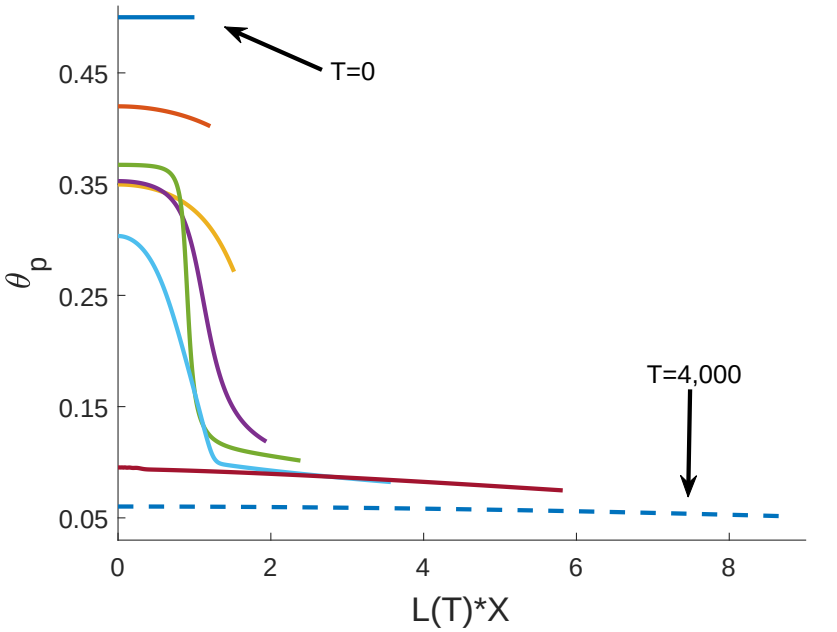

Figure 3.36: Spatial profile of polymer for the case seen in Fig. 3.35 as the polymer fraction oscillates. Lines with increasing length correspond to increasing points at time. Profiles are plotted (with increasing gel length) at $T = 0$, 50, 200, 350, 500, 1000, 2000, 4000. Values as given in Fig. 3.35.

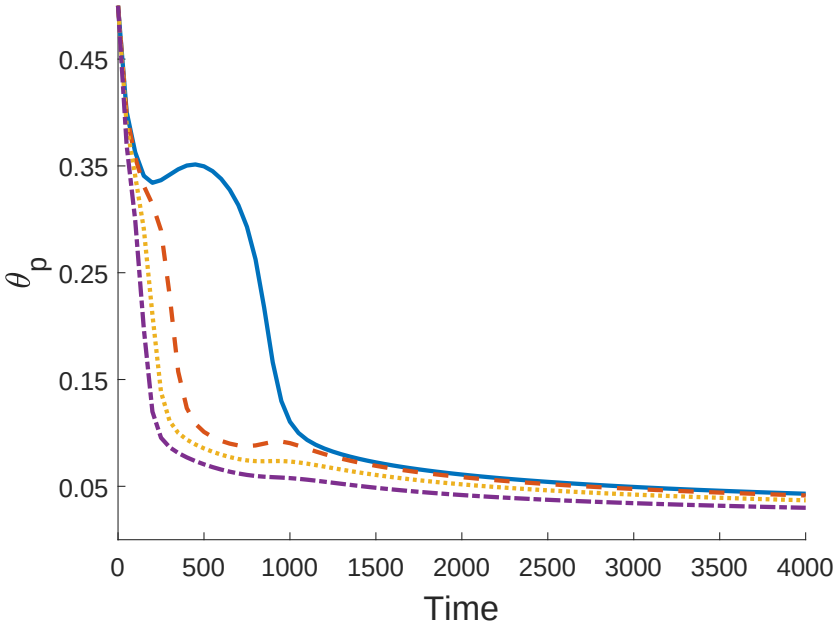

Figure 3.37: Reduced oscillations are seen in θ_p as the resistance parameter is reduced to $\mathcal{R} = 0.5$. $\theta_p(X = 0)$ is the solid blue line, $\theta_p(X = 0.33)$ is the dashed red line, $\theta_p(X = 0.66)$ is the dotted gold line, $\theta_p(X = 1)$ is the dash-dotted purple line. Values otherwise as given in Fig. 3.35.

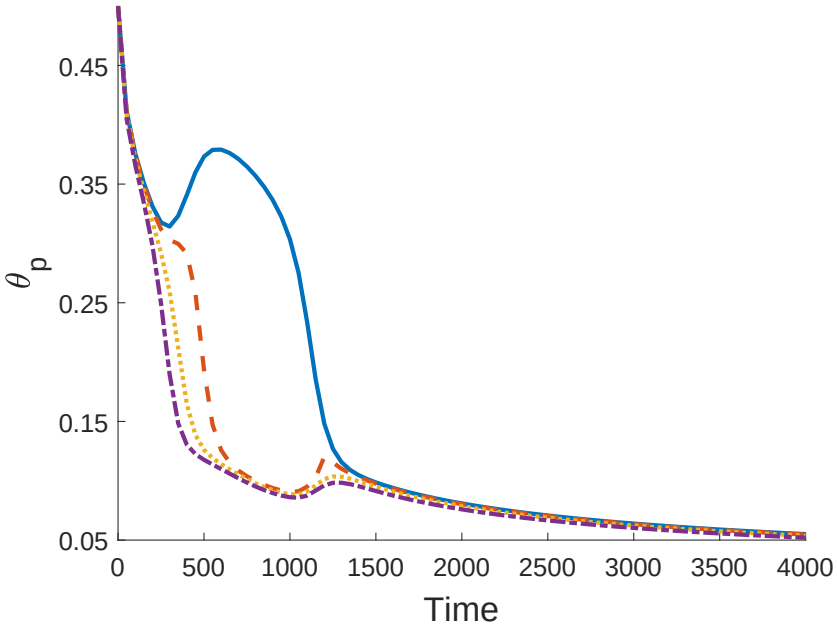

Figure 3.38: Reduced oscillations are also seen in θ_p as drag is reduced to $\xi = 0.5$. $\theta_p(X = 0)$ is the solid blue line, $\theta_p(X = 0.33)$ is the dashed red line, $\theta_p(X = 0.66)$ is the dotted gold line, $\theta_p(X = 1)$ is the dash-dotted purple line. Values otherwise as given in Fig. 3.35.

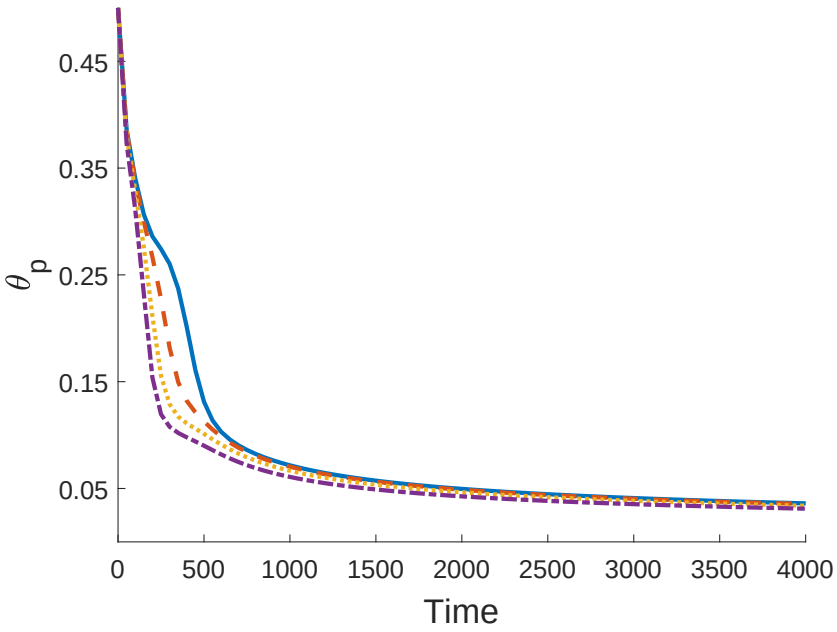

Figure 3.39: With $\xi = \mathcal{R} = 0.5$, oscillations are no longer seen in θ_p as the gel swells. $\theta_p(X = 0)$ is the solid blue line, $\theta_p(X = 0.33)$ is the dashed red line, $\theta_p(X = 0.66)$ is the dotted gold line, $\theta_p(X = 1)$ is the dash-dotted purple line. Values otherwise as given in Fig. 3.35.

3.8 DISCUSSION

In this chapter, we have analysed the cell-gel model developed in Chapter 2 in 1D Cartesian coordinates. This has allowed us to develop a thorough understanding of the conditions under which the gel equilibrates, the conditions affecting the early time behaviour and the stability of the system, and, through numerical analysis, the qualitative behaviours that can occur. Throughout this chapter, we have seen that the balance between chemical potentials and cell-derived forces is crucial in the gel's mechanical behaviour. We have shown that the presence of cells can cause a gel that would otherwise swell to contract; meanwhile, sufficiently strong osmotic forces can cause a gel to swell even with cells present. Moreover, the initial fraction of polymer was shown to negatively correlate with the final polymer fraction in cell-gel systems, and negatively correlate with the final gel length with or without cells present.

In Sections 3.4 - 3.6, we studied the long and short time behaviour of the gel, showing that it is governed by the balance between cell and osmotic forces. The gel equilibrates

when the cell and solvent potentials inside the gel are in balance with the external free energy; similarly, the early time behaviour and stability of equilibria is determined by the gradients of these functions inside the gel. Through deriving an analytic solution for the system's short time behaviour, we investigated how steady states respond to spatial perturbations and determined whether these perturbations will grow or decay.

This analysis also allowed us to evaluate how steady state values and stability change with variations in parameter values. As discussed in Section 2.4, due to the boundary conditions we use, the standard free energy constants μ_s^0 and μ_p^0 do not appear in the final system of equations. As a result of this, we are not able to reproduce the examples of bistable equilibria presented in Keener *et al.* (2011a) where μ_p^0 is varied against θ_p. However, as mentioned in Section 2.4, the parameters μ_p^0 and μ_s^0 are typically not present in studies using the Flory-Huggins free energy.

In a laboratory setting, this analysis of parameter values and steady state outcomes can be used to predict experimental outcomes given specific gel configurations, *e.g.* suggesting whether a gel will equilibrate or dissolve, or if a different configuration is needed to reach a desired experimental result. This analysis may also allow for physical parameter values to be determined given comparison with experimental results. For example, if we are given experimental data for an initial gel configuration and its subsequent equilibrium state, we may be able to determine that particular parameters must lie within certain ranges through comparison with such steady state diagrams as presented in 3.6.6.

In Section 3.7, we presented novel results relating to the gel's evolution, these being the presence of non-uniform equilibria and the case where the polymer fraction and cell density oscillate between increases and decreases. Spatially non-uniform steady states were found to eventuate in the cell-gel system from non-uniform initial conditions in the polymer fraction or cell density in the absence of diffusion. With small diffusion, quasi-steady states were found where the gel evolved to a state with spatial variations present in the variables, but which then gradually smoothed over time. In the oscillating case, due to competition between the free energy and cell traction, we see the fraction of polymer and the cell density repeatedly fluctuate within a spatial region

as the gel swells, before it eventually dissolves. To our knowledge, this behaviour has not been described in the literature before; this could be investigated experimentally.

Recent experimental work has suggested using osmotic pressure as a way to impose a desired mechanical compression on cells cultured *in vitro* (Dolega *et al.*, 2017; Monnier *et al.*, 2016). Our model provides a framework to quantify and evaluate such methods. Although to our knowledge, no one has yet used osmotic pressure to impose dynamic cycles of compression or tension on cells within a gel, our results suggest that this might be possible by, for example, changing the composition of the solution in the solvent bath surrounding the gel as a function of time. Again, this model could be used to predict the ensuing cycles of gel expansion and contraction, as well as to match the frequency and amplitude of these cycles to those seen *in vivo*. This might be beneficial in culturing cartilage cells for example, where oscillating stresses can lead to better mechanical and cell properties in the cells and tissues grown *in vitro* (Salinas *et al.*, 2018). Oscillating fluid flow has also been seen to be an important mechanism in areas like proteoglycan production (Eifler *et al.*, 2006) and regulating calcium concentrations (Edlich *et al.*, 2001).

Our analysis has focussed on the qualitative behaviours predicted by our model in a simple 1D setting. To facilitate greater comparison with experiments, for example that presented in Moon and Tranquillo (1993), a couple of different steps could be taken. An extension to our work here, if a consistent set of data for relevant experiments was available, would be to fit such experimental data for our model parameters and initial conditions, allowing for a more direct comparison between these experiments and simulations like those presented in Section 3.7. Transforming the model to spherically symmetric coordinates would also help in comparing our results with models looking at spheres of gel like those in Moon and Tranquillo (1993) and Green *et al.* (2013), although we note that, given that such a model would be one-dimensional in the gel's radius r, we would not expect significantly different qualitative outcomes to those seen with our model here, which is one-dimensional in the gel's length.

In Figs. 3.21 and 3.22, we saw the contraction of a gel with a small initial polymer fraction. In this instance, the polymer fraction and cell density increased gradually at the beginning and end of the gel's evolution, bookending a period of rapid contrac-

tion where θ_p and n increased significantly. This behaviour is comparable to examples of mechanically-driven gel contraction presented in Moon and Tranquillo (1993) and Green *et al.* (2013). There was an initial lag in the evolution of the gel's radius seen in Green's model which replicates experimental observations from Moon and Tranquillo (1993). This initial lag was not present in Moon and Tranquillo's mathematical model, and similarly, we did not see an initial lag in changes to the gel's length in our simulations. Moon and Tranquillo posit that the initial delay seen experimentally is a consequence of the cells spreading after being seeded; it may not be present in our simulations as a consequence of the cells being smoothly distributed at initial time, therefore not requiring a lead time to redistribute themselves through the gel as may happen *in vitro*.

We also saw in Section 3.7.6 that, with all else held constant, the gel reached a smaller equilibrium length with a smaller initial polymer fraction. Similarly, with cells present, a smaller initial polymer fraction resulted in a larger value for the polymer fraction at equilibrium. Our model therefore captures the negative correlation between the initial polymer concentration and final concentration highlighted in the experimental study presented by Stevenson *et al.* (2010), who also reference this behaviour occurring in experiments such as Zhu *et al.* (2001) and Evans and Barocas (2009).

In the absence of cells, in Fig. 3.23 and associated simulations, we saw that decreasing the initial polymer fraction θ_i similarly led to gels with a smaller equilibrium length, *i.e.* gels that have contracted further. Without cells, the equilibrium value of the polymer fraction θ^* is determined by the parameters in the free energy function; therefore, unlike what was seen for cell-gel systems, θ^* remained the same with increases in θ_i. We can therefore see that cell forces play an important role in the negative correlation between initial and final polymer concentrations seen experimentally.

Studies such as Barocas *et al.* (1995) that estimate the value of the cell traction parameter τ_0 typically do so using models that focus on cell-gel mechanics, *i.e.* they do not include the presence of chemical potentials. We have demonstrated herein that chemical potentials can counteract cell traction and affect the degree of gel contraction witnessed. This therefore indicates that without considering the free energy in the gel-solvent system, current models may in fact underestimate the magnitude of cell

traction stresses, since the degree of compaction in the experiment will also depend on the mixing energy of the polymer and solvent. It also highlights that the measure of the traction parameter may be quite experiment-specific, depending on the particular configuration of the gel and surrounding fluid. This is supported by Fig. 3.4, where we see the balance between cell traction τ_0 and mixing energy χ that maintains the same equilibrium value of polymer; increasing χ indicates that the gel can equilibrate with a smaller value of τ_0, and vice versa.

We remark that while we have chosen a particular form for the cell force function G here, other modelling choices have been used. Green *et al.* (2013) for example numerically investigate numerous different cell force functions: the Murray force function similar to that described in Section 2.3; a 'preferred ECM density' function; and functions incorporating chemical concentration. Green *et al.* also consider whether contact inhibition should be incorporated in the form $\lambda\theta_p^2$ as opposed to the form λn^2, *i.e.* acting on the polymer network instead of the cell density. An extension to this work would be to consider different forms of the cell force function, and again, given consistent experimental data to fit the model, to determine if better agreement is found with particular choices.

In the Moon and Tranquillo (1993) study, the gel is constructed as a microsphere; however, in cell-gel experiments, the gels are often thin layers, where the height of the gel is small relative to its length or radius. Therefore, another extension to this model is to study the gel as a two-dimensional thin film, exploiting the ratio of the film's vertical and horizontal length scales as a small parameter to rescale the system and derive a reduced system of equations. In this way, gel behaviour in different experimental settings might be compared and analysed. We derive such a model in the following chapter.

4

2D THIN FILM MODEL

4.1 INTRODUCTION

Having considered the cell-gel model in a one-dimensional geometry in Chapter 3, we now investigate gel behaviour in a two-dimensional, thin film geometry. Many experiments into gel mechanics investigate such thin layers and discs of gel (see *e.g.* Barocas *et al.* (1995); Stevenson *et al.* (2010)), again focusing on the contraction of gels and the impact of cell-gel interactions. A key reason for the use of these thin films is that they are easier to construct in experiments compared to gel microspheres (such spheres were used in Moon and Tranquillo (1993) for example) (Green *et al.*, 2013). In studying the gel in this geometry, we therefore have two aims. Firstly, we would like to better understand the mechanics of the gel in the thin film environment, and secondly, we wish to compare the emergent behaviours in this system to those in the 1D case. Such a model considering the interacting effects of cell traction and osmotic pressure in the thin film geometry has not previously been presented.

We study the 2D Cartesian coordinate system for simplicity of modelling and to facilitate comparison with the 1D Cartesian model presented in the previous chapter. To develop a tractable model in the thin film setting, we will exploit the small inverse aspect ratio of the thin film (the ratio of the film's vertical and horizontal length scales) to simplify our 2D model. Our goal is to derive a new leading order, 1D model which again incorporates osmotically-driven solvent flow alongside cell traction stress in the gel. Once more, we hypothesise that the balance between chemical potentials and cell traction stress will be crucial in determining the equilibrium outcome for the gel.

In this chapter, we first briefly discuss studies into thin film flows. We then move into the model derivation, adapting the model presented in Chapter 2 to fit a 2D Cartesian thin film geometry. We demonstrate how, through our choice of scaling, we can derive a leading order, extensional flow model, wherein the system is reduced to a 1D set of equations in the x-coordinate. To conclude this chapter, we discuss this reduced model in comparison to the 1D model derived in Chapter 3. The thin film model will be further studied both analytically and numerically in Chapters 5 and 6.

A review of thin film and extensional flow models relevant to this chapter was presented in Section 1.4. We will build on such techniques in developing the thin film model in this chapter. The thin film models presented earlier do not consider the effects of osmotic swelling; to our knowledge, osmotic pressure has not been included in a multiphase, mechanical thin film model such as these.

The influence of osmotic pressure in a thin film environment has been looked at in the context of biofilm growth, in studies such as Trinschek *et al.* (2016, 2017). The aim of this work was to study the spreading of bacterial biofilms, driven by the osmotic movement of solution into the biofilm. The biofilm is modelled as a thin, biphasic material which is a mixture of solvent and biomass. The free energy in the system drives the influx of water from substrate into the biofilm as an osmotic pressure gradient; this drives the growth of the biofilm over time. As in our modelling, osmotic pressure is included as a chemical potential, with their models consisting of advection-diffusion equations for the thin film height and surfactant concentration.

While neither the modelling approach used in these studies by Trinschek *et al.* nor the biological problems themselves bear direct relevance to our work here (*e.g.* we consider a free boundary problem in the thin layer and solve for the velocities of the phases), one result which may be of interest in the thin gel environment is that of continuously spreading biofilms. This describes films which swell in a relatively uniform manner both vertically and horizontally until the film height reaches a particular level, at which point the film then only spreads out horizontally (see Fig. 3 in Trinschek *et al.* (2017) for example). In analysing the thin film model we develop here, we will consider whether the gel length and height change at the same relative rate or if any differences emerge as the gel swells or contracts.

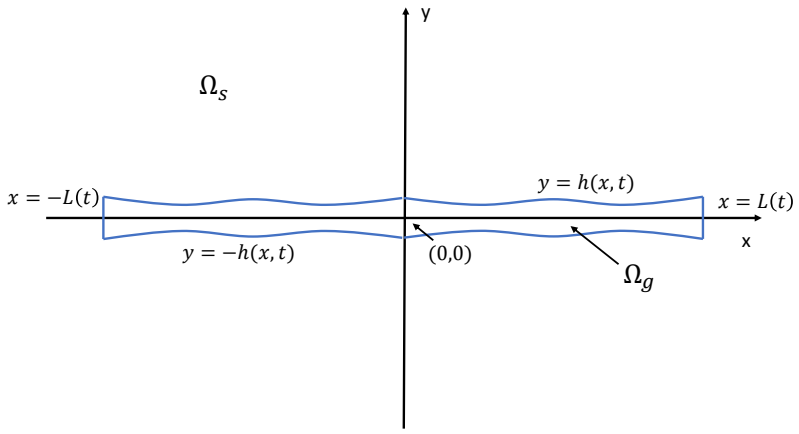

Figure 4.1: Thin film domain $\Omega = \Omega_g + \Omega_s$. Ω_g is the gel region with $\theta_p > 0$, $\theta_s > 0$ and cell density $n \geqslant 0$. Ω_s is the region of pure solvent surrounding the gel wherein $\theta_p = n = 0$ and $\theta_s = 1$. The gel is symmetric about the x-axis and y-axis, and the ratio of gel height to length is small.

4.3 2D MODEL FOR A THIN FILM OF GEL WITH CELLS

In this chapter, we consider a thin film of gel consisting of polymer and solvent; this gel is seeded with cells. We again study the model developed in Chapter 2, now using a two-dimensional, Cartesian coordinate system with spatial coordinates $\mathbf{x} = (x, y)$. The thin film is characterised by a small inverse aspect ratio, that is, a small vertical length scale relative to the horizontal length scale. The small parameter ε describes this inverse aspect ratio.

As seen in Fig. 4.1, the gel exists in the domain Ω_g, which is surrounded by the pure solvent domain Ω_s. We consider a gel that is symmetric about $y = 0$ and $x = 0$, with free boundaries for the gel height at $y = h(x,t)$ and $y = -h(x,t)$, as well as vertical free boundaries for the gel length at $x = L(t)$ and $x = -L(t)$. The centre-line of the gel is fixed at $y = 0$. We assume that all quantities are continuous and differentiable at $x = 0$ and $y = 0$. Due to the gel's symmetry, we restrict our attention to the region $0 \leqslant y \leqslant h$ and $0 \leqslant x \leqslant L$. As in Chapter 3, terms in the solvent region Ω_s will be denoted with the superscript e; all other terms refer to quantities in the gel region Ω_g.

The conservation of mass equations (2.2), (2.3) and (2.5) for the volume fractions of polymer and solvent as well as the cell density are

$$\frac{\partial \theta_p}{\partial t} + \frac{\partial}{\partial x}(\theta_p v_p) + \frac{\partial}{\partial y}(\theta_p w_p) = 0, \tag{4.1}$$

$$\frac{\partial \theta_s}{\partial t} + \frac{\partial}{\partial x}(\theta_s v_s) + \frac{\partial}{\partial y}(\theta_s w_s) = 0, \tag{4.2}$$

$$\frac{\partial n}{\partial t} + \frac{\partial}{\partial x}(n v_p) + \frac{\partial}{\partial y}(n w_p) = D\left(\frac{\partial^2 n}{\partial x^2} + \frac{\partial^2 n}{\partial y^2}\right). \tag{4.3}$$

We note here that our velocity vectors have the form

$$\boldsymbol{v_p} = (v_p, w_p), \quad \boldsymbol{v_s} = (v_s, w_s), \tag{4.4}$$

where v_p is the polymer velocity in the horizontal direction and w_p is the polymer velocity in the vertical direction, and similarly for the solvent. Adding equations (4.1) and (4.2) and using the no-voids condition $\theta_p + \theta_s = 1$ gives

$$\frac{\partial}{\partial x}(\theta_p v_p + \theta_s v_s) + \frac{\partial}{\partial y}(\theta_p w_p + \theta_s w_s) = 0. \tag{4.5}$$

For simplicity, we will henceforth take the solvent viscosities η_s and κ_s to be zero as in Green *et al.* (2017), which implies that the solvent stress tensor $\boldsymbol{\sigma}_s = 0$. We recall equations (2.8) and (2.9) describing conservation of momentum for the polymer and solvent phases,

$$\nabla \cdot (\theta_p \boldsymbol{\sigma_p}) - \theta_p \nabla \mu_p - \theta_p \nabla P + \nabla(\theta_p G) = \xi \theta_p \theta_s (\boldsymbol{v_p} - \boldsymbol{v_s}), \tag{4.6}$$

$$-\theta_s \nabla \mu_s - \theta_s \nabla P = -\xi \theta_p \theta_s (\boldsymbol{v_p} - \boldsymbol{v_s}). \tag{4.7}$$

Taking the sum of these equations and using the relation $\theta_p \nabla \mu_p = -\theta_s \nabla \mu_s$ (see (2.12) and (2.13)), we can express equation (4.6) in the form

$$\nabla \cdot (\theta_p \boldsymbol{\sigma}_p) - \nabla P + \nabla(\theta_p G) = 0. \tag{4.8}$$

Equations (4.7) and (4.8) are used as our momentum balance equations hereafter.

These momentum balance equations have the following two-dimensional forms,

$$\frac{\partial}{\partial x}\left(2\eta_p\theta_p\frac{\partial v_p}{\partial x}+\kappa_p\theta_p\left(\frac{\partial v_p}{\partial x}+\frac{\partial w_p}{\partial y}\right)\right)+\frac{\partial}{\partial y}\left(\eta_p\theta_p\left(\frac{\partial w_p}{\partial x}+\frac{\partial v_p}{\partial y}\right)\right) - \frac{\partial P}{\partial x}+\frac{\partial}{\partial x}(\theta_p G)=0, \tag{4.9}$$

$$\frac{\partial}{\partial x}\left(\eta_p\theta_p\left(\frac{\partial w_p}{\partial x}+\frac{\partial v_p}{\partial y}\right)\right)+\frac{\partial}{\partial y}\left(2\eta_p\theta_p\frac{\partial w_p}{\partial y}+\kappa_p\theta_p\left(\frac{\partial v_p}{\partial x}+\frac{\partial w_p}{\partial y}\right)\right) - \frac{\partial P}{\partial y}+\frac{\partial}{\partial y}(\theta_p G)=0, \tag{4.10}$$

$$\theta_s\frac{\partial \mu_s}{\partial x}+\theta_s\frac{\partial P}{\partial x}-\xi\theta_p\theta_s(v_p-v_s)=0, \tag{4.11}$$

$$\theta_s\frac{\partial \mu_s}{\partial y}+\theta_s\frac{\partial P}{\partial y}-\xi\theta_p\theta_s(w_p-w_s)=0. \tag{4.12}$$

We have the kinematic boundary conditions at $y=h(x,t)$ and $x=L(t)$,

$$w_p=\frac{\partial h}{\partial t}+v_p\frac{\partial h}{\partial x} \quad \text{at } y=h, \tag{4.13}$$

$$v_p=\frac{dL}{dt} \quad \text{at } x=L. \tag{4.14}$$

On $y=h(x,t)$, the zero normal stress boundary condition on the gel-solvent interface (2.24) becomes

$$-\left(2\eta_p\theta_p\frac{\partial v_p}{\partial x}+\kappa_p\theta_p\left(\frac{\partial v_p}{\partial x}+\frac{\partial w_p}{\partial y}\right)-P_\triangle+\theta_p G\right)\frac{\partial h}{\partial x} +\eta_p\theta_p\left(\frac{\partial w_p}{\partial x}+\frac{\partial v_p}{\partial y}\right)=0, \tag{4.15}$$

$$-\left(\eta_p\theta_p\left(\frac{\partial w_p}{\partial x}+\frac{\partial v_p}{\partial y}\right)\right)\frac{\partial h}{\partial x}+2\eta_p\theta_p\frac{\partial w_p}{\partial y}+\kappa_p\theta_p\left(\frac{\partial v_p}{\partial x}+\frac{\partial w_p}{\partial y}\right) -P_\triangle+\theta_p G=0, \tag{4.16}$$

with the permeability condition (2.25) given as

$$-\mathcal{R}\theta_s(v_s-v_p)\frac{\partial h}{\partial x}\frac{1}{\sqrt{\frac{\partial h}{\partial x}^2+1}}+\mathcal{R}\theta_s(w_s-w_p)\frac{1}{\sqrt{\frac{\partial h}{\partial x}^2+1}}=P_\triangle+\mu_{s_\triangle}, \tag{4.17}$$

where $P_\triangle=P-P^e$ and $\mu_{s_\triangle}=\mu_s-\mu_s^e$. We note that the normal vector at $y=h$ is

$$\hat{\mathbf{n}}_h=\frac{1}{\sqrt{\frac{\partial h}{\partial x}^2+1}}\left(-\frac{\partial h}{\partial x},1\right). \tag{4.18}$$

Similarly, at $x = L$, the interface condition (2.24) becomes

$$2\eta_p\theta_p\frac{\partial v_p}{\partial x} + \kappa_p\theta_p\left(\frac{\partial v_p}{\partial x} + \frac{\partial w_p}{\partial y}\right) - P_\triangle + \theta_p G = 0, \tag{4.19}$$

$$\eta_p\theta_p\left(\frac{\partial w_p}{\partial x} + \frac{\partial v_p}{\partial y}\right) = 0, \tag{4.20}$$

with the permeability condition (2.25),

$$\mathcal{R}\theta_s(v_s - v_p) = P_\triangle + \mu_{s\,\triangle}, \tag{4.21}$$

where we have used the normal vector $\hat{\mathbf{n}}_L = (1, 0)$ at $x = L$.

Evaluating the force balance equations (4.9) - (4.10) in the solvent domain Ω_s, we find that the external pressure P^e is at most a function of time, *i.e.* $P^e = P^e(t)$; we also note that $\mu_s^e = f(0)$, where $f(0)$ is constant (see Chapter 3 for further details).

Given symmetry of n about $x = 0$, we have the boundary condition

$$\frac{\partial n}{\partial x} = 0 \quad \text{at } x = 0. \tag{4.22}$$

The no-flux cell boundary condition (2.22) indicates that

$$D\frac{\partial n}{\partial x} = 0 \quad \text{at } x = L, \tag{4.23}$$

and

$$-D\frac{\partial n}{\partial x}\frac{\partial h}{\partial x} + D\frac{\partial n}{\partial y} = 0 \quad \text{at } y = h. \tag{4.24}$$

By symmetry at $x = 0$, we have

$$v_p(0, y, t) = 0, \tag{4.25}$$

which indicates that

$$\frac{\partial v_p}{\partial y} = 0 \quad \text{at } x = 0. \tag{4.26}$$

Given that v_p is an even function about $y = 0$, we also have

$$\frac{\partial v_p}{\partial y} = 0 \quad \text{at } y = 0, \tag{4.27}$$

where we have assumed v_p is differentiable at $y = 0$. We similarly have by symmetry at $y = 0$,

$$w_p(x, 0, t) = 0, \tag{4.28}$$

which gives that

$$\frac{\partial w_p}{\partial x} = 0 \quad \text{at } y = 0. \tag{4.29}$$

Likewise, w_p is an even function about $x = 0$, such that

$$\frac{\partial w_p}{\partial x} = 0 \quad \text{at } x = 0, \tag{4.30}$$

where we have similarly assumed that w_p is differentiable at $x = 0$.

We now re-scale our system. As in Chapter 3, we let $\mathfrak{L} = L(0)$ be the length scale, $\mathfrak{N}$ be a characteristic cell density (typically set as the average cell density at $t = 0$), and choose the time scale to be the ratio of polymer viscosity η_p to the free energy scale $k_B\mathcal{T}/\nu_m$. We let $\mathcal{H}$ be the height scale, typically set as the average height at $t = 0$. Thus, the inverse aspect ratio is $\varepsilon = \mathcal{H}/\mathfrak{L}$. We therefore non-dimensionalise the independent variables as follows, where tildes denote dimensionless quantities,

$$x = \mathfrak{L}\tilde{x}, \quad y = \varepsilon\mathfrak{L}\tilde{y}, \quad t = \frac{\eta_p \nu_m}{k_B\mathcal{T}}\tilde{t},$$

with the dependent variables and functions being non-dimensionalised thus,

$$\begin{aligned}
&n = \mathfrak{N}\tilde{n}, \quad L(t) = \mathfrak{L}\tilde{L}(\tilde{t}), \quad h = \varepsilon\mathfrak{L}\tilde{h} = \mathcal{H}\tilde{h},\\
&v_p = \frac{\mathfrak{L}k_B\mathcal{T}}{\eta_p\nu_m}\tilde{v}_p, \quad v_s = \frac{\mathfrak{L}k_B\mathcal{T}}{\eta_p\nu_m}\tilde{v}_s, \quad w_p = \frac{\varepsilon\mathfrak{L}k_B\mathcal{T}}{\eta_p\nu_m}\tilde{w}_p, \quad w_s = \frac{\varepsilon\mathfrak{L}k_B\mathcal{T}}{\eta_p\nu_m}\tilde{w}_s,\\
&P = \frac{k_B\mathcal{T}}{\varepsilon^2\nu_m}\tilde{P}, \quad \mu_s = \frac{k_B\mathcal{T}}{\varepsilon^2\nu_m}\tilde{\mu}_s.
\end{aligned}$$

We note that the variables which are common to the 1D Cartesian model are scaled as previously in Chapter 3, with the exception of the pressure P and chemical potential μ_s which are scaled to be large at $\mathcal{O}(1/\varepsilon^2)$. The new variables which did not previously appear in the model – y, h, w_p and w_s – are assumed to be $\mathcal{O}(\varepsilon)$ in line with our thin film approximation.

After re-scaling, equation (4.3) becomes

$$\frac{\partial \tilde{n}}{\partial \tilde{t}} + \frac{\partial}{\partial \tilde{x}}(\tilde{n}\tilde{v}_p) + \frac{\partial}{\partial \tilde{y}}(\tilde{n}\tilde{w}_p) = \tilde{D}\frac{\partial^2 \tilde{n}}{\partial \tilde{x}^2} + \frac{\tilde{D}}{\varepsilon^2}\frac{\partial^2 \tilde{n}}{\partial \tilde{y}^2}, \tag{4.31}$$

where we have defined the non-dimensional diffusion coefficient

$$\tilde{D} = \frac{\eta_p \nu_m}{\mathfrak{L}^2 k_B \mathcal{T}} D, \tag{4.32}$$

which is scaled as in Chapter 3. The mass conservation equations (4.1) and (4.2) and kinematic boundary conditions (4.13) and (4.14) are unchanged after being re-scaled.

Following re-scaling, the momentum balance equations (4.9) - (4.12) have the form

$$\begin{aligned}
&\varepsilon^2\left\{\frac{\partial}{\partial \tilde{x}}\left(2\theta_p\frac{\partial \tilde{v}_p}{\partial \tilde{x}} + \tilde{\kappa}_p\theta_p\left(\frac{\partial \tilde{v}_p}{\partial \tilde{x}} + \frac{\partial \tilde{w}_p}{\partial \tilde{y}}\right)\right) + \frac{\partial}{\partial \tilde{y}}\left(\theta_p\frac{\partial \tilde{w}_p}{\partial \tilde{x}}\right)\right\} - \frac{\partial \tilde{P}}{\partial \tilde{x}} \\
&\quad + \frac{\partial}{\partial \tilde{x}}\left(\theta_p\frac{\tilde{\tau}_0\tilde{n}^2}{1+\tilde{\lambda}\tilde{n}^2}\right) + \frac{\partial}{\partial \tilde{y}}\left(\theta_p\frac{\partial \tilde{v}_p}{\partial \tilde{y}}\right) = 0, &(4.33)\\
&\varepsilon^2\left\{\frac{\partial}{\partial \tilde{x}}\left(\theta_p\frac{\partial \tilde{w}_p}{\partial \tilde{x}}\right)\right\} + \frac{\partial}{\partial \tilde{x}}\left(\theta_p\frac{\partial \tilde{v}_p}{\partial \tilde{y}}\right) + \frac{\partial}{\partial \tilde{y}}\left(2\theta_p\frac{\partial \tilde{w}_p}{\partial \tilde{y}} + \tilde{\kappa}_p\theta_p\left(\frac{\partial \tilde{v}_p}{\partial \tilde{x}} + \frac{\partial \tilde{w}_p}{\partial \tilde{y}}\right)\right) \\
&\quad - \frac{1}{\varepsilon^2}\left\{\frac{\partial \tilde{P}}{\partial \tilde{y}} - \frac{\partial}{\partial \tilde{y}}\left(\theta_p\frac{\tilde{\tau}_0\tilde{n}^2}{1+\tilde{\lambda}\tilde{n}^2}\right)\right\} = 0, &(4.34)\\
&\theta_s\frac{\partial \tilde{\mu}_s}{\partial \tilde{x}} + \theta_s\frac{\partial \tilde{P}}{\partial \tilde{x}} - \tilde{\xi}\theta_p\theta_s(\tilde{v}_p - \tilde{v}_s) = 0, &(4.35)\\
&\theta_s\frac{\partial \tilde{\mu}_s}{\partial \tilde{y}} + \theta_s\frac{\partial \tilde{P}}{\partial \tilde{y}} - \varepsilon^2\tilde{\xi}\theta_p\theta_s(\tilde{w}_p - \tilde{w}_s) = 0, &(4.36)
\end{aligned}$$

where we have defined the non-dimensional parameters

$$\tilde{\kappa}_p = \frac{\kappa_p}{\eta_p}, \quad \tilde{\xi} = \frac{\varepsilon^2\mathfrak{L}^2\xi}{\eta_p}, \quad \tilde{\tau}_0 = \frac{\varepsilon^2\nu_m\mathfrak{N}^2\tau_0}{k_B\mathcal{T}}, \quad \tilde{\lambda} = \mathfrak{N}^2\lambda. \tag{4.37}$$

Note that $\tilde{\xi}$ and $\tilde{\tau}_0$ are taken to be $\mathcal{O}(1)$. Hence, they encode our assumptions about the strength of the unscaled drag and cell traction parameters, *i.e.* they are assumed to be large here at $\mathcal{O}(1/\varepsilon^2)$. The terms in (4.37) are otherwise scaled as in the 1D model.

We non-dimensionalise the interface conditions (4.15) - (4.17) at $y = h$ to obtain

$$
\begin{aligned}
&-\varepsilon^2\left\{2\theta_p\frac{\partial\tilde{v}_p}{\partial\tilde{x}}+\tilde{\kappa}_p\theta_p\left(\frac{\partial\tilde{v}_p}{\partial\tilde{x}}+\frac{\partial\tilde{w}_p}{\partial\tilde{y}}\right)\right\}\frac{\partial\tilde{h}}{\partial\tilde{x}}+\varepsilon^2\theta_p\frac{\partial\tilde{w}_p}{\partial\tilde{x}}\\
&\quad-\left(\tilde{P}_\triangle-\theta_p\frac{\tilde{\tau}_0\tilde{n}^2}{1+\tilde{\lambda}\tilde{n}^2}\right)\frac{\partial\tilde{h}}{\partial\tilde{x}}+\theta_p\frac{\partial\tilde{v}_p}{\partial\tilde{y}}=0, \qquad (4.38)\\
&-\varepsilon^2\theta_p\frac{\partial\tilde{w}_p}{\partial\tilde{x}}\frac{\partial\tilde{h}}{\partial\tilde{x}}-\theta_p\frac{\partial\tilde{v}_p}{\partial\tilde{y}}\frac{\partial\tilde{h}}{\partial\tilde{x}}+2\theta_p\frac{\partial\tilde{w}_p}{\partial\tilde{y}}+\tilde{\kappa}_p\theta_p\left(\frac{\partial\tilde{v}_p}{\partial\tilde{x}}+\frac{\partial\tilde{w}_p}{\partial\tilde{y}}\right)\\
&\quad-\frac{1}{\varepsilon^2}\left(\tilde{P}_\triangle-\theta_p\frac{\tilde{\tau}_0\tilde{n}^2}{1+\tilde{\lambda}\tilde{n}^2}\right)=0, \qquad (4.39)\\
&-\tilde{\mathcal{R}}\theta_s(\tilde{v}_s-\tilde{v}_p)\frac{\partial\tilde{h}}{\partial\tilde{x}}\frac{1}{\sqrt{\varepsilon^2\frac{\partial\tilde{h}}{\partial\tilde{x}}^2+1}}+\tilde{\mathcal{R}}\theta_s(\tilde{w}_s-\tilde{w}_p)\frac{1}{\sqrt{\varepsilon^2\frac{\partial\tilde{h}}{\partial\tilde{x}}^2+1}}\\
&\quad=\tilde{P}_\triangle+\tilde{\mu}_{s\triangle}, \qquad (4.40)
\end{aligned}
$$

where the non-dimensional resistance parameter is defined

$$\tilde{\mathcal{R}}=\frac{\varepsilon^3\mathfrak{L}\mathcal{R}}{\eta_p}. \qquad (4.41)$$

As with the drag and cell traction parameters ($\tilde{\xi}$ and $\tilde{\tau}_0$ respectively) above, the scaled resistance parameter is taken to be $\mathcal{O}(1)$, indicating that resistance is a significant influence in the thin film model. The resistance here is scaled to be large at $\mathcal{O}(1/\varepsilon^3)$, as distinct from the scaling in the 1D Cartesian model.

The interface conditions (4.19) - (4.21) at $x = L$ after re-scaling have the form

$$
\begin{aligned}
2\theta_p\frac{\partial\tilde{v}_p}{\partial\tilde{x}}+\tilde{\kappa}_p\theta_p\left(\frac{\partial\tilde{v}_p}{\partial\tilde{x}}+\frac{\partial\tilde{w}_p}{\partial\tilde{y}}\right)-\frac{1}{\varepsilon^2}\left(\tilde{P}_\triangle-\theta_p\frac{\tilde{\tau}_0\tilde{n}^2}{1+\tilde{\lambda}\tilde{n}^2}\right)&=0, \qquad (4.42)\\
\varepsilon^2\theta_p\frac{\partial\tilde{w}_p}{\partial\tilde{x}}+\theta_p\frac{\partial\tilde{v}_p}{\partial\tilde{y}}&=0, \qquad (4.43)\\
\tilde{\mathcal{R}}\theta_s(\tilde{v}_s-\tilde{v}_p)&=\varepsilon(\tilde{P}_\triangle+\tilde{\mu}_{s\triangle}). \qquad (4.44)
\end{aligned}
$$

The no-flux boundary condition (4.24) at $y = h$ is re-scaled such that

$$-\varepsilon^2\tilde{D}\frac{\partial\tilde{n}}{\partial\tilde{x}}\frac{\partial\tilde{h}}{\partial\tilde{x}}+\tilde{D}\frac{\partial\tilde{n}}{\partial\tilde{y}}=0. \qquad (4.45)$$

We henceforth drop tildes from non-dimensional quantities.

We have scaled a number of variables and parameters in the model to be large. We assume a balance between the pressure P and cell traction parameter τ_0 at $\mathcal{O}(1/\varepsilon^2)$ in the force balance equation (4.34) and interface condition (4.39) with both P and τ_0 scaled to be large; this is necessary to derive a non-trivial reduction to the model. This then leads to a relation at leading order in equation (4.33) between pressure, cell force and viscous terms. Scaling the chemical potential to be large in equations (4.35) and (4.36) is also required for a non-trivial model reduction and ensures that both chemical and cell potentials contribute to the leading order momentum balance, while large drag in equation (4.35) is needed to couple together the polymer and solvent axial velocities. A large resistance parameter is required in interface condition (4.38) to maintain continuity as solvent flows across the long gel-solvent interface.

We now expand our variables in powers of ε as follows, and substitute these expansions into our model equations,

$$\begin{aligned}
\theta_p &= \theta_{p_0} + \varepsilon\theta_{p_1} + \varepsilon^2\theta_{p_2} + ..., \\
n &= n_0 + \varepsilon n_1 + \varepsilon^2 n_2 + ..., \\
h &= h_0 + \varepsilon h_1 + \varepsilon^2 h_2 + ..., \\
v_p &= v_{p_0} + \varepsilon v_{p_1} + \varepsilon^2 v_{p_2} + ...,
\end{aligned}$$

and similarly for θ_s, v_s, w_p, w_s, P and L. Unlike previous work discussed in Section 1.4, we expand our variables here in powers of ε instead of ε^2. This is due to the $\mathcal{O}(\varepsilon)$ term which appears in interface condition (4.44) after the model is re-scaled. The $\mathcal{O}(\varepsilon)$ terms do not contribute to the leading order model derived in this chapter, but they are included here for completeness.

4.3.1 *Demonstrating the y-independence of leading order dependent variables*

We begin by showing that the leading order cell density n_0, pressure P_0, polymer fraction θ_{p_0} and polymer axial velocity v_{p_0} do not depend on y. This facilitates the

derivation of simplified mass and momentum equations, as we will demonstrate subsequently.

Now, from equation (4.31) at $\mathcal{O}(1/\varepsilon^2)$,

$$D\frac{\partial^2 n_0}{\partial y^2} = 0. \tag{4.46}$$

At leading order, the no-flux boundary condition (4.45) gives $D\partial n_0/\partial y = 0$ at $y = h_0$. Integrating (4.46) and applying this no-flux boundary condition, we have

$$D\frac{\partial n_0}{\partial y} = 0, \tag{4.47}$$

and so $n_0 = n_0(x,t)$. Note that we have assumed $D \neq 0$ here to derive this condition for n_0. We will look at equation (4.31) at $\mathcal{O}(1)$ later in the model derivation to obtain a leading order expression for $\partial n_0/\partial t$.

Considering (4.34) at $\mathcal{O}(1/\varepsilon^2)$, we have

$$\frac{\partial \Pi_0}{\partial y} = 0, \tag{4.48}$$

where we have defined $\Pi_0 = P_0 - \theta_{p_0} G_0$, noting that $G_0 = G(n_0(x,t))$. This implies that

$$\Pi_0 = \Pi_0(x,t). \tag{4.49}$$

From interface condition (4.39), at $y = h_0$,

$$P_0 - P_0^e(t) - \theta_{p_0} G_0 = 0. \tag{4.50}$$

We have found that $P_0^e(t)$ and higher order equivalent terms do not feature in the final system of equations; therefore, without loss of generality, we now set $P^e = 0$, and as such, $P_\triangle = P$ for each order of ε. Accordingly, applying (4.50), we find

$$\Pi_0 = 0, \tag{4.51}$$

and so

$$P_0 = \theta_{p_0} G_0. \tag{4.52}$$

We note that this result holds for all y and, accordingly, holds everywhere in our system.

At $\mathcal{O}(1)$, equation (4.36) yields

$$\theta_{s_0} \frac{\partial}{\partial y} (\mu_{s_0} + \theta_{p_0} G_0) = 0, \tag{4.53}$$

where $\mu_{s_0} = \mu_s(\theta_{p_0})$; therefore,

$$\theta_{s_0} \left(\frac{\partial \mu_{s_0}}{\partial \theta_p} + G_0 \right) \frac{\partial \theta_{p_0}}{\partial y} = 0. \tag{4.54}$$

Now, for (4.54) to hold, we must have that $\partial \theta_{p_0}/\partial y = 0$ or that $\partial \mu_{s_0}/\partial \theta_p = -G_0$. Given that G_0 is independent of y and that $\mu_{s_0} = \mu_s(\theta_{p_0})$, both these conditions imply that we must have

$$\theta_{p_0} = \theta_{p_0}(x, t), \tag{4.55}$$

i.e. at leading order, θ_{p_0} is independent of y, and accordingly, μ_{s_0} is as well. Similarly, we have now found that $P_0 = P_0(x, t)$ by equation (4.52). We note that for equation (4.55) to be true at all times, it must also hold for the initial polymer fraction $\theta_i(x, y)$, *i.e.* our initial condition must satisfy $\partial \theta_i(x, y)/\partial y = 0$.

Using our definition for Π_0 together with equation (4.33) at leading order, we have

$$-\frac{\partial \Pi_0}{\partial x} + \frac{\partial}{\partial y} \left(\theta_{p_0} \frac{\partial v_{p_0}}{\partial y} \right) = 0. \tag{4.56}$$

Noting from (4.51) that $\Pi_0 = 0$, this becomes

$$\frac{\partial}{\partial y} \left(\theta_{p_0} \frac{\partial v_{p_0}}{\partial y} \right) = 0, \tag{4.57}$$

$$\implies \theta_{p_0} \frac{\partial v_{p_0}}{\partial y} = F_1(x, t). \tag{4.58}$$

From boundary condition (4.38) at $\mathcal{O}(1)$,

$$\theta_{p_0} \frac{\partial v_{p_0}}{\partial y} = 0 \text{ at } y = h_0, \tag{4.59}$$

and thus $F_1(x,t) = 0$. Accordingly,

$$\theta_{p_0} \frac{\partial v_{p_0}}{\partial y} = 0, \tag{4.60}$$

$$\implies v_{p_0} = v_{p_0}(x,t), \tag{4.61}$$

i.e. our leading order polymer axial velocity is independent of y.

From equation (4.35) at leading order,

$$v_{s_0} = v_{p_0} - \frac{1}{\xi \theta_{p_0}} \left(\frac{\partial \mu_{s_0}}{\partial x} + \frac{\partial}{\partial x} \left(\theta_{p_0} G_0 \right) \right). \tag{4.62}$$

Therefore, we also have leading order solvent axial velocity $v_{s_0} = v_{s_0}(x,t)$.

4.3.2 y-*independence of* $\mathcal{O}(\varepsilon)$ *terms*

We now follow the same process to show that the $\mathcal{O}(\varepsilon)$ terms in cell density n_1, pressure P_1, polymer fraction θ_{p_1}, and polymer axial velocity v_{p_1} are also independent of y. This simplifies later steps in our derivation of a leading order model.

Integrating equation (4.31) at $\mathcal{O}(1/\varepsilon)$ and using the no-flux boundary condition $\partial n_1/\partial y = 0$ at $y = h_0$, we find that $n_1 = n_1(x,t)$. This indicates that the first order correction to the cell force function is also independent of y, that is, $G_1 = G_1(x,t)$. Evaluating (4.34) at $\mathcal{O}(1/\varepsilon)$ yields

$$\frac{\partial \Pi_1}{\partial y} = 0, \tag{4.63}$$

$$\implies \Pi_1 = \Pi_1(x,t), \tag{4.64}$$

where $\Pi_1 = P_1 - \theta_{p_0} G_1 - \theta_{p_1} G_0$. Using (4.39), we find that

$$P_1 - \theta_{p_0} G_1 - \theta_{p_1} G_0 = 0 \tag{4.65}$$

at $y = h_0$, and hence $\Pi_1 = 0$. Therefore,

$$P_1 = \theta_{p_0} G_1 + \theta_{p_1} G_0 \tag{4.66}$$

everywhere in the domain. Now, equation (4.36) at $\mathcal{O}(\varepsilon)$ becomes

$$\theta_{s_0} \frac{\partial}{\partial y} \left(\mu_{s_1} + G_0 \theta_{p_1} \right) = 0, \tag{4.67}$$

where μ_{s_1} is the first order correction to μ_s; therefore,

$$\theta_{s_0} \left(\frac{\partial \mu_{s_1}}{\partial \theta_p} + G_0 \right) \frac{\partial \theta_{p_1}}{\partial y} = 0. \tag{4.68}$$

As in the leading order case, either possible solution to this equation requires that $\theta_{p_1} = \theta_{p_1}(x, t)$; hence μ_{s_1} must also be independent of y. We also therefore have that $P_1 = P_1(x, t)$ from equation (4.66).

We evaluate equation (4.33) at $\mathcal{O}(\varepsilon)$, finding

$$-\frac{\partial \Pi_1}{\partial x} + \frac{\partial}{\partial y} \left(\theta_{p_0} \frac{\partial v_{p_1}}{\partial y} + \theta_{p_1} \frac{\partial v_{p_0}}{\partial y} \right) = 0. \tag{4.69}$$

This simplifies to the condition

$$\frac{\partial}{\partial y} \left(\theta_{p_0} \frac{\partial v_{p_1}}{\partial y} \right) = 0, \tag{4.70}$$

from which, after integrating with respect to y and applying interface condition (4.38), we have

$$\theta_{p_0} \frac{\partial v_{p_1}}{\partial y} = 0, \tag{4.71}$$

$$\implies v_{p_1} = v_{p_1}(x, t). \tag{4.72}$$

From (4.36) at $\mathcal{O}(\varepsilon)$, we find that

$$v_{s_1} = v_{p_1} - \frac{1}{\xi\theta_{p_1}}\frac{\partial}{\partial x}\left(\mu_{s_1} + \theta_{p_0}G_1 + \theta_{p_1}G_0\right). \tag{4.73}$$

Thus, the solvent axial velocity must also be independent of y at first order, *i.e.* $v_{s_1} = v_{s_1}(x,t)$.

4.3.3 *Derivation of thin film mass balance equations*

Having established that θ_{p_0} and v_{p_0} are independent of y, the mass conservation equation (4.1) at leading order gives,

$$\begin{aligned}
&\frac{\partial\theta_{p_0}}{\partial t} + \frac{\partial}{\partial x}(\theta_{p_0}v_{p_0}) + \frac{\partial}{\partial y}(\theta_{p_0}w_{p_0}) = 0,\\
&\implies \frac{\partial}{\partial y}(\theta_{p_0}w_{p_0}) = -\left(\frac{\partial\theta_{p_0}}{\partial t} + \frac{\partial}{\partial x}(\theta_{p_0}v_{p_0})\right),\\
&\implies \theta_{p_0}w_{p_0} = -\left(\frac{\partial\theta_{p_0}}{\partial t} + \frac{\partial}{\partial x}(\theta_{p_0}v_{p_0})\right)y + F_2(x,t).
\end{aligned} \tag{4.74}$$

Since $w_{p_0} = 0$ at $y = 0$, we have $F_2(x,t) = 0$ in equation (4.74), and so our polymer velocity in the y-direction is governed by

$$\theta_{p_0}w_{p_0} = -\left(\frac{\partial\theta_{p_0}}{\partial t} + \frac{\partial}{\partial x}(\theta_{p_0}v_{p_0})\right)y; \tag{4.75}$$

accordingly, w_{p_0} is a linear function of y.

We have the kinematic boundary condition at $y = h_0$,

$$w_{p_0} = \frac{\partial h_0}{\partial t} + v_{p_0}\frac{\partial h_0}{\partial x}. \tag{4.76}$$

Applying this kinematic condition in equation (4.75) at $y = h_0$, we find

$$\frac{\partial}{\partial t}\left(\theta_{p_0}h_0\right) + \frac{\partial}{\partial x}\left(\theta_{p_0}v_{p_0}h_0\right) = 0. \tag{4.77}$$

This equation describes the mass conservation of polymer across the height of the thin film.

Similarly, integrating the solvent conservation of mass equation (4.2) from $y = 0$ to $y = h_0$,

$$\begin{aligned}\theta_{s_0} w_{s_0}\Big|_0^{h_0} &= -\int_0^{h_0} \frac{\partial \theta_{s_0}}{\partial t} dy - \int_0^{h_0} \frac{\partial}{\partial x}\left(\theta_{s_0} v_{s_0}\right) dy, \\ &= \left(-\frac{\partial \theta_{s_0}}{\partial t} y - \frac{\partial}{\partial x}\left(\theta_{s_0} v_{s_0}\right) y\right)\Big|_0^{h_0}. \end{aligned} \tag{4.78}$$

By symmetry at $y = 0$, $w_{s_0}(y = 0) = 0$. Therefore,

$$\theta_{s_0} w_{s_0}\Big|_{y=h_0} = -\frac{\partial \theta_{s_0}}{\partial t} h_0 - \frac{\partial}{\partial x}\left(\theta_{s_0} v_{s_0}\right) h_0. \tag{4.79}$$

From interface condition (4.40) at leading order, we also have

$$\theta_{s_0} w_{s_0}\Big|_{y=h_0} = \frac{1}{\mathcal{R}}\left(\mu_{s_0} - \mu_{s_0}^e + \theta_{p_0} G_0\right) + \theta_{s_0}(v_{s_0} - v_{p_0})\frac{\partial h_0}{\partial x} + \theta_{s_0} w_{p_0}\Big|_{y=h_0}. \tag{4.80}$$

Combining equations (4.79) and (4.80) and using the kinematic boundary condition (4.76) for w_{p_0} at $y = h_0$, we find

$$\begin{aligned}&\frac{\partial}{\partial t}\left(\theta_{s_0} h_0\right) + \frac{\partial}{\partial x}\left\{\theta_{s_0} h_0\left(v_{p_0} - \frac{1}{\xi \theta_{p_0}}\left(\frac{\partial \mu_{s_0}}{\partial x} + \frac{\partial}{\partial x}(\theta_{p_0} G_0)\right)\right)\right\} \\ &\quad = -\frac{1}{\mathcal{R}}\left(\mu_{s_0} - \mu_{s_0}^e + \theta_{p_0} G_0\right), \end{aligned} \tag{4.81}$$

where we have substituted for v_{s_0} using equation (4.62). Equation (4.81) describes the advection of solvent mass across the height of the gel.

Taking linear combinations of equations (4.81) and (4.77), we can obtain the mass conservation equations for h_0 and θ_{p_0},

$$\begin{aligned}&\frac{\partial h_0}{\partial t} + \frac{\partial}{\partial x}\left(h_0 v_{p_0} - \frac{h_0 \theta_{s_0}}{\xi \theta_{p_0}}\left(\frac{\partial \mu_{s_0}}{\partial x} + \frac{\partial}{\partial x}(\theta_{p_0} G_0)\right)\right) \\ &\quad = -\frac{1}{\mathcal{R}}\left(\mu_{s_0} - \mu_{s_0}^e + \theta_{p_0} G_0\right), \end{aligned} \tag{4.82}$$

$$\begin{aligned}&\frac{\partial \theta_{p_0}}{\partial t} + v_{p_0}\frac{\partial \theta_{p_0}}{\partial x} + \frac{\theta_{p_0}}{h_0}\frac{\partial}{\partial x}\left(\frac{h_0 \theta_{s_0}}{\xi \theta_{p_0}}\left(\frac{\partial \mu_{s_0}}{\partial x} + \frac{\partial}{\partial x}(\theta_{p_0} G_0)\right)\right) \\ &\quad = \frac{\theta_{p_0}}{\mathcal{R} h_0}\left(\mu_{s_0} - \mu_{s_0}^e + \theta_{p_0} G_0\right). \end{aligned} \tag{4.83}$$

To derive an expression for $\partial n_0/\partial t$, we evaluate equation (4.31) at $\mathcal{O}(1)$. This gives

$$\frac{\partial n_0}{\partial t} + \frac{\partial}{\partial x}(n_0 v_{p_0}) + \frac{\partial}{\partial y}(n_0 w_{p_0}) = D\frac{\partial^2 n_0}{\partial x^2} + D\frac{\partial^2 n_2}{\partial y^2}. \tag{4.84}$$

We express this in the following form, noting that all terms on the right-hand side are independent of y,

$$D\frac{\partial^2 n_2}{\partial y^2} = \frac{\partial n_0}{\partial t} + \frac{\partial}{\partial x}(n_0 v_{p_0}) + n_0\frac{\partial w_{p_0}}{\partial y} - D\frac{\partial^2 n_0}{\partial x^2}. \tag{4.85}$$

After integrating between $y = 0$ and $y = h_0$, we have

$$D\frac{\partial n_2}{\partial y}\bigg|_0^{h_0} = \left(\frac{\partial n_0}{\partial t} + \frac{\partial}{\partial x}(n_0 v_{p_0}) + n_0\frac{\partial w_{p_0}}{\partial y} - D\frac{\partial^2 n_0}{\partial x^2}\right) h_0. \tag{4.86}$$

We note that $\partial n_2/\partial y = 0$ at $y = 0$ from the symmetry condition (4.22). From the no-flux boundary condition (4.45) at $y = h_0$, we find that at $\mathcal{O}(\varepsilon^2)$,

$$D\frac{\partial n_2}{\partial y} = D\frac{\partial n_0}{\partial x}\frac{\partial h_0}{\partial x}. \tag{4.87}$$

Equation (4.86) then becomes

$$D\frac{\partial n_0}{\partial x}\frac{\partial h_0}{\partial x} = \left(\frac{\partial n_0}{\partial t} + \frac{\partial}{\partial x}(n_0 v_{p_0}) + n_0\frac{\partial w_{p_0}}{\partial y}\right) h_0 - D\frac{\partial^2 n_0}{\partial x^2} h_0, \tag{4.88}$$

which simplifies to

$$\left(\frac{\partial n_0}{\partial t} + \frac{\partial}{\partial x}(n_0 v_{p_0}) + n_0\frac{\partial w_{p_0}}{\partial y}\right) h_0 - D\frac{\partial}{\partial x}\left(h_0\frac{\partial n_0}{\partial x}\right) = 0. \tag{4.89}$$

Given that $h_0 > 0$ in the gel, we divide by h_0 and use (4.75) to substitute for w_{p_0}, obtaining the mass conservation equation for n_0,

$$\frac{\partial n_0}{\partial t} + \frac{\partial}{\partial x}(n_0 v_{p_0}) - \frac{n_0}{\theta_{p_0}}\frac{\partial \theta_{p_0}}{\partial t} - \frac{n_0}{\theta_{p_0}}\frac{\partial}{\partial x}(\theta_{p_0} v_{p_0}) - \frac{D}{h_0}\frac{\partial}{\partial x}\left(h_0\frac{\partial n_0}{\partial x}\right) = 0. \tag{4.90}$$

4.3.4 *Derivation of an equation for* v_{p_0}

Having derived equations for the advection of polymer and solvent across the height of the film and for advection-diffusion of cells, we now aim to find an expression for v_{p_0}. Equation (4.33) at $\mathcal{O}(\varepsilon^2)$ gives

$$\frac{\partial}{\partial x}\left(2\theta_{p_0}\frac{\partial v_{p_0}}{\partial x}+\kappa_p\theta_{p_0}\left(\frac{\partial v_{p_0}}{\partial x}+\frac{\partial w_{p_0}}{\partial y}\right)\right)-\frac{\partial \Pi_2}{\partial x}+\frac{\partial}{\partial y}\left(\theta_{p_0}\frac{\partial w_{p_0}}{\partial x}\right)+\frac{\partial}{\partial y}\left(\theta_{p_0}\frac{\partial v_{p_2}}{\partial y}\right)=0, \tag{4.91}$$

where $\Pi_2 = P_2 - \theta_{p_0}G_2 - \theta_{p_2}G_0 - \theta_{p_1}G_1$.

Next we integrate equation (4.91) with respect to y from $y = 0$ to $y = h_0$ to obtain

$$h_0\frac{\partial}{\partial x}\left(2\theta_{p_0}\frac{\partial v_{p_0}}{\partial x}\right)+h_0\frac{\partial}{\partial x}\left(\kappa_p\theta_{p_0}\frac{\partial v_{p_0}}{\partial x}\right)+\int_0^{h_0}\left(\frac{\partial}{\partial x}\left(\kappa_p\theta_{p_0}\frac{\partial w_{p_0}}{\partial y}-\Pi_2\right)\right)dy = -\left[\theta_{p_0}\frac{\partial w_{p_0}}{\partial x}+\theta_{p_0}\frac{\partial v_{p_2}}{\partial y}\right]_0^{h_0}. \tag{4.92}$$

From boundary condition (4.38) at $\mathcal{O}\left(\epsilon^2\right)$, we have at $y = h_0$

$$\theta_{p_0}\frac{\partial w_{p_0}}{\partial x}+\theta_{p_0}\frac{\partial v_{p_2}}{\partial y}=\left(2\theta_{p_0}\frac{\partial v_{p_0}}{\partial x}+\kappa_p\theta_{p_0}\left(\frac{\partial v_{p_0}}{\partial x}+\frac{\partial w_{p_0}}{\partial y}\right)-\Pi_2\right)\frac{\partial h_0}{\partial x}. \tag{4.93}$$

Further, by symmetry at $y = 0$, we have $w_{p_0}(x, 0, t) = 0$, and so $\partial w_{p_0}/\partial x = 0$ at $y = 0$. We also have that v_{p_2} is an even function of y about $y = 0$, and thus $\partial v_{p_2}/\partial y = 0$ at $y = 0$. Therefore, from equation (4.92),

$$h_0\frac{\partial}{\partial x}\left(2\theta_{p_0}\frac{\partial v_{p_0}}{\partial x}\right)+h_0\frac{\partial}{\partial x}\left(\kappa_p\theta_{p_0}\frac{\partial v_{p_0}}{\partial x}\right)+\int_0^{h_0}\frac{\partial}{\partial x}\left(\kappa_p\theta_{p_0}\frac{\partial w_{p_0}}{\partial y}-\Pi_2\right)dy = -\left(2\theta_{p_0}\frac{\partial v_{p_0}}{\partial x}+\kappa_p\theta_{p_0}\left(\frac{\partial v_{p_0}}{\partial x}+\frac{\partial w_{p_0}}{\partial y}\bigg|_{y=h_0}\right)-\Pi_2\bigg|_{y=h_0}\right)\frac{\partial h_0}{\partial x}. \tag{4.94}$$

Using the Leibniz integral rule, we have

$$\int_0^{h_0}\frac{\partial}{\partial x}\left(\kappa_p\theta_{p_0}\frac{\partial w_{p_0}}{\partial y}-\Pi_2\right)dy=\frac{\partial}{\partial x}\int_0^{h_0}\left(\kappa_p\theta_{p_0}\frac{\partial w_{p_0}}{\partial y}-\Pi_2\right)dy-\left[\kappa_p\theta_{p_0}\frac{\partial w_{p_0}}{\partial y}-\Pi_2\right]_{y=h_0}\frac{\partial h_0}{\partial x}, \tag{4.95}$$

and substituting equation (4.95) into (4.94) yields,

$$\frac{\partial}{\partial x}\left(2\theta_{p_0}\frac{\partial v_{p_0}}{\partial x}h_0+\kappa_p\theta_{p_0}\frac{\partial v_{p_0}}{\partial x}h_0\right)+\frac{\partial}{\partial x}\int_0^{h_0}\left(\kappa_p\theta_{p_0}\frac{\partial w_{p_0}}{\partial y}-\Pi_2\right)dy$$
$$-\left[\kappa_p\theta_{p_0}\frac{\partial w_{p_0}}{\partial y}-\Pi_2\right]_{y=h_0}\frac{\partial h_0}{\partial x}=-\left(\kappa_p\theta_{p_0}\frac{\partial w_{p_0}}{\partial y}\bigg|_{y=h_0}-\Pi_2\bigg|_{y=h_0}\right)\frac{\partial h_0}{\partial x}. \quad (4.96)$$

This reduces to the expression

$$\frac{\partial}{\partial x}\left(2\theta_{p_0}\frac{\partial v_{p_0}}{\partial x}h_0+\kappa_p\theta_{p_0}\frac{\partial v_{p_0}}{\partial x}h_0\right)+\frac{\partial}{\partial x}\int_0^{h_0}\left(\kappa_p\theta_{p_0}\frac{\partial w_{p_0}}{\partial y}-\Pi_2\right)dy=0. \quad (4.97)$$

We will return to this further on in our derivation.

We now consider (4.34) at $\mathcal{O}(1)$, finding

$$\frac{\partial}{\partial y}\left(2\theta_{p_0}\frac{\partial w_{p_0}}{\partial y}+\kappa_p\theta_{p_0}\frac{\partial v_{p_0}}{\partial x}+\kappa_p\theta_{p_0}\frac{\partial w_{p_0}}{\partial y}\right)-\frac{\partial\Pi_2}{\partial y}=0,$$
$$\implies 2\theta_{p_0}\frac{\partial w_{p_0}}{\partial y}+\kappa_p\theta_{p_0}\frac{\partial v_{p_0}}{\partial x}+\kappa_p\theta_{p_0}\frac{\partial w_{p_0}}{\partial y}-\Pi_2=F_3(x,t). \quad (4.98)$$

From boundary condition (4.39) on $y=h_0$ at $\mathcal{O}(1)$,

$$2\theta_{p_0}\frac{\partial w_{p_0}}{\partial y}+\kappa_p\theta_{p_0}\frac{\partial v_{p_0}}{\partial x}+\kappa_p\theta_{p_0}\frac{\partial w_{p_0}}{\partial y}-\Pi_2=0. \quad (4.99)$$

Therefore, we find

$$F_3(x,t)=0, \quad (4.100)$$

and from (4.98),

$$\Pi_2=(2+\kappa_p)\theta_{p_0}\frac{\partial w_{p_0}}{\partial y}+\kappa_p\theta_{p_0}\frac{\partial v_{p_0}}{\partial x}. \quad (4.101)$$

We can therefore simplify the integral term in (4.97), and after substituting in the expression for Π_2 above, equation (4.97) becomes

$$\begin{aligned}\frac{\partial}{\partial x}\left(2\theta_{p_0}\frac{\partial v_{p_0}}{\partial x}h_0+\kappa_p\theta_{p_0}\frac{\partial v_{p_0}}{\partial x}h_0\right)\\ -\frac{\partial}{\partial x}\int_0^{h_0}\left(2\theta_{p_0}\frac{\partial w_{p_0}}{\partial y}+\kappa_p\theta_{p_0}\frac{\partial v_{p_0}}{\partial x}\right)dy=0.\end{aligned}\tag{4.102}$$

Noting that the integrand is independent of y, this becomes

$$\begin{aligned}\frac{\partial}{\partial x}\left(2\theta_{p_0}\frac{\partial v_{p_0}}{\partial x}h_0+\kappa_p\theta_{p_0}\frac{\partial v_{p_0}}{\partial x}h_0\right)\\ -\frac{\partial}{\partial x}\left[\left(2\theta_{p_0}\frac{\partial w_{p_0}}{\partial y}+\kappa_p\theta_{p_0}\frac{\partial v_{p_0}}{\partial x}\right)y\right]_0^{h_0}=0,\end{aligned}\tag{4.103}$$

from which,

$$\frac{\partial}{\partial x}\left(2\theta_{p_0}\frac{\partial v_{p_0}}{\partial x}h_0-2\theta_{p_0}\frac{\partial w_{p_0}}{\partial y}h_0\right)=0.\tag{4.104}$$

Now, using equation (4.75), we find

$$\begin{aligned}&\frac{\partial}{\partial x}\left(2\theta_{p_0}\frac{\partial v_{p_0}}{\partial x}h_0+2\frac{\partial\theta_{p_0}}{\partial t}h_0+2\frac{\partial}{\partial x}(\theta_{p_0}v_{p_0})h_0\right)=0,\\ &\implies 2\frac{\partial}{\partial x}\left(h_0\left(2\theta_{p_0}\frac{\partial v_{p_0}}{\partial x}+\frac{\partial\theta_{p_0}}{\partial t}+v_{p_0}\frac{\partial\theta_{p_0}}{\partial x}\right)\right)=0.\end{aligned}\tag{4.105}$$

We integrate (4.105) with respect to x, finding

$$2h_0\left(2\theta_{p_0}\frac{\partial v_{p_0}}{\partial x}+\frac{\partial\theta_{p_0}}{\partial t}+v_{p_0}\frac{\partial\theta_{p_0}}{\partial x}\right)=F_4(y,t).\tag{4.106}$$

Since the left-hand side of this expression is independent of y, we must have $F_4=F_4(t)$. From equation (4.75), we have

$$\frac{\partial\theta_{p_0}}{\partial t}=-\theta_{p_0}\frac{\partial w_{p_0}}{\partial y}-\frac{\partial}{\partial x}\left(\theta_{p_0}v_{p_0}\right).\tag{4.107}$$

Substituting this into equation (4.106), we find

$$2h_0\left(\theta_{p_0}\frac{\partial v_{p_0}}{\partial x}-\theta_{p_0}\frac{\partial w_{p_0}}{\partial y}\right)=F_4(t), \tag{4.108}$$

while from equation (4.101),

$$-2\theta_{p_0}\frac{\partial w_{p_0}}{\partial y}=-\Pi_2+\kappa_p\theta_{p_0}\left(\frac{\partial v_{p_0}}{\partial x}+\frac{\partial w_{p_0}}{\partial y}\right). \tag{4.109}$$

Hence, equation (4.108) becomes

$$h_0\left(2\theta_{p_0}\frac{\partial v_{p_0}}{\partial x}-\Pi_2+\kappa_p\theta_{p_0}\left(\frac{\partial v_{p_0}}{\partial x}+\frac{\partial w_{p_0}}{\partial y}\right)\right)=F_4(t). \tag{4.110}$$

From the interface condition (4.42) at $x=L_0$,

$$2\theta_{p_0}\frac{\partial v_{p_0}}{\partial x}+\kappa_p\theta_{p_0}\left(\frac{\partial v_{p_0}}{\partial x}+\frac{\partial w_{p_0}}{\partial y}\right)-\Pi_2=0; \tag{4.111}$$

thus we find

$$F_4=0, \tag{4.112}$$

and equation (4.106) simplifies to

$$2\theta_{p_0}\frac{\partial v_{p_0}}{\partial x}+\frac{\partial \theta_{p_0}}{\partial t}+v_{p_0}\frac{\partial \theta_{p_0}}{\partial x}=0; \tag{4.113}$$

this gives us a leading order expression for the polymer axial velocity v_{p_0}.

Now, at $x=L_0$, from the interface condition (4.44) at leading order, we have

$$v_{s_0}=v_{p_0}. \tag{4.114}$$

Substituting this into (4.62), we find that, at $x=L_0$,

$$\frac{\partial \mu_{s_0}}{\partial x}=-\frac{\partial}{\partial x}\left(\theta_{p_0}G_0\right). \tag{4.115}$$

We also have no cell flux at $x = L_0$, therefore $\partial n_0/\partial x = 0$, and we can express equation (4.115) as

$$\left(\frac{\partial \mu_{s_0}}{\partial \theta_{p_0}} + G_0\right) \frac{\partial \theta_{p_0}}{\partial x} = 0; \tag{4.116}$$

this indicates that at $x = L_0$ we have the extra boundary condition

$$\frac{\partial \theta_{p_0}}{\partial x} = 0. \tag{4.117}$$

For consistency, we will always use initial conditions such that this boundary condition is satisfied, *i.e.*

$$\frac{\partial \theta_i(L)}{\partial x} = 0, \tag{4.118}$$

where $\theta_i(x)$ is the initial polymer fraction. We note that physically this may not always be true; this may lead to more complicated scenarios (such as the existence of boundary layers) which we do not address here.

4.3.5 *Transformation to a 1D fixed domain*

Finally, as in Chapter 3, we transform our model to a fixed domain with the coordinate transformation $t = T$, $x = L_0(T)X$.

The leading order governing equations, (4.77), (4.81), (4.90) and (4.113), become

$$\frac{\partial}{\partial T}\left(\theta_{p_0} h_0\right) - X\frac{\dot{L}_0}{L_0}\frac{\partial}{\partial X}\left(\theta_{p_0} h_0\right) + \frac{1}{L_0}\frac{\partial}{\partial X}\left(\theta_{p_0} h_0 v_{p_0}\right) = 0, \tag{4.119}$$

$$\begin{aligned}\frac{\partial}{\partial T}\left(\theta_{s_0} h_0\right) &- X\frac{\dot{L}_0}{L_0}\frac{\partial}{\partial X}\left(\theta_{s_0} h_0\right) \\ &+ \frac{1}{L_0}\frac{\partial}{\partial X}\left\{\theta_{s_0} h_0\left(v_{p_0} - \frac{1}{\xi L_0 \theta_{p_0}}\left(\frac{\partial \mu_{s_0}}{\partial X} + \frac{\partial}{\partial X}\left(\theta_{p_0} G_0\right)\right)\right)\right\} \\ &= -\frac{1}{\mathcal{R}}\left(\mu_{s_0} - \mu^e_{s_0} + \theta_{p_0} G_0\right),\end{aligned} \tag{4.120}$$

$$\begin{aligned}\frac{\partial n_0}{\partial T} &- X\frac{\dot{L}_0}{L_0}\frac{\partial n_0}{\partial X} + \frac{1}{L_0}\frac{\partial}{\partial X}(n_0 v_{p_0}) \\ &- \frac{n_0}{\theta_{p_0}}\left\{\frac{\partial \theta_{p_0}}{\partial T} - X\frac{\dot{L}_0}{L_0}\frac{\partial \theta_{p_0}}{\partial X} + \frac{1}{L_0}\frac{\partial}{\partial X}\left(\theta_{p_0} v_{p_0}\right)\right\} - \frac{D}{L_0^2 h_0}\frac{\partial}{\partial X}\left(h_0\frac{\partial n_0}{\partial X}\right) = 0,\end{aligned} \tag{4.121}$$

$$\frac{2\theta_{p_0}}{L_0}\frac{\partial v_{p_0}}{\partial X} + \frac{\partial \theta_{p_0}}{\partial T} - X\frac{\dot{L}_0}{L_0}\frac{\partial \theta_{p_0}}{\partial X} + \frac{v_{p_0}}{L_0}\frac{\partial \theta_{p_0}}{\partial X} = 0, \tag{4.122}$$

respectively.

Transforming equation (4.83) and substituting into (4.122) for the $\partial\theta_{p_0}/\partial T$ term, we obtain

$$\begin{aligned}\frac{2h_0}{L_0}\frac{\partial v_{p_0}}{\partial X} &- \frac{1}{L_0^2}\frac{\partial}{\partial X}\left\{\frac{\theta_{s_0} h_0}{\xi \theta_{p_0}}\left(\frac{\partial \mu_{s_0}}{\partial X} + \frac{\partial}{\partial X}\left(\theta_{p_0} G_0\right)\right)\right\} \\ &+ \frac{1}{\mathcal{R}}\left(\mu_{s_0} - \mu^e_{s_0} + \theta_{p_0} G_0\right) = 0.\end{aligned} \tag{4.123}$$

We can substitute this into (4.120), giving

$$\frac{\partial}{\partial T}\left(\theta_{s_0} h_0\right) - X\frac{\dot{L}_0}{L_0}\frac{\partial}{\partial X}\left(\theta_{s_0} h_0\right) + \frac{1}{L_0}\frac{\partial}{\partial X}\left(\theta_{s_0} h_0 v_{p_0}\right) - \frac{2h_0}{L_0}\frac{\partial v_{p_0}}{\partial X} = 0. \tag{4.124}$$

We can also substitute equation (4.122) into equation (4.121) to eliminate the $\partial\theta_{p_0}/\partial T$ term there, finding

$$\frac{\partial n_0}{\partial T} - X\frac{\dot{L}_0}{L_0}\frac{\partial n_0}{\partial X} + \frac{1}{L_0}\frac{\partial}{\partial X}(n_0 v_{p_0}) + \frac{n_0}{L_0}\frac{\partial v_{p_0}}{\partial X} - \frac{D}{L_0^2 h_0}\frac{\partial}{\partial X}\left(h_0\frac{\partial n_0}{\partial X}\right) = 0. \tag{4.125}$$

The mass conservation equations (4.119) and (4.124) can be expressed in the non-conservative forms

$$\frac{\partial \theta_{p_0}}{\partial T} - X\frac{\dot{L}_0}{L_0}\frac{\partial \theta_{p_0}}{\partial X} + \frac{1}{L_0}\frac{\partial}{\partial X}\left(\theta_{p_0} v_{p_0}\right) + \frac{\theta_{p_0}}{L_0}\frac{\partial v_{p_0}}{\partial X} = 0, \tag{4.126}$$

$$\frac{\partial h_0}{\partial T} - X\frac{\dot{L}_0}{L_0}\frac{\partial h_0}{\partial X} + \frac{1}{L_0}\frac{\partial}{\partial X}\left(h_0 v_{p_0}\right) - \frac{2h_0}{L_0}\frac{\partial v_{p_0}}{\partial X} = 0. \tag{4.127}$$

From equation (4.126), we find that, as in Chapter 3, the polymer advection equation has characteristics on $X = 0$ and $X = L$; as such, the polymer fraction θ_{p_0} is determined by the initial condition $\theta_i(X)$ and velocity v_{p_0}. From equation (4.127), we see that the height h_0 similarly has characteristics on $X = 0$ and $X = L$, and is determined by its initial condition $h_i(X)$ and v_{p_0}.

We have again taken the initial condition $\theta_i(X)$ to be differentiable and to satisfy $\partial\theta_i(0)/\partial X = 0$, so that for all time, $\partial\theta_{p_0}(0,T)/\partial X = 0$ (see Section 3.2). We have similarly taken the initial height $h_i(X)$ to be differentiable and satisfy $\partial h_i(0)/\partial X = 0$, such that $\partial h_0(0,T)/\partial X = 0$ for all time.

Therefore, our reduced 1D model is made up of the following system of equations,

$$\theta_{s_0} = 1 - \theta_{p_0} \tag{4.128}$$

$$\frac{\partial}{\partial T}\left(\theta_{p_0} h_0\right) - X\frac{\dot{L}_0}{L_0}\frac{\partial}{\partial X}\left(\theta_{p_0} h_0\right) + \frac{1}{L_0}\frac{\partial}{\partial X}\left(\theta_{p_0} h_0 v_{p_0}\right) = 0, \tag{4.129}$$

$$\frac{\partial}{\partial T}\left(\theta_{s_0} h_0\right) - X\frac{\dot{L}_0}{L_0}\frac{\partial}{\partial X}\left(\theta_{s_0} h_0\right) + \frac{1}{L_0}\frac{\partial}{\partial X}\left(\theta_{s_0} h_0 v_{p_0}\right) - \frac{2h_0}{L_0}\frac{\partial v_{p_0}}{\partial X} = 0, \tag{4.130}$$

$$\frac{\partial n_0}{\partial T} - X\frac{\dot{L}_0}{L_0}\frac{\partial n_0}{\partial X} + \frac{1}{L_0}\frac{\partial}{\partial X}(n_0 v_{p_0}) + \frac{n_0}{L_0}\frac{\partial v_{p_0}}{\partial X} - \frac{D}{L_0^2 h_0}\frac{\partial}{\partial X}\left(h_0\frac{\partial n_0}{\partial X}\right) = 0, \tag{4.131}$$

$$\begin{aligned}\frac{2h_0}{L_0}\frac{\partial v_{p_0}}{\partial X} - \frac{1}{L_0^2}\frac{\partial}{\partial X}\left\{\frac{\theta_{s_0} h_0}{\xi\theta_{p_0}}\left(\frac{\partial \mu_{s_0}}{\partial X} + \frac{\partial}{\partial X}\left(\theta_{p_0} G_0\right)\right)\right\} \\ + \frac{1}{\mathcal{R}}\left(\mu_{s_0} - \mu_{s_0}^e + \theta_{p_0} G_0\right) = 0,\end{aligned} \tag{4.132}$$

subject to boundary conditions

$$\frac{\partial \theta_{p_0}}{\partial X} = 0 \quad \text{at } X = 0, X = 1, \tag{4.133}$$

$$\frac{\partial n_0}{\partial X} = 0 \quad \text{at } X = 0, X = 1, \tag{4.134}$$

$$\frac{\partial h_0}{\partial X} = 0 \quad \text{at } X = 0, \tag{4.135}$$

$$v_{p_0} = 0 \quad \text{at } X = 0, \tag{4.136}$$

$$\dot{L}_0 = v_{p_0}(X = 1), \tag{4.137}$$

and initial conditions

$$\theta_p(X, 0) = \theta_i(X), \quad n(X, 0) = n_i(X), \quad h(X, 0) = h_i(X), \quad L(0) = 1, \tag{4.138}$$

where we assume

$$\frac{\partial \theta_i(0)}{\partial X} = \frac{\partial \theta_i(1)}{\partial X} = 0, \qquad \frac{\partial h_i(0)}{\partial X} = 0. \tag{4.139}$$

As noted earlier, the mass conservation equations (4.129) and (4.130) can be expressed in the non-conservative form given in equations (4.126) and (4.127) (repeated here for convenience),

$$\frac{\partial \theta_{p_0}}{\partial T} - X\frac{\dot{L}_0}{L_0}\frac{\partial \theta_{p_0}}{\partial X} + \frac{1}{L_0}\frac{\partial}{\partial X}(\theta_{p_0} v_{p_0}) + \frac{\theta_{p_0}}{L_0}\frac{\partial v_{p_0}}{\partial X} = 0, \tag{4.140}$$

$$\frac{\partial h_0}{\partial T} - X\frac{\dot{L}_0}{L_0}\frac{\partial h_0}{\partial X} + \frac{1}{L_0}\frac{\partial}{\partial X}(h_0 v_{p_0}) - \frac{2h_0}{L_0}\frac{\partial v_{p_0}}{\partial X} = 0. \tag{4.141}$$

We will use both the conservative and non-conservative forms at different points in subsequent chapters when analysing the thin film model.

4.3.6 *Discussion*

In this chapter, we developed a model to study the behaviour of a thin film of gel. We exploited the small parameter in the system, namely the inverse aspect ratio ε, and showed that under a particular set of scalings, the original two-dimensional system

of equations can be reduced to a one-dimensional system of four coupled PDEs. This leading order model consists of mass conservation equations for the volume fractions of polymer and solvent across the height of the gel, equations (4.129) and (4.130) respectively, a mass conservation equation for the cell density (4.131), and a force balance equation governing the polymer axial velocity (4.132) which is first order in v_p. Such a model considering cell traction stresses and osmotic pressure in this thin film setting has not been presented previously.

This reduced system of equations provides significant benefits when studying the model both analytically and numerically. To solve the initial 2D model, we must not only account for free boundaries defining the height and length of the gel, but also solve the governing equations for θ_p, n and v_p in two spatial coordinates. Having shown that the solution is uniform across the gel height at leading order, we avoid the complexity of solving our equations in the y-coordinate. Instead of needing to solve for the free boundaries in 2D, our thin film model tracks the height of the gel through mass conservation equations (4.129) and (4.130). We can then transform our free boundary at $x = L_0(T)$ onto a fixed domain as was previously done in Chapter 3. This allows us to solve the model numerically in a conventional manner, using, for example, a Crank-Nicolson scheme. The thin film model is also tractable for analytic study; we will present a reduced ODE solution in Chapter 5 and small time solution in Chapter 6, together with numerical results.

The model as presented in equations (4.128)-(4.139) has some key differences to the 1D model presented in Chapter 3, driven by the geometry of the thin film. In the previous geometry, all solvent flowed in or out of the gel horizontally through the gel's endpoint at $X = 1$. In contrast, in the thin film model, we can have solvent flow into the gel across the long boundary at $y = h_0$. This manifests itself in the additional terms seen in equation (4.120). This equation describes mass conservation of the solvent fraction across the thickness of the gel, and includes a source term which depends on the balance of chemical and cell potentials, scaled by the resistance of the interface to fluid flow. This source term effectively emerges as a result of integrating over the height of the gel.

In the model presented in Chapter 3, the cell density is governed by an advection-diffusion equation. In the thin film setting, cell density can additionally evolve as a result of solvent flux across the $y = h_0$ boundary (seen by substituting for $\partial v_{p_0}/\partial X$ using (4.132) in (4.131)); as solvent flows across this boundary causing the gel to swell or shrink, the cell density will decrease or increase accordingly. The model derivation here uses the presence of diffusive terms to find that n_0 is independent of y; therefore, unlike the previous 1D case, we cannot set $D = 0$ without violating one of the assumptions underpinning the thin film reduction of the model.

Another key difference is that we have a first order equation (4.132) for the polymer velocity in the thin film model as opposed to a second order equation previously. The continuity of stress boundary condition which was required to close the system in Chapter 3 is integrated into the velocity equation in the thin film setting.

As was previously discussed with reference to Howell (1996) in Chapter 1, the classic Trouton model for a two-dimensional Newtonian sheet has a Trouton ratio of 4. We note that taking the limit $\theta_{p_0} = 1$ in equations (4.77) and (4.105), we recover the Trouton model describing the leading order height and axial velocity of a thin sheet as given in equations (1.11) and (1.12), with the Trouton ratio appearing in equation (4.105).

The scaling used to derive the thin film model here, with pressure taken to be large, resulted in a relation between pressure and viscous stress emerging at leading order in the momentum equation (4.33). This is typically seen in lubrication theory, leading to parabolic solutions in y for the leading order axial velocity (Green, 2006). In our model, the absence of a no-slip condition on the gel's boundary leads to the leading order axial velocity v_p being uniform across the y-coordinate, which is typical of an extensional flow such as in Howell (1996). The pressure in our system, scaled to be large, is found to be created by the cell potentials in the gel; this pressure, together with the large chemical potentials, drives the movement of solvent and polymer. In the case without cells, it is the chemical potentials alone driving the flow, with the leading order pressure contribution being zero.

As an aside, we note that if we take a cell-free system wherein $n = 0$, we can derive the same model as that given by equations (4.129) - (4.132) (with $n = 0$ throughout) by using a typical extensional flow scaling limit where pressure is not large. The deriva-

tion in this alternative case follows largely the same methodology as that presented in this chapter, with the key difference being that pressure P is scaled to be $\mathcal{O}(1)$ and does not contribute to the leading order solution. This is consistent with the model derived in this chapter, where the leading order pressure contribution is zero in the case of no cells being present.

As has been discussed here, the thin film model contains key differences to the model presented in Chapter 3. We will therefore now explore this thin film model both analytically and numerically in Chapters 5 and 6. We aim to investigate the behaviours arising from the model in this geometry and assess the results in comparison to those presented previously. Chapter 5 will study the thin film with uniform initial conditions, while in Chapter 6, non-uniform initial conditions are considered.

5

THIN FILM ANALYSIS: UNIFORM INITIAL CONDITIONS

5.1 INTRODUCTION

In Chapter 4, we developed a new model for a two-dimensional thin film of gel. We exploited the thinness of the gel to derive an extensional flow model, where the longitudinal velocity, polymer volume fraction and cell density are independent of the y-coordinate; the evolution of the gel is therefore driven by the balance of cell traction stresses and chemical potentials along the length of the gel with the surrounding solvent across the interface. In the next chapters, we investigate our thin film model both analytically and numerically. We restrict our focus to spatially uniform initial conditions in this chapter, while in Chapter 6, we study spatially non-uniform initial conditions.

We first demonstrate that if the initial gel height, polymer fraction and cell density are spatially uniform, a reduced, ordinary differential equation model can be derived. We then develop a small time solution to this model. We present numerical solutions for the ODE model, studying the qualitative behaviours predicted in this thin film setting. Comparisons will be made to the results presented in Chapter 3 to better understand gel evolution in this new scenario.

5.2 REDUCED MODEL FOR UNIFORM INITIAL CONDITIONS

We start this chapter studying the leading order model derived in Chapter 4 for a thin film on a fixed spatial domain; this model is given by equations (4.128) - (4.139). For notational convenience, we now drop the subscript zeroes on leading order variables. We will consider the non-conservative forms of mass conservation equations (4.129)

and (4.130), *i.e.* equations (4.140) and (4.141). We repeat the mass and momentum conservation equations here for convenience, these being,

$$\frac{\partial \theta_p}{\partial T} - X\frac{\dot{L}}{L}\frac{\partial \theta_p}{\partial X} + \frac{1}{L}\frac{\partial}{\partial X}(\theta_p v_p) + \frac{\theta_p}{L}\frac{\partial v_p}{\partial X} = 0, \tag{5.1}$$

$$\frac{\partial h}{\partial T} - X\frac{\dot{L}}{L}\frac{\partial h}{\partial X} + \frac{1}{L}\frac{\partial}{\partial X}(h v_p) - \frac{2h}{L}\frac{\partial v_p}{\partial X} = 0, \tag{5.2}$$

$$\frac{\partial n}{\partial T} - X\frac{\dot{L}}{L}\frac{\partial n}{\partial X} + \frac{1}{L}\frac{\partial}{\partial X}(n v_p) + \frac{n}{L}\frac{\partial v_p}{\partial X} - \frac{D}{L^2 h}\frac{\partial}{\partial X}\left(h\frac{\partial n}{\partial X}\right) = 0, \tag{5.3}$$

$$\frac{2h}{L}\frac{\partial v_p}{\partial X} - \frac{1}{L^2}\frac{\partial}{\partial X}\left\{\frac{\theta_s h}{\xi \theta_p}\left(\frac{\partial \mu_s}{\partial X} + \frac{\partial}{\partial X}(\theta_p G)\right)\right\} + \frac{1}{\mathcal{R}}(\mu_s - \mu_s^e + \theta_p G) = 0. \tag{5.4}$$

For uniform initial conditions in θ_p, n and h, we now show that we can reduce this thin film system of equations to a simpler model. This model is governed by an ODE for h as a function of time, with the other variables specified in terms of h.

Given uniform initial conditions, the free energy and cell force are also initially uniform in X. This means that the velocity equation (5.4) at initial time is

$$\frac{\partial v_p}{\partial X}(T = 0) = -\frac{L}{2\mathcal{R}h}(\mu_s - \mu_s^e + \theta_p G), \tag{5.5}$$

and given that the terms on the right hand side are all initially independent of X, the initial velocity is given by

$$v_p(T = 0) = -\frac{L}{2\mathcal{R}h}(\mu_s - \mu_s^e + \theta_p G)\, X, \tag{5.6}$$

where we have used the condition $v_p = 0$ at $X = 0$. At initial time, equations (5.1), (5.2) and (5.3) become

$$\frac{\partial \theta_p}{\partial T}(T = 0) = -\frac{2\theta_p}{L}\frac{\partial v_p}{\partial X}, \tag{5.7}$$

$$\frac{\partial h}{\partial T}(T = 0) = \frac{h}{L}\frac{\partial v_p}{\partial X}, \tag{5.8}$$

$$\frac{\partial n}{\partial T}(T = 0) = -\frac{2n}{L}\frac{\partial v_p}{\partial X}. \tag{5.9}$$

Given that v_p is linear in X at $T = 0$, these equations indicate that the solutions for h, θ_p and n remain uniform in X at the next time step. Therefore, $\partial v_p/\partial X$ must also be constant in space at the next time step, and this process continues on as time progresses, with no spatial dependency being introduced in θ_p, h or n.

Accordingly, given uniform initial conditions, our model reduces to the following system of first order ODEs, together with an equation for v_p,

$$v_p(T, X) = -\frac{L}{2\mathcal{R}h}\left(\mu_s - \mu_s^e + \theta_p G\right) X, \tag{5.10}$$

$$\frac{dh}{dT} = -\frac{1}{2\mathcal{R}}\left(\mu_s - \mu_s^e + \theta_p G\right), \tag{5.11}$$

$$\frac{d\theta_p}{dT} = \frac{\theta_p}{\mathcal{R}h}\left(\mu_s - \mu_s^e + \theta_p G\right), \tag{5.12}$$

$$\frac{dn}{dT} = \frac{n}{\mathcal{R}h}\left(\mu_s - \mu_s^e + \theta_p G\right). \tag{5.13}$$

The kinematic condition gives

$$\frac{dL}{dT} = v_p(X = 1), \tag{5.14}$$

and we take the initial conditions

$$h(T = 0) = 1, \quad \theta_p(T = 0) = \theta_i, \quad n(T = 0) = 1, \quad L(T = 0) = 1, \tag{5.15}$$

where we have scaled h and n on the initial height and cell density respectively.

We now demonstrate that this system can be reduced to a single ODE for the height h. We substitute equation (5.11) into equation (5.10) to find

$$v_p = \frac{LX}{h}\frac{dh}{dT}, \tag{5.16}$$

$$= LX\frac{d}{dT}\left(\log(h(T))\right). \tag{5.17}$$

Similarly, substituting equation (5.11) into equation (5.12), we have

$$\frac{d\theta_p}{dT} = -2\frac{\theta_p}{h}\frac{dh}{dT}, \tag{5.18}$$

which can be written in the form

$$\frac{d}{dT}\left(\log(\theta_p(T))\right) = \frac{d}{dT}\left(\log(h^{-2}(T))\right). \tag{5.19}$$

Integrating this, we find that

$$\log(\theta_p(T)) = \log(h^{-2}(T)) + C, \tag{5.20}$$

where, from our initial conditions, the constant C has the value

$$C = \log(\theta_i). \tag{5.21}$$

We thus have

$$\theta_p = \frac{\theta_i}{h^2}, \tag{5.22}$$

and similarly, we find the solution for the cell density as

$$n = \frac{1}{h^2}. \tag{5.23}$$

Substituting for $v_p(X = 1)$ using equation (5.17), the kinematic boundary condition (5.14) becomes

$$\frac{dL}{dT} = L\frac{d}{dT}\left(\log(h)\right), \tag{5.24}$$

and thus

$$\frac{d}{dT}\left(\log(L)\right) = \frac{d}{dT}\left(\log(h)\right). \tag{5.25}$$

Given that $L(0) = h(0) = 1$, we find that

$$L(T) = h(T). \tag{5.26}$$

Having found solutions θ_p and n as functions of h, we can also express the chemical potential $\mu_s(\theta_p)$ and cell force function $G(n)$ as functions of h, and accordingly, reduce our model to the following system in $h(T)$,

$$\frac{dh}{dT} = -\frac{1}{2\mathcal{R}}\left(\mu_s(\theta_p) - \mu_s^e + \theta_p G(n)\right), \tag{5.27}$$

$$\theta_p(T) = \frac{\theta_i}{h^2}, \tag{5.28}$$

$$n(T) = \frac{1}{h^2}, \tag{5.29}$$

$$L(T) = h, \tag{5.30}$$

$$v_p(X,T) = X\frac{dh}{dT}. \tag{5.31}$$

We note that while the solution for $v_p(X,T)$ has been included here, it is not required to understand how h, and subsequently θ_p, n and L, evolve in time.

From this reduced model, we can draw a number of conclusions about how the gel behaves under spatially uniform initial conditions. The foremost result here is that if there is no initial spatial variation in the volume fractions and cell density, the gel will remain uniform in space for all time. We see that the length of the gel is equal to its height as it evolves, therefore any movement in the free boundaries of the gel will occur in the same manner both length-wise and height-wise. We also see that the polymer fraction and cell density are inversely proportional to the squared height, scaled by the initial conditions.

The entire system is driven by the balance between the solvent chemical potential μ_s and the cell potential $\theta_p G$ inside the gel with the external chemical potential μ_s^e. If these forces are in balance, the system is in equilibrium, as expected. For the height to be increasing, and accordingly, the gel to be swelling, we require that μ_s^e is greater than the sum of $\theta_p G$ and μ_s; the opposite holds for the gel to contract. The gel equilibrates when these forces are in balance, that is

$$\mu_s(\theta_p) - \mu_s^e + \theta_p G(n) = 0. \tag{5.32}$$

We note that this is equivalent to the equilibrium condition given for the 1D model in equation (3.46).

The rate at which the gel evolves is determined by equation (5.27). Accordingly, increasing the resistance of the interface $\mathcal{R}$ slows the rate of change of h and the rest of the system. Similarly, larger values of parameters such as the mixing energy χ and cell traction τ_0 appearing in μ_s and G respectively will increase the rate of gel evolution. The reduced model is independent of drag; with no dependence on the X-coordinate, there is no relative motion between the polymer and solvent as the gel evolves and so no shearing takes place.

We further note that one can arrive at the model given by equations (5.27) - (5.31) by substituting the ansatz $\theta_p = \theta_p(T)$, $n = n(T)$, $h = h(T)$, and $v_p = XL(T)V(T)$ (where $V(T)$ is to be determined) into equations (5.1) - (5.4) and simplifying as done above. This ansatz encodes from the outset that θ_p, n and h are independent of X for all time, whereas in the derivation above, we only assume that the initial conditions are independent of X and demonstrate from there that, as time progresses, these variables must remain spatially independent.

5.2.1 *Short time solution*

As in Section 3.5, we develop a short time solution to the reduced gel model given by equations (5.27) - (5.31). This allows us to compute analytic solutions over early time; these analytic solutions provide a means of understanding how the gel behaves as it initially evolves from its initial conditions, as well as a method to validate our numerical solution in Section 5.3.

We define the short time scale $T = \delta\hat{T}$, where $\delta \ll 1$. We expand the dependent variables about the initial conditions as power series in δ,

$$h(\hat{T}) = 1 + \delta h_1(\hat{T}) + \delta^2 h_2(\hat{T}) + ..., \tag{5.33}$$

and similarly for θ_p, n, L and v_p. For these series, we have the initial conditions $L_0 = 1$, $\theta_0 = \theta_i$, $n_0 = 1$ and $h_0 = 1$.

After substituting these expansions into the model equations, from equation (5.27) at $\mathcal{O}(\delta)$ we find

$$\frac{\partial h_1}{\partial \hat{T}} = -\frac{1}{2\mathcal{R}}(\mu_s(\theta_i) - \mu_s^e(0) + \theta_i G(1)); \tag{5.34}$$

therefore,

$$h_1 = -\frac{\hat{T}}{2\mathcal{R}}(\mu_s(\theta_i) - \mu_s^e(0) + \theta_i G(1)). \tag{5.35}$$

Using this expression for h_1 in equations (5.28) - (5.30), we find the small time solutions,

$$h = 1 + \delta h_1, \tag{5.36}$$

$$L = 1 + \delta h_1, \tag{5.37}$$

$$\theta_p = \theta_i(1 - 2\delta h_1), \tag{5.38}$$

$$n = 1 - 2\delta h_1, \tag{5.39}$$

where

$$h_1 = -\frac{\hat{T}}{2\mathcal{R}}(\mu_s(\theta_i) - \mu_s^e(0) + \theta_i G(1)). \tag{5.40}$$

As in the ODE (5.27), the small time behaviour is governed by the difference between the external chemical potential and the internal cell and chemical potential energies. We will use this solution to confirm our numerical results are evolving in the correct manner in Section 5.3.

5.3 THIN FILM NUMERICS

We solve the reduced model described by equations (5.27) - (5.30) using an inbuilt MATLAB ODE solver, specifically *ode15s* which is designed to handle stiff systems. We use the short time solution (5.36) - (5.39) to verify this numerical method. As illustrated by Fig. 5.1, we find good agreement between the two solutions, demonstrating that our

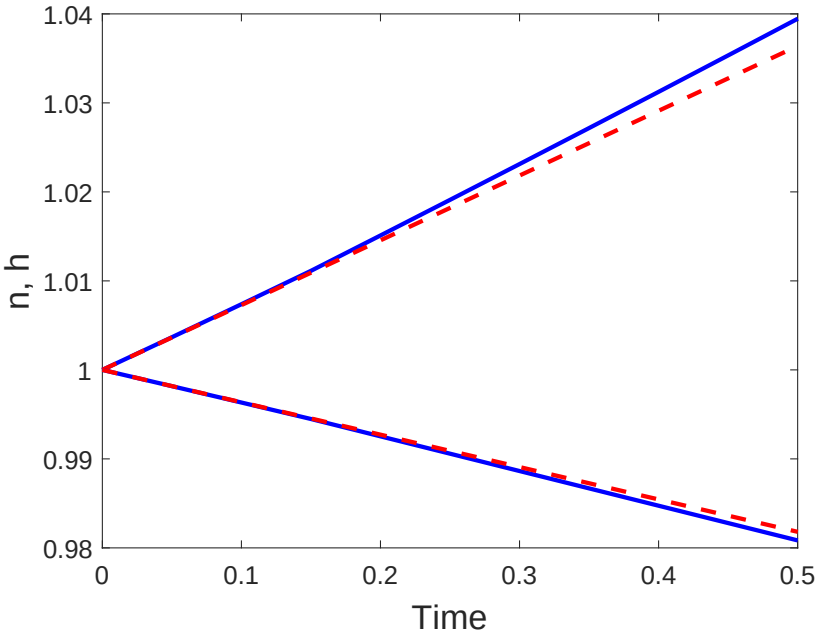

Figure 5.1: Comparing the small time solution for uniform initial conditions (red dashed lines) with the numerical ODE solution (blue solid lines) over early time for n (increasing over time) and h (decreasing over time). The solutions are closely matched over small time. Values: $\theta_i = 0.4$, $n_i = 1$, $h_i = 1$, $\chi = -0.1$, $N = 100$, $\mathcal{R} = 1.5$, $\tau_0 = 1.2$, $\lambda = 1$.

ODE scheme is evolving in the right manner from its initial conditions. In the next chapter, we will compare the solutions given by the ODE solver and those given by our full numerical scheme (described in Section 6.4), confirming that the two agree in their description of the gel's evolution and steady state values (see Fig. 6.2). We can also solve the equilibrium condition (5.32) for the system with uniform initial conditions to confirm that the simulation has reached an appropriate steady state.

5.3.1 *Numerical simulations*

We study a thin film with uniform initial conditions in the polymer fraction, cell density and height. Recall that the solutions remain spatially uniform for all time and that $h(T) = L(T)$.

For a gel without cells, we can see either swelling and contraction take place, depending on the chemical potentials in the system. Fig. 5.2, for example, demonstrates swelling induced by osmotic pressure (with mixing parameter $\chi = 0.75$), while, con-

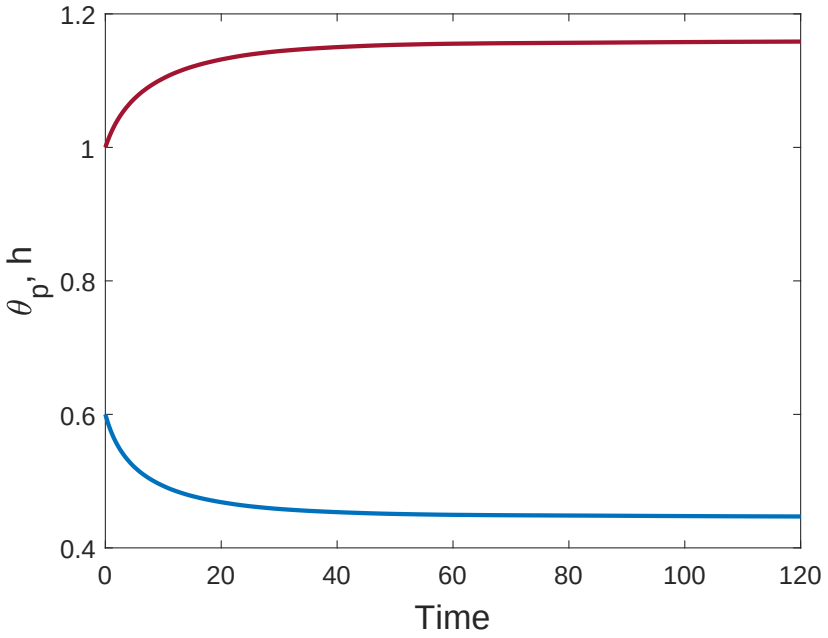

Figure 5.2: Time evolution of a cell-free thin gel. The gel swells to equilibrium uniformly across its domain. θ_p is the solid blue line, h is the solid maroon line (note that $h = L$). Values: $\theta_i = 0.6$, $n_i = 0$, $h_i = 1$, $\chi = 0.75$, $N = 100$, $\mathcal{R} = 1$. $(\theta^*, h^*, L^*) = (0.45, 1.16, 1.16)$.

versely, Fig. 5.3 shows a case where the gel contracts (with mixing increased to $\chi = 1.5$, promoting separation between the polymer and solvent). The equilibria reached here, $\theta^* = 0.45$ for the swelling case and $\theta^* = 0.86$ for the contracting case, are the same values as found for the equivalent initial conditions and parameters in the 1D Cartesian gel (see Figs. 3.8 and 3.9 respectively).

Introducing cells into this system can precipitate a switch to contraction in a gel that would otherwise swell. We take the same parameter values as in the swelling gel above (Fig. 5.2) and introduce a cell population ($n_i = 1$, $\tau_0 = 1$). In Fig. 5.4, we see that this gel now contracts due to the presence of cells, reaching a steady state with a significant reduction in height and length. This highlights that in this thin film geometry, given sufficient traction stress, the presence of cells can outweigh the osmotic swelling pressure created by chemical potentials in a gel. Reducing the traction parameter ($\tau_0 = 0.1$), we see that the presence of cells does not necessitate contraction. In Fig. 5.5, it is evident that due to a weak cell contribution, osmotic pressure is still the dominant driver of the gel's behaviour, and the thin film will still swell to an equilibrium. The equilibrium

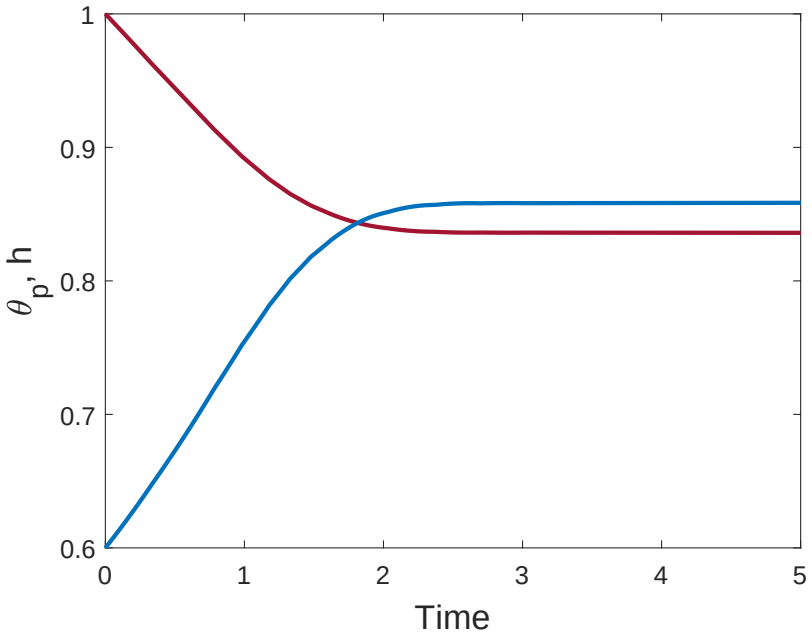

Figure 5.3: Time evolution of a cell-free thin gel. The gel contracts to equilibrium with sufficiently large χ. θ_p is the solid blue line, h is the solid maroon line (note that $h = L$). Values: $\theta_i = 0.6$, $n_i = 0$, $h_i = 1$, $\chi = 1.5$, $N = 100$, $\mathcal{R} = 1$. $(\theta^*, h^*, L^*) = (0.86, 0.84, 0.84)$.

values of polymer and cell density again match those found for the 1D case for the same initial conditions and parameters (see Figs. 3.12 and 3.11 for the contraction and swelling examples respectively).

Increasing the resistance parameter $\mathcal{R}$ slows the evolution of the gel and hence increases the time taken to reach a steady state; however, it does not affect the eventual equilibrium reached. Fig. 5.6 shows the effect of increasing the resistance parameter from $\mathcal{R} = 1$ to $\mathcal{R} = 5$, which increases the time taken for the gel to reach its steady state approximately five-fold, from $T \approx 2$ to $T \approx 10$. This relation between $\mathcal{R}$ and T is expected, given that the solution for h in equation (5.27) is of the form $F(T/R)$.

For both the contracting and expanding examples here, the gel remains spatially uniform throughout its evolution and at its steady state. As expected, the changes in height and length are identical given $h_i = L_i = 1$, indicating that the gel grows in a uniform ratio horizontally and vertically. Next, we will explore whether this remains the case when the gel is constructed with non-uniform initial conditions.

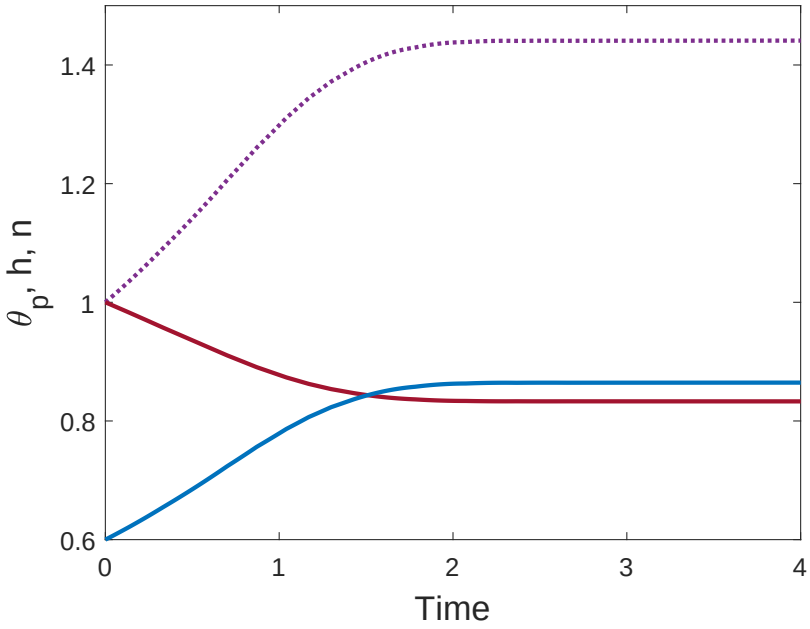

Figure 5.4: Time evolution of a thin cell-gel system. The gel contracts to equilibrium due to the presence of cells. θ_p is the solid blue line, h is the solid maroon line (note that $h = L$), n is the dotted purple line. Values: $\theta_i = 0.6$, $n_i = 1$, $h_i = 1$, $\chi = 0.75$, $N = 100$, $\mathcal{R} = 1$, $\tau_0 = 1$, $\lambda = 1$. $(\theta^*, n^*, h^*, L^*) = (0.86, 1.44, 0.83, 0.83)$.

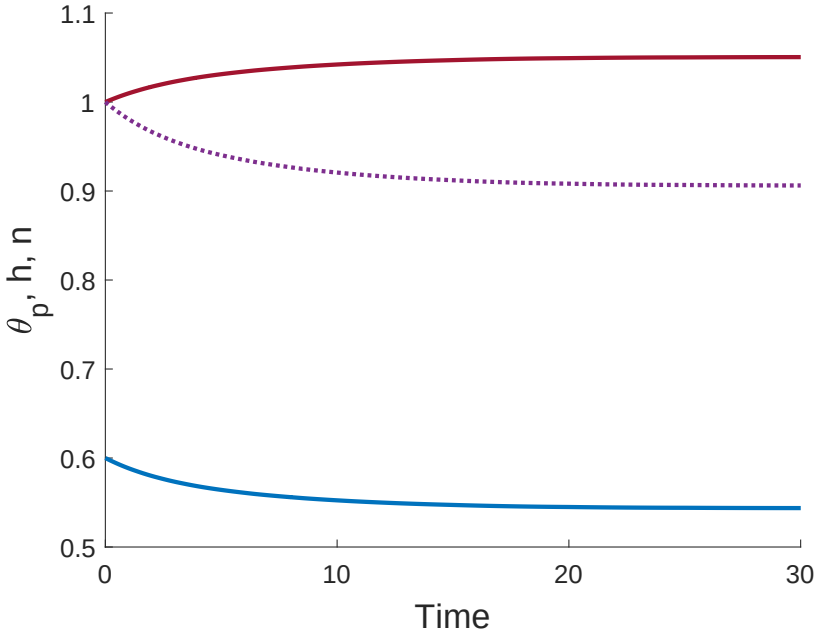

Figure 5.5: Time evolution of a thin cell-gel system. The gel swells to a steady state due to osmotic pressure counteracting weak cell traction. θ_p is the solid blue line, h is the solid maroon line (note that $h = L$), n is the dotted purple line. Values: $\theta_i = 0.6$, $n_i = 1$, $h_i = 1$, $\chi = 0.75$, $N = 100$, $\mathcal{R} = 1$, $\tau_0 = 0.1$, $\lambda = 1$. $(\theta^*, n^*, h^*, L^*) = (0.54, 0.91, 1.05, 1.05)$.

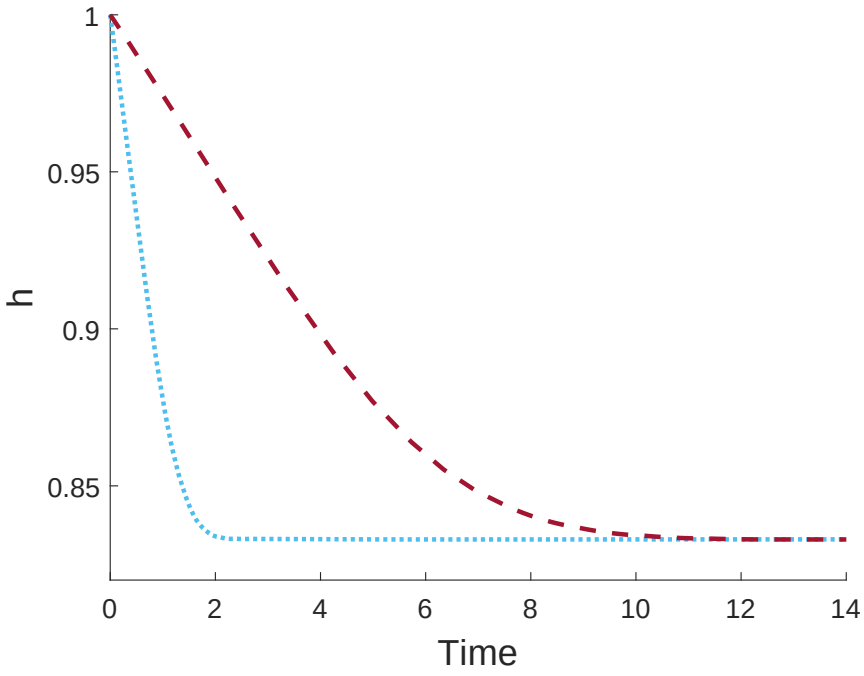

Figure 5.6: Comparing the effect of the size of the resistance parameter on the evolution of the gel height. $\mathcal{R} = 1$ is the light blue dotted line, $\mathcal{R} = 5$ is the maroon dashed line. Values otherwise as given in Fig. 5.4.

5.4 DISCUSSION

In this chapter, we have used analytic and numerical methods to study a new model for a thin film cell-gel system. Given uniform initial conditions, we have developed a reduced ODE model driven by the difference in chemical and cell potentials. Small time solutions were found, which provided an analytic solution for the gel's early time behaviour. We then presented a numerical solution to the model, analysing the dynamics seen as the gel evolves from uniform initial conditions. We found both gel swelling and contraction possible depending on the balance of potentials.

A key finding here is that, for uniform initial conditions, the system of equations reduces to a model defined by an ODE in time for the height h. From the reduced model, we see that, given uniform initial conditions, there are no spatial gradients in the dependent variables θ_p, n and h; accordingly, the gel evolves in a spatially-invariant manner. This is a consequence of the 2D geometry, where due to the thinness of the gel and the significant length of the boundary across $y = h$ compared to that

at $X = 1$, solvent flows into or from the gel across the horizontal boundary in much greater amounts than across the vertical interface at $X = 1$.

This manner of evolution is a significant difference between the thin film and 1D model of Chapter 3. In the 1D case, fluid only flows into or out of the gel through the boundary at $X = 1$. This means that even with uniform initial conditions, any non-zero drag creates a shearing effect as the gel evolves, and non-uniform spatial profiles arise in the dependent variables (these non-uniformities generally smooth out by the time the gel equilibrates). Meanwhile, with uniform initial conditions in the thin film, the gel's contraction or swelling is driven by solvent flow in the thin direction; accordingly, drag does not influence the gel's behaviour. Given no such shearing occurs between the polymer and solvent, the gel maintains its spatially uniform structure as it evolves and reaches equilibrium. This is highlighted by the drag parameter not contributing to the ODE model.

In this thin film case, the spatial uniformity is a product of the gel's geometry, with no assumptions necessary beyond taking uniform initial conditions. We note that we can derive an ODE solution for uniform initial conditions in the 1D Cartesian model (as was done in Keener *et al.* (2011b)); however, this is only possible by imposing the assumption that drag $\xi = 0$. We remark that Moon and Tranquillo (1993) also derived an ODE reduction to their 1D mechanochemical model on assuming that the velocity was linear in space.

The ODE model is driven by the balance in cell and chemical potentials internally with the external chemical potential. The simulations reach the same equilibrium values for θ^* and n^* given the same parameter values and initial conditions as in the 1D model; this is to be expected given the same equilibrium conditions exist in both cases.

We note that the modelling assumption is made in Stevenson *et al.* (2010) when calculating cell traction that the ratio of gel height to radius remains constant during the gel's evolution. The results seen here, where the scaled thin film length and height are equal, add support to this modelling assumption.

Given uniform initial conditions, we have seen different dynamics at work in the thin film problem compared to the 1D case. The extra source of solvent across the large horizontal interface allows the gel to equilibrate more rapidly and in a spatially

uniform manner. We will now study the thin film with non-uniform initial conditions and consider the emergent behaviours that follow.

6

THIN FILM ANALYSIS: NON-UNIFORM INITIAL CONDITIONS

6.1 INTRODUCTION

In this chapter, we study the thin film model developed in Chapter 4 using spatially varying initial conditions. In Chapter 5, we found that with uniform initial conditions, we can reduce the thin film model to a system driven by a single ODE for the gel height h; this simplified both analytic and numerical analysis of the model. For non-uniform initial conditions, the gel need not remain spatially uniform as it evolves, and therefore, we must solve the full PDE system given by (4.128) - (4.139). We firstly discuss the equilibrium conditions for the model. We then develop a small time solution to examine the stability of equilibria to spatial perturbations. Finally, we develop a numerical scheme and present solutions for non-uniform initial conditions. We evaluate a range of initial conditions and parameter choices, finding that spatial non-uniformities will persist at equilibrium with non-uniform initial conditions in the gel.

In this chapter, we again evaluate the leading order thin film model on a fixed spatial domain which was derived in Chapter 4; this model is given by equations (4.128) - (4.139).

6.2 STEADY STATE CONDITIONS

In studying the steady state conditions, we use the non-conservative mass conservation equations (4.140) and (4.141) in place of (4.129) and (4.130). We again repeat the mass and momentum balance equations, where the subscript zeroes have been dropped from leading order variables for notational convenience,

$$\frac{\partial h}{\partial T} - X\frac{\dot{L}}{L}\frac{\partial h}{\partial X} + \frac{1}{L}\frac{\partial}{\partial X}\left(h v_p\right) - \frac{2h}{L}\frac{\partial v_p}{\partial X} = 0, \tag{6.1}$$

$$\frac{\partial \theta_p}{\partial T} - X\frac{\dot{L}}{L}\frac{\partial \theta_p}{\partial X} + \frac{1}{L}\frac{\partial}{\partial X}\left(\theta_p v_p\right) + \frac{\theta_p}{L}\frac{\partial v_p}{\partial X} = 0, \tag{6.2}$$

$$\frac{\partial n}{\partial T} - X\frac{\dot{L}}{L}\frac{\partial n}{\partial X} + \frac{1}{L}\frac{\partial}{\partial X}\left(n v_p\right) + \frac{n}{L}\frac{\partial v_p}{\partial X} - \frac{D}{L^2 h}\frac{\partial}{\partial X}\left(h\frac{\partial n}{\partial X}\right) = 0, \tag{6.3}$$

$$\frac{2h}{L}\frac{\partial v_p}{\partial X} - \frac{1}{L^2}\frac{\partial}{\partial X}\left\{\frac{\theta_s h}{\xi \theta_p}\left(\frac{\partial \mu_s}{\partial X} + \frac{\partial}{\partial X}\left(\theta_p G\right)\right)\right\} + \frac{1}{\mathcal{R}}\left(\mu_s - \mu_s^e + \theta_p G\right) = 0. \tag{6.4}$$

The steady state system here is

$$\frac{1}{L}\frac{\partial}{\partial X}(h v_p) - \frac{2h}{L}\frac{\partial v_p}{\partial X} = 0, \tag{6.5}$$

$$\frac{1}{L}\frac{\partial}{\partial X}(\theta_p v_p) + \frac{\theta_p}{L}\frac{\partial v_p}{\partial X} = 0, \tag{6.6}$$

$$\frac{1}{L}\frac{\partial}{\partial X}(n v_p) + \frac{n}{L}\frac{\partial v_p}{\partial X} - \frac{D}{L^2 h}\frac{\partial}{\partial X}\left(h\frac{\partial n}{\partial X}\right) = 0, \tag{6.7}$$

$$\frac{2h}{L}\frac{\partial v_p}{\partial X} - \frac{1}{L^2}\frac{\partial}{\partial X}\left\{\frac{\theta_s h}{\xi\theta_p}\left(\frac{\partial \mu_s}{\partial X} + \frac{\partial}{\partial X}(\theta_p G)\right)\right\} + \frac{1}{\mathcal{R}}(\mu_s - \mu_s^e + \theta_p G) = 0. \tag{6.8}$$

To demonstrate that there is zero velocity at a steady state, we return briefly to the conservative advection equation (4.129). At equilibrium, this becomes

$$\frac{1}{L}\frac{\partial}{\partial X}(\theta_p h v_p) = 0. \tag{6.9}$$

Integrating with respect to X and applying zero velocity at $X = 0$, we find

$$\theta_p h v_p = 0; \tag{6.10}$$

given $\theta_p > 0$ and $h > 0$, this means that we must have $v_p = 0$ at equilibrium.

From equation (4.62) (translated to the fixed spatial domain), we then have

$$v_s = -\frac{1}{\xi L\theta_p}\frac{\partial}{\partial X}(\mu_s + \theta_p G). \tag{6.11}$$

We will see in this section that the right-hand side of this expression must be zero at a steady state, demonstrating that $v_s = 0$.

Thus, this system equilibrates when θ_p, n and h reach such values that there is zero net force everywhere, there is zero velocity, and the gel length and height are not changing.

We saw that in the case of uniform initial conditions, the equilibrium condition for the thin film model was given by equation (5.32) as follows,

$$\mu_s - \mu_s^e + \theta_p G = 0. \tag{6.12}$$

For the system to be at a steady state with non-uniform initial conditions, the following condition in the momentum balance equation (6.4) must be satisfied,

$$-\frac{1}{L^2}\frac{\partial}{\partial X}\left\{\frac{\theta_s h}{\xi\theta_p}\left(\frac{\partial \mu_s}{\partial X}+\frac{\partial}{\partial X}\left(\theta_p G\right)\right)\right\}+\frac{1}{\mathcal{R}}\left(\mu_s-\mu_s^e+\theta_p G\right)=0. \tag{6.13}$$

From the cell advection-diffusion equation (6.3), we also have

$$\frac{D}{h}\frac{\partial}{\partial X}\left(h\frac{\partial n}{\partial X}\right)=0. \tag{6.14}$$

Given the model derivation in Chapter 4, we must take $D \neq 0$. Therefore, integrating (6.14) and applying the no-flux boundary condition (4.134), we find,

$$h\frac{\partial n}{\partial X}=0; \tag{6.15}$$

given $h > 0$, this indicates that, at equilibrium,

$$\frac{\partial n}{\partial X}=0, \tag{6.16}$$

and accordingly, n must be spatially uniform.

Given that $G = G(n)$, we can then express (6.13) in the form

$$-\frac{1}{L^2}\frac{\partial}{\partial X}\left\{\frac{\theta_s h}{\xi\theta_p}\left(\frac{\partial \mu_s}{\partial \theta_p}+G\right)\frac{\partial \theta_p}{\partial X}\right\}+\frac{1}{\mathcal{R}}\left(\mu_s-\mu_s^e+\theta_p G\right)=0. \tag{6.17}$$

We note that

$$\frac{\partial}{\partial X}\left(\mu_s-\mu_s^e+\theta_p G\right)=\left(\frac{\partial \mu_s}{\partial \theta_p}+G\right)\frac{\partial \theta_p}{\partial X}, \tag{6.18}$$

and therefore, if $\mu_s-\mu_s^e+\theta_p G=0$, equation 6.17 must be satisfied. We saw in equations (3.49) - (3.52) that for the right-hand side of (6.18) to equal zero, we must have

$$\frac{\partial \theta_p}{\partial X}=0. \tag{6.19}$$

Therefore, sufficient conditions for equilibrium in the thin film are spatially uniform values $\theta_p = \theta^*$ and $n = n^*$ that satisfy (6.12). These are the same conditions as seen in Chapter 3 when $D \neq 0$. We note that there are no restrictions on h, *i.e.* the height can be non-uniform in space at the gel's steady state.

As mentioned, these equilibrium conditions match those discussed in Section 3.4 for a 1D gel with $D \neq 0$. Therefore, we expect any equilibrium solution for θ_p and n in the 1D Cartesian model with $D \neq 0$ (Chapter 3) and the reduced thin film model (Chapter 5) to be an equilibrium here, and similarly, any equilibrium found herein to be a steady state in these earlier models.

We now demonstrate that equation (6.12) together with uniform n and θ_p are the necessary conditions for equilibrium. To see this, we revert back to the 2D model before it is re-scaled. From equations (4.9) and (4.10), at a steady state we have,

$$\nabla P = \nabla (\theta_p G). \tag{6.20}$$

From (4.11) and (4.12), we then see that, at equilibrium,

$$\nabla (\mu_s + \theta_p G) = 0. \tag{6.21}$$

We integrate this to find the steady state condition,

$$\mu_s + \theta_p G = C(t), \tag{6.22}$$

where $C(t)$ is to be determined. From the interface conditions (4.19) and (4.21) at $x = L$, we find that

$$\theta_p G + \mu_s - \mu_s^e = 0, \tag{6.23}$$

and accordingly, we see that $C = \mu_s^e$, where μ_s^e is constant. We therefore have the following equilibrium condition for the 2D system of equations,

$$\theta_p G + \mu_s = \mu_s^e. \tag{6.24}$$

We can also reinforce here that θ_p must be constant at a steady state. Firstly, from equation (4.3) with no flux boundary conditions, we find that n is constant at equilibrium. Upon expanding μ_s and with constant n, (6.24) then becomes,

$$F(\theta_p) = \log(1-\theta_p) + \chi\theta_p^2 + \theta_p\left(G + 1 - \frac{1}{N}\right) = 0. \tag{6.25}$$

Now, in the limit $\theta_p \to 0$, $F \to 0$. Meanwhile, $F \to -\infty$ as $\theta_p \to 1$. Differentiating F yields,

$$F'(\theta_p) = -\frac{1}{1-\theta_p} + 2\chi\theta_p + G + 1 - \frac{1}{N}. \tag{6.26}$$

Setting $F' = 0$, we see that F has at most two turning points, and consequently, (6.25) has at most two unique, non-zero solutions in θ_p. Accordingly, given that θ_p must be continuous, we see that only constant values for the polymer fraction will satisfy the equilibrium condition.

Therefore, spatially uniform values for θ_p and n satisfying equation (6.12) are the necessary conditions for equilibrium in the thin film.

6.3 SMALL TIME EVOLUTION OF SPATIALLY PERTURBED EQUILIBRIA

We now develop a short time solution to the thin film model. We evaluate the short time behaviour of equilibrium initial conditions subject to spatial perturbations. As was the case with the 1D model in Chapter 3, this analysis will allow us to suggest the stability of equilibria through studying the behaviour of the spatially varying perturbations: unstable equilibria will see an increase in the amplitude of the perturbations, while for stable equilibria, the amplitude of the perturbations will decay. Alongside θ_p and n, which we have found must be spatially uniform at equilibrium, we restrict our analysis to spatially uniform equilibrium values of h, owing to the difficulty of finding analytic solutions for non-uniform examples.

We denote the dimensionless equilibrium values by asterisks, L^*, θ^*, n^*, h^*, v^* (where $v^* = 0$). The equilibrium values of h, n and L are used as the characteristic

values to scale these variables; this means that $h^* = n^* = L^* = 1$. We take spatial perturbations with amplitude ϵ, where $\delta \ll \epsilon \ll 1$; δ is the short time scale described previously, such that $T = \delta\hat{T}$. Note that the amplitude ϵ is distinct from the inverse aspect ratio ε seen in Chapter 4. We expand our variables as power series in ϵ and δ as described in equations (3.73), (3.74), and so on, and take the initial conditions

$$L_0 = 1, \tag{6.27}$$

$$v_0 = \epsilon v_{01} + \epsilon^2 v_{02} + ..., \tag{6.28}$$

$$\theta_0 = \theta^* + \epsilon\theta_{01}(X), \tag{6.29}$$

$$n_0 = 1 + \epsilon n_{01}(X), \tag{6.30}$$

$$h_0 = 1 + \epsilon h_{01}(X). \tag{6.31}$$

Note that we set $L_0 = L^* = 1$, *i.e.* we do not perturb the initial length of the gel from its equilibrium value. Also note that higher order terms of v_0 are determined through analysis of the momentum balance equation (6.4). We again set $\theta_{01} = \cos(\gamma X)$, $n_{01} = N_{01}\cos(\gamma X)$, and take $h_{01} = -H_{01}\cos(\gamma X)$, where N_{01} and H_{01} are constants that are $\mathcal{O}(1)$. Given that we expect h to move in the opposite direction to θ_p and n, we have taken h_{01} to have the opposite sign to that of n_{01} and θ_{01} without loss of generality. The initial conditions for θ_p, n and h therefore become

$$\theta_0 = \theta^* + \epsilon\cos(\gamma X), \tag{6.32}$$

$$n_0 = 1 + \epsilon N_{01}\cos(\gamma X), \tag{6.33}$$

$$h_0 = 1 - \epsilon H_{01}\cos(\gamma X). \tag{6.34}$$

We require θ_0, n_0 and h_0 to satisfy the symmetry boundary conditions (4.133), (4.134) and (4.135) at $X = 0$ for any choice of γ. The no-flux boundary conditions (4.133) and (4.134) at $X = 1$ require that $\gamma = Z\pi$ for some positive integer Z.

We ensure that, for any choices of the constants H_{01} and N_{01}, the masses of polymer and cells under the perturbed initial conditions are, to $\mathcal{O}(\epsilon)$, equal to the masses for the

unperturbed initial conditions (which are θ^* for the polymer and 1 for the cell density) Integrating $\theta_0 h_0 L_0$ across the spatial domain $0 \leqslant X \leqslant 1$, we have

$$\begin{aligned}\theta^* &= \int_0^1 (\theta_0 h_0 L_0) dX, \\ &= \int_0^1 (\theta^* + \epsilon \cos(\gamma X)(1 - \epsilon H_{01} \cos(\gamma X)) dX, \\ &= \theta^* + \epsilon \frac{1}{\gamma} \sin(\gamma) - \epsilon \frac{\theta^* H_{01}}{\gamma} \sin(\gamma) + \mathcal{O}(\epsilon^2).\end{aligned}$$

Since $\sin(\gamma) = 0$ for all valid choices of γ, we see that mass is conserved to $\mathcal{O}(\epsilon)$, regardless of our choice of H_{01}. Therefore, we are free to set H_{01} to any $\mathcal{O}(1)$ value. On evaluating $n_0 h_0 L_0$, we find that we are similarly free to set N_{01} to any $\mathcal{O}(1)$ value.

To find v_{01}, we use equation (6.4) at $\mathcal{O}(\epsilon)$, obtaining the expression

$$\begin{aligned}\frac{\partial v_{01}}{\partial X} = \frac{(1-\theta^*)}{2\xi\theta^*} \frac{\partial}{\partial X} \left(-\theta^* f''(\theta^*) \frac{\partial \theta_{01}}{\partial X} + \frac{\tau_0}{1+\lambda} \frac{\partial \theta_{01}}{\partial X} + \theta^* \frac{2\tau_0 N_{01}}{(1+\lambda)^2} \frac{\partial n_{01}}{\partial X} \right) - \\ \frac{1}{2\mathcal{R}} \left(-\theta^* f''(\theta^*) \theta_{01} + \frac{\tau_0}{1+\lambda} \theta_{01} + \theta^* \frac{2\tau_0 N_{01}}{(1+\lambda)^2} n_{01} \right),\end{aligned} \tag{6.35}$$

After substituting for θ_{01} and n_{01}, this simplifies to

$$\frac{\partial v_{01}}{\partial X} = \left(\frac{(1-\theta^*)}{2\xi\theta^*} \gamma^2 + \frac{1}{2\mathcal{R}} \right) z \cos(\gamma X), \tag{6.36}$$

where, as in equation (3.89) in the 1D Cartesian model,

$$z = \theta^* f''(\theta^*) - \frac{\tau_0}{1+\lambda} - \theta^* \frac{2\tau_0 N_{01}}{(1+\lambda)^2}. \tag{6.37}$$

We therefore have the solution

$$v_{01} = \left(\frac{(1-\theta^*)}{2\xi\theta^*} \gamma + \frac{1}{2\mathcal{R}\gamma} \right) z \sin(\gamma X). \tag{6.38}$$

Solving the mass conservation equations (6.1) - (6.3) at $\mathcal{O}(\delta)$, we find that $\theta_{10} = n_{10} = h_{10} = 0$, as these terms depend on $v^* = 0$. The kinematic boundary condition (4.137) for L similarly gives $L_{10} = 0$.

We therefore consider the mass conservation equations at $\mathcal{O}(\delta\epsilon)$. From equation (6.1), we find

$$\frac{\partial h_{11}}{\partial \hat{T}} = \frac{\partial v_{01}}{\partial X}, \tag{6.39}$$

so that

$$h_{11} = \frac{\partial v_{01}}{\partial X}\hat{T}. \tag{6.40}$$

Similarly, we find from equations (6.2) and (6.3) respectively that

$$\theta_{11} = -2\theta^* \frac{\partial v_{01}}{\partial X}\hat{T}, \tag{6.41}$$

$$n_{11} = \left(-2\frac{\partial v_{01}}{\partial X} + D\frac{\partial^2 n_{01}}{\partial X^2}\right)\hat{T}. \tag{6.42}$$

From the kinematic boundary condition at $\mathcal{O}(\delta\epsilon)$, we find that $L_{11} = v_{01}(X = 1) = 0$.

Thus, we have the small time analytic solutions

$$\theta_p(X, \hat{T}) = \theta^* + \epsilon\cos(\gamma X) - \epsilon\delta\hat{T}\theta^*\left(\frac{(1-\theta^*)}{\xi\theta^*}\gamma^2 + \frac{1}{\mathcal{R}}\right) z\cos(\gamma X) + \mathcal{O}(\delta^2), \tag{6.43}$$

$$\begin{aligned} n(X, \hat{T}) = 1 &+ \epsilon N_{01}\cos(\gamma X) \\ &- \epsilon\delta\hat{T}\left\{\left(\frac{(1-\theta^*)}{\xi\theta^*}\gamma^2 + \frac{1}{\mathcal{R}}\right) z + DN_{01}\gamma^2\right\}\cos(\gamma X) + \mathcal{O}(\delta^2), \end{aligned} \tag{6.44}$$

$$h(X, \hat{T}) = 1 - \epsilon H_{01}\cos(\gamma X) + \epsilon\delta\hat{T}\left(\frac{(1-\theta^*)}{2\xi\theta^*}\gamma^2 + \frac{1}{2\mathcal{R}}\right) z\cos(\gamma X) + \mathcal{O}(\delta^2), \tag{6.45}$$

$$L(\hat{T}) = 1 + \mathcal{O}(\delta^2). \tag{6.46}$$

We note that these solutions satisfy the no-flux boundary conditions at $X = 1$.

We are again interested in the temporal growth or decay of the spatial perturbations to our equilibrium initial conditions. We therefore evaluate how the amplitude of terms involving $\cos(\gamma X)$ evolves over the small time scale. From our solution for θ_p given by equation (6.43), we have the terms,

$$\left\{1 - \left(\frac{(1-\theta^*)}{\xi\theta^*}\gamma^2 + \frac{1}{\mathcal{R}}\right) z\theta^*\delta\hat{T}\right\}\epsilon\cos(\gamma X). \tag{6.47}$$

From the solution for n (6.44), we have,

$$\left\{1-\left(\left(\frac{(1-\theta^*)}{\xi\theta^*}\gamma^2+\frac{1}{\mathcal{R}}\right)\frac{z}{N_{01}}+D\gamma^2\right)\delta\hat{T}\right\}N_{01}\epsilon\cos(\gamma X), \tag{6.48}$$

and similarly for h in (6.45),

$$\left\{1-\left(\frac{(1-\theta^*)}{2\xi\theta^*}\gamma^2+\frac{1}{2\mathcal{R}}\right)\frac{z}{H_{01}}\delta\hat{T}\right\}H_{01}\epsilon\cos(\gamma X). \tag{6.49}$$

Given the absence of the $\cosh(\alpha X)$ terms we saw previously in Section 3.6, the results here can be interpreted in a straightforward manner with respect to stability and instability in the gel. The terms multiplying $\cos(\gamma X)$ in each variable represent the spatial perturbations. The growth or decay of the perturbations in equations (6.43) and (6.45) is governed by the sign of z. For $z > 0$, the magnitude of the spatial perturbations is decreasing, and accordingly, the local spatial variations decay over time. With $z < 0$ on the other hand, the polymer fraction and height grow away from steady state, signalling that the equilibrium is unstable. The cell density (6.44) follows this same behaviour; however, the presence of diffusion may smooth unstable behaviour, depending on the balance of parameters.

The equilibrium and stability conditions for the thin film model, including the value of z, are equivalent to those presented in Chapter 3 for the 1D Cartesian gel. Therefore, the results presented in Section 3.6.6 also remain valid for the thin film case. Accordingly, we do not present these again here. We will use these small time solutions to confirm that our numerical simulations are evolving in the correct manner in the following section.

6.4 THIN FILM NUMERICS

We develop a numerical scheme to evaluate the thin film described in equations (4.128) - (4.139). We now consider both uniform and non-uniform initial conditions under a variety of parameter choices to understand the forces driving gel swelling and contrac-

tion. We find that it is possible for spatially non-uniform equilibria in the gel's height to emerge numerically in this thin film setting.

To study the thin film model for spatially varying initial conditions, we use a similar numerical scheme to that presented in Chapter 3, and again solve using MATLAB. We use a finite difference scheme to discretise the system of equations with a uniform spatial grid between $X = 0$ and $X = 1$. The force balance equation (6.4) is first-order in velocity v_p, therefore we use a cumulative trapezoidal scheme to numerically integrate the expression across the spatial domain and update the velocity at each new time step. Central differencing is used for spatial derivatives in (6.4), except for the derivatives of (6.55) at the endpoints of the domain, where one-sided differences are used. A Crank-Nicolson method is used to solve equations (6.1) - (6.3) in the conservative form detailed below.

We find that this scheme conserves mass effectively. Using a time step dT between 10^{-6} and 10^{-5} and spatial step $dX = 0.025$ in the simulations which follow, the worst-case change in mass between initial time and end time for the cell density or polymer fraction was $2.69 \times 10^{-5}\%$. To further check our numerical scheme, in Section 6.4.1 we compare the full numerical solution with the small time solution detailed in Section 6.3, and in Section 6.4.2 we compare this numerical solution with the ODE solution from Chapter 5, finding good agreement in each case. While this numerical scheme has performed well over a wide range of parameter choices and initial conditions, we note that some instability and non-convergence has been encountered for particular parameter combinations where the gel evolution is rapid, *e.g.* with large values of τ_0 or χ.

We numerically solve the conservative form of the mass and momentum balance equations given by (4.129) - (4.132). We define the quantities $Q(X,T) = \theta_p h$ and $W(X,T) = \theta_s h$, and note the relations that follow,

$$h = Q + W, \quad \theta_p = \frac{Q}{Q+W}, \quad \theta_s = \frac{W}{Q+W}.$$

We transform the chemical potential μ_s into a function of Q and W as follows,

$$\mu_s = f(\theta_p) - \theta_p f'(\theta_p) = \log(\theta_s) + \left(1 - \frac{1}{N}\right)\theta_p + \chi\theta_p^2 + \mu_s^0,$$
$$\implies \mu_s(Q, W) = \log\left(\frac{W}{W+Q}\right) + \left(1 - \frac{1}{N}\right)\frac{Q}{Q+W} + \chi\left(\frac{Q}{Q+W}\right)^2 + \mu_s^0. \tag{6.50}$$

Similarly, its derivative becomes

$$\frac{\partial \mu_s}{\partial X} = \left(-\frac{1}{\theta_s} + 1 - \frac{1}{N} + 2\chi\theta_p\right)\frac{\partial \theta_p}{\partial X},$$
$$\implies \frac{\partial \mu_s}{\partial X} = \left(-\frac{Q+W}{W} + 1 - \frac{1}{N} + 2\chi\left(\frac{Q}{Q+W}\right)\right)\frac{\partial}{\partial X}\left(\frac{Q}{Q+W}\right). \tag{6.51}$$

Equations (4.129), (4.130) and (4.132) can then be expressed respectively as

$$\frac{\partial Q}{\partial T} - X\frac{\dot{L}}{L}\frac{\partial Q}{\partial X} + \frac{1}{L}\frac{\partial}{\partial X}(Qv_p) = 0, \tag{6.52}$$
$$\frac{\partial W}{\partial T} - X\frac{\dot{L}}{L}\frac{\partial W}{\partial X} + \frac{1}{L}\frac{\partial}{\partial X}(Wv_p) - \frac{2(Q+W)}{L}\frac{\partial v_p}{\partial X} = 0, \tag{6.53}$$
$$\frac{2(Q+W)}{L}\frac{\partial v_p}{\partial X} - \frac{1}{L^2}\frac{\partial}{\partial X}(V_1(Q, W, n)) + V_2(Q, W, n) = 0, \tag{6.54}$$

where

$$V_1(Q, W, n) = \frac{1}{\xi}\left(-(Q+W) - \frac{W}{N}\left(1 + \frac{W}{Q}\right) + 2\chi W\right)\frac{\partial}{\partial X}\left(\frac{Q}{Q+W}\right) + \frac{\tau_0}{\xi}\frac{W(Q+W)}{Q}\frac{\partial}{\partial X}\left(\frac{Q}{Q+W}\frac{n^2}{1+\lambda n^2}\right), \tag{6.55}$$
$$V_2(Q, W, n) = \frac{1}{\mathcal{R}}\left(\log\left(\frac{W}{W+Q}\right) + \left(1 - \frac{1}{N}\right)\frac{Q}{Q+W} + \chi\left(\frac{Q}{Q+W}\right)^2 + \frac{Q}{Q+W}\frac{\tau_0 n^2}{1+\lambda n^2}\right) = 0. \tag{6.56}$$

The cell advection-diffusion equation remains as given in equation (4.131).

We evaluate these equations using the following algorithm:

1. Set parameter values and initial conditions in variables θ_p, n, h, L.

2. Compute Q and W at $T = 0$.

3. Solve equation (6.54) for the velocity v_p at $T = 0$ using the cumulative trapezoidal rule to integrate the first-order PDE in space, subject to boundary condition (4.136).

4. For $i = 1, 2, ...$

   a) Increment T by time step dT.

   b) Solve the polymer mass advection equation (6.52) using a Crank-Nicolson scheme, subject to boundary conditions (4.133) and (4.135).

   c) Solve the solvent mass advection equation (6.53) using a Crank-Nicolson scheme, subject to boundary conditions (4.133) and (4.135).

   d) Solve the cell advection-diffusion equation (4.131) using a Crank-Nicolson scheme, subject to boundary conditions (4.134).

   e) Update the velocity by solving equation (6.54) using the new values of θ_p, h and n as in step 3, subject to boundary condition (4.136).

   f) Use the kinematic boundary condition (4.137) with an explicit Euler time step to update the length of the gel.

The end time is chosen to be large enough that the gel reaches a steady state or θ_p approaches 0 or 1, in which case our model breaks down. We then analyse the solutions for n, θ_p, h and L over time to understand the evolution of the gel.

Throughout the simulations presented in this section, we will again keep certain parameters fixed and study the effects of changing others between simulations. The fixed parameters retain the values given in Table 3.1 (noting that the solvent viscosities η_s and κ_s have already been set to zero in Chapter 4). The ranges of values used for the parameters and initial conditions which may vary between examples are presented in Table 6.1. We note that the initial conditions for θ_p, n and h will have spatially varying components included on occasion in the simulations which follow; accordingly, we scale the initial conditions for height and cell density on the average initial value for each, such that the mean values $\bar{h}_i = \int_0^1 h_i(X)dX = 1$ and $\bar{n}_i = \int_0^1 n_i(X)dX = 1$. Similarly, when spatial perturbations are added to θ_p, these are such that $\bar{\theta}_i = \int_0^1 \theta_i(X)dX$.

Table 6.1: Initial conditions (excluding spatially varying components) and parameters which we change between simulations

Term	Symbol	Values
Initial polymer fraction	θ_i	0.3 - 0.6
Initial cell density	n_i	0 - 1
Initial height	h_i	1
Cell traction coefficient	τ_0	0.75 - 1
Cell diffusion coefficient	D	0 - 1
Mixing parameter	χ	-0.5869 - 0.75
Interface resistance	$\mathcal{R}$	0.4 - 4
Drag coefficient	ξ	0.2 - 4

6.4.1 *Comparison with small time solution*

In Fig. 6.1, we compare the numerical solution for θ_p with the small time analytic solution given by equation (6.43) over early time. We solve condition (6.12) to find an equilibrium θ^* and n^* using an arbitrary choice of parameters. We see that the two solutions for θ_p are in good agreement at different points in the spatial domain, albeit for a short time frame. The presence of a significant diffusion coefficient here quickly draws the numerical solutions back to equilibrium. We see similar behaviour in the solutions for n and h (results not shown). For this equilibrium, $z = 0.3$, indicating a stable equilibrium; we see in Fig. 6.1 that the polymer fraction accordingly reverts back towards a uniform steady state.

6.4.2 *Uniform initial conditions*

In Chapter 5, we presented a numerical method for solving the reduced thin film model, given by equations (5.27) - (5.30), which arises for uniform initial conditions. We also presented simulations for different cases of gel swelling and contraction, both with and without cells. Therefore, we do not repeat similar analysis for uniform initial conditions here.

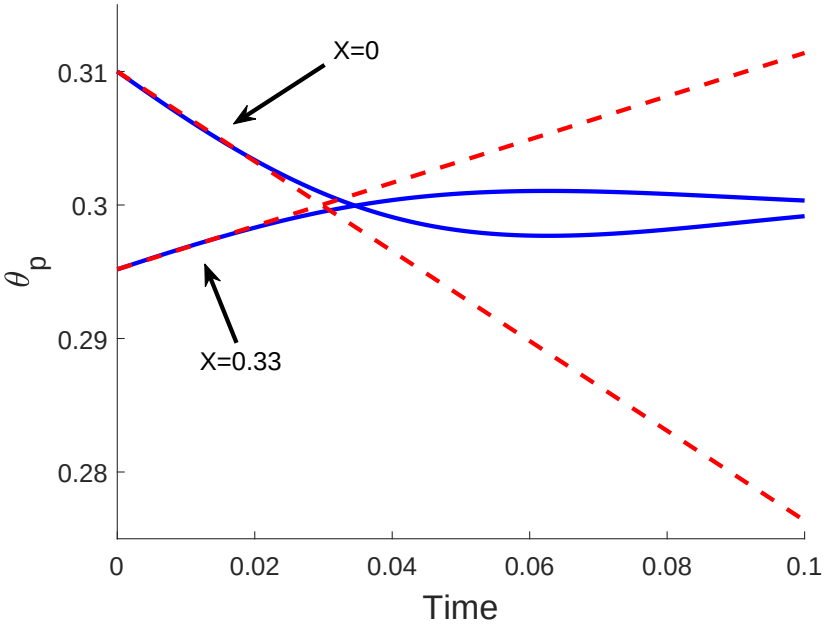

Figure 6.1: Comparing the small time solution (6.43) for θ_p with perturbed equilibrium initial conditions (red dashed lines) with the numerical solution (blue solid lines) over early time at $X = 0$ and $X = 0.33$. The solutions are closely matched over small time. Values: $\theta_i = 0.3 + 0.01\cos(2\pi X)$, $n_i = 1 + 0.01\cos(2\pi X)$, $h = 1 - 0.01\cos(2\pi X)$, $\chi = -0.5869$, $\xi = 0.25$, $\mathcal{R} = 0.75$, $\tau_0 = 0.75$, $D = 1$, $\gamma = 2\pi$, $\epsilon = 0.01$, $N_{01} = H_{01} = 1$.

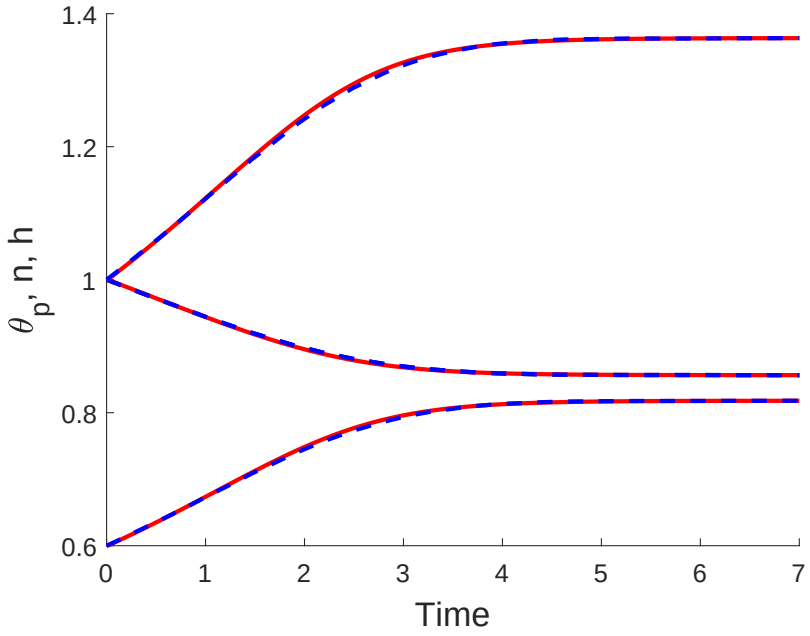

Figure 6.2: Comparison of simulations for a gel with uniform initial conditions using the ODE solver (blue dashed lines) and full numerical scheme (red solid lines) for cell density, height and polymer fraction (in descending vertical order). Values: $\theta_i = 0.6$, $n_i = 1$, $h_i = 1$, $\chi = 0.7$, $\xi = 1$, $\mathcal{R} = 1.5$, $\tau_0 = 0.8$, $D = 1$.

We note that the full numerical scheme described here behaves in agreement with the numerical solutions for the reduced model. Fig. 6.2 compares the solutions for the time evolution of a contracting gel with cells between the full numerics and the ODE solver used in the previous chapter. We see that the two simulations are equivalent as the gel evolves to its steady state.

6.4.3 *Non-uniform initial conditions: introduction*

We now consider spatially varying initial conditions in one or more of the polymer fraction, cell density and height. We analyse the gel behaviours emerging in these different cases, in particular evaluating whether spatial non-uniformities persist or are smoothed out as the gel evolves over time, and whether perturbing particular dependent variables has different impacts on the system's outcomes.

6.4.4 *Spatially varying initial polymer, cell-free gel*

We first consider a cell-free gel with a non-uniform initial polymer distribution. We take the initial condition $\theta_i = 0.6 + 0.02\cos(\pi X)$, noting that θ_i satisfies the boundary conditions $\partial\theta_p/\partial X = 0$ at $X = 0$ and $X = 1$, and that the initial mass of polymer in the gel remains 0.6 under this initial condition. This resembles a gel where the polymer is initially slightly bunched around the centre of the thin film at $X = 0$. We will firstly discuss the equilibrium outcomes for the gel, then describe how the variables change over time.

We see in this environment that spatially varying steady states can be found without the presence of cells. Fig. 6.3 displays the time evolution of $\theta_p(X, T)$ at $X = 0$ and $X = 1$, while Fig. 6.4 shows the time evolution of $h(X, T)$ at $X = 0$ and $X = 1$ as well as $L(T)$. We see that the gel height h evolves to a non-uniform equilibrium here. The mixing parameter $\chi = 0.75$ is at a value that promotes mixing between the polymer and solvent. This drives an osmotic pressure gradient, causing the gel to swell to an equilibrium state, with solvent flowing into the gel. The polymer fraction converges to a uniform value as it evolves, reaching a steady state where $\theta^* = 0.45$. Meanwhile, we see that non-uniformities develop in the gel height; these spatial variations persist at equilibrium where the mean equilibrium value $\bar{h}^* = 1.16$ and the amplitude $A_{h^*} = 0.019$, where $A_{h^*} = (h^*_{max} - h^*_{min})/2$. The amplitude A_{h^*} is of a similar magnitude to the amplitude of the initial polymer fraction. The gel length at equilibrium $L^* = 1.16$ is equal to the mean equilibrium value of the height $\bar{h}^*$.

Figs. 6.5 and 6.6 show the spatial distributions of θ_p and h respectively across the gel length at increasing points in time. As seen in Fig. 6.5, the initial non-uniformity in the polymer distribution quickly smooths out so that θ_p is uniform across the spatial domain. Meanwhile, Fig. 6.6 demonstrates that sinusoidal variations matching the shape of those in the initial polymer arise in the gel height. These variations persist over time, resulting in varying height at the gel's steady state.

In response to the osmotic pressure gradient here driven by the free energy, we see more solvent enter the gel over early time (*e.g.* $T = 0$ to $T = 0.5$) in the regions of higher polymer fractions near $X = 0$, resulting in these areas of the gel becoming

locally thicker. This is seen in the gel height increasing to a greater degree close to $X = 0$ since more solvent is entering the gel in that region. Conversely, we see θ_p increase near $X = 1$ over this time period, *i.e.* there is some localised contraction in the gel due to the initial presence of more solvent in this region. This corresponds to decreases in h seen at corresponding times. By $T = 1$, the gel swells across the spatial domain, with a uniform polymer profile developing as solvent continues to enter the gel more rapidly in areas of greater polymer concentration. The height continues to increase as the gel swells, maintaining its non-uniform distribution. These variations that develop and persist in h correspond to local variations in mass across the spatial domain that exist from the initial non-uniformity in θ_i. Accordingly, while the fraction of polymer is constant by the time the gel equilibrates, the mass of polymer per unit length $\theta^* h^*(X)$ varies in space.

In Section 6.2, we found that $\partial\theta_p/\partial X = 0$ is a necessary condition for equilibrium in the thin film. We see here that the polymer is redistributed evenly such that there is a balance in chemical potential from gel to solvent and within the gel itself. The extra mass at different points in space (coming from the spatially varying height) enables a constant polymer fraction to be maintained at equilibrium. We note that this model does not consider surface tension. With surface tension present, we might expect the variations in height to smooth over time as well; however, in its absence, there is no force driving the surface to flatten out and we see the non-uniformities persist at equilibrium.

The equilibrium polymer fraction $\theta^* = 0.45$ matches that in Fig. 3.8 where $\theta_i = 0.6$ and $\chi = 0.75$, indicating that the spatial perturbation does not affect the equilibrium quantity of polymer found. We also note that the same behaviour is evident in a cell-free contracting gel, *i.e.* θ_p is uniform at equilibrium with spatially varying h (results not shown).

We see the same qualitative outcome for the gel when taking non-uniform h_i with uniform θ_i, *i.e.* at the resulting steady state, h^* will vary in space while θ^* is uniform (results not shown). As seen in the previous example, the variations in mass across the spatial domain allow for a uniform polymer fraction to be maintained at equilibrium.

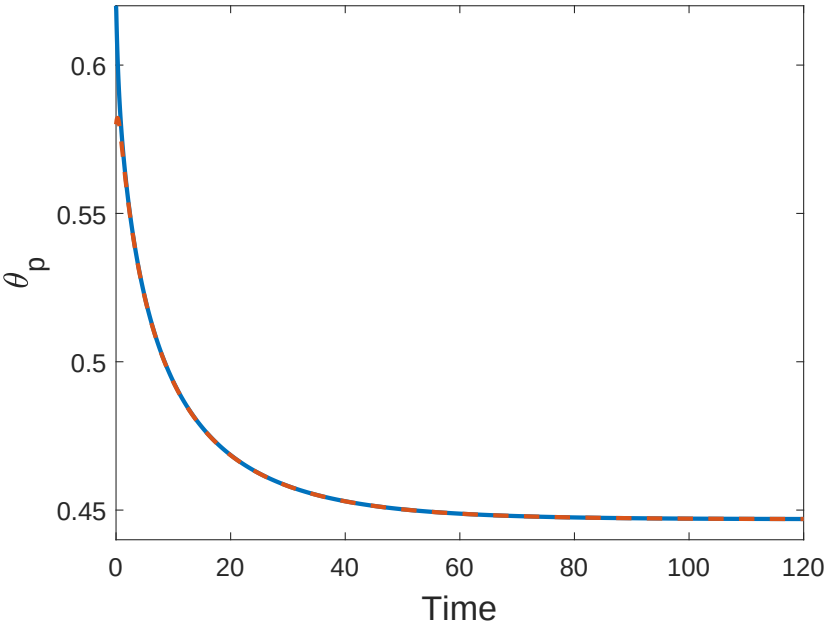

Figure 6.3: Time evolution of a cell-free gel with non-uniform initial polymer fraction. The polymer fraction evens out to a uniform equilibrium as the gel swells. $\theta_p(X=0)$ is the solid blue line, $\theta_p(X=1)$ is the dashed red line. Values: $\theta_i = 0.6 + 0.02\cos(\pi X)$, $n_i = 0$, $h_i = 1$, $\chi = 0.75$, $\xi = 1$, $\mathcal{R} = 1$. $(\theta^*, \bar{h}^*, L^*) = (0.45, 1.16, 1.16)$.

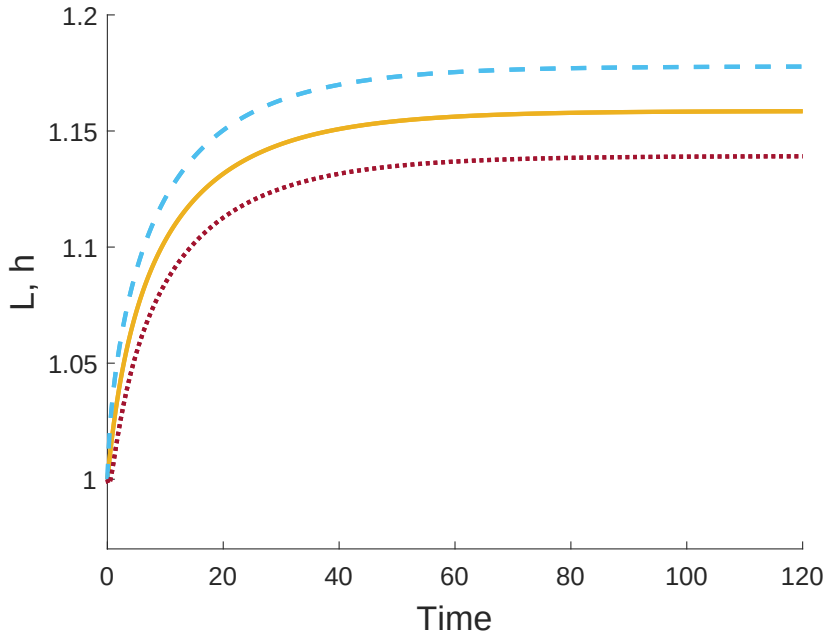

Figure 6.4: Time evolution of a cell-free gel with non-uniform initial polymer fraction. Spatial variations develop in the height in response to the initial non-uniform polymer distribution; these variations persist to equilibrium. L is the solid gold line, $h(X=0)$ is the dashed light blue line, $h(X=1)$ is the dotted maroon line. Values as in Fig. 6.3.

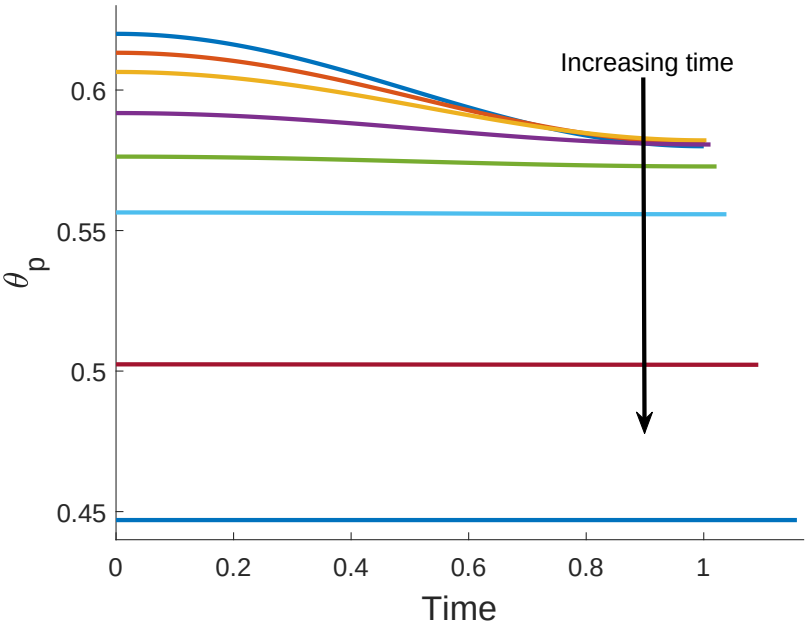

Figure 6.5: Spatial profile of θ_p as the gel swells from non-uniform polymer initial condition. Spatial variations in the polymer profile decay quickly over time. Profiles are plotted (from top to bottom) at $T = 0, 0.1, 0.2, 0.5, 1, 2, 8, 120$. Values as in Fig. 6.3.

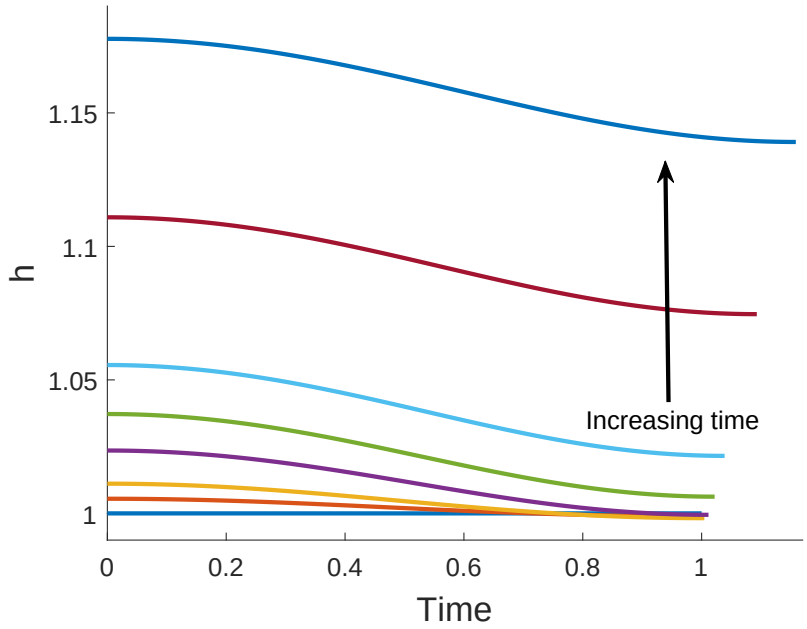

Figure 6.6: Spatial profile of h as the gel swells from a non-uniform polymer initial condition. Spatial variations emerge in the height which are maintained at equilibrium. Profiles are plotted (from bottom to top) at $T = 0, 0.1, 0.2, 0.5, 1, 2, 8, 120$. Values as in Fig. 6.3.

6.4.5 *Spatially varying initial polymer, cell-gel system*

We now take the system presented in Section 6.4.4 and introduce a cell population where $n_i = 1$ and $\tau_0 = 1$. We maintain the non-uniform initial condition for polymer, $\theta_{p_i} = 0.6 + 0.02\cos(\pi X)$. Figs. 6.7 and 6.8 display this system's evolution. While the gel was previously seen to swell, the introduction of cells switches the gel's behaviour to contraction, with the forces the cells generate outweighing the chemical potential gradient. The gel reaches a steady state where $\theta^* = 0.86$, $n^* = 1.44$, $\bar{h}^* = 0.83$, $L^* = 0.83$. We note that this is the same equilibrium in θ^* and n^* as the example presented in Fig. 3.12.

As in Section 6.4.4, the non-uniformity in θ_p evens out over time, with h developing spatial variations that remain present at equilibrium; Figs. 6.9 and 6.11 show how the spatial profiles of θ_p and h respectively change over time. Meanwhile, variations also appear in the cell density n while the gel contracts. As in the example presented in Figs. 3.26 - 3.28, the cell density increases more around $X = 1$ in response to the smaller initial polymer fraction there; however, as time progresses, the variation in n decays due to the presence of diffusion (see Fig. 6.10).

6.4.6 *Spatially varying initial cell density, cell-gel system*

We now take the initial cell density to be spatially varying, such that $n_i = 1 + 0.02\cos(\pi X)$, with a uniform initial polymer fraction $\theta_i = 0.6$. Small spatial variations arise in both the polymer fraction and height here as the gel evolves (see Figs. 6.12 - 6.13). The non-uniform cell distribution, shown in Fig. 6.14, leads to greater forces initially being applied in the negative X-direction; this cell traction induces spatial gradients in the polymer profile and, accordingly, the height, as more solvent is forced from the gel. Fig. 6.16 shows θ_p increasing towards $X = 0$ over early time in response to the cell force gradient, while in Fig. 6.15, we see a corresponding decrease in height around $X = 0$. Contrary to the previous examples seen in this chapter, the non-uniformity that arises in the height as the gel evolves does not continue to equilibrium. In this instance, with

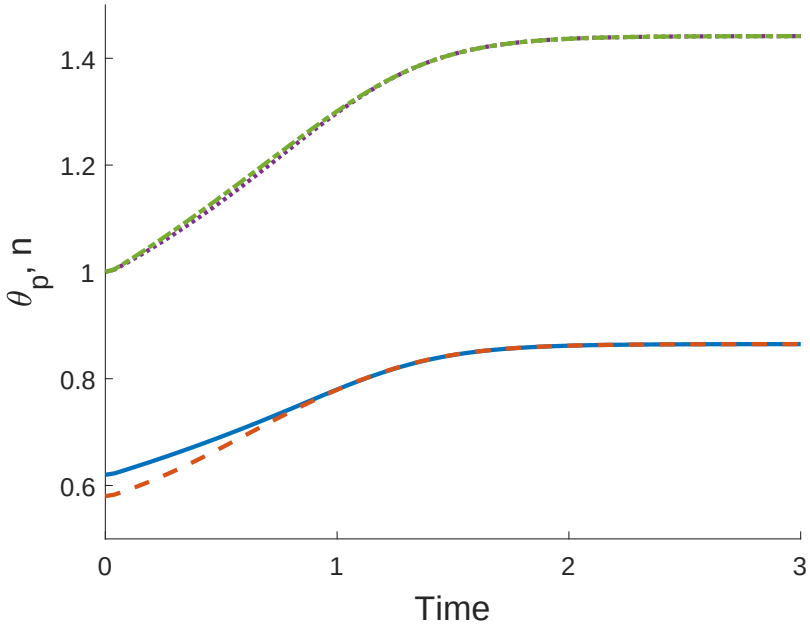

Figure 6.7: Time evolution of a cell-gel system with non-uniform initial polymer fraction. The polymer fraction evens out to a uniform equilibrium as the gel contracts. Small variations appear in the cell density which also even out over time. $\theta_p(X=0)$ is the solid blue line, $\theta_p(X=1)$ is the dashed red line, $n(X=0)$ is the dotted purple line, $n(X=1)$ is the dash-dotted green line. Values: $\theta_i = 0.6 + 0.02\cos(\pi X)$, $n_i = 1$, $h_i = 1$, $\chi = 0.75$, $\xi = 1$, $\mathcal{R} = 1$, $\tau_0 = 1$, $D = 1$. $(\theta^*, n^*, \bar{h}^*, L^*) = (0.86, 1.44, 0.83, 0.83)$.

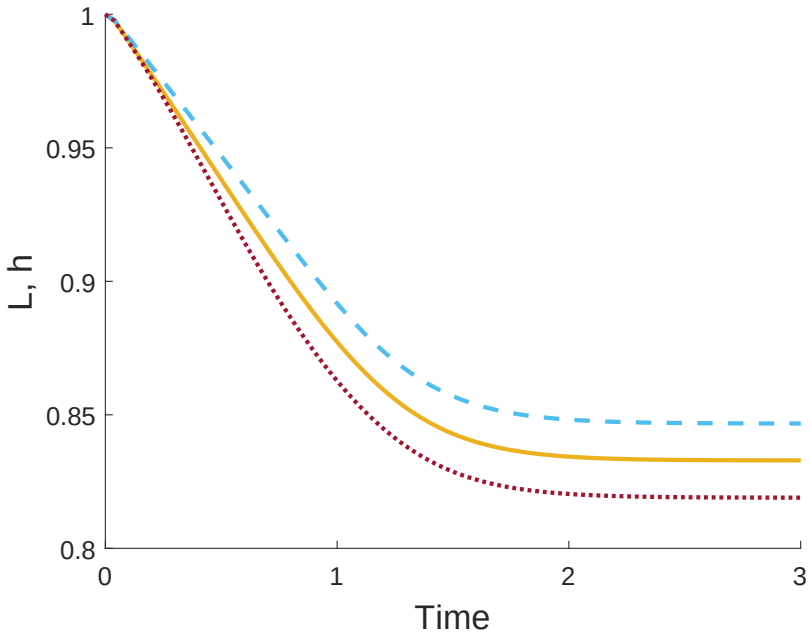

Figure 6.8: Time evolution of a cell-gel system with non-uniform initial polymer fraction. Spatial variations develop in the height in response to the initial non-uniform polymer distribution; these variations persist to equilibrium. L is the solid gold line, $h(X=0)$ is the dashed light blue line, $h(X=1)$ is the dotted maroon line. Values as in Fig. 6.7.

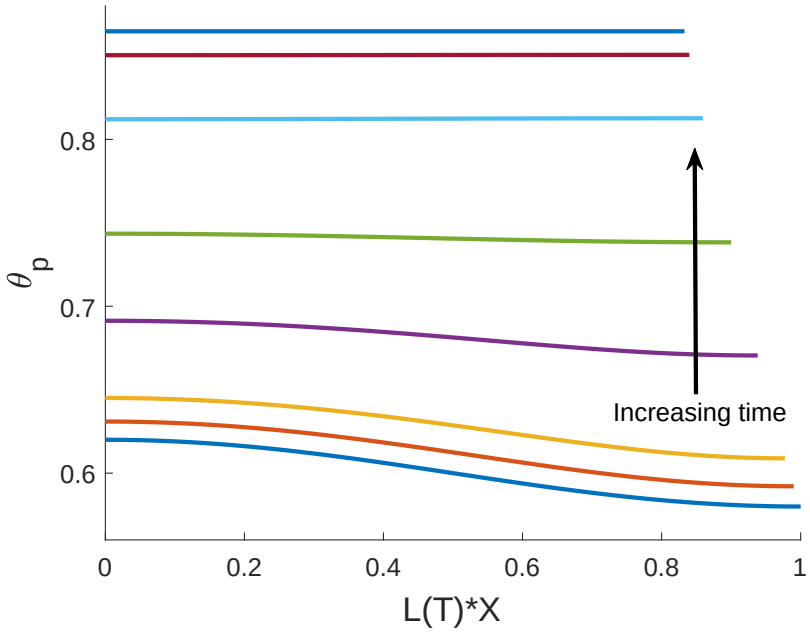

Figure 6.9: Spatial profile of θ_p as the gel contracts from non-uniform polymer initial condition. Spatial variations in the polymer profile decay quickly over time. Profiles are plotted (from bottom to top) at $T = 0, 0.1, 0.2, 0.5, 0.8, 1.2, 1.6, 3$. Values as in Fig. 6.7.

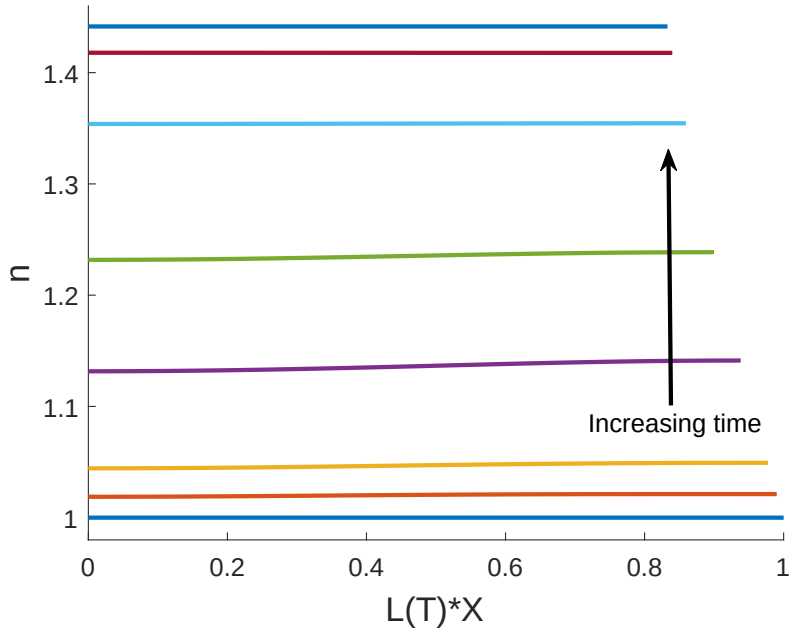

Figure 6.10: Spatial profile of n as the gel contracts from a non-uniform polymer initial condition. Small spatial variations briefly emerge in the cell density which dissipate before the gel equilibrates. Profiles are plotted (from bottom to top) at $T = 0, 0.1, 0.2, 0.5, 0.8, 1.2, 1.6, 3$. Values as in Fig. 6.7.

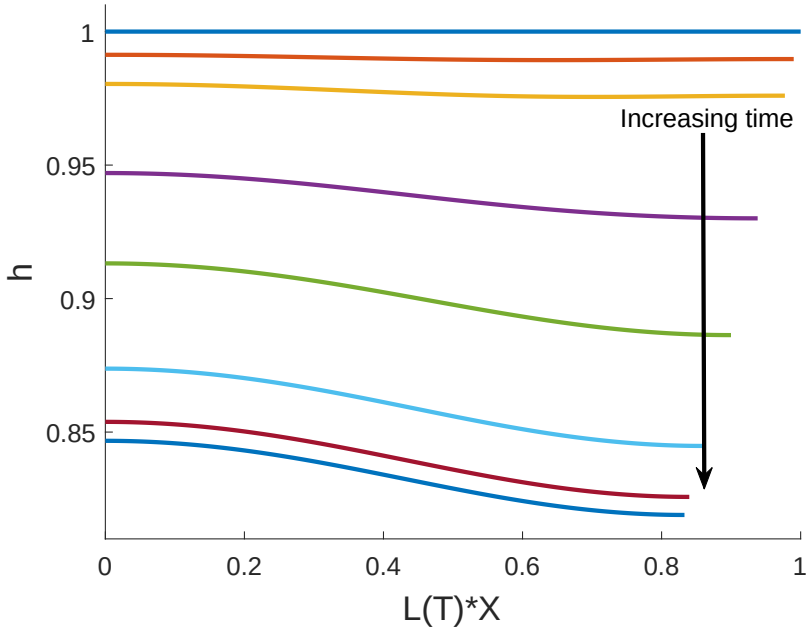

Figure 6.11: Spatial profile of h as the gel contracts from a non-uniform polymer initial condition. Spatial variations emerge in the height which are maintained at equilibrium. Profiles are plotted (from top to bottom) at $T = 0, 0.1, 0.2, 0.5, 0.8, 1.2, 1.6, 3$. Values as in Fig. 6.7.

the polymer initially uniform, the small local variations in the gel's thickness do not persist at equilibrium. As required, the cell density is constant when the gel equilibrates, with the strong diffusion coefficient playing a significant role in smoothing out the initial variations. The gel reaches the same steady state as the previous example with $\theta_p^* = 0.86$, $n^* = 1.44$, $h^* = L^* = 0.83$; therefore, we see that varying the initial cell distribution does not led to greater contraction in the gel.

6.4.7 *Spatially varying initial height, cell-gel system*

We now vary the initial height for this gel, such that $h_i = 1 + 0.02\cos(\pi X)$, while taking $\theta_i = 0.6$ and $n_i = 1$ to be constant. The gel again contracts to an equilibrium with θ_p and n being constant, while spatial variations in h persist through to the gel's steady state. The mean equilibrium values of the model variables are unchanged from previous examples. As this example does not demonstrate any new qualitative outcomes, we do not include any figures.

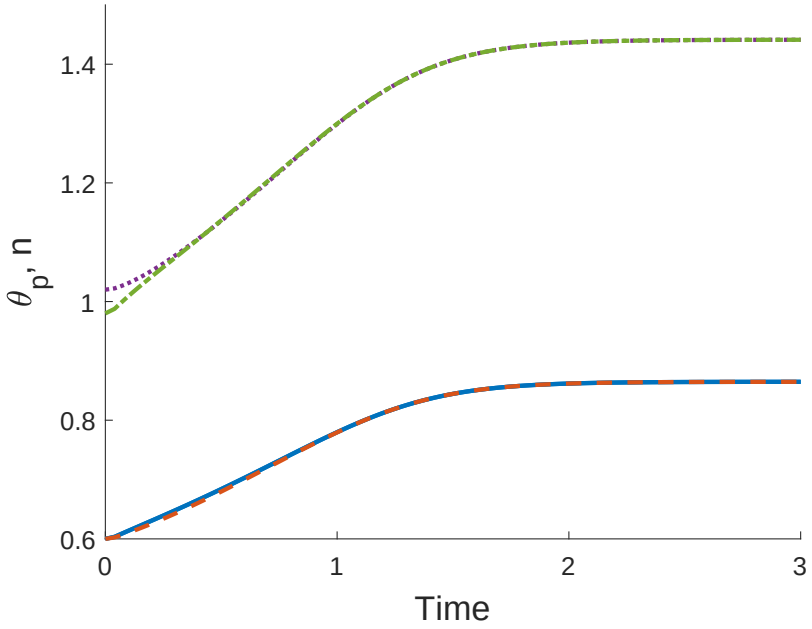

Figure 6.12: Time evolution of a cell-gel system with non-uniform initial cell density. n evens out to a uniform equilibrium as the gel contracts, while small variations appear in θ_p which then smooth out over time. $\theta_p(X = 0)$ is the solid blue line, $\theta_p(X = 1)$ is the dashed red line, $n(X = 0)$ is the dotted purple line, $n(X = 1)$ is the dash-dot green line. Values: $\theta_i = 0.6$, $n_i = 1 + 0.02\cos(\pi X)$, $h_i = 1$, $\chi = 0.75$, $\xi = 1$, $\mathcal{R} = 1$, $\tau_0 = 1$, $D = 1$. $(\theta^*, n^*, \bar{h}^*, L^*) = (0.86, 1.44, 0.83, 0.83)$.

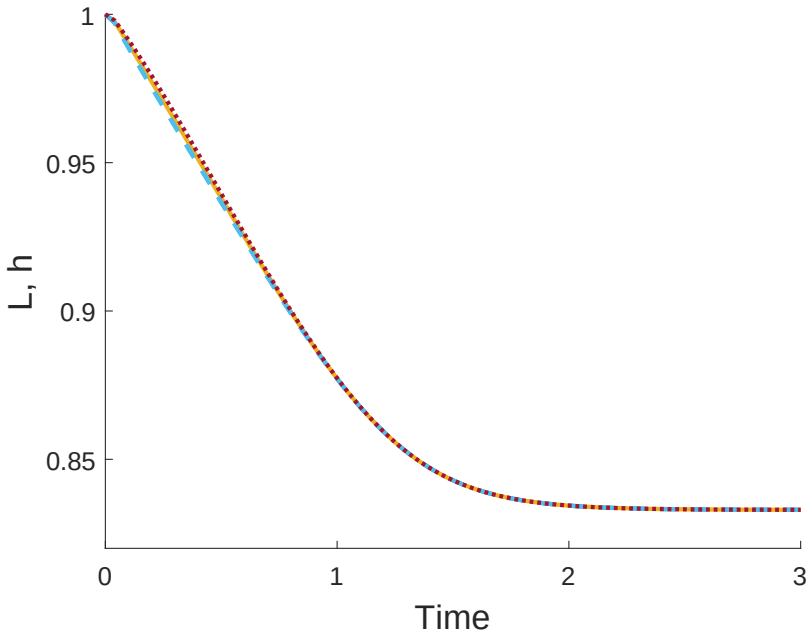

Figure 6.13: Time evolution of a cell-gel system with non-uniform initial cell density. Spatial variations develop in the height in response to the initial non-uniform cell distribution; however, these variations decay before the gel equilibrates. L is the solid gold line, $h(X = 0)$ is the dashed light blue line, $h(X = 1)$ is the dotted maroon line. Values as in Fig. 6.12.

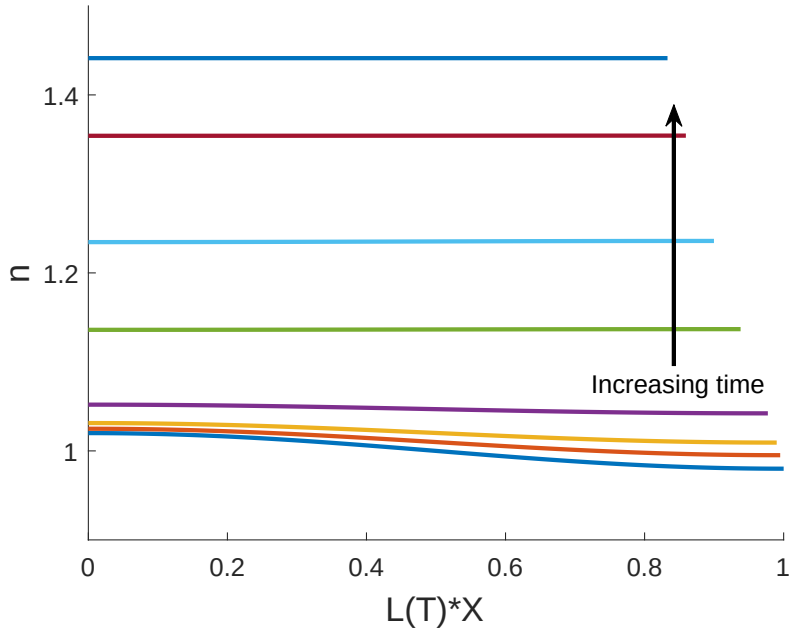

Figure 6.14: Spatial profile of n as the gel contracts from non-uniform cell initial condition. Spatial variations in the cell profile decay quickly over time. Profiles are plotted (from bottom to top) at $T = 0, 0.06, 0.1, 0.2, 0.5, 0.8, 1.2, 3$. Values as in Fig. 6.12.

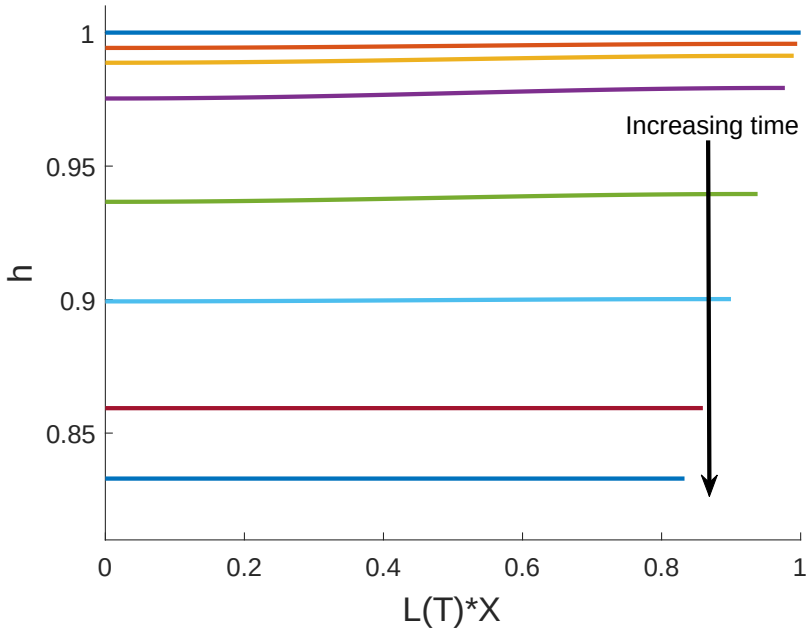

Figure 6.15: Spatial profile of h as the gel contracts from a non-uniform cell initial condition. Spatial variations briefly emerge in the height which dissipate before the gel equilibrates. Profiles are plotted (from top to bottom) at $T = 0, 0.06, 0.1, 0.2, 0.5, 0.8, 1.2, 3$. Values as in Fig. 6.12.

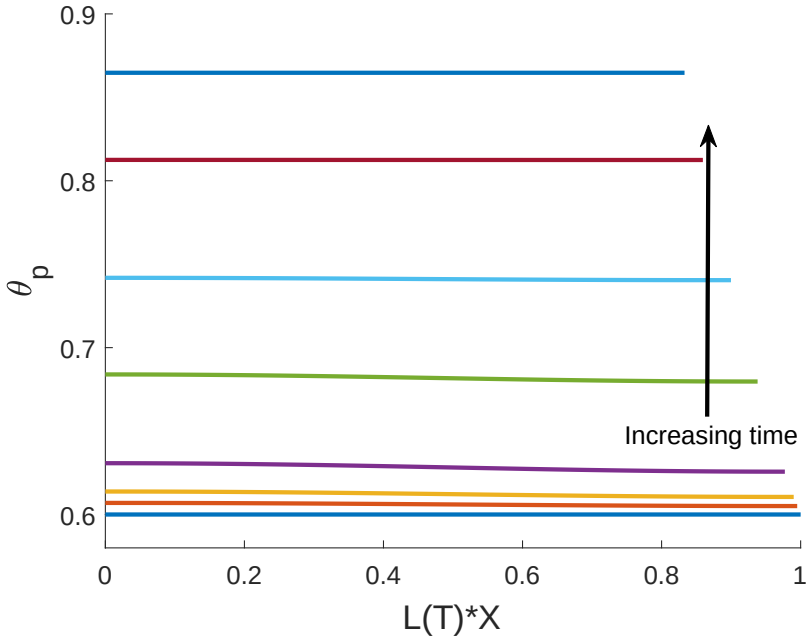

Figure 6.16: Spatial profile of θ_p as the gel contracts from a non-uniform cell initial condition. Spatial variations briefly emerge in the polymer fraction which dissipate before the gel equilibrates. Profiles are plotted (from bottom to top) at $T = 0, 0.06, 0.1, 0.2, 0.5, 0.8, 1.2, 3$. Values as in Fig. 6.12.

We note that taking different combinations of spatially varying initial conditions in h, n and θ_p will result in the same qualitative outcomes for the system – if θ_p or h are spatially varying initially, then h will be spatially dependent at equilibrium, regardless of the initial cell density; only varying n initially will not induce a non-uniform equilibrium by itself.

6.4.8 *Influence of drag and resistance*

We now investigate the effect that the drag parameter ξ and the resistance parameter $\mathcal{R}$ have on the gel's evolution. We take a contracting gel with cells with parameter values and initial conditions as given in Fig. 6.7, where the initial polymer fraction is non-uniform. We reiterate that in this case, the gel will equilibrate to a uniform value of polymer, $\theta^* = 0.86$. We now modify the drag parameter ξ. In Figs. 6.17 and 6.18 we compare the polymer fraction's spatial evolution over early time (up to $T = 0.8$) for high drag ($\xi = 4$) and low drag ($\xi = 0.2$) respectively. In the high drag case, we see little

change over this time to the spatial structure of the gel as it contracts. The amplitude of the variations in the polymer fraction decreases over time (amplitude $\mathcal{A}_{\theta_p} = 0.007$ at $T = 0.8$); however, it retains the sinusoidal shape of the initial condition. In this case, the large drag coefficient slows down solvent flow across the gel in the x-direction. It is therefore easier for solvent to flow out of the gel primarily in the thin direction. It does this at a relatively uniform rate across the domain, hence the spatial distribution only slowly decreases in amplitude. With low drag on the other hand, we see that the polymer fraction changes more rapidly near $X = 1$ than in the high drag case. The polymer moves quickly towards a uniform spatial distribution, since it is now easier for fluid to flow longitudinally within the gel as well as in the vertical direction. With more cell forces being applied in the area near $X = 1$, the polymer fraction increases at one point (at around $T = 0.4$) as it evolves, before evening out again as the gel moves towards its equilibrium state. We note that the polymer fraction reaches a uniform steady state at $T \approx 3$ in both the low and high drag cases here (results not shown).

The resistance parameter $\mathcal{R}$ affects the speed at which fluid can flow across the gel-solvent interface at both $y = h$ and $X = 1$. We see dramatic differences comparing the evolution in θ_p for low resistance with $\mathcal{R} = 0.4$ in Fig. 6.20 compared to high resistance, $\mathcal{R} = 4$ in Fig. 6.19 (we note that in both these examples $\xi = 1$). For low resistance, the gel quickly contracts, with θ_p smoothing out as it moves towards its steady state. With this small value of $\mathcal{R}$, the gel has equilibrated by $T = 0.8$. For high resistance, the evolution is significantly slower. Indeed, by $T = 0.8$, the polymer fraction has only increased to approximately $\theta_p = 0.64$ at its maximum. Interestingly, in this case, while the fraction of polymer is only changing slowly, the amplitude has halved from its initial value by $T = 0.8$. This indicates that, while the resistance is slowing the flow of solvent across the gel's boundary, solvent inside the gel is flowing quickly enough to flatten the polymer's distribution.

6.4.9 *Zero-diffusion case*

The derivation of the thin film model, wherein the diffusive flux terms are used to derive that n is independent of y, requires D to be $\mathcal{O}(1)$. Accordingly, the examples

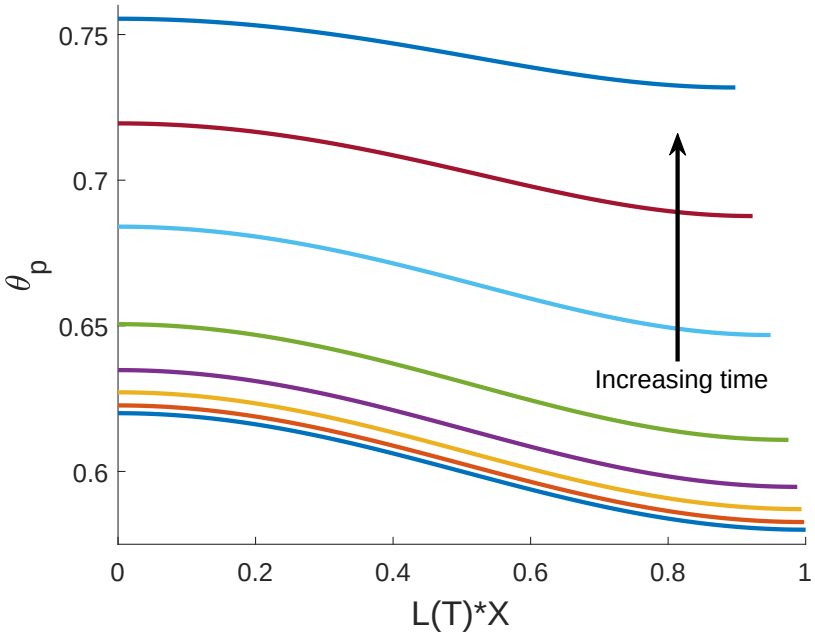

Figure 6.17: Spatial profile of θ_p between $T = 0$ and $T = 0.8$ as the gel contracts from a non-uniform polymer initial condition with high drag $\xi = 4$. Spatial variations slowly recede as the gel contracts over this time. Profiles are plotted (from bottom to top) at $T = 0, 0.02, 0.05, 0.1, 0.2, 0.4, 0.6, 0.8$. Values otherwise as given in Fig. 6.7.

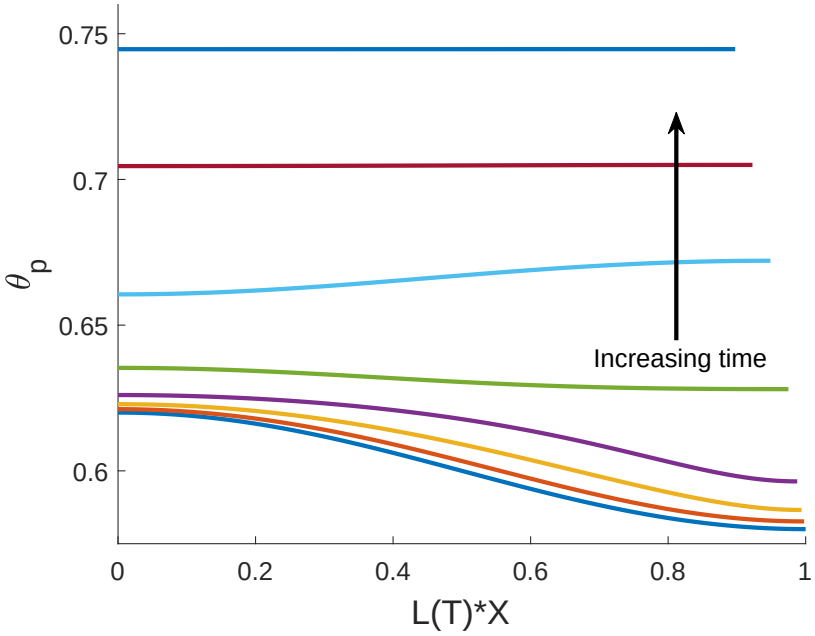

Figure 6.18: Spatial profile of θ_p between $T = 0$ and $T = 0.8$ as the gel contracts from a non-uniform polymer initial condition with low drag $\xi = 0.2$. Over this time, spatial variations quickly smooth out as the gel contracts. Profiles are plotted (from bottom to top) at $T = 0, 0.02, 0.05, 0.1, 0.2, 0.4, 0.6, 0.8$. Values otherwise as given in Fig. 6.7.

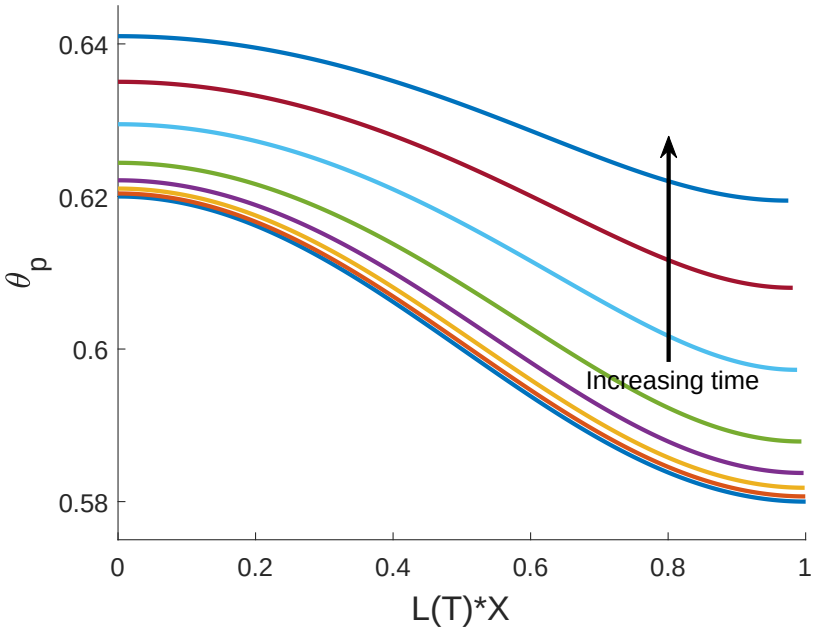

Figure 6.19: Spatial profile of θ_p between $T = 0$ and $T = 0.8$ as the gel contracts from a non-uniform polymer initial condition with high resistance $\mathcal{R} = 4$. The polymer fraction decreases very slowly due to the impermeability of the boundary. Profiles are plotted (from bottom to top) at $T = 0$, 0.02, 0.05, 0.1, 0.2, 0.4, 0.6, 0.8. Values otherwise as given in Fig. 6.7.

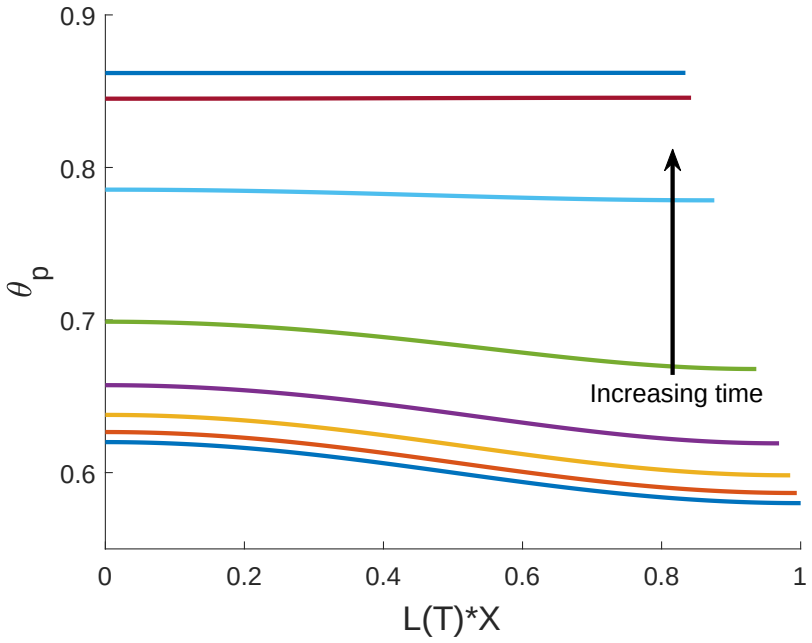

Figure 6.20: Spatial profile of θ_p between $T = 0$ and $T = 0.8$ as the gel contracts from a non-uniform polymer initial condition with low resistance $\mathcal{R} = 0.4$. The gel quickly contracts to its equilibrium state. Profiles are plotted (from bottom to top) at $T = 0$, 0.02, 0.05, 0.1, 0.2, 0.4, 0.6, 0.8. Values otherwise as given in Fig. 6.7.

presented in this chapter so far have been generated with $D = 1$. Nevertheless, for the sake of completeness, we investigate the outcomes for the system here without diffusion, although we cannot guarantee the validity of our thin film reduction in this case. With zero diffusion, cells must move with the polymer and the cell distribution does not need to be uniform at steady state, indicating that θ_p in turn is also not required to be uniform at equilibrium.

We take $D = 0$ with initial conditions $n_i = 1 + 0.02\cos(\pi X)$, $\theta_i = 0.6$, $h_i = 1$. We note here that due to issues with code convergence, we have run these examples with a smaller interaction energy than previously, taking $\chi = 0.4$. We show in Figs. 6.21 - 6.24 that with no diffusion and a non-uniform initial cell density, we obtain equilibria that are non-uniform in the cell density, polymer fraction and height. This reflects similar examples in the 1D model (see Figs. 3.26 and 3.29). In this instance, the gel reaches a mean equilibrium cell density $\bar{n}^* = 1.29$ with amplitude $\mathcal{A}_{n^*} = 0.033$, which is greater than the initial amplitude. The polymer fraction evolves to mean equilibrium value $\bar{\theta}^* = 0.78$ with amplitude $\mathcal{A}_{\theta^*} = 0.004$, while for the height, $\bar{h}^* = 0.88$ with amplitude $\mathcal{A}_{h^*} = 0.002$. Fig. 6.25 demonstrates the time evolution of velocity v_p at different points in the spatial domain. We see that the velocity goes to zero at all shown spatial points, confirming that the gel is at a steady state. With only cells taken to be initially non-uniform, the gel reaches a steady state where the cells, polymer and height are all non-uniform. This is a significant difference to the case with diffusion, where non-uniform initial cell profiles did not lead to spatially varying steady states. While this simulation does not fit with the particular derivation of the thin film system here, it does demonstrate the possibility that spatially dependent solutions may occur in both the polymer and cells. Examples with a small diffusion coefficient (*e.g.* $D \approx 1\text{x}10^{-3} - 1\text{x}10^{-5}$) were found to reach a similar non-uniform quasi-steady state; however, given the presence of the small diffusive flux, cells and polymer very slowly moved towards a uniform distribution (results not shown).

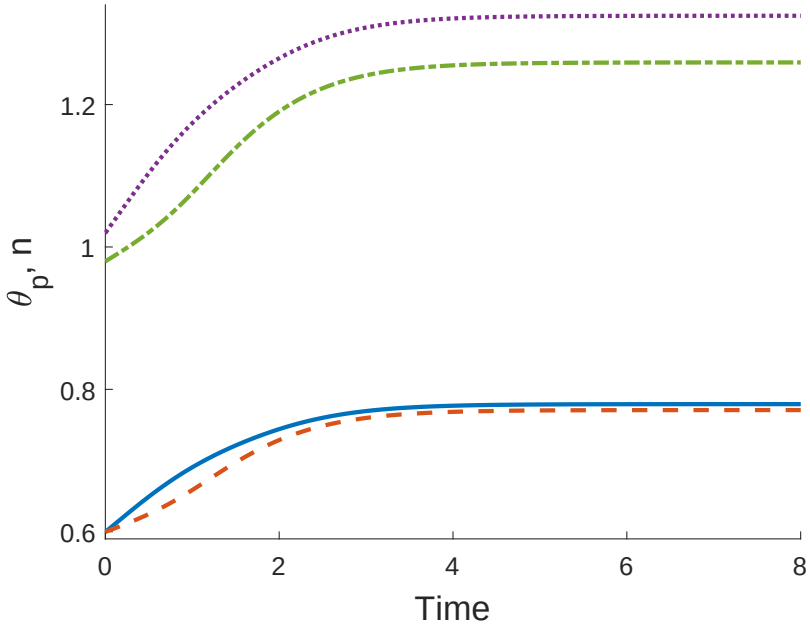

Figure 6.21: Time evolution of a cell-gel system with zero diffusion and a non-uniform initial cell density. Spatial variations develop in the polymer in response to the non-uniform initial cell distribution; both θ_p and n remain non-uniform at the gel's steady state. $\theta_p(X=0)$ is the solid blue line, $\theta_p(X=1)$ is the dashed red line, $n(X=0)$ is the dotted purple line, $n(X=1)$ is the dash-dot green line. Values: $\theta_i = 0.6$, $n_i = 1 + 0.02\cos(\pi X)$, $h_i = 1$, $\chi = 0.4$, $\xi = 1$, $\mathcal{R} = 1$, $\tau_0 = 1$, $D = 0$. $(\bar{\theta}^*, \bar{n}^*, \bar{h}^*, L^*) = (0.78, 1.29, 0.88, 0.88)$.

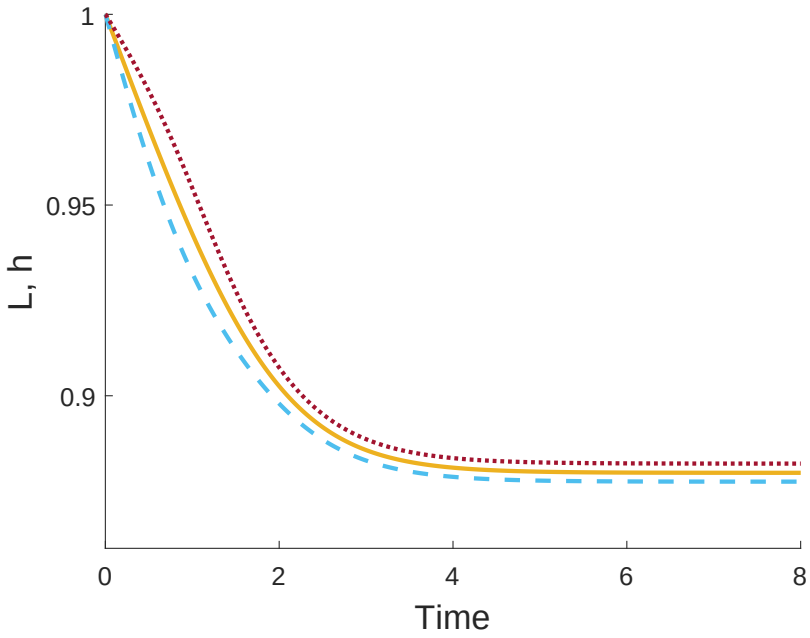

Figure 6.22: Time evolution of a cell-gel system with zero diffusion and a non-uniform initial cell density. Spatial variations develop in the height in response to the non-uniform initial cell distribution, this persists at the gel's steady state. L is the solid gold line, $h(X=0)$ is the dashed light blue line, $h(X=1)$ is the dotted maroon line. Values as in Fig. 6.21.

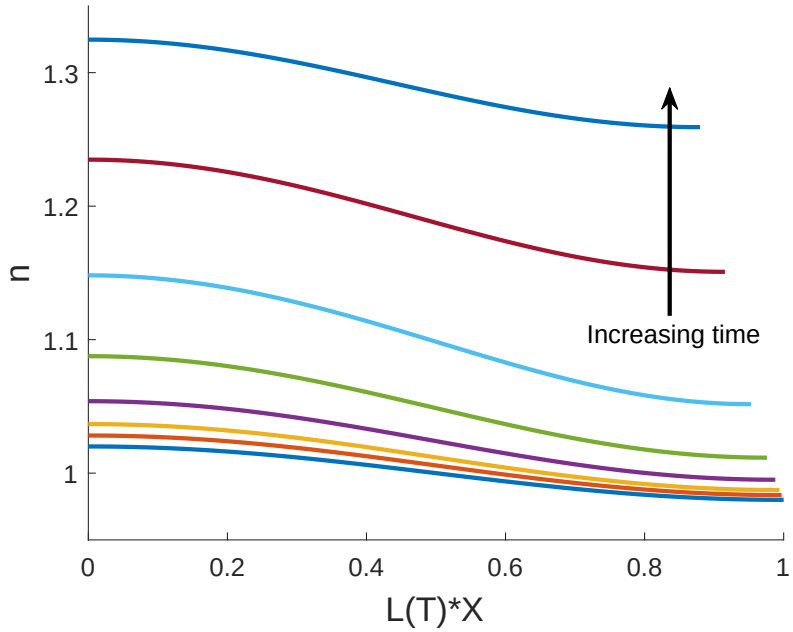

Figure 6.23: Spatial profile of n as the gel contracts from non-uniform cell initial condition with zero diffusion. Spatial variations in the cell profile grow and persist at equilibrium. Profiles are plotted (from bottom to top) at $T = 0$, 0.05, 0.1, 0.2, 0.4, 0.8, 1.6, 8. Values as in Fig. 6.21.

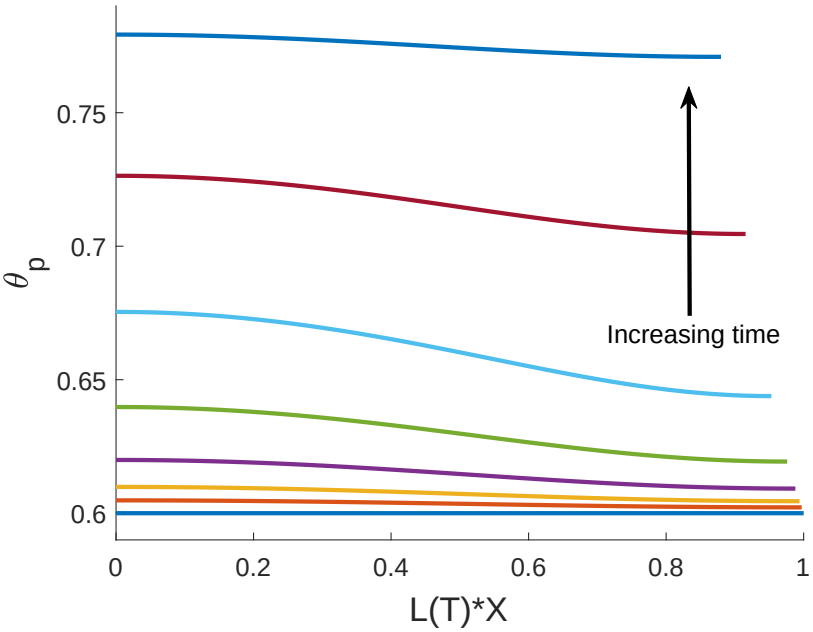

Figure 6.24: Spatial profile of θ_p as the gel contracts from non-uniform cell initial condition with zero diffusion. Spatial variations in the polymer profile emerge and persist at equilibrium. Profiles are plotted (from bottom to top) at $T = 0$, 0.05, 0.1, 0.2, 0.4, 0.8, 1.6, 8. Values as in Fig. 6.21.

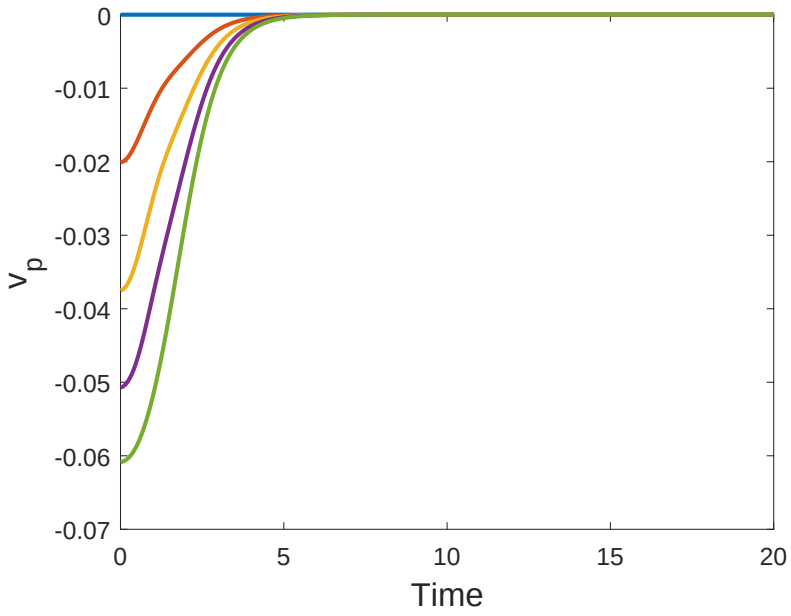

Figure 6.25: Time evolution of velocity v_p at different points in the spatial domain. The velocity goes to zero across the spatial domain as the gel reaches its spatially varying equilibrium. In descending order initially, $v_p(0,T)$ is the blue line, $v_p(0.25,T)$ is the red line, $v_p(0.5,T)$ is the yellow line, $v_p(0.75,T)$ is the purple line, $v_p(1,T)$ is the green line. Values as in Fig. 6.21.

6.5 DISCUSSION

In this chapter, we have used analytic and numerical methods to study the thin film cell-gel system with non-uniform initial conditions. Equilibrium conditions and small time solutions were derived, allowing for predictions to be made about the stability of steady states. We then presented a numerical scheme for the thin film, studying gels with non-uniform initial conditions in θ_p, n and h. We found the novel result that spatially non-uniform solutions can persist in the height of the thin film at equilibrium, with or without cells present.

In the reduced model presented in Chapter 5, we saw that, with constant initial conditions, the gel expanded or contracted uniformly, driven by fluid flow in the y-direction. In the full model presented here, we see that more complicated dynamics emerge with spatially varying initial conditions. The gel is still primarily driven by flow in the thin direction; however, the terms involving drag and spatial derivatives in the dependent variables are now active. Accordingly, we see spatial variations arising in

θ_p, n and h as the gel evolves. We have found that solutions exist where the gel height is non-uniform at steady state, even though the polymer fraction and cell density are constant. When θ_i is non-uniform, local variations in the polymer induce solvent flow into or out of the gel to even out this polymer fraction; this correlates with spatial variations in the gel height at these points, reflecting the variations in mass. Similarly, when h_i is non-uniform, the height maintains its spatial dependency to ensure θ_p remains constant.

A significant difference in this thin geometry from the 1D case is that increasing drag now reduces spatial changes in the velocity. This is evident from equation (6.4), where we see that increasing ξ decreases the influence of the spatial derivative terms on the velocity. A consequence of this is evident in Fig. 6.17, where we see that, with large drag, initial spatial variations persist longer through the gel's evolution, as it is easier for fluid to flow vertically out of the gel than across the spatial domain due to the shearing forces present with a large drag coefficient. In the 1D case, we saw that increases in the drag coefficient tended to induce greater spatial gradients in the polymer and cells, as solvent could only enter and leave the gel through the endpoint at $X = 1$, and so had to flow across the entire spatial domain. Like in the 1D Cartesian model, the resistance parameter $\mathcal{R}$ has the expected effect of slowing gel evolution by slowing the rate of solvent flow across the free boundaries.

Differences from the 1D Cartesian case are also found in the small time solutions for perturbed equilibria presented in Section 6.3. In the 1D case, the solution for v_{01} (the first correction to the spatial perturbation in the velocity solution) is a function of sinh and sin terms (see equation (3.90)). The hyperbolic term describes how the gel length changes in response to the perturbation away from equilibrium, while the trigonometric term describes the growth or decay of the spatial perturbations over time. In the small time solution for v_{01} in the thin film case (equation (6.38)), there is no hyperbolic term present. Mathematically, this is because the PDE for v_{01} is first-order, rather than second-order like in the 1D case; this allows a solution to be found as a function of sin only. It also reflects how the thin film predominantly evolves in the thin y-direction; this solution indicates that L does not change to at least $\mathcal{O}(\epsilon\delta)$ over the small time scale. In the 1D case, there is also the presence of a boundary layer in the

cells at $X = 1$; this does not appear in the thin film model due to the condition arising from the thin film approximation that $\partial\theta_p/\partial X = 0$ at $X = 1$.

We have noted that our thin film model derivation assumes that the non-dimensional diffusion coefficient D is $\mathcal{O}(1)$. Under this assumption, as seen in Section 6.2, we cannot find equilibria in the thin film system with non-uniform polymer or cell distributions. Diffusion causes the cells to spread until a uniform cell density is reached across the gel. We note that examples with diffusion $D \neq 0$ in the 1D case (such as in Fig. 3.20) also resulted in uniform equilibria. We have presented simulations with zero diffusion in the thin film here, finding examples where non-uniform equilibria persist in θ_p and n. While we cannot definitively say that $n = n(x,t)$ for the zero diffusion case, we have shown that, if such y-independent solutions can exist for $D = 0$, then we can find non-uniform equilibria in the thin film environment as well. We note that with small diffusion ($D \approx 0.0001$), we do see quasi-steady states in θ_p and n, where non-uniform states are found which slowly drift towards uniformity as a result of diffusive flux.

Unlike the studies by Trinschek *et al.* (2016, 2017) discussed in Section 4.2, we do not see situations where, at a certain point, the gel continues expanding lengthwise while its vertical swelling has stopped. Indeed, throughout these simulations, we see that the scaled height (or its mean value) is equal to the scaled gel length at equilibrium. As discussed in Section 5.4, this supports modelling assumptions used in Stevenson *et al.* (2010), although we do note that, given its spatial dependency, h does not equal L for all times in these results, counter to this assumption. In our model, there is no mechanism to cause a change in behaviour and decouple the lengthwise expansion from the vertical movement of the gel. This could possibly occur if the domain was somehow vertically or horizontally limited, or if an additional external pressure was imposed from one particular direction. A different cell force function might also see more emphasis on horizontal forces. An avenue for future work may be to explore whether these dynamics can be factored in, allowing for the expansion or contraction of a gel to be tailored in a certain direction, not just a situation wherein the length and height evolve similarly as seen here.

In this chapter, we have studied the qualitative behaviours emerging from the thin film model with non-uniform initial conditions. There is significant scope to extend

this research and validate the model's behaviours through experimental collaboration. This would allow for parameter values to be fit and suggest particular regions in the parameter space for deeper analysis to be carried out. The numerical results in this chapter suggest further avenues to investigate experimentally, for example, confirming whether gels which are initially uniform in space retain this uniformity as they evolve, and whether small variations in the initial polymer profile do indeed result in spatially varying height profiles. A modelling extension to consider is to include surface tension and study its effect in cases where the gel height is found to vary; the aim would be to establish whether surface tension smooths out the height in such cases.

7

CONCLUSION

This thesis explored the mechanical behaviour of biological gels. We developed a new multiphase model to study the mechanics of cell-seeded gels, accounting for both cell-derived forces and osmotically-driven solvent flow. The primary contribution of this work has been to consider how cell traction stresses compete with chemical potentials and the effect that this has on equilibrium outcomes for the gel. Previous mathematical models have either investigated how chemical potential gradients can cause gel swelling or contraction in the absence of cells, or have only considered the forces exerted by the cells, excluding solvent flux across the gel's boundary. Our results have demonstrated that the presence of cells can cause a gel to contract when it would otherwise swell; on the other hand, the strength of the interaction energy between polymer and solvent can cause a gel to swell even with cells present. The level of interaction energy can lead to either gel swelling or contraction in the absence of cells. Considering these effects together is important in gaining a more comprehensive understanding of the system.

In Chapter 2, we presented our multiphase model governing the behaviour of a cell-gel system. Mass and momentum conservation equations described the evolution of polymer and solvent volume fractions as well as the cell density. The velocity of the system was driven by cell and chemical potential functions appearing in the momentum balance equations, as well as interface conditions which described continuity of stress and fluid flow across the free boundary. This system of equations, complete with appropriate initial and boundary conditions, provided the framework to explore gel swelling and contraction under different assumptions and in different dimensions.

Throughout the subsequent analysis in both one and two spatial dimensions, we saw that the system is driven by the balance between osmotic pressure gradients and cell traction stresses. The magnitude of these forces inside the gel and in the surrounding solvent was found to determine, firstly, whether the gel swells or contracts, and secondly, whether an equilibrium state is found and, if so, the values of model variables at this steady state. The conditions needed for the system of equations to equilibrate were found to be the same in different gel geometries, relying on this balance of cell and chemical potentials. Physical parameters like drag and viscosity affected the manner in which the gel evolved both temporally and spatially, although did not

affect the equilibrium state found. For example, the size of the drag coefficient influenced the movement of polymer and solvent across the spatial domain, impacting the gel's behaviour differently in the 1D and 2D settings. Meanwhile, the resistance of the interface changed the speed at which fluid moved across the gel's free boundaries, and accordingly, affected the rate at which the gel evolved.

Chapter 3 provided an investigation of the model in 1D Cartesian coordinates. This simple geometry allowed us to gain an understanding of the qualitative behaviours demonstrated by the gel. We showed the novel result that cell forces can cause contraction in a gel which would otherwise swell due to osmotic pressure. Increasing the effects of drag relative to viscosity encourages steeper spatial gradients in polymer and cell density as the gel evolves, leading to lags in evolution between the end and centre of the gel. We found that our model agreed with existing experimental results (such as Stevenson *et al.* (2010)) showing a negative correlation between the initial polymer volume fraction and equilibrium volume fraction for the cell-gel system. We also demonstrated novel results in the existence of spatially varying steady states when taking non-uniform initial conditions, as well as oscillatory behaviour as the gel swells, driven by competing traction and osmotic forces.

We presented a new, leading order model for a 2D thin gel incorporating osmotic effects in Chapter 4. By taking a scaling limit in which, amongst other parameters, the pressure and resistance of the boundary were assumed to be large, we derived an extensional flow model in which key model variables were found to be independent of the y-coordinate. This allowed for a system of equations describing the gel's mechanics in one spatial coordinate to be found. The presence of cell potentials was found to generate the pressure in the thin film which, along with the chemical potentials, drives the velocity of polymer and solvent and, accordingly, the gel's evolution.

Owing to the different behaviour emerging in the thin film with uniform and non-uniform initial conditions, we studied these separately. In Chapter 5, we considered uniform initial conditions for the thin film, and found that the system reduced to an ODE for h with all other variables given by algebraic expressions involving h. Significantly, when θ_p, n and h are initially uniform, no spatial gradients develop in the thin

film as the gel evolves. This is a consequence of the 2D geometry, wherein the primary flow of solvent is in the thin direction.

In Chapter 6, we studied non-uniform initial conditions in the thin film. We found novel behaviour in the existence of spatially varying steady states; initial variations in polymer result in non-uniform height profiles at equilibrium, as the height changes while the gel swells or contracts to accommodate local variations in mass. As in the 1D Cartesian case, the balance of cell traction and chemical potentials determines equilibrium states and their stability. Increasing drag in this setting was found to maintain existing spatial variations, as it is easier for fluid to flow out in the y-direction with large drag than flow across the gel in the axial direction. This is different to the 1D case, where large drag creates spatial gradients moving back from $X = 1$ as fluid can only enter and leave the gel through this endpoint.

There are a number of directions that future work could take, both mathematically and experimentally. We have discussed these exploratory avenues within each chapter; some of these are touched on again here amongst other ideas. The availability of relevant and consistent experimental data would allow for realistic parameter ranges to be developed. With this, we could study the fit of our model in the different geometries presented here, as well as other features such as the form of the cell force function. Transforming the models developed here into radial and spherically symmetric coordinates would reflect experiments performed using thin discs and gel spheres respectively, facilitating more direct comparison with experimental results in these settings. We would not expect significant shifts in the qualitative behaviours predicted by our models under such changes to the geometry; however, analysing the model in the appropriate coordinate system would allow for better comparisons between our models and experiments to be made.

If the gel contracts significantly or there is a high cell seeding density, it may be the case that the volume fraction of the cells is no longer negligible. To account for this fact, we could extend our model to include the cells as an additional phase alongside the polymer and solvent. This would add considerable complexity to the modelling problem, and is left for future work.

In this thesis, we have considered what are essentially floating gels surrounded only by solvent, without any external pressure such as a piston or plates. Often experiments are performed where such external compressive forces are applied to the gel from either one or numerous directions (see *e.g.* Kim *et al.* (2006); Vervoort *et al.* (2005)). Our cell-gel model could be adapted to consider such problems, with appropriate adjustments made to features like boundary conditions to incorporate the external forces.

Our work has not considered the potential role of chemical signalling on cell behaviour. Models of chemotactic cell aggregation consider cells and culture medium (see *e.g.* Byrne and Owen (2004)) as well as ECM (see *e.g.* Green *et al.* (2017)), together with a chemoattractant concentration. The chemoattractant induces the movement of cells in response to a chemical stimulus produced by the cells themselves; this is an important process in areas such as wound healing and tissue growth. Incorporating chemotaxis in our model would facilitate better understanding of how the additional non-random cell motion created by chemotactic gradients affects cell and polymer behaviour as well as the gel's overall evolution. To consider these effects, our model needs to be modified to include equations for the chemical concentration and its effect on cells, following methods like those used in the references above.

The oscillating results found in Chapter 3 indicate that, with fine tuning of parameters such as the chemical potential of the solvent, such behaviours might emerge in a spherical gel. This suggests experimental investigation into this behaviour, potentially using methods like those in Monnier *et al.* (2016) for example. Situations where the thin film height and length change at different rates were discussed in the context of biofilms in Chapter 4. Considering anisotropy in the alignment of the polymers, which have been assumed here to be isotropic, would be a significant extension to this work which may lead to different patterns of evolution in the gel height and length (see *e.g.* Green and Friedman (2008); Holloway *et al.* (2018) for studies of transversely isotropic fluids).

This thesis has studied the mechanics of biological gels under the competing forces of cell traction and osmotic pressure. The utility of this cell-gel model can be seen in the range of results presented for different geometries and under different initial con-

ditions and parameter choices. This work can therefore be extended to model different problems and influence future biological experiments, which would, in turn, help to refine the system presented in this thesis. This will yield better understanding of cell-gel mechanics that has the potential to impact tissue engineering.

BIBLIOGRAPHY

Barocas, V., Moon, A., Tranquillo, R., *et al.* (1995). The fibroblast-populated collagen microsphere assay of cell traction force-part 2: measurement of the cell traction parameter. *Journal of Biomechanical Engineering*, **117**(2), 161–170. (Cited on pages 4, 88, and 91.)

Barocas, V. H. and Tranquillo, R. T. (1994). Biphasic theory and in vitro assays of cell-fibril mechanical interactions in tissue-equivalent gels. In *Cell Mechanics and Cellular Engineering*, pages 185–209. Springer. (Cited on pages 6 and 18.)

Byrne, H. M. and Owen, M. R. (2004). A new interpretation of the keller-segel model based on multiphase modelling. *Journal of mathematical biology*, **49**(6), 604–626. (Cited on page 175.)

Cogan, N. and Guy, R. D. (2010). Multiphase flow models of biogels from crawling cells to bacterial biofilms. *HFSP journal*, **4**(1), 11–25. (Cited on page 7.)

Cogan, N. and Keener, J. (2004). The role of the biofilm matrix in structural development. *Mathematical medicine and biology: a journal of the IMA*, **21**(2), 147–166. (Cited on page 7.)

Doi, M. (2011). Onsager's variational principle in soft matter. *Journal of Physics: Condensed Matter*, **23**(28), 284118. (Cited on page 7.)

Doi, M. and Onuki, A. (1992). Dynamic coupling between stress and composition in polymer solutions and blends. *Journal de Physique II*, **2**(8), 1631–1656. (Cited on page 7.)

Dolega, M., Delarue, M., Ingremeau, F., Prost, J., Delon, A., and Cappello, G. (2017). Cell-like pressure sensors reveal increase of mechanical stress towards the core of multicellular spheroids under compression. *Nature communications*, **8**(1), 1–9. (Cited on page 87.)

Drew, D. (1983). Mathematical modeling of two-phase flow. *Annual review of fluid mechanics*, **15**(1), 261–291. (Cited on page 8.)

Edlich, M., Yellowley, C. E., Jacobs, C. R., and Donahue, H. J. (2001). Oscillating fluid flow regulates cytosolic calcium concentration in bovine articular chondrocytes. *Journal of biomechanics*, **34**(1), 59–65. (Cited on page 87.)

Eifler, R. L., Blough, E. R., Dehlin, J. M., and Haut Donahue, T. L. (2006). Oscillatory fluid flow regulates glycosaminoglycan production via an intracellular calcium pathway in meniscal cells. *Journal of orthopaedic research*, **24**(3), 375–384. (Cited on page 87.)

Evans, M. C. and Barocas, V. H. (2009). The modulus of fibroblast-populated collagen gels is not determined by final collagen and cell concentration: experiments and an inclusion-based model. *Journal of biomechanical engineering*, **131**(10). (Cited on page 88.)

Frantz, C., Stewart, K. M., and Weaver, V. M. (2010). The extracellular matrix at a glance. *Journal of cell science*, **123**(24), 4195–4200. (Cited on page 2.)

Green, J., Bassom, A., and Friedman, A. (2013). A mathematical model for cell-induced gel compaction in vitro. *Mathematical Models and Methods in Applied Sciences*, **23**(01), 127–163. (Cited on pages 5, 6, 12, 20, 21, 87, 88, 89, and 91.)

Green, J., Whiteley, J., Oliver, J., Byrne, H., and Waters, S. (2017). Pattern formation in multiphase models of chemotactic cell aggregation. *Mathematical medicine and biology: a journal of the IMA*, **35**(3), 319–346. (Cited on pages 12, 13, 14, 15, 94, and 175.)

Green, J. E. F. (2006). *Mathematical modelling of cell aggregation in liver tissue engineering*. Ph.D. thesis, University of Nottingham. (Cited on pages 12, 15, and 117.)

Green, J. E. F. and Friedman, A. (2008). The extensional flow of a thin sheet of incompressible, transversely isotropic fluid. *European Journal of Applied Mathematics*, **19**(3), 225–257. (Cited on page 175.)

Holloway, C. R., Cupples, G., Smith, D. J., Green, J. E. F., Clarke, R. J., and Dyson, R. J. (2018). Influences of transversely isotropic rheology and translational diffusion on

the stability of active suspensions. *Royal Society open science*, **5**(8), 180456. (Cited on page 175.)

Hong, W., Zhao, X., and Suo, Z. (2010). Large deformation and electrochemistry of polyelectrolyte gels. *Journal of the Mechanics and Physics of Solids*, **58**(4), 558–577. (Cited on pages 3 and 10.)

Howell, P. (1996). Models for thin viscous sheets. *European Journal of Applied Mathematics*, **7**(4), 321–343. (Cited on pages 12, 13, and 117.)

Keener, J., Sircar, S., and Fogelson, A. (2011a). Influence of the standard free energy on swelling kinetics of gels. *Physical Review E*, **83**(4), 041802. (Cited on pages 7, 9, 10, 23, and 86.)

Keener, J., Sircar, S., and Fogelson, A. (2011b). Kinetics of swelling gels. *SIAM Journal on Applied Mathematics*, **71**(3), 854–875. (Cited on pages 7, 9, 10, 11, 12, 13, 18, 19, 20, 22, 23, 25, 36, 60, 61, 72, and 132.)

Kim, S. J., Spinks, G. M., Prosser, S., Whitten, P. G., Wallace, G. G., and Kim, S. I. (2006). Surprising shrinkage of expanding gels under an external load. *Nature Materials*, **5**(1), 48–51. (Cited on page 175.)

King, J. and Oliver, J. (2005). Thin-film modelling of poroviscous free surface flows. *European Journal of Applied Mathematics*, **16**(4), 519–553. (Cited on pages 12, 14, and 15.)

Krause, S., Maffini, M. V., Soto, A. M., and Sonnenschein, C. (2008). A novel 3d in vitro culture model to study stromal–epithelial interactions in the mammary gland. *Tissue Engineering Part C: Methods*, **14**(3), 261–271. (Cited on page 2.)

Kumar, A. and Gupta, R. (2003). *Fundamentals of Polymer Engineering, Revised and Expanded*. CRC Press. (Cited on pages 9 and 10.)

Monnier, S., Delarue, M., Brunel, B., Dolega, M. E., Delon, A., and Cappello, G. (2016). Effect of an osmotic stress on multicellular aggregates. *Methods*, **94**, 114–119. (Cited on pages 3, 87, and 175.)

Moon, A. and Tranquillo, R. (1993). Fibroblast-populated collagen microsphere assay of cell traction force: Part 1. continuum model. *AIChE journal*, **39**(1), 163–177. (Cited on pages 2, 4, 5, 6, 7, 12, 20, 21, 87, 88, 89, 91, and 132.)

Mori, Y., Chen, H., Micek, C., and Calderer, M.-C. (2013). A dynamic model of polyelectrolyte gels. *SIAM Journal on Applied Mathematics*, **73**(1), 104–133. (Cited on pages 7, 9, 11, 13, 18, 20, 21, 22, 23, and 25.)

Morton, K. W. and Mayers, D. F. (2005). *Numerical solution of partial differential equations: an introduction*. Cambridge University Press. (Cited on page 54.)

Murray, J. (2001). *Mathematical biology II: spatial models and biomedical applications*. Springer New York. (Cited on pages 4, 5, 6, and 21.)

Murray, J., Oster, G., and Harris, A. (1983). A mechanical model for mesenchymal morphogenesis. *Journal of Mathematical Biology*, **17**(1), 125–129. (Cited on page 4.)

Oliver, J., King, J., McKinlay, K., Brown, P., Grant, D., Scotchford, C., and Wood, J. (2005). Thin-film theories for two-phase reactive flow models of active cell motion. *Mathematical medicine and biology: a journal of the IMA*, **22**(1), 53–98. (Cited on pages 7, 8, and 10.)

Oster, G., Murray, J., and Maini, P. (1985). A model for chondrogenic condensations in the developing limb: the role of extracellular matrix and cell tractions. *Development*, **89**(1), 93–112. (Cited on page 7.)

Oster, G. F. (1984). On the crawling of cells. *Development*, **83**(Supplement), 329–364. (Cited on page 7.)

Oster, G. F. and Perelson, A. S. (1985). Cell spreading and motility: a model lamellipod. *Journal of Mathematical Biology*, **21**(3), 383–388. (Cited on page 7.)

Rozario, T. and DeSimone, D. (2010). The extracellular matrix in development and morphogenesis: a dynamic view. *Developmental biology*, **341**(1), 126–140. (Cited on page 2.)

Rubinstein, M., Colby, R. H., *et al.* (2003). *Polymer physics*, volume 23. Oxford University Press New York. (Cited on pages 22, 23, and 56.)

Salinas, E. Y., Hu, J. C., and Athanasiou, K. (2018). A guide for using mechanical stimulation to enhance tissue-engineered articular cartilage properties. *Tissue Engineering Part B: Reviews*, **24**(5), 345–358. (Cited on page 87.)

Shoulders, M. D. and Raines, R. T. (2009). Collagen structure and stability. *Annual review of biochemistry*, **78**, 929–958. (Cited on page 2.)

Sircar, S., Keener, J., and Fogelson, A. (2013). The effect of divalent vs. monovalent ions on the swelling of mucin-like polyelectrolyte gels: Governing equations and equilibrium analysis. *The Journal of chemical physics*, **138**(1), 014901. (Cited on pages 11 and 23.)

Stevenson, M. D., Sieminski, A. L., McLeod, C. M., Byfield, F. J., Barocas, V. H., and Gooch, K. J. (2010). Pericellular conditions regulate extent of cell-mediated compaction of collagen gels. *Biophysical journal*, **99**(1), 19–28. (Cited on pages 2, 69, 88, 91, 132, 169, and 173.)

Trinschek, S., John, K., and Thiele, U. (2016). From a thin film model for passive suspensions towards the description of osmotic biofilm spreading. *AIMS Materials Science*, **3**(3), 1138–1159. (Cited on pages 12, 92, and 169.)

Trinschek, S., John, K., Lecuyer, S., and Thiele, U. (2017). Continuous versus arrested spreading of biofilms at solid-gas interfaces: The role of surface forces. *Physical review letters*, **119**, 078003. (Cited on pages 12, 92, and 169.)

Vervoort, S., Patlazhan, S., Weyts, J., and Budtova, T. (2005). Solvent release from highly swollen gels under compression. *Polymer*, **46**(1), 121–127. (Cited on page 175.)

Wayne, J. S., McDowell, C. L., Shields, K. J., and Tuan, R. S. (2005). In vivo response of polylactic acid–alginate scaffolds and bone marrow-derived cells for cartilage tissue engineering. *Tissue engineering*, **11**(5-6), 953–963. (Cited on page 2.)

Winstanley, H., Chapwanya, M., McGuinness, M., and Fowler, A. (2011). A polymer–solvent model of biofilm growth. *Proceedings of the Royal Society A: Mathematical, Physical and Engineering Science*, **467**(2129), 1449–1467. (Cited on pages 7 and 10.)

Wolgemuth, C. W., Mogilner, A., and Oster, G. (2004). The hydration dynamics of polyelectrolyte gels with applications to cell motility and drug delivery. *European Biophysics Journal*, **33**(2), 146–158. (Cited on page 7.)

Zhang, T., Cogan, N., and Wang, Q. (2008). Phase-field models for biofilms ii. 2-d numerical simulations of biofilm-flow interaction. *Communications in Computational Physics*, **4**(1), 72–101. (Cited on page 22.)

Zhu, Y., Umino, T., Liu, X., Wang, H., Romberger, D., Spurzem, J., and Rennard, S. (2001). Contraction of fibroblast-containing collagen gels: initial collagen concentration regulates the degree of contraction and cell survival. *In Vitro Cellular & Developmental Biology-Animal*, **37**(1), 10–16. (Cited on page 88.)